Lateral Shear Strength Estimation of Rectangular RC Bridge Piers

A Thesis
by
Aysha Zeneeb Majeed

for the award of the degree of
Doctor of Philosophy

Department of Civil Engineering
Indian Institute of Technology Madras
August 2016

Lateral Shear Strength Estimation of Rectangular RC Bridge Piers

A Thesis
by
Aysha Zeneeb Majeed
(Roll No. CE12D035)

for the award of the degree of
Doctor of Philosophy

Department of Civil Engineering
Indian Institute of Technology Madras
August 2016

Certificate

This is to certify that the thesis titled **Lateral Shear Strength Estimation of Rectangular RC Bridge Piers** submitted by **Aysha Zeneeb Majeed** (Roll No. CE12D035) to the Indian Institute of Technology Madras for the award of the degree of Doctor of Philosophy is a bona fide record of the research work done by her under our supervision. The contents of this thesis, in full or in parts, have not been submitted to any other Institute or University for the award of any degree or diploma.

C.V.R. Murty
Professor
Department of Civil Engineering
Indian Institute of Technology Madras

Rupen Goswami
Assistant Professor
Department of Civil Engineering
Indian Institute of Technology Madras

Blank page

Abstract

Reinforced concrete (RC) bridge piers exhibit complex behavior owing to combined actions of axial force *P*, shear force *V*, and bending moment *M* during earthquake shaking. A simple method is presented to efficiently estimate lower bound lateral load required to cause failure, including identification of mode of failure and location of failure, in prismatic and flared RC members of solid rectangular cross-section under combined stresses. A well established *shear capacity model* for concrete (using Bresler's failure envelope criteria) is integrated with the conventional section analysis model (for capturing axial-flexure interaction). Then, shear strength, of transverse reinforcement obtained using a basic truss model, is combined to estimate overall shear strength capacity of RC members. The latter accounts for variation in crack angle due to combined effect of normal (due to axial and flexural actions) and shear stresses. Contribution of dowel action by longitudinal reinforcement is considered towards residual shear strength. *Shear Force – Bending Moment* (*V-M*) *strength interaction capacity diagram*, viewed alongside the demand diagram, helps depict failure load and failure mode, and provides insights into the shear resistance mechanism of RC members. Analytical results of failure load of RC members obtained using the proposed method are compared with published experimental results of 107 RC members (tested with different axial loads, transverse reinforcement ratios, longitudinal reinforcement ratios, shear span to depth ratios, and loading conditions). Further, the analytically obtained results are compared with those obtained using other available models to estimate lateral load (or shear) capacity of RC members; in all cases, reasonable accuracy is observed of shear capacity predicted by the proposed method, which is simple and intuitive too.

Subsequently, the proposed method is used to evaluate *mode of failure* (*i.e.*, flexure or shear) and *location of failure* in RC bridge piers, both with uniform rectangular cross-sections and those varying along the length of the pier, under combined actions of gravity load and seismic effects. The mode and location of failure vary depending on (1) *geometry*: *i.e.*, plan aspect ratio of cross-section and slenderness, including shear span to depth ratio, of member, (2) *design and detailing*: *i.e.*, longitudinal and transverse reinforcement ratio including distribution of reinforcement within cross-section and along the length of the member, and (3) *gravity load*: *i.e.*, axial load ratio, in addition to grade of constituent materials. In particular, the proposed method helps identifying the mode and location of damage in piers, where either reinforcement detailing changes (as within and outside potential plastic hinge region) or size of cross-section changes (as in flared piers). Also, limits are recommended of the amount of transverse reinforcement required, depending on slenderness, to ensure ductile flexural mode of failure in prismatic RC piers of solid rectangular cross-section.

Blank page

Acknowledgement

I express my sincere appreciation to my thesis supervisors, Professors Rupen Goswami and C.V.R. Murty, for their relentless commitment, enlightening guidance and unwavering support. I relish the energy and enthusiasm we had during countless discussions over these years, and cherish my learning in developing a simplified view of complex issues.

Also, I am grateful to all other Faculty Members of the Structural Engineering Laboratory, for their timely support towards the successful completion of my studies at IIT Madras. Further, I thank my friends and colleagues, Sunitha P. Menon, A. R. Vijayanarayanan, G. Tamizharasi, B. Bijili, M. Velmurugan and Tharun J. Joseph for their understanding, and the modest get-togethers we had, which made my stay and studies at IIT Madras more enjoyable.

I am deeply indebted to my husband, Azeem K., for the unconditional support and motivation, putting up with all my mood swings, to my parents for the prayers, care and struggle over the years, to my in-laws for the prayers and perseverance, and to my sisters for the moral support. It would not have been possible for me to complete the doctoral work without the unyielding love of my son Afraz, who has been exceptionally understanding and caring throughout our stay in campus.

Aysha Zeneeb Majeed

10 August 2016
Chennai

Blank page

Table of Contents

Page

Page

Blank page

List of Tables

Blank page

List of Figures

List of Symbols

Symbol	Description
A_b	Area of individual reinforcing bar
A_c	Area of core concrete of cross-section
A_{ci}	Area of i^{th} fiber of concrete
A_g	Gross area of member cross-section
A_h	Sectional area of transverse reinforcement
A_l	Area of longitudinal reinforcement
A_v	Cross-sectional area of stirrup legs
A_{si}	Area of i^{th} fiber of longitudinal steel
A_{sl}	Area of longitudinal reinforcement in tension
A_{st}	Total cross-sectional area of stirrups intercepting the crack at a given section
A_{sti}	Total cross-sectional area of stirrup *i* intercepting the crack at a given section
A_{sw}	Area of stirrups in one direction of confinement
C	Cantilever member
2C	Double ended cantilever member
C_{k1}	Compressive force acting on the face of concrete layer k at section 1
C_{k2}	Compressive force acting on the face of concrete layer k at section 2
B	Width of the member cross-section
D	Overall depth of the member cross-section
DC	Member in double bending
E	Modulus of elasticity
E_c	Initial tangent modulus of concrete
$E_{c,sec}$	Secant modulus of concrete
F_k	Horizontal shear force acting on k^{th} layer of concrete
F_{k-1}	Horizontal shear force acting on $(k-1)^{th}$ layer of concrete
F_y	Yield strength of longitudinal reinforcing steel
F_{yi}	Yield strength of stirrup *i*
H	Horizontal force
H_d	Shear demand on a member corresponding to factored load
H_{max}	Maximum lateral shear force carrying capacity of piers at failure
H_Ω	Flexural overstrength based shear demand on a member
I	Moment of inertia of cross-section of longitudinal bar
L	Length of the member
L_1, L_2, L_3	Distance from the loading point at top to the stirrup at level 1,2 and 3
L_b	Length of column between the point of maximum moment and point of contra-flexure
M	Bending moment of a cross section
M_{cap}	Moment capacity of a cross-section at a given axial load level
$M_{cap@0.5P}$	Moment capacity of a cross-section at an axial load level $P/P_u = 0.5P$
$M_{cap@fck60}$	Moment capacity of a cross-section with concrete grade M60, at a given axial load level
M_d	Moment demand corresponding to factored load

Symbol	Description
M_l	Maximum bending moment capacity as per code provisions
M_{max}	Maximum experimental bending moment capacity
M_p	Plastic moment in the bar
M_Ω	Flexural overstrength capacity
M_u	Ultimate bending moment capacity of the section
N	Total number of fibres in a cross-section
N_{cf}	Total number of concrete fibres in a cross-section
N_{sf}	Total number of steel layers in a cross-section
P	Compressive axial force
P_b	Axial load at balanced failure
P_{ext}	External compressive axial load acting on the section
P_u	Ultimate compressive axial load capacity of the section
S	Distance between two sections considered along the length of member
S_L	Spacing of stirrups in longitudinal direction
S_v	Spacing of stirrups
V	Lateral shear force
V_c	Shear capacity of concrete cross-section
V_d	Shear demand on concrete cross-section
V_{di}	Shear demand at the level of i^{th} stirrup
$V_{c,@M=o}$	Shear capacity of concrete cross-section at zero bending moment
$V_{@P=o,\ M=o}$	Shear capacity at zero moment and zero axial load
$V_{c@P=pPu,\ M=o}$	Shear capacity of concrete cross-section at zero bending moment at a given axial load level pP_u
$V_{c@P=pPu,\ M=Mu}$	Shear capacity of concrete cross-section at maximum bending moment at a given axial load level pP_u
$V_{c,max@fck6o}$	Maximum shear capacity of cross-section with concrete grade M60
V_{exp}	Estimated failure load from experiments
V_k	Nominal shear force at k^{th} layer
V_n	Nominal shear capacity of cross-section
V_o	Overstrength shear
V_p	Shear component of prestressing
V_{prop}	Failure load using proposed model
V_s	Shear capacity of reinforcing steel
V_{sl}	Shear resistance offered by dowel action of n_l longitudinal bars
V_{st}	Shear resistance offered by transverse reinforcement
V_{sti}	Contribution of i^{th} stirrup towards shear resistance of RC member
V^*	Design shear force obtained considering overstrength flexural actions
V_Ω	Flexural overstrength based shear demand
V_{theo}	Theoretical estimates of lateral load capacity
V_u	Factored shear force at a section
a	Plan aspect ratio
a'	Shear span
b	Width of member cross-section
b_c	Width of concrete core cross-section
b_v	Width of concrete web including adjustments for presence of ducts
C_c	Modification factor accounting for reversed cyclic load effect

Symbol	Description
C_e	Modification factor accounting for size effect
C_{pt}	Modification factor accounting for increase in shear capacity of concrete with increase in longitudinal steel
d	Depth from compression face to centroid of tension reinforcement
d_c	Depth of concrete core cross-section
d_l	Diameter of longitudinal reinforcement
d_v	Effective shear depth
f_c	Normal stress in concrete
$f_{c,i}$	Average normal stress in i^{th} fiber of concrete
f_s	Normal stress in i^{th} fiber of longitudinal steel
$f_{s,i}$	Normal stress in longitudinal steel
$f_{sc,i}$	Normal stress in longitudinal steel in compression
$f_{st,i}$	Normal stress in longitudinal steel in tension
f'_c	Cylinder strength of unconfined concrete in compression
$f_{c,max}$	Maximum concrete compressive strength
f'_{cc}	Confined compressive strength of concrete
f'_{co}	Unconfined compressive strength of concrete
f_{cd}	Design compressive stress
f_{cr}	Concrete tension at initiation of cracking
f'_l	Effective confining stress
f_{ck}	Characteristic compressive strength of concrete cube
f_v	Tensile stress in stirrups
f_y	Yield strength of reinforcing steel
f_{yl}	Yield strength of longitudinal reinforcement
f_{yt}	Yield strength of transverse reinforcement
f_{yi}	yield strength of stirrup *i*
f_2	Principal compressive stress
m	Lower characteristic yield strength of longitudinal steel
m'	Number of concrete layers
n	Total number of stirrups intercepting the crack along the length of the member
n_l	Total number of longitudinal bars
p	Axial load ratio
r	Radius of longitudinal bar
s_v	Spacing of transverse reinforcement
s	Slenderness ratio
y_i	Distance to the centroid of the fiber *i* from the geometric centroidal axis of the cross-section
$y_{c,i}$	Distance to the centroid of the concrete fiber *i*, from the geometric centroidal axis of the cross-section
$y_{s,i}$	Distance to the centroid of the steel layer *i*, from the geometric centroidal axis of the cross-section
α	Crack angle
α'	Safety coefficient
β	Concrete contribution factor
Δ_y	Maximum displacement of longitudinal stirrups between adjacent stirrups
δ	Displacement of the member

Symbol	Description
δ_u	Ultimate displacement of the member
δ_y	Yield displacement of the member
$\Delta\varepsilon$	Strain gradient
ε_{bot}	Average strain in the bottom concrete fiber
ε_c	Normal strain in concrete
ε'_c	Concrete strain at peak stress
ε_{co}	Strain corresponding to f'_{co}
ε_{cc}	Strain corresponding to f'_{cc}
$\varepsilon_{c,i}$	Average compressive strain in i^{th} fiber of concrete
$\varepsilon_{c,max}$	Limiting strain for confined concrete
ε_{cr}	Strain in concrete at initiation of cracking
ε_o	Average normal strain in the middle fiber
ε_s	Normal strain in steel
ε_{si}	Average normal strain in i^{th} fiber of longitudinal steel
ε_{sci}	Average normal strain in i^{th} fiber of longitudinal steel in compression
ε_{sti}	Average normal strain in i^{th} fiber of longitudinal steel in tension
ε_{su}	Fracture strain of transverse steel
ε_{top}	Average strain in the top concrete fiber
ε_y	Yield strain in reinforcing steel
μ	Ductility
μ_a	Allowable ductility factor
μ_d	Displacement ductility factor
υ_c	Nominal shear stress
υ_{cr}	Concrete contribution in terms of nominal shear stress at initiation of diagonal cracking
φ	Curvature of cross-section
ϕ	Safety factor, strength reduction factor
ρ_a	Area ratio of transverse reinforcement
ρ_l	Longitudinal reinforcement ratio
ρ_L	Area ratio of longitudinal reinforcement
ρ_s	Volumetric ratio of hoop reinforcement with respect to core concrete
ρ_T	Transverse reinforcement ratio
ρ_v	Volumetric ratio of transverse reinforcement
ρ_w	Effective area of flexural reinforcement
τ_c	Shear stress in concrete
τ_{ci}	Average shear stress of i^{th} fiber of concrete
θ	Strut angle
σ_{cp}	Axial compressive stress

1
Introduction

1.0 RC BRIDGE PIERS

A simple but critical structure is the single pier bridge; it consists primarily of a vertical cantilever supporting bridge *superstructure*. A bridge is a lifeline structure, and its structural *integrity* and *functionality* should be maintained even after major earthquakes. Hence, the behaviour of the pier in a single pier bridge plays a crucial role in the structural performance of the bridge during strong earthquake shaking. Earthquake-resistant design of structures relies on *ductility* of structural components to dissipate input seismic energy. In bridges, *failure* of superstructure renders the bridge dysfunctional, and therefore, is not acceptable. Further, connection failures are *brittle*, and therefore, cannot be allowed either. Furthermore, foundations are inaccessible for inspection and repair after earthquakes, and hence, damage cannot be permitted even in them either. Therefore, in conventional bridges without additional energy dissipation devices, the pier (also called *substructure*) is the only structural component where controlled inelasticity can be allowed to dissipate the input seismic energy, provided the damage in it does not cause collapse of the bridge. This requirement can be fulfilled by ensuring these piers to undergo *ductile flexural damage*; brittle shear failure of piers is unacceptable, particularly in *reinforced concrete (RC)* bridges.

Single column RC bridge piers are used more commonly in bridges owing to their *aesthetics* and *lesser space use* (Figure 1.1). Prismatic (circular or rectangular cross-section) piers are used most commonly; also, often, non-prismatic piers with flaring along the elevation are used for their *architectural*, *functional* and *structural* advantages (Figure 1.2). But, at the same time, single piers pose two *unique* challenges from structural behaviour point of view under seismic applications, namely:

(i) They lack redundancy; and
(ii) They are subjected to *high magnitude* combined actions of axial force P, shear force V and bending moment M, during strong earthquake shaking.

Figure 1.1: Single pier reinforced concrete bridge: (a) Most commonly used substructure type due to architectural, functional and structural reasons, (b) schematic elevation showing components of RC bridge pier

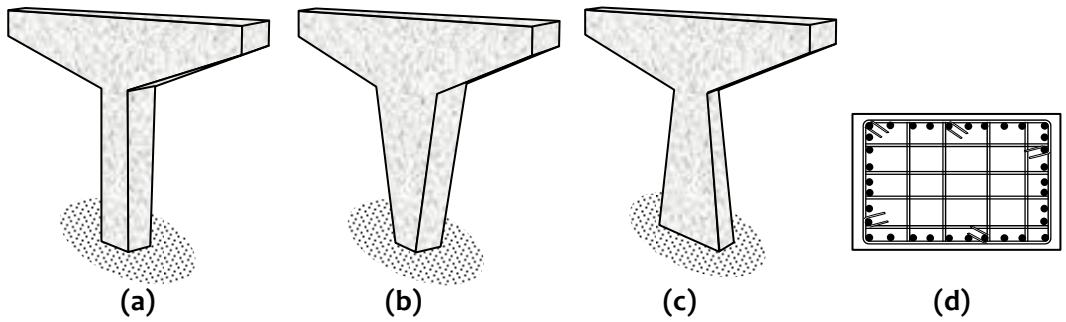

Figure 1.2: Elevation of commonly used single column RC piers: (a) pier with uniform cross-section, (b) pier with flaring towards top, (c) pier with flaring towards bottom, and (d) typical detail of piers with solid rectangular cross-section

Many RC bridges with single piers suffered severe *damage* in the piers or *collapse* during past earthquakes worldwide. These damages or collapses could have been avoided, if expected response of such piers had been envisaged and they had been designed to resist the effects imposed on them during strong earthquake shaking.

1.1 EARTHQUAKE BEHAVIOUR OF RC BRIDGE PIERS

Bridge piers sustain inelastic response under the combined actions of induced axial force P, shear force V, and bending moment M; this involves *stiffness degradation* and *strength deterioration* of the pier, and results in increased lateral deformation. This combined *P-V-M* action during strong earthquake shaking induces *high normal and shear stresses* in single pier RC bridges. Considering the interaction of normal and shear

stresses is necessary for accurate estimation of lateral *load*, lateral *deformation* and lateral *ductility* capacities of piers [Lee and Elnashai, 2001]. Therefore, while it is important to quantify the *lateral load carrying capacity* of such piers, it is critical to determine the likely *mode of failure*. Together, these two inputs give insightful understanding of behaviour of RC piers towards ensuring earthquake safety of bridges.

1.2 EARTHQUAKE DESIGN OF RC BRIDGE PIERS

Structural design involves proportioning of members and providing capacities in members to meet the demands imposed by expected loads. For single pier RC bridges, strong earthquake shaking imposes interaction between axial force P, shear force V and bending moment M, which in turn, results in nonlinear actions in the piers. These nonlinear actions include cracking of concrete in tension, yielding of steel reinforcement in tension, and crushing of concrete in compression. But, simplified design procedures normally adopted consider separately the actions imposed by P and M (through nonlinear P-M interaction), and that by V. P-V-M interaction is considered only in few design codes through shear capacity enhancement factor due to axial compression, while shear capacity reduction with increase in bending moment demand is considered in CALTRANS and AASHTO documents [*e.g.,* CALTRANS, 2013; AASHTO, 2010]. On the other hand, P-V-M interaction can be significant in stocky RC piers (with low slenderness). And, in general, V-M interaction leads to degradation in shear strength, and thereby to premature brittle failure of RC piers.

The critical parameters that govern behaviour of RC members subjected to lateral loading include *slenderness*, *plan aspect ratio*, *longitudinal and transverse reinforcement ratios* (along with detailing of longitudinal and transverse reinforcement bars), and *axial load ratio*. Analytical methods (*e.g., Equilibrium Plasticity Truss Models*, *Modified Compression Field Theory Models*, *Softened Truss Model*, and *Truss Arch Models*) are available to predict closely the strength of RC members under combined loading. But, these methods provide little understanding of mechanisms of internal resistance offered by RC members to combined P-V-M load effects. Further, these methods are complex, and are rarely used in design practise.

The mode of failure of RC members under earthquake shaking effects is governed by relative strengths of members in shear and flexure; the prominent modes of

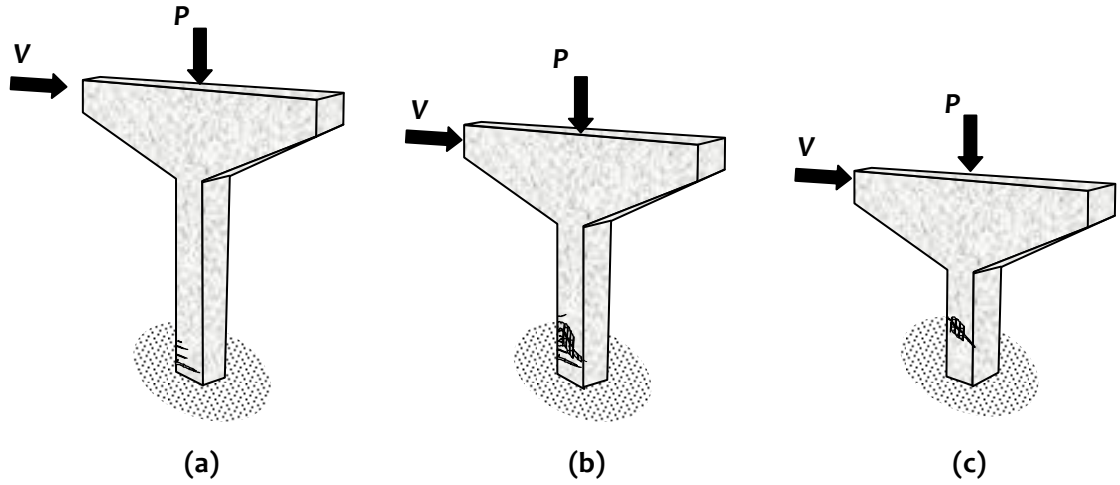

Figure 1.3: Predominant modes of failure in RC members: (a) flexure failure, (b) combined flexure-shear failure, and (c) shear failure

failure are *flexure failure*, *combined flexure-shear failure*, and *shear failure* (Figure 1.3). Shear failure is less ductile than flexure failure [Mergos and Kappos, 2012], and hence, not desirable. Thus, estimating shear strength (as a function of bending moment and axial load imposed) is critical to identifying the possible mode of failure of RC members. In addition, identifying the location of such failure is important; this is particularly critical in non-prismatic members or in members with longitudinal or transverse reinforcement varying along the length of the member. Thus, a simple, yet robust, method is required to determine *failure load*, *failure mode* and *failure location* in RC members.

1.3 OBJECTIVES OF THE PRESENT STUDY

The present study investigates the influence of combined *P-V-M* load effects on response of RC members of solid rectangular cross-sections. It aims to develop a simple method to determine *failure load*, *failure mode* and *failure location* in RC members. Thus, specific objectives of the present study are:

(1) To *develop* a simple analytical method for getting insights into internal resistance mechanism of RC members considering *P-V-M* interaction;

(2) To *estimate failure load*, *failure mode* and *failure location* of single cantilever RC members subjected to lateral action, using the said analytical method developed; and

(3) To *identify* the critical parameters influencing *failure load*, *failure mode* and *failure location* of single RC members with solid rectangular cross-section, using the said analytical method developed.

The analytical method combines traditional flexure model (using *classical section analysis* approach) with a shear model (using *equilibrium*, *compatibility* and *constitutive relations* approach) to account for *P-V-M* interaction.

1.4 ORGANISATION OF THESIS

The content of the thesis is presented in five relatively independent chapters. In Chapter 1, an introduction is presented to the subject matter of the thesis and specific issues addressed in this thesis. In Chapter 2, a review is presented of the pertinent literature on the subject, including behaviour of RC bridges during past earthquakes, experimental and analytical research studies, and design provisions adopted worldwide. In particular, important experimental and analytical studies are evaluated with emphasis on understanding resistance mechanism of RC members under action of combined load effects, and gap areas identified for possible investigations. And, finally Chapter 2 presents the scope of present study.

In Chapters 3 and 4, mechanisms of resistance are presented of lateral load at the section level and member level, respectively. In Chapter 3, a simplified *mechanics-driven* analytical method is proposed for estimating load carrying capacity of prismatic RC sections with solid rectangular cross-sections subjected to combined *P-V-M* load effects; using this method, behaviour is studied of *RC Section*s. Effects are explained of axial force P and bending moment M on shear strength V_c of concrete.

And, in Chapter 4, behaviour is studied of *RC Members*. Lateral load capacity of RC members is estimated by superposing sectional shear capacity of concrete, and that of transverse reinforcement using basic truss analogy. Simple expressions are derived for estimating effects of crack angle and dowel action of longitudinal reinforcement. Shear resisting mechanism of RC members is explained with *shear-flexure interaction diagrams* obtained using the proposed analytical method, which helps determining *failure load*, *failure mode* and *failure location* in RC members. Also, detailed parametric study is presented on *prismatic* and *non-prismatic* RC members to understand influence of various parameters on lateral load capacity of RC members. In particular, the minimum transverse reinforcement is identified, which is required to prevent brittle shear failure in RC bridge piers.

In Chapter 5, the work done in this study is summarised, along with salient conclusions drawn from it. The chapter closes with a discussion on limitations of present study and the scope for possible future work on the subject.

2
Review of Literature

2.0 INTRODUCTION

Bridges constructed in seismically active areas are exposed to risk of damage from earthquakes. Severity of earthquake damage to bridges ranges from minor cracks and residual lateral deformations, to complete collapse. Failure is unacceptable for these lifeline facilities during earthquakes, because their failure jeopardizes immediate post-earthquake services (especially *rescue and relief* operations). Thus, bridges are required to remain *functional* after a design level earthquake.

Past earthquakes revealed vulnerability of bridges to strong ground motions. Collapses of bridges during past earthquakes were mainly owing to failure of all its components – *superstructure*, *bearings*, *substructure* and *foundations*. The key deficiencies of bridges, which led to damage or even collapse, are: (i) insufficient seat width to prevent unseating of superstructure, (ii) inadequate transverse reinforcement in piers to provide shear resistance and ductility, (iii) inadequate anchorage length of longitudinal reinforcement bars in piers resulting in pull-out of the piers from the foundations, (iv) improper location of expansion joints leading to unstable configuration of spans, where only one column is spaced between two joints, and (v) inadequacy of wing walls and abutments to minimize displacement and reduce damage at piers [Saadeghvaziri and Foutch, 1988]. Because foundations are not easy to retrofit and damage in superstructure renders the bridge dysfunctional in post-earthquake conditions, the substructures or piers are the components wherein inelasticity can be allowed to dissipate energy in ductile flexure mode; piers are amenable for repair and retrofit.

Of the various types of bridges, the *simple bridges* (those with balanced spans with low skew and approximately equal stiffness) are most commonly built on highways. Usually, the superstructures of these bridges consist of cast-in-place girders. The girders and piers act as *separate* structural units, when connected by bearings, or as an *integrated* unit, when cast monolithically. The piers are of four types, namely *wall type*

with single members with height to maximum plan dimension ratio less than 2.5 (Figure 2.1a), *linked column frame type* with two or more piers connected at intermediate levels with link beams to reduce displacements and moments (Figure 2.1b), *multiple column frame type* with two or more piers connected together by a cap beam resulting in frame action (Figure 2.1c), and *single column type* with single members of height to maximum plan dimension ratio greater than 2.5 (Figure 2.1d). Geometry and aspect ratio play significant role in the behaviour of bridge piers during earthquake shaking. Earthquake shear behaviour of RC bridge piers, with different elevation and plan aspect ratios, is a critical aspect, which has not been adequately explored. Other parameters that influence the shear behaviour of RC bridge piers include the shear span to depth ratio, percentage of transverse and longitudinal reinforcements, frequency of the applied load and the level of axial compressive stresses [Higai *et al*, 1985].

In general, under strong earthquake ground motion, bridge piers are subjected to combined effect of axial forces, bending moments and shear forces. *Flexural strength* of pier is dependent on the imposed *axial force*, and *shear strength* is influenced by the imposed *bending moment*. Neglecting the interaction of these combined load effects can result in *overestimation* of lateral *load* capacity and *underestimation* of lateral *deformation* demand [Lee and Elnashai, 2001]. Shear strength deserves particular care, because the nonlinear interaction between *bending*, *shearing* and *compressing/elongating* actions lead to reduction in shear strength, particularly in the regions of inelasticity (plastic hinges), leading to premature failure of such piers.

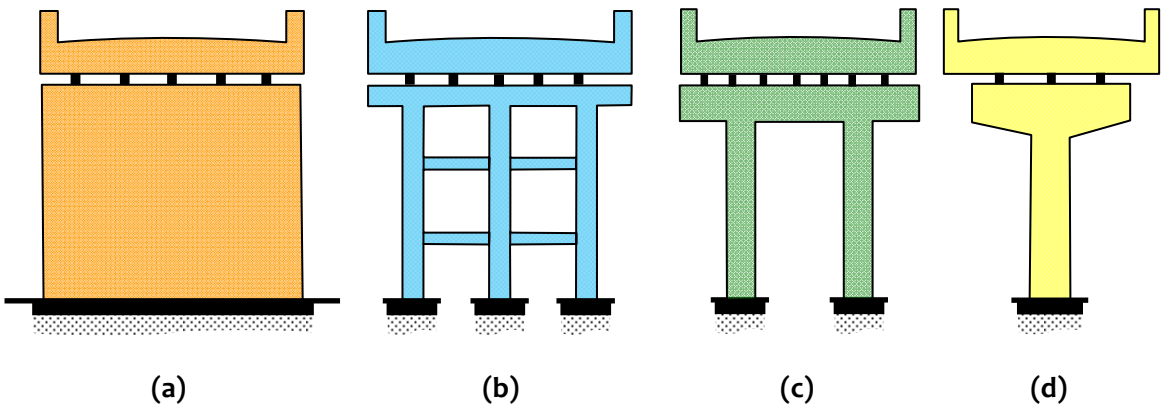

Figure 2.1: Classification of RC bridge piers: (a) Wall type, (b) Linked column frame type, (c) Multiple column frame type, and (d) Single column type

This chapter provides an overview of performance of bridge piers in the past earthquakes, with emphasis on behaviour of single column RC bridge piers. Analytical and experimental studies are examined on how the behaviour of piers is predicted during expected strong earthquake ground motion, and design and detailing specifications reviewed as provided by national and international codes, towards ensuring earthquake safety of piers.

2.1 SINGLE COLUMN RC BRIDGE PIERS

Single column piers are appropriate, when superstructure is connected to substructure through bearings and width of superstructure is small; superstructure with large width results in high eccentric live loads in single column piers. Continuous box girder supported on single piers is a common choice of highway bridge configuration, mainly owing to *less space requirement* and *better aesthetics*. Single pier bridges with superstructure resting on bearings behave like cantilever columns in all directions. These single column piers lack redundancy, and hence, rely on ductility capacity to resist the displacement loading imposed during earthquake ground shaking. Further, confinement effect in single column piers is lesser than that in frame type pier, owing to large size of piers, thus limiting *strength* and *ductility* of plastic hinges at the pier bases.

2.1.1 Geometry

Pier capacities (especially lateral strength and ductility capacities) and response are greatly affected by geometry of RC bridge piers – shape and size of cross-section in plan, and slenderness and variation of cross-section (prismatic or flared) in elevation.

2.1.1.1 Cross–Section

RC bridge piers can be classified based on their cross-sectional geometry in plan as *solid rectangular* (Figure 2.2a), *hollow rectangular* (Figure 2.2b), *solid circular* (Figure 2.2c), *hollow circular* (Figure 2.2d), and *polygonal* (Figure 2.2e). Circular and rectangular sections are most commonly used; within that the secondary choice is between solid and hollow section shapes.

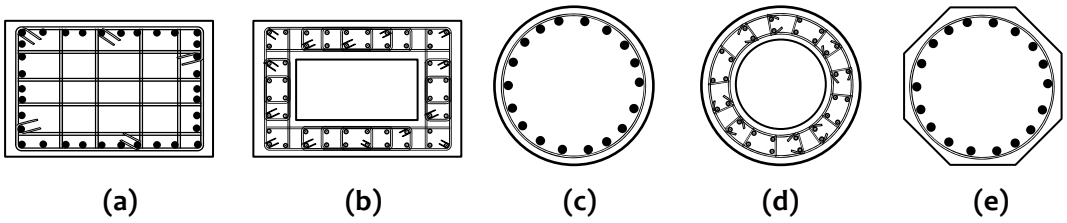

Figure 2.2: Cross-sections of commonly built RC bridge piers: (a) Solid rectangular, (b) Hollow rectangular, (c) Solid circular, (d) Hollow circular, and (e) Polygonal

Circular sections are generally considered to be more efficient and easy to construct; spiral confinement provided in them results in better confinement of the core concrete and restrains longitudinal reinforcement from buckling. Square sections are the most efficient section among other shapes and as the plan aspect ratio increases; effect of confinement of core is lesser in them. Mass of hollow piers is significantly smaller than that of piers with solid cross-section, thus reducing the amount of material used and decreasing the inertia forces induced by earthquake effects. In general, piers with hollow sections show enhanced deformability and have higher shear capacity when compared to solid ones with the same cross-sectional area, owing to presence of two curtains of transverse reinforcement. Also, rectangular piers show enhanced *deformability and shear capacity*, than circular ones when provided with intermediate ties [Goswami, 2002; Goswami and Murty, 2005].

2.1.1.2 Slenderness

Slenderness of a RC pier (the ratio of its height to width of cross-section) determines the level of flexure-shear interaction. For a pier with uniform cross-section along the height, an increase in height leads to an increase in slenderness. With increase in slenderness, geometric and material nonlinearities play significant role in their response; stocky piers with less slenderness are susceptible to brittle shear failure.

2.1.1.3 Prismatic and Non Prismatic

Depending on the geometry in elevation, single column type bridge piers can be classified as *hammerhead shaped pier* (Figure 2.3a) or *flared shaped pier* (Figure 2.3b and 2.3c). Behaviour of flared shaped is complex owing to its varying cross-section the varying capacity of the cross-section moves the location of failure away from the assumed locations. Even a lightly reinforced flare contributes to increasing the section capacity in flared region [Nada *et al*, 2003], which alters the expected behaviour.

2.1.2 Constituent Materials

Response of a pier depends on those of its individual constituent materials – longitudinal reinforcing steel, transverse reinforcing steel, and concrete. Configuration, amount and placement of transverse reinforcement, and percentage and distribution of longitudinal reinforcement affect the *stress-strain characteristics* of concrete. Both design and detailing of longitudinal and transverse reinforcement play a vital role in the earthquake response of bridge piers, along with other influencing factors (such as ratio of core and gross cross-sectional areas, and load history) [Sakai, 1989].

2.1.2.1 Reinforcing Steel

Depending on the choice of cross-section shape and type of elevation, reinforcement layout and detailing have to be carefully done to ensure the required seismic displacement capacity without significant strength degradation. In RC piers, transverse reinforcement offers three functions, namely *(i)* enhancing shear strength by resisting shear force through tensile action, *(ii)* confining concrete by protecting it from outward bulging due to normal compressive stress and *(iii)* preventing buckling of longitudinal bars. Longitudinal reinforcement contributes mainly towards the flexural strength of piers, in addition to affecting the overall confinement of concrete. By limiting the amount of longitudinal steel in relation to cross-section dimensions, yield strength and adequate ductility can be ensured.

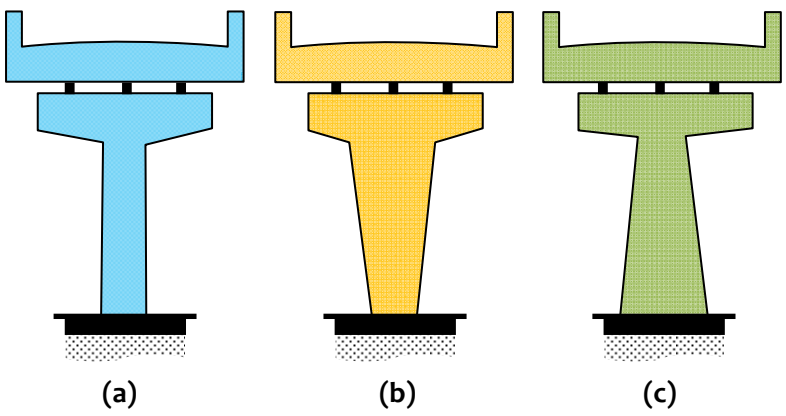

Figure 2.3: Elevation of commonly built single column RC bridge piers: (a) Hammerhead shaped; (b) and (c) Flared shaped pier

Also, inadequate lap splices of longitudinal and transverse reinforcements limit the available flexural strength and ductility capacity [Boys, 2009]. Lapping of foundation starter bars at the base of the pier has many construction advantages. But, this leads to de-bonding of lap splice resulting from insufficient development length of longitudinal bars during seismic shaking, particularly in a cantilever column where inelasticity is expected to develop at its base [Kim *et al*, 2006]. Studies suggest that lapped splices in potential plastic hinge regions should be used, only when the design level of structure ductility μ is less than or equal to 3. Lapping of longitudinal bars should be done by cranking bars into the core concrete, rather than by lapping side-by-side [Priestley and Park, 1987]. Providing lap splices requires concrete to carry *tension* and *shear*. As a result of this load transfer, longitudinal reinforcement bars go into axial tension or compression. Distribution of tensile stresses in the concrete normal to the axis of the bar is as shown in Figure 2.4. Lapping of bars generates additional forces in concrete, which tend to push the bars apart. If the cover provided is not strong enough to prevent this bursting force, spalling of cover concrete happens, followed by splice failure. Large cross-sections of bridge pier necessitate lapping of transverse reinforcement also. Simple lapping of transverse bars is ineffective during earthquake loading, because variation in axial compressive load dilates the core concrete owing to Poisson's effect. This will lead to opening up of the transverse reinforcement, and thus, make the lap ineffective at high ductility demand. Use of splice weld or mechanical couplers (Figure 2.5) enables the reinforcing steel bar to behave in a manner similar to continuous length bars. Mechanically coupled longitudinal bars exhibit better performance when subjected to reversed cyclic loading.

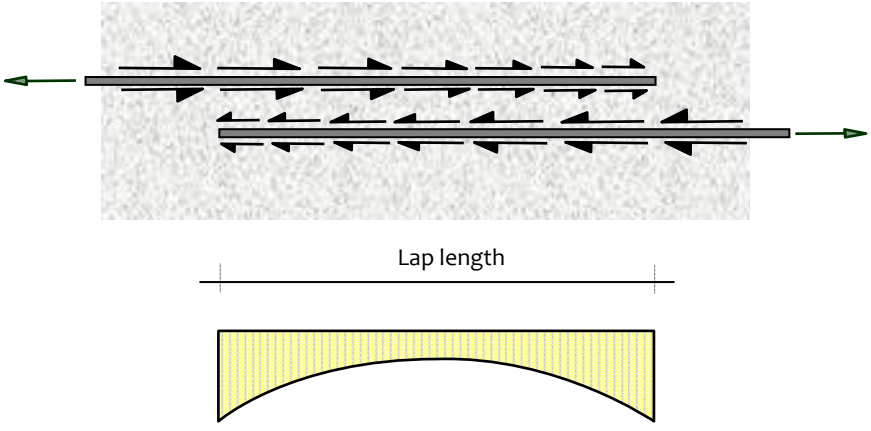

Figure 2.4: Distribution of tensile stresses transferred to concrete along lap length

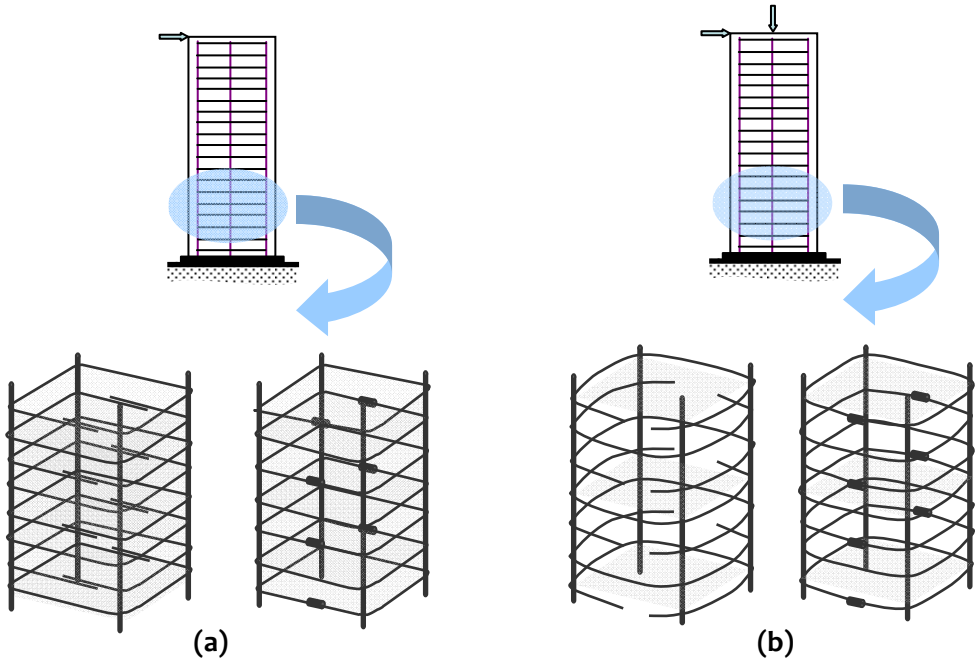

Figure 2.5: Effect of transverse reinforcement on confinement using Lap splices and Mechanical couplers: (a) without axial load, and (b) with axial load

Proper anchorage of longitudinal reinforcement allows the required composite action of steel and concrete, and ensures sufficient ductility. To prevent anchorage failure, hoops and cross-tie reinforcement should be provided with 135˚ hook-ends anchored around longitudinal reinforcement; the anchorage length provided should be sufficient enough to develop full tensile capacity of reinforcing bars. Within the potential plastic hinge region, anchorage of confining steel must be done by welding of stirrups. For well-controlled ductile anchorage behaviour, adequate confinement from transverse reinforcement must be ensured; else brittle, unpredictable splitting failures can occur [CEB-FIP, 2000; Priestley and Park, 1987].

In non-prismatic piers, flared part is usually supplemented with additional longitudinal reinforcement; this enhances flexural capacity of flare and results in premature damage in non-flared region. Also, sufficient anchorage should be provided to transverse reinforcement to ensure that shear strength is not compromised. Confinement through peripheral hoop reinforcement is more effective in circular piers than that in rectangular RC members without any cross-ties; also, rectangular hoops provide less restraint against longitudinal bar buckling and hence are not recommended when ductile response is required. Similarly, premature termination of longitudinal reinforcement and their inadequate lap splicing at the critical regions limits the ductility capacity of piers and can lead to anchorage failure [FIB, 2007].

2.1.2.2 Concrete

RC bridge piers are expected to undergo ductile actions under strong ground motions to dissipate large earthquake energy input without significant deterioration in strength. Ductility can be achieved by carefully detailing the transverse reinforcement in piers; this improves the confined properties of core concrete. In general, confinement of concrete is enhanced by increasing transverse reinforcement ratio, which leads to increase in concrete strain capacity, and thereby, ductility capacity.

Most existing confinement models available in literature are based on limited sets of tests on specimen with different details. Early confinement models [Chan, 1955; Roy and Sozen, 1964; Kent and Park, 1971] do not consider the effect of arrangement of transverse ties across the cross-section. Also, the use of these confinement models is limited to RC members with circular or square cross-sections; only a few of them are extended to RC members with rectangular cross-section. Later, in the 1980's, the effect was recognised of arrangement of transverse ties and positioning of longitudinal reinforcement, on confinement of concrete [Sheikh and Uzumeri, 1982, Scott *et al*, 1982; Mander *et al*, 1988; Saatcioglu and Razvi, 1992]. Among the available models, only few are applicable to circular, square, rectangular and wall-type RC piers [Mander *et al*, 1988; Saatcioglu and Razvi, 1992; Hoshikuma *et al*, 1997]. Confinement models were further refined to describe the envelope curve under cyclic loading conditions more accurately to match with the curve corresponding to monotonic loading conditions [Martinez-Rueda, 1997; Konstantinidis *et al*, 2004].

A number of models are available for unified stress-strain curve of confined concrete. One of these, the Mander Model [Mander *et al*, 1988] (Figure 2.6a) considers the effect of strain rate and cyclic loading, and has been used to predict the experimental behaviour of RC piers with various geometry and reinforcement configurations. Also, the model was developed based on results of tests on large-sized RC members, to investigate the ductility of bridge piers, under dynamic loading, and is applicable to most of the cross-section geometries. A significant contribution of this model is introduction of an energy balance approach to estimate longitudinal strain capacity; the energy stored in transverse hoops is equated to sum of energies stored in the concrete confined by it and the energy required to maintain the yield in the longitudinal steel in compression. This model is simple, provides ease in numerical computations, and is

based on studies done on bridge piers. In this model, confined stress-strain curve of concrete are obtained as

$$f_c = \frac{f_{cc}^{'} x\, r}{r - 1 + x^r}, \tag{2.1}$$

where

$$x = \frac{\varepsilon_c}{\varepsilon_{cc}}, \tag{2.2}$$

$$\varepsilon_{cc} = \varepsilon_{co}\left[1 + 5\left(\frac{f_{cc}^{'}}{f_{co}^{'}} - 1\right)\right], \tag{2.3}$$

$$r = \frac{E_c}{(E_c - E_{c,sec})}, \text{ and} \tag{2.4}$$

$$f_{cc}^{'} = f_{co}^{'}\left[-1.254 + 2.254\sqrt{1 + \frac{7.94 f_l^{'}}{f_{co}^{'}}} - 2\frac{f_l^{'}}{f_{co}^{'}}\right], \tag{2.5}$$

in which $f_{co}^{'}$ is the unconfined compressive strength of concrete (taken as 0.85 times the cylinder strength), $f_{cc}^{'}$ the confined compressive strength of concrete, $f_l^{'}$ the effective confining stress calculated considering arrangement bars, ε_c, ε_{co} and ε_{cc} the strains corresponding to $f_c^{'}$, $f_{co}^{'}$ and $f_{cc}^{'}$ respectively, and E_c and $E_{c,sec}$ the initial tangent modulus and secant modulus of concrete, respectively. The limiting strains for unconfined concrete is assumed as 0.004, and for confined concrete a conservative estimate based on energy balance is used given by:

$$\varepsilon_{c,max} = 0.004 + \frac{1.4\rho_s f_{yt}\varepsilon_{su}}{f_{cc}^{'}}, \tag{2.6}$$

where f_{yt} and ε_{su} are the yield strength and fracture strain of transverse steel. But, the ultimate concrete strain predicted by this model was found to be inferior to those resulting from other models [Konstantinidis *et al*, 2007]. Also, this model leads to numerical instability under large displacements, causing convergence problem during numerical computation [Martinez-Rueda, 1997]. Also, the ultimate strain estimate using Eq.(2.6) of sections subjected to bending or combined bending and axial compression is found to be conservative by almost 50% [Priestley et al, 1996].

The mechanism of failure of concrete is complex, particularly in the presence of combined effect of normal and shear stresses. Many mathematical models and theories

were developed to describe the failure surface of concrete subjected to simultaneous actions of normal and shear stresses. Two of the simplest models are the *Drucker-Prager Failure Criterion* and *Mohr-Coulomb Failure Criterion*, where shear stress is represented as a linear function of the normal stress. But, experimental results represent shear stress as a curvilinear function of normal stress. These models are commonly referred to as two parameter models, and are suited for hand calculations. Commonly, Drucker-Prager Criterion is used for modelling soils, and Mohr-Coulomb Criterion for modelling concrete. The Drucker-Prager Criterion was modified later, as *Bresler-Pister Failure Criterion* [Bresler and Pister, 1958], where a parabolic dependence is postulated of shear stress on normal stress, using three parameters and *octagonal stress*. The three parameters are established by curve fitting of available experimental test data from a number of RC members tested to failure under different combinations of compressive and shear stresses. As per this criterion (Figure 2.6b), shear stress is related to the normal stress in concrete by a quadratic parabola, given by:

$$\tau_{c,i} = 0.1 f_c \sqrt{0.62 + 7.86\left(\frac{f_c}{f_c^{'}}\right) - 8.46\left(\frac{f_c}{f_c^{'}}\right)^2}\ , \tag{2.7}$$

where τ_{ci} is the average shear stress and f_c the average normal stress of i^{th} fiber of concrete, and $f_c^{'}$ the compressive strength of concrete. Later, models developed using *four* parameters (*e.g.*, Willam-Warnke Criteria) and *five* parameters (*e.g.*, Ottosen Criteria, Reimann Criteria and Hsieh-Ting-Chen Criteria) provided results closer to experimental test data, but are complex and require more computational effort [Chen, 2007].

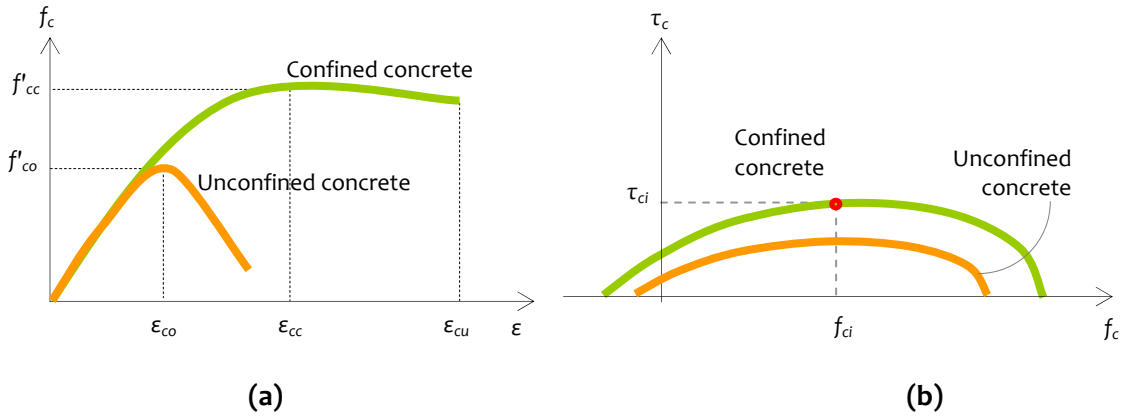

Figure 2.6: Constitutive relationships of concrete: (a) Mander's Model for confined and unconfined concrete [Mander *et al*, 1988], and (b) Bresler's Failure Envelope for normal and shear stresses for confined and unconfined concrete [Bresler and Pister, 1958]

2.1.3 Grades of Reinforcing Steel and Concrete

Ductile response of bridge piers relies on the capacity of reinforcing steel to sustain repeated cyclic loads at high levels of plastic strain without significant reduction in stress. Use of high strength steels (those with yield strength of 550 MPa and above) helps in reduction of material use, and thereby, improves constructability. But, use of high strength steel reduces energy dissipation capacity , and therefore ductility capacity, when compared to piers constructed with lower strength steel reinforcements [Tim, 2014]. Hence, an upper limit on grade of steel is specified by various standards to ensure minimum ductility.

Also, in seismic design, the actual yield strain of steel used should not be significantly higher than that used in design; this may result in excessive strength in plastic hinge regions, and members have to be made strong enough to avoid unanticipated brittle mode of failure Also, ratio of ultimate strength to yield strength of a minimum 1.2 is accepted as reasonable value (Figure 2.7). Low ratios result in shortening of plastic hinge length, and hence, an increase in reinforcement strain for a given ductility level, which increases the propensity of buckling. Considering these factors, grade of steel in the range 400–500 MPa is recommended by various standard codes [Priestley and Benzoni, 1996; FIB, 2007].

With increase in compressive strength of concrete, enhancement in *shear strength* of RC sections is more than their *flexural strength*, which changes failure mode from *shear* to *flexure* (Figure 2.8) [Sotoud and Aboutaha, 2014]. Also, experimental studies on RC structural walls with high strength concrete demonstrated enhancement in ductility. But, high strength leads to inelastic shear stiffness degradation and damage accumulation under reversed cyclic loading. Such effect is due to lower fracture toughness of high strength concrete (of compressive strength 103 MPa and more), which leads to rapid shear stiffness degradation and strength deterioration [Burgueno *et al*, 2014]. Hence, higher grades of concrete are not preferred in earthquake-resistant structures; compressive strengths of commonly used concretes are in the range 22.5–45 MPa for seismic applications [Paulay and Priestley, 1992; Priestley and Benzoni, 1996].

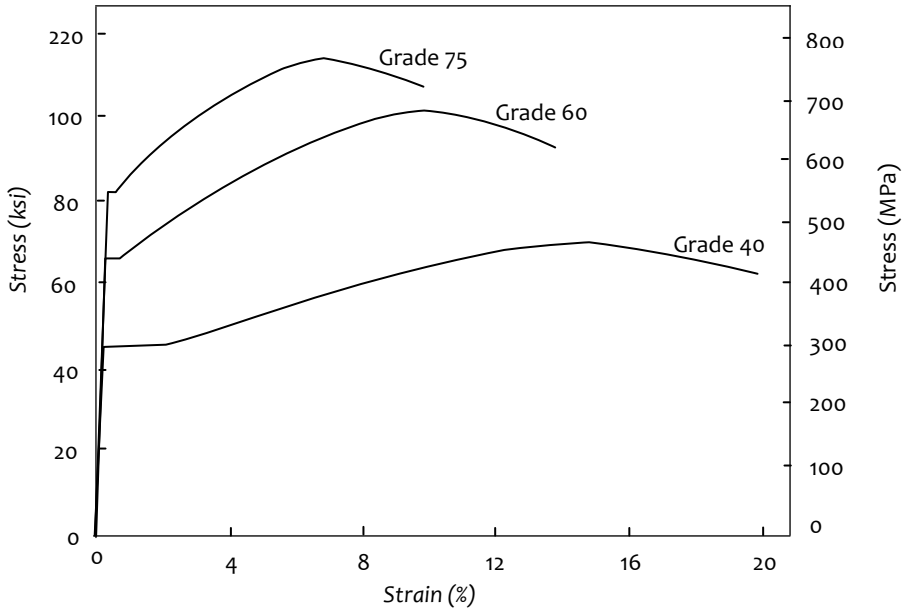

Figure 2.7: Monotonic tensile stress-strain characteristics of reinforcing steel: Effect of reinforcement grade [*reproduced from* Paulay and Priestley, 1992]

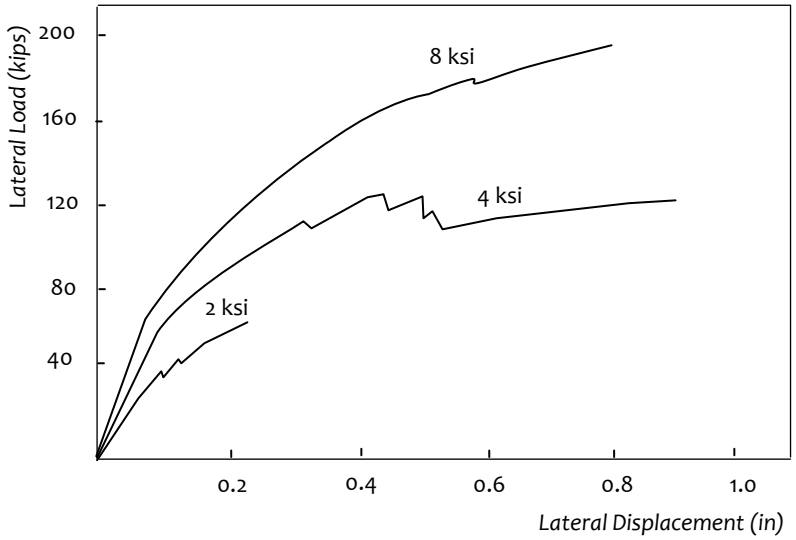

Figure 2.8: Effect of concrete grade on lateral load capacity of columns [*reproduced from* Sotoud and Aboutaha, 2014]

2.2 PERFORMANCE OF RC BRIDGES IN PAST EARTHQUAKES

Main factor governing damage and collapse of bridges in past earthquakes has been failure of piers. Inadequacy of single column RC piers against strong ground motion is evident in past earthquakes (*e.g.*, 1971 San Fernando, 1987 Whittier Narrows, 1989 Loma Prieta, 1994 Northridge, 1995 Kobe, 1999 Chi-Chi, and 2004 Mid-Niigata Prefecture Earthquakes). Severity of their damage ranges from minor cracks and lateral

deformations to complete collapse (Figure 2.9). Deficiencies in behaviour of bridges are associated with shortcomings in earthquake design and detailing, construction practices, deterioration in structures, and structural modifications. Some common causes of failure or damage in bridge piers during past earthquakes include: (i) inadequate flexural capacity, (ii) inadequate shear capacity, (iii) lack of transverse reinforcement, confinement and ductility, (iv) bond slip, lap splice and anchorage, and bond splitting, (v) abrupt change in cross-sectional properties, and (vi) large deformations. A discussion on behaviour of RC bridges during past earthquakes is presented in this section.

2.2.1 Flexure Failure

Piers designed to withstand earthquake loading were found to perform satisfactorily with adequate ductile behaviour. Failure of piers in the 2004 Mid-Niigata earthquake illustrates failures associated with inadequate flexural capacity. Improper reinforcement detailing and inadequate transverse reinforcement in the regions of inelasticity predominantly led to flexure failure at the base of piers of the Hanshin Expressway in the 1995 Kobe earthquake and 1999 Chi-Chi earthquake (Figure 2.10).

2.2.2 Shear Failure

Most failures observed in the past earthquakes were due to failure in shear. The 1987 Whittier Narrows, 1994 Northridge, 1995 Kobe and 1999 Chi-Chi earthquakes demonstrated inherent weakness of piers in their lateral strength. The magnitude of earthquake and its accompanying ground motion in Whittier Narrows earthquake was less severe than what is commonly believed to represent a threat to bridges, but bridges incurred extensive damages. This unexpected damageability led to an accelerated effort to understand how bridges perform in earthquakes and how to better design them to

Figure 2.9: Complete Collapse of Bridge, 1995 Kobe Earthquake [CALTRANS, 2006]

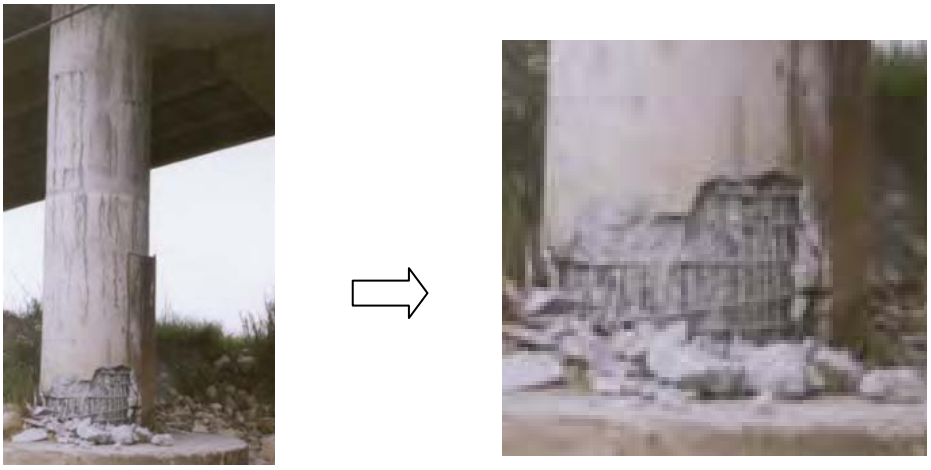

Figure 2.10: Flexure failure of Bridge Piers, 1999 Chi-Chi Earthquake [CALTRANS, 2006]

prevent future failures [Priestley and Park, 1987; Penzien *et al*, 2003]. The reasons for failures include inadequacy in transverse reinforcement (in terms of spacing, bar size and detailing), poor anchoring of ties leading to opening up of transverse ties, and insufficient lap splices, and buckling of longitudinal reinforcement followed by crushing of core concrete. Shear failure was observed within and outside plastic hinge zones, in these earthquakes. Inelasticity inside the plastic hinge zone led to more reduction in shear capacity than expected and wide spacing of stirrups in the less critical zones led to failure of piers in shear. Seismic strength and ductility of such piers to resist strong earthquake ground motion were inadequate.

Near field effects of ground motions also played an important role in these failures. Rigid body motion was noticed in several bridges with short piers due to high stiffness in the transverse direction in the 1999 Chi-Chi earthquake. Torsional movement in single column piers was evident from spiral cracks incurred (Figure 2.11). Inclined cracks at top of RC piers resulted in imbalance in superstructure, and thus in severe out-of-plane movement. Large vertical movements induced high stresses at the continuous supports, resulting in shear cracks [Hsu and Fu, 2004].

2.2.3 Combined Flexure–Shear Failure

A large number of piers experienced severe damage in combined flexure-shear failure mode during 1994 Northridge, 1995 Kobe, 1999 Chi-Chi and 2008 Wenchuan earthquakes [Mitchell *et al*, 1995; Hsu and Fu, 2004]. Main factors contributing to this failure mode were: discontinuing longitudinal bars just above the footing, creating a

weak cross-section in the high moment region of the column and inadequate confining reinforcement. Poor seismic behaviour of these piers was compounded due to lap splicing of confining reinforcements and large spacing between them. The outer layer of lap spliced hoops become ineffective in confining core concrete when the cover concrete is lost, thereby jeopardizing the capacity of the section to form a stable plastic hinge. Also, piers with large cross-sections (and hence low shear span to depth ratio and slender piers with low axial loads) mainly suffered this type of failure (Figure 2.12) [Sun *et al*, 2008].

(a) **(b)** **(c)**

Figure 2.11: Shear failures of bridge piers*:* (a) Shear failure in short column pier during 1999 Chi-Chi Earthquake, (b) Shear failure of wall pier during 1995 Kobe Earthquake owing to lack of transverse ties in the cross-section, and (c) Severe damage of non-prismatic column piers during 1994 Northridge Earthquake at the transition point in geometry owing to combined factors of shear, compression and axial actions [CALTRANS, 2006]

(a) **(b)**

Figure 2.12: Combined flexure –shear failures of bridge piers during 1995 Kobe Earthquake: (a) low shear span-to-depth ratio, and (b) low axial loads in slender piers [Sun *et al,* 2008]

2.2.4 Other Failures

The major reason for the two-level elevated Cypress Viaduct collapse in Oakland during 1989 Loma Prieta earthquake was inadequate lap splice length of longitudinal bars. Extensive cracking of joints due to improper shear reinforcement at joints regions was also evident [Tarakji, 1992; Penzien *et al*, 2003]. The collapse of upper deck at a section of the 2-level San Francisco-Oakland Bay Bridge was attributed to insufficient seating width, rendering the bridge out–of-service during 1989 Loma Prieta earthquake. Loss of bond between column reinforcing steel and footing due to inadequate development length resulted in pull-out failure in a bridge pier that collapsed completely during the 1971 San Fernando earthquake (Figure 2.13a) [James, 2001]. These inadequacies in reinforcement detailing led to premature *failure in flexure.*

Stocky piers with high axial loads in 1971 San Fernando earthquake, and piers located near fault zones in 1994 Northridge earthquake, were subjected to substantial vertical accelerations and suffered axial compression failure (Figure 2.13b). Complete collapse of piers occurred prior to diagonal shear cracking. Lack of redundancy is another crucial factor that resulted in failure and collapse of the support structure in single column bridge piers. At the same time, inherent redundancy in the frame system with multiple column bents, helped sustain severe damage without collapse, in spite of a non-ductile design and detail. This earthquake caused bridge designers to revise structural design and details to provide increased resistance to *forces* and *displacements* imposed by earthquakes. Prior to this, seismic design criteria for *bridges* in USA were based on lateral *force* requirements for *buildings* [James, 2001; Penzien *et al* 2003].

Failure due to pounding was another common cause for failure of bridge piers during earthquake shaking. Underestimation of deformation capacity causes damage to piers due to pounding with nearby structures; pounding was observed in the 1989 Loma Prieta and 1987 Whittier Narrows Earthquakes. Typical failure in regions of longitudinal rebar cut-off was exposed in the 2004 Mid-Niigata Prefecture earthquake (Figure 2.13c); these piers were located in near fault region, which induced vertical accelerations.

(a) (b) (c)

Figure 2.13: Additional types of failures in bridge piers: (a) Pull-out failures of bridge piers during 1971 San Fernando Earthquake, (b) Axial compression failure of bridge piers during 1994 Northridge Earthquake, and (c) Shear failure at rebar cut-off point during Mid-Niigata Prefecture Earthquake [CALTRANS, 2006]

2.2.5 Salient Observations

The devastating earthquakes during the past several decades resulted in severe damage to bridges, especially due to failure of bridge piers. Many valuable lessons were learned from the field studies conducted after these earthquakes, which helped in understanding performance of bridge piers during earthquakes. Most pier failures were brittle. Shear strength deterioration with increase in flexural demand in the plastic hinge regions and wider spacing of transverse reinforcement outside the plastic hinge zone, were main causes of shear failures. The main reasons for flexure failures include inadequate and improper detailing of transverse reinforcement (leading to ineffective confinement) and lapping of longitudinal reinforcement at critical sections (reducing the flexural capacity). Other factors like vertical acceleration mobilising high axial loads, inadequate anchorage of reinforcement, and location of bridges near fault zones, also led to brittle mode of failures in the past earthquakes.

2.3 PAST STUDIES ON RC BRIDGE PIERS

Following the 1971 San Fernando earthquake, there was an upsurge in research on seismic performance of concrete bridges – experimental and analytical studies to better understand their earthquake behaviour. Initially, experimental studies were carried out in New Zealand and Japan, and then in USA and Europe, to develop revised seismic design specifications. In line with experimental studies, analytical studies were

also carried out, to estimate ultimate strength of RC members subjected to combined axial force, bending moment and shear force actions, during seismic events. In spite of extensive and sustained research, consensus on a general theory to estimate shear strength of RC sections under combined seismic actions has not been arrived at. In the conventional approach, (a) flexural strength is estimated considering the interaction of *axial force* and *bending moment*, and (b) shear strength is estimated independent of other actions. Various methods were developed based on different mechanisms of shear transfer, based on failure modes observed in test specimens.

2.3.1 Experimental Studies

Reasonable understanding of earthquake behaviour of RC piers through experimental investigations is the first step towards reliable prediction of their earthquake behaviour. Although experimental research is limited on earthquake response of bridge piers, there is a substantial database of experimental investigations on RC elements subjected to cyclic loading [*e.g.*, Wight and Sozen, 1973; Atalay and Penzien, 1975; Gill, 1979; Nagasaka, 1982; Umehara and Jirsa, 1982; Zhou *et al*, 1985; Zahn *et al*, 1986; Soesianawati *et al*, 1986; Ang *et al*, 1989; Mander *et al*, 1988; Tanaka and Park, 1990; Priestley and Benzoni, 1996; Saatcioglu and Grira, 1999; Sezen, 2002; Ousalem *et al*, 2003 and 2004; Pan and Li, 2012]. In this section, experimental research studies on the response of RC members subjected to seismic loading are summarized. From each study, the parameters in focus are extracted; these include slenderness, longitudinal and transverse reinforcement ratio, axial load ratio, and type of loading.

2.3.1.1 Slenderness

Slenderness is expressed either in terms of (i) shear span-to-depth ratio (L/D for a cantilever specimen, where L is the length of the member and D its depth), (ii) bending moment M to shear force V ratio, or (iii) M/VD (Figure 2.14). Early studies include tests on three octagonal shaped RC members with increasing slenderness ranging from 1.75 to 3.25 under cyclic loading condition with axial load $0.06f_c'A_g$ [Davey, 1974]. The ratio M/V is varied by applying a fixed end moment to the top of the column, simulating piers of different lengths. The studies examined influence of slenderness, on mode of failure, flexural ductility and shear strength [Stone and Geraldine, 1989; Geraldine and Stone, 1990; Lehman and Moehle, 2000]. The significant observations made are:

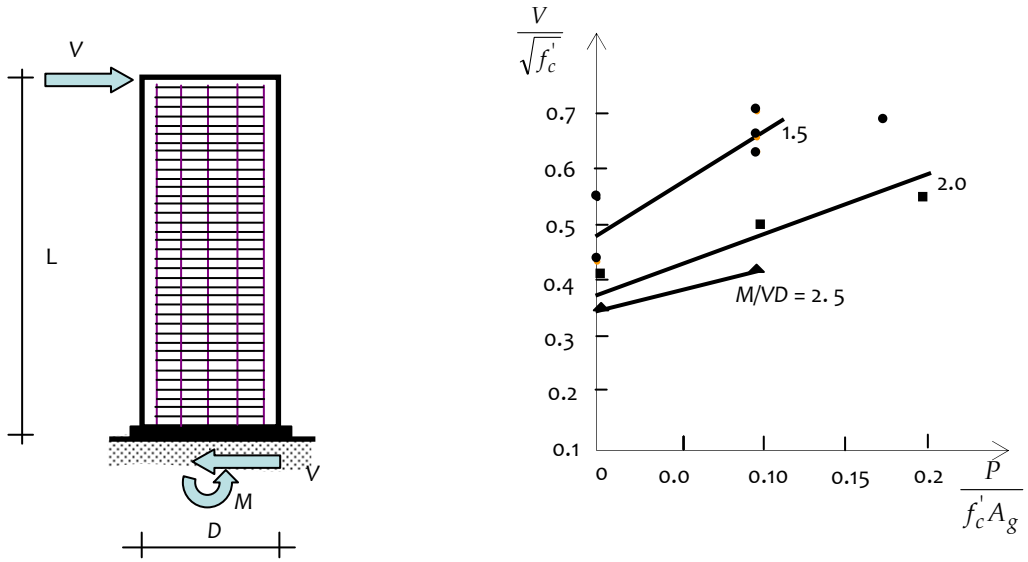

Figure 2.14: Effect of varying slenderness and axial load on shear capacity of RC members [*reproduced from* Ang *et al*, 1989]

(i) Column displacement ductility capacity increase with increase in *M/V*,

(ii) Shear demand increases with a reduction in the *M/V*, and

(iv) Shearing deformations of slender RC members are less than 5% of the total deformation.

Slender RC members, which are flexure dominated, exhibit failure modes similar to conventional beams under flexure. Reducing slenderness leads to intricate interaction in flexure and shear behaviour – local stresses in concrete and steel vary along the length of member and depth of cross-section. Clarity is lacking still on understanding of load carrying mechanisms and shear-flexure interaction under a given axial load [Davey, 1974; Ang *et al*, 1989; Wong *et al*, 1993].

2.3.1.2 *Size Effect*

Limited experimental studies were carried out to examine size effect on inelastic behaviour of RC members subjected to combined actions of axial force, bending moment and shear force. In one of these studies, a series of cyclic loading tests were conducted on full scale circular RC members of 1.5 m diameter and their scaled replica. The effect of size on failure mode, energy absorption property and ductility capacity was found to be less significant [Stone and Geraldine, 1989]. This observation was supported by findings made from testing of a full-scale column of 2.4 m square section and a 1:4 scale replica subjected to quasi-static cyclic lateral load till complete failure [Hoshikuma *et al*, 2001]. The size effect did not appear when reinforcement details, including bar diameter

and vertical hoop spacing, were scaled down precisely based on scale factor. But, this conclusion was not supported by tests done on 1:3 scale models of prototype cross-section 1.5 m x 1.5 m [Yeh *et al*, 2002]. The prototype had more ductility than the scale models. Possible sources for this discrepancy were reported as

(i) difference in yield strength of longitudinal reinforcement bars and

(ii) low cycle fatigue has more influence on small size reinforcement bars used in scaled models.

But, the scale criteria applied in the previous experiments were not completely satisfied in this model. This could be the reason for the strong *scale effect* observed in both of the previous tests [Carlo *et al*, 2007].

2.3.1.3 Reinforcement Ratio

Longitudinal and transverse reinforcement ratios affect strength and ductility of piers under seismic loading. Also, for a prismatic pier with constant axial load demand, varying the reinforcement ratios alters the response and failure mode. The influence of transverse and longitudinal reinforcement ratios is discussed in the following sub-sections.

(a) Transverse reinforcement

Transverse reinforcement ratio has significant effect on ductility of RC members under seismic loading. Core concrete dilates in the transverse direction, with increase in compressive stress on core concrete, arising from combined action of bending moment and axial load. Main role of transverse reinforcement is to prevent the dilation by restraining the concrete core laterally; also increased transverse reinforcement ratio reduces likelihood of buckling of longitudinal reinforcement. Transverse reinforcement is quantified by *(i)* its cross-sectional *area*, expressed in terms of ratio of *transverse steel area* to *concrete area*, and *(ii)* its *volume*, expressed in terms of ratio of *transverse steel volume* to *concrete volume*. *Area ratio* is used commonly in static design equations, to determine the web reinforcement required to control cracking of concrete due to shear; it relates area of steel to area of concrete at a given cross-section defined as,

$$\rho_a = \frac{A_h}{b s_v}, \tag{2.8}$$

where A_h is the cross-sectional area of transverse reinforcement, s the spacing of transverse reinforcement, and b the width of the specimen. *Volumetric ratio* is preferred

usually to describe the transverse reinforcement required for confinement, as it is directly related to the amount of confinement provided in the column. A change in volumetric ratio influences the maximum compressive stress and strain in the RC member. It is defined as,

$$\rho_v = \frac{2(b_c + d_c)A_h}{b_c d_c s_v}, \tag{2.9}$$

where b_c and d_c are the concrete core dimensions. In experimental studies, this ratio is found to range from 0.1% to 3.6%.

Several experiments were carried out by varying the amount of reinforcement ratio and their arrangement, to study the effect of transverse reinforcement ratios on the response of RC members, under monotonic and cyclic loading [Davey, 1974; Munro, 1976; Gill *et al*, 1979; Mander *et al*, 1988; Ang, 1981; Soesianawati *et al*, 1986; Zahn *et al*, 1986]. Another set of studies were carried out to understand the role of transverse reinforcement in enhancing ductile behaviour of RC bridge piers [*e.g*., Sheikh and Uzumeri, 1982; Mander *et al*, 1988; Razvi and Saatcioglu, 1994]. Increase in concrete compressive strength, decrease in the slope of falling branch of stress-strain curve of concrete, and increase in longitudinal strain at which hoop fractures, were observed with increase in the transverse reinforcement ratio.

Similar studies were performed to understand the effect of transverse reinforcement in possible improvement of ductile behaviour on short RC members with slenderness of 2 [Gill *et al*, 1979], and on slender RC members with slenderness of 4 [Ang, 1981; Soesianawati *et al*, 1986; Zahn *et al*, 1986]. Good ductile behaviour with little strength deterioration up to displacement ductility of 6, and considerable enhancement in flexural strength at high axial loads, were observed by providing sufficient amount of transverse reinforcement. In slender RC members, the extreme compression strain of core concrete reached values up to 2 times that reached in short RC members with similar amounts and arrangements of confining steel. Behaviour of specimens with more stringent transverse steel ratios substantially improved behaviour in shear critical RC members, with slenderness in the range 1.75–3.25 [Davey, 1974]. Also, transverse reinforcement was found to influence the failure mode; by reducing their spacing, it changed from *shear* to *flexure* mode, as evident from the angle of cracks sustained by the specimen (Figure 2.15; δ is the transverse displacement of the RC member) [Watson and Park, 1989; and Machida and Abdelkereem, 2000].

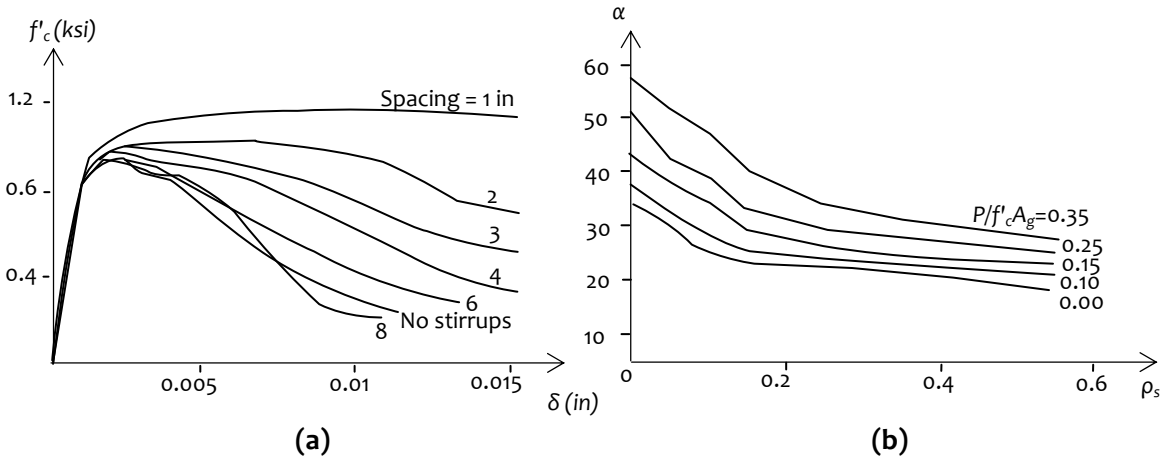

Figure 2.15: Effect of spacing of transverse reinforcement on (a) compressive strength due to confinement [*reproduced from* Tanaka and Park, 1990], and (b) maximum angle of crack α [*reproduced from* Machida and Abdelkareem, 2000], of RC members

(b) Longitudinal Reinforcement

Longitudinal reinforcement of the RC member is quantified as ratio of *total area of longitudinal steel* at a cross-section to *gross cross-sectional area* of that section. On an average, longitudinal reinforcement ratio provided in pier sections was in the range 1%-3% [Dawn, 2000]. Doubly-reinforced RC members demonstrate different behaviours under monotonic and cyclic loading conditions. Under monotonic loading, the ultimate curvature and ultimate curvature ductility decrease with increase in longitudinal tensile reinforcement [Lehman and Moehle, 2000; *original source* Iwasaki, 1985; Priestley and Benzoni, 1996]. On the other hand, under cyclic loading, the ultimate curvature and ultimate curvature ductility increase with increase in longitudinal tensile reinforcement. This requires that both positive and negative longitudinal reinforcements are about the same; when this is not maintained, the results obtained are on the contrary [Tim, 2014].

2.3.1.4 Materials

The effect of yield strength of reinforcement on response of RC members under seismic loading conditions were studied in tests on square and octagonal specimens of cross-section 400 mm and aspect ratio of 4. Specimens were subjected to constant axial load and cyclically varying lateral load applied at mid-height [Zahn *et al*, 1986]. The yield strength of transverse reinforcing steel considered was *380* MPa. Performances of these specimens were compared with those of another set of similar specimens with Grade 275 steel [Ang, 1981]. No significant difference was observed in stiffness, strength and deformation characteristics (Figure 2.16), apart from early fracture of hoops in the specimen with lesser grade of steel.

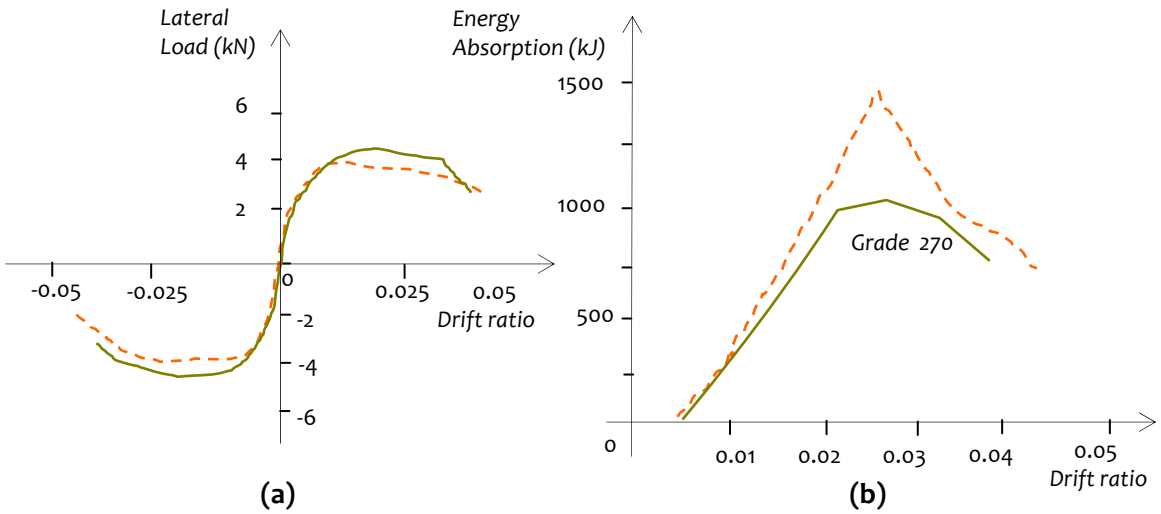

Figure 2.16: Effect of reinforcement grade on response of RC members: (a) Contour of hysteretic loop, and (b) comparison of energy absorption [Zahn *et al*, 1986]

2.3.1.5 Type of Loading

Variation in response, due to static and dynamic loading, was compared in a study conducted on two octagonal specimens. One unit with 1:2 scale subjected to static loading and another identical with 1:6 scale were tested on shaking table (Figure 2.17) [Munro, 1976]. Dynamic load was applied as slow cyclic load reversals of increasing displacement amplitude. The moment-displacements curves of 1:6 scale model tested dynamically and 1:3 scale model tested statically were in good agreement from the point of view of ductility capacity, providing assurance in continuing experimental research on ductility using statically tested models. Shear failure mechanism of bridges collapsed in 1995 Kobe earthquake was investigated by conducting tests on four 1:7 scale model piers, with similar properties, using different loading cases [Kawashima *et al*, 2007]. Loading cases include: *(i)* pushover loading, *(ii)* unidirectional cyclic loading, and *(iii)* bidirectional cyclic loading. All specimens were loaded under a constant compressive stress of *1.75 MPa*. One specimen was loaded to failure under displacement-controlled pushover loading with loading speed of *1 mm/sec* until 2.4% drift. In the case of unidirectional cyclic loading, displacement was increased step-wise from 0.5% drift to failure with increments of 0.5% drift. In the case of bidirectional cyclic loading, a circular orbit was used, with loading displacement similar to unidirectional cyclic loading. The failure mode of the specimen subjected to unidirectional cyclic loading resembled closely the flexure-shear failure in the piers during 1995 Kobe earthquake. Also, under bidirectional loading, the flexural cracks occurred at wider spacing, and core concrete

sustained more damage than the specimen subjected to unidirectional loading. Hence, the effect of bidirectional loading cannot be ignored.

Similar observations were reported by another study, where four types of full-scale rectangular and square RC members were tested under unidirectional and bidirectional loading (Figure 2.18) [Rodrigues *et al*, 2013]. Stiffness degradation and strength deterioration were more significant under bidirectional loading than under unidirectional loading, for ductility demands larger than three. Also, ultimate ductility of RC members subjected to bidirectional loading were significantly lower than of those subjected to unidirectional loading.

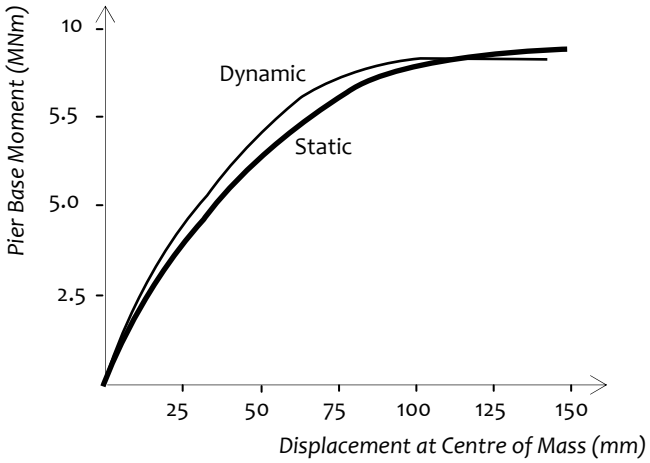

Figure 2.17: Comparison of static and dynamic response (moment – displacement) curves [*reproduced from* Munro, 1976]

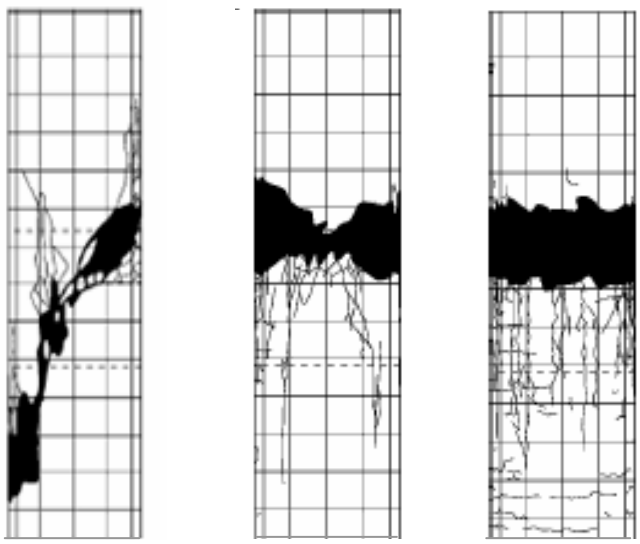

(a) **(b)** **(c)**

Figure 2.18: Influence of loading type: (a) unidirectional pushover loading, (b) unidirectional cyclic loading, and (c) bidirectional cyclic loading [Rodrigues *et al*, 2013]

2.3.1.6 Influence of Axial Load

Under strong earthquake ground motion, piers are subjected to variable axial load conditions. Both strength and deformation capacities of piers are dependent on the magnitude and direction of axial load. In particular, axial compressive load is important in mitigating premature failure of piers due to sliding shear [Penelis and Kappos, 1997]. Several experiments were conducted to study ductile behaviour of RC members with varying axial load; axial load ratio 0.0 – $0.7f_c'A_g$ was used in the experiments. But, axial load ratio of $0.2f_c'A_g$ or less was used in slender bridge piers.

Enhancement of strength with increase in axial load was investigated in RC members by testing four full-size rectangular RC members with different transverse reinforcement ratios and subjected to different level of axial loads ($0.1f_c'A_g$–$0.6f_c'A_g$) under simulated earthquake loadings [Gill *et al*, 1979]. The specimens had square cross-section (side 550mm; length 1.2m). The tests were conducted using a double-ended specimen with a central stub. All specimens behaved in ductile manner showing little strength deterioration up to displacement ductility of 6, with maximum extreme fibre concrete compression strain of about 0.02. Also, considerable enhancement of flexural strength was observed compared to that computed as per the then code provisions [ACI 318-77, 1977], particularly for members carrying high axial loads. Similar observations were made from another set of experimental tests carried out to investigate the flexural strength and ductility capacity with varying axial load, on RC members with same slenderness (of 2.2) and compared with ideal flexural strength calculated as per code provisions [ACI 318-83, 1983; Priestley and Park, 1987]. In Figure 2.19, M_{max} is the maximum experimental bending moment capacity and M_I the moment estimated based on code provisions. The flexural strength enhancement depends strongly on the axial load ratio. Also, with very high axial loads, failure modes changed from *ductile flexure* behaviour to *brittle shear* behaviour. In another set of experiments, 1:6 RC scaled models were tested, of slenderness 3 and axial load ratios $0.1f_c'A_g$ and $0.2f_c'A_g$ [Geraldine and Stone, 1990]; the specimens had circular cross-section of 1.5m diameter and height of 4.5m. Ultimate moment and displacement ductility were larger in specimens with larger axial load; also, specimen with larger axial load ratio had ~8.8% higher energy absorption capacity than the specimen with smaller axial load ratio. Also, increase in axial load: *(i)* reduced ultimate lateral displacement capacity, and *(ii)* increased stiffness degradation and strength deterioration.

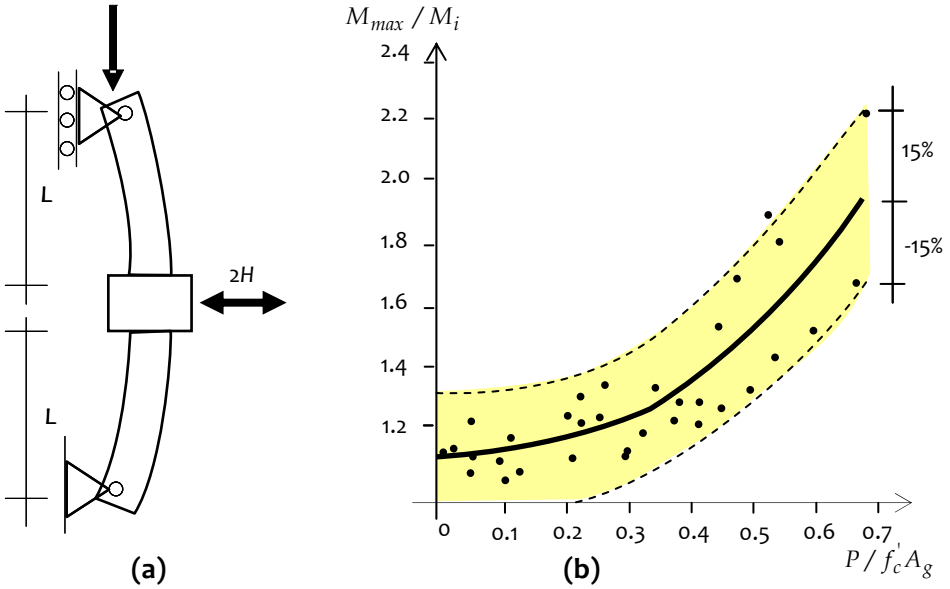

Figure 2.19: Influence of axial load: (a) schematic of double ended specimen, and (b) moment enhancement ratio [*reproduced from* Priestley, 1987]

Response of RC members subjected to slowly applied reversed cyclic loading were examined in another study conducted on full-scale specimen (350 mm square cross-section; 900 mm long; six 25 mm Grade 415 steel deformed bars as longitudinal reinforcement, and Grade 475 steel bars as transverse reinforcement) with and without axial load [Saatcioglu and Ozcebe, 1989]. Out of 14 specimens, two specimens were tested without axial load, another two under variable axial load, and the rest 10 under constant axial load of $0.11 f_c' A_g$. Constant axial compression accelerated stiffness degradation and strength deterioration. Variable compressive axial load increased flexural yield strength, followed by rapid strength deterioration, but variable *tensile* axial load was found to reduce flexural yield strength, but with delayed strength deterioration. Irrespective of constant or variable compressive axial load, member displacement ductility reduced.

In another study, 12 cantilever specimens were subjected to cyclic loading (Figure 2.19a) of square cross-section (305 mm side) with L/D = 6.0. Axial loads equal to approximately 25%, 50% and 75% of the balanced axial load of the cross-section was applied to the specimens [Atalay and Penzien, 1975]. Increasing the applied axial load from zero to axial load at balanced failure resulted in increase in deformations at yield. Stiffness, strength and deformation characteristics were found to deteriorate with

increase in axial load above the balanced axial load. Influence of axial load on shear strength and deformation of circular members, under different levels of axial load, was investigated on tests carried out on 16 circular RC specimens with aspect ratio 2 and various axial load ratios [Wong *et al*, 1993]. One specimen was subjected to uniaxial cyclic loading and another to random cyclic loading. Remaining 14 specimens were subjected to biaxial loading conditions. All members were reinforced with 20 longitudinal bars of 16mm diameter. Amount of spiral reinforcement was varied from 0.39% to 2.46%, and axial load ratios from zero to $0.19f_c'A_g$, and to $0.39f_c'A_g$. Specimens under biaxial loading sustained severe stiffness degradation and strength deterioration leading to large energy dissipation, compared to those under uniaxial loading .

2.3.2 Analytical Studies

Predicting the response of RC bridge piers analytically is challenging, owing to nonlinear behaviour, and interaction of stresses developed due to combined loading under earthquake ground motion. The nonlinear response of RC is caused by initial cracking of concrete, followed by yielding of reinforcement and crushing of concrete in compression. Under earthquake shaking, large shear and flexural forces are generated in the pier in addition to axial compression; this results in coupling of nonlinearities due to these forces. To capture realistic behaviour of bridge piers under earthquake shaking, analytical methods are essential.

Many analytical methods were developed to predict the response of RC piers subjected to combined actions of axial force, shear force, and bending moment. Prediction of *flexural behaviour* based on *sectional approach* has been accepted universally for more than a century now, where simple Bernoulli's Hypothesis forms the basis; simple experiments (*e.g.,* with two point loading) verified the theory. Traditionally, the same experiments with two point loading were used for shear tests also. While the region between the two loads in the two point loading test provides a constant flexure region with zero shear, the shear spans are subjected to constant shear and linearly varying bending moment; the behaviour changes from section to section. Thus, if a relationship is sought between the magnitude of shear force and the strain in transverse reinforcement, the strains are different for every transverse bar and also differ along the height of each bar. This makes it difficult to use results of such test to develop a general theory for *pure shear* behaviour.

Hence, in shear, there is no agreed basis for a rational theory yet, and experiments are difficult to be conducted in RC members subjected to pure shear. Therefore, in contrast to the small variation in flexural strengths estimated by the current national and international codes, shear strength estimated by the same codes vary by a factor more than 2. Modelling approaches developed so far for estimating shear strength of RC members can be broadly categorized as: (i) Discrete Models, and (ii) Finite Element Models.

2.3.2.1 Discrete Models

These models provide an approximate method, where approximate theoretical expressions are arrived at from first principles for predicting the response of members. The main advantage of these models is the efficiency in computation. This may not give good results when detailed behaviour at plastic hinge locations needs to be investigated, as local effects cannot be monitored and strength deterioration due to cyclic nonlinear loading cannot be addressed.

(a) 45° Truss Model

Significant effort has been made during the last century to develop *sectional models* and *semi-empirical theories* based on available experimental data to evaluate response of RC members under the action of *combined stresses*, including *shear*. During the early 20th century, truss models (Figure 2.20) were the widely adopted analytical tools for analysis and design of flexural members [Collins and Mitchell, 1991; *original source* Ritter, 1899; and Moersch, 1902]. These truss models are based on the concept that after cracking of concrete, the diagonal tensile stresses (arising from applied shear stresses) can be idealized as a parallel chord truss with diagonal compression struts of concrete inclined at 45˚ with respect to longitudinal axis. Even though this model overestimates strength by 30-50% over the test results, it is still the basis of some refined

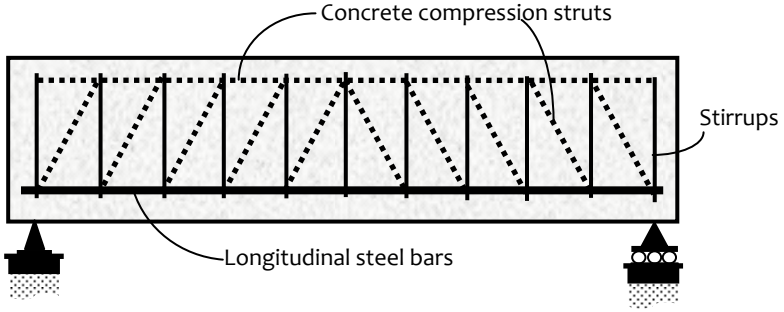

Figure 2.20: Ritter's Truss Model [*adapted from*: Collins and Mitchell, 1991]

new models [Tegos and Penelis, 1988; Moretti and Tassios, 2006; Park and Eom, 2007; Tureyen and Frosch, 2003; Park *et al*, 2006 and 2012; Mari *et al*, 2014; Cladera *et al*, 2015].

(b) Variable Angle Truss Model

Further research on truss models was mobilised by generalising the angle of inclination of concrete struts and incorporating the effect of transverse reinforcement [Kupfer, 1964; and Lampert and Thurlimann, 1971]. Three equilibrium equations were derived with varying strut angle, which explains the reason for yielding of both transverse and longitudinal reinforcements at failure. This is known as *Variable Angle Truss Model* (Figure 2.21). Since plasticity is assumed at failure and only equilibrium equations were satisfied, it is known as *Equilibrium Plasticity Truss Model*. Strut angles were predicted using minimum energy principles [Recupero *et al*, 2003]. Models developed based on the theory of plasticity allow selecting the strut angle depending on the amount of transverse and longitudinal reinforcements. Since concrete shear failure is brittle, some arbitrary limits are placed on strut angles by different models, in the range 25^{o}-65^{o}. The main limitation of this model is that, it does not consider the contribution of concrete; also, shear carrying mechanism of concrete is neglected. This makes it a conservative method, particularly when amount of transverse reinforcement is low.

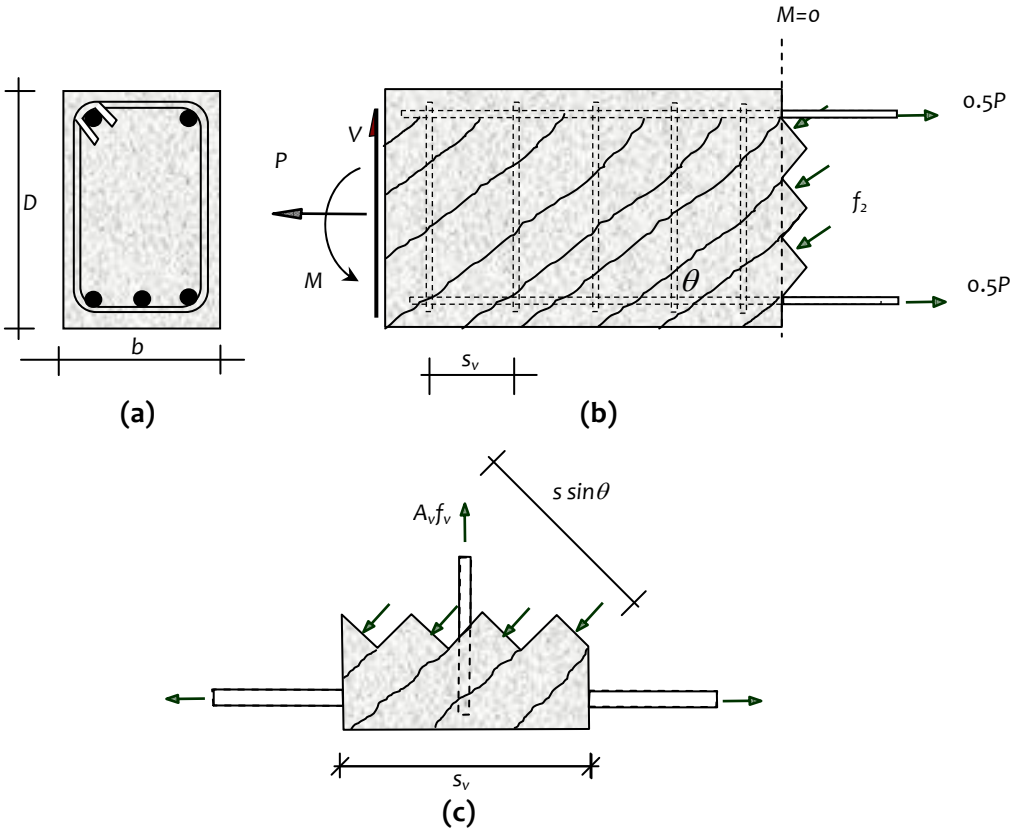

Figure 2.21: Equilibrium Conditions for Truss Model: (a) cross-section, (b) diagonal stresses and longitudinal equilibrium, and (c) forces in transverse reinforcement [a*dapted from*: Collins and Mitchell, 1991]

(c) Concrete Tooth Model

Alongside the development of truss models, a more realistic approach was proposed, the *Concrete Tooth Models*, which brought in the idea of shear transfer mechanism in concrete. The plain concrete (without transverse reinforcement) between two adjacent flexural cracks is considered analogous to the tooth in a comb (Figure 2.22). These teeth were assumed to be free cantilevers fixed in the compression zone and loaded by horizontal shear arising from bond stress on reinforcement. Although the model was not successful in covering the entire shear mechanism, it initiated more rational approaches. Additional research done on these models revealed the significance of the forces transferred across cracks, through crack friction. Later, this was quantified based on the test results on RC flexural members and a general expression for *ultimate shear force* was proposed by carrying out nonlinear calculations [Birgisson, 2011].

These plasticity models were unable to explain *shear resistance mechanism* of concrete; also they provided only an upper bound solution and that too for members with low reinforcement ratios. This theory was extended further to the non-yielding domains, where interface shear transfer was accounted for [Ramirez and Breen, 1991]. A combination of variable angle truss and concrete contribution is proposed, known as *Modified Truss Model Approach*, where an additional concrete contribution term is included. As per this approach for beams, concrete contribution diminishes with the level of shear stress. Vertical axis of Figure 2.23 represents concrete contribution in terms of nominal shear stress, and horizontal axis represents shear stress level produced by applied loading. Essentially, this model is applicable for regions with minimum or no transverse reinforcement.

(d) Strut and Tie Models

The section analysis of cracked concrete is applicable for regions where *Bernoulli's Hypothesis* is valid. Behaviour of regions, where this *Bernoulli's Hypothesis* is invalid, commonly known as the *Disturbed Regions* or *D regions*, was not well understood until the development of *Strut and Tie Models* [Schlaich *et al*, 1987]. *Strut and Tie Models* are based on *Truss Analogy* [Collins and Mitchell, 1991; *original source* Ritter, 1899 and Morsch, 1902] with the key elements resisting the flow of forces as per Truss Analogy (Figure 2.24). Flow of compression forces is idealized with compression chords (called *struts*) and of tensile force with tension chords (called *ties*). Idealization of flow of forces with *struts* and *ties* as per *Truss Models* for various shear span to depth ratios is depicted

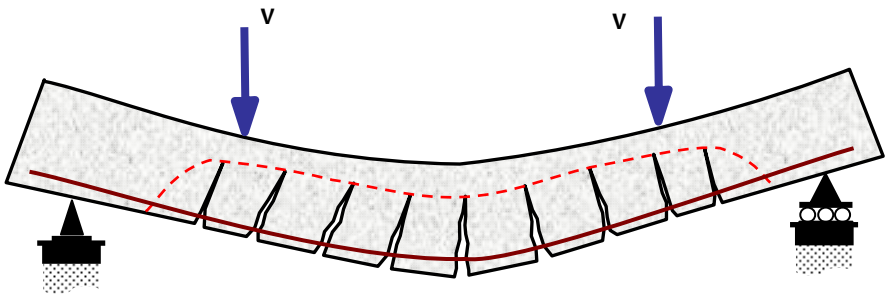

Figure 2.22: Kani's concrete teeth and backbone of the concrete comb [*source:* Birgisson, 2011]

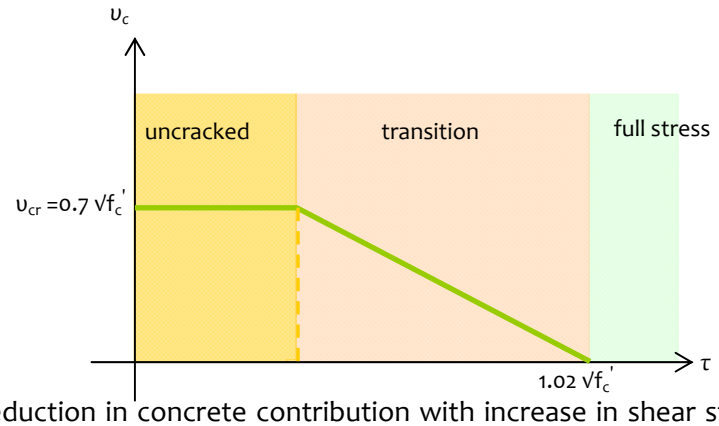

Figure 2.23: Reduction in concrete contribution with increase in shear stress level [Ramirez and Breen, 1991]

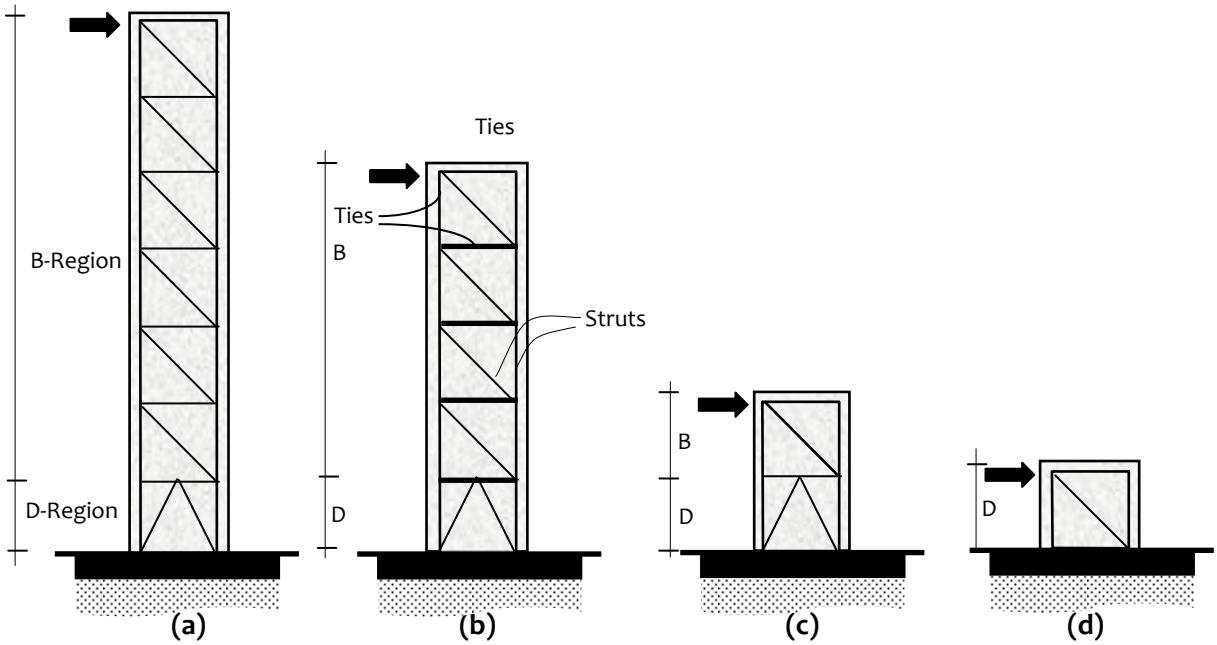

Figure 2.24: Truss models showing idealization of flow of forces for varying span-to-depth ratios; span-to-depth ratio: (a) 6, (b) 4, (c) 1.5, and (d) 1

in Figure 2.24. Regions, where the force flow is uniform, are referred to as *Beam Regions* or *B regions*. For slender piers, lateral load and support reactions cause disturbance in the internal flow of forces at the supports. The *D regions* are smaller in size, when compared to *B regions*, if the members have high span-to-depth ratios; the *D Regions* may occupy the entire structure, if the members have small span-to-depth ratios. Hence, behaviour of such *RC bridge piers*, can be predicted realistically using *Beam Theory* as their failure is governed by flexure [Yap, 2012], provided shear and other undesirable modes of failure are precluded. As the aspect ratio reduces, major portion of the pier becomes *D Region*, where the assumption of linear strain variation across the cross-section becomes inappropriate; in these regions, failure is governed by shear.

Strut and Tie Models are useful particularly in the design of RC piers, characterised by a complex flow of internal stresses. Selecting a *Strut and Tie Model* is an iterative process starting with the selection of centreline truss model. Member forces are evaluated, followed by dimensioning of the elements (*struts and ties*) based on the internal member forces and strengths of steel and concrete elements. Then, the nodal zones connecting truss members are analysed, and the dimensions of struts and ties checked with geometrical constraints of structure, for compatibility. The Truss Model, its geometry, or both, needs to be modified, if compatibility condition is not satisfied, and the procedure repeated, until the solution is acceptable. The initial *Strut and Tie Models* were formulated based on the failure crack patterns observed during experiments, on the pattern of loading and support conditions, and on the strains in the materials, documented in experiments. Basically, a *Strut and Tie Model* representing a structure should satisfy: *(i)* force equilibrium between internal stress resultants and applied loads, *(ii)* failure criteria of steel and concrete, where factored internal design stresses must be within the limiting design strengths of these elements, and *(iii)* strain compatibility, where the elements must be able to withstand sufficient rotation before the assumed stresses develop in the *struts* and *ties* [Muttoni and Ruiz, 2008]. The above three conditions differentiate *Strut and Tie Models* from *Classical Truss Analogy*, in which only force equilibrium is considered and the truss system may not be stable.

(e) Truss Arch Models

The truss models discussed in the previous section, to estimate shear strength of a pier, fail to consider the arch action developed in the member, and therefore, is more conservative. The *Truss Arch Model* is composed of a truss consisting of transverse and longitudinal reinforcement bars, inclined concrete members between the inclined cracks,

and an arch consisting of concrete bearing normal stresses [Xie *et al*, 2011]. Arch action in RC members was recognised during 1960's, where a *truss model* together with an additional compression chord was used to describe behaviour of flexural members. Shear was assumed to be carried by *truss mechanism* and *arch mechanism* (Figure 2.25).

Beam action alone is found to give conservative results, particularly in shear critical members. *Arch action* becomes significant when shear span-to-depth ratio is small. The contribution of concrete and transverse reinforcement bars to shear, in the *truss model,* is described by established truss models, and in the *arch model* by inclined compression chords (where the chord width is estimated using semi-empirical approaches). Unlike truss models, in the *Truss Arch Model*, the concrete contribution towards shear considers parameters, such as aggregate interlock on cracked surface.

2.3.2.2 *Finite Element Models*

A large number of studies have been attempted using *Finite Element Method (FEM)*; *beam elements* were used for nonlinear analysis of bridge piers. The early work using FEM was the analysis of RC beams with a predefined crack pattern [Ngo and Scordelis, 1967]. The model included effect of cracking and bond simulation capability that aids in computing stresses near the crack. This was called the *Discrete Crack Model*. Since then many models were developed taking into account cracking of concrete and yielding of reinforcement. Some salient models that gained wide acceptance and were received with great interest are explained in the sections below.

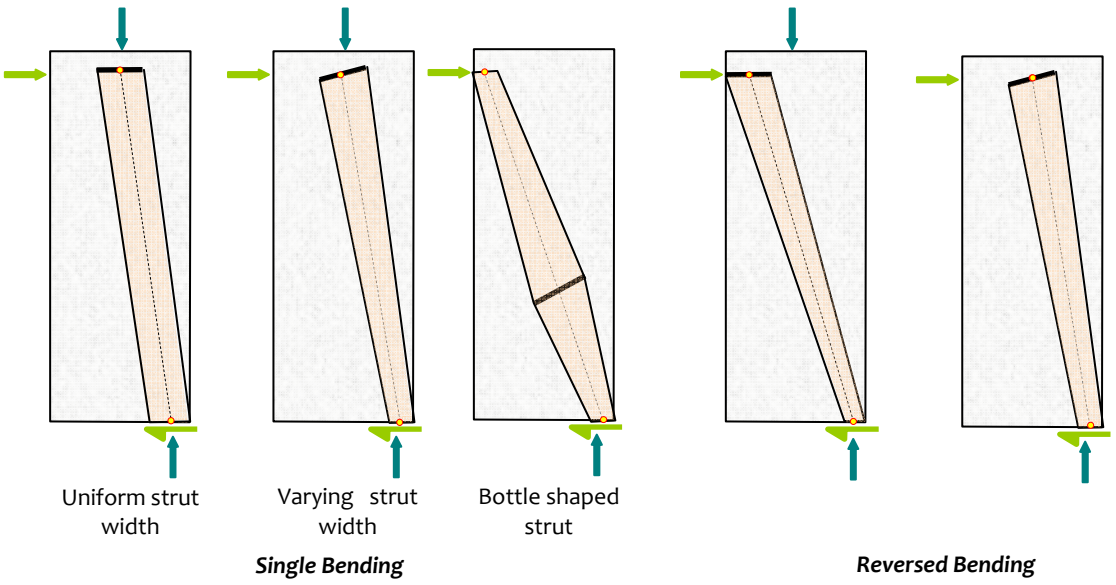

Figure 2.25: Arch models with various strut geometries [Leondardt, 1965; Priestley *et al*, 1994; Pan and Li, 2012; Rossi, 2013]

(a) Compression Field Theory

Compression Field Theory considers effects of bending moment, shear force and axial force for predicting the response of RC elements subjected to combined stresses, thus satisfying both *equilibrium* and *deformation* compatibility conditions. Compatibility conditions were incorporated in predicting the strut angles [Vecchio and Collins, 1986]; strut angles were assumed to coincide with the principal compression strain directions. After cracking of concrete, the shear force is assumed to be resisted by a field of diagonal compression, in line with the concept of *Tension Field Theory* applied for the post-buckling shear resistance problems of plate girders (Figure 2.26) [Pillai and Menon, 2009; *original source* Wagner, 1929]. Hence, this theory is known as *Compression Field Theory*. This model is capable of estimating biaxial stress and strain conditions in a RC element subjected to combined stresses. But, tensile stresses in the cracked concrete were neglected, which led to overestimation of deformation.

(b) Modified Compression Field Theory

After verifying the Compression Field Theory with tests on RC members subjected to combined shear and axial stresses, it was further modified; the modified theory was called *Modified Compression Field Theory (MCFT)* [Vecchio and Collins, 1988]. Based on the experimental data, stress-strain relation of RC was considered for *compression* and *tension* concrete, including that for tensile concrete also (Figure 2.27). The accuracy of MCFT depends on *actual collapse mechanism* of RC member and *width of crack*. More shear reinforcement reduced the width of the crack and thereby enhancing the contribution of concrete, unlike in truss models, where concrete contribution was considered equal to that of member without shear reinforcement. This model required an iterative procedure to determine stress and strain distributions. Beam cross-section was discretized into thin fibres (Figure 2.28). Plane sections were assumed to remain plane even after deformation, and shear stresses were computed as the finite difference of normal stress on either side of the finite length layer (Figure 2.29); in the figure, C_{k1} and C_{k2} denote the compressive force acting on the face of concrete layer k at sections 1 and 2 separated by a distance S (which is usually taken as D/6), with D being the overall depth of the member cross-section. F_k and F_{k-1} are horizontal shear forces acting on k^{th} and $(k-1)^{th}$ layer of concrete, respectively, and m denotes the number of discretized concrete layers along the length.

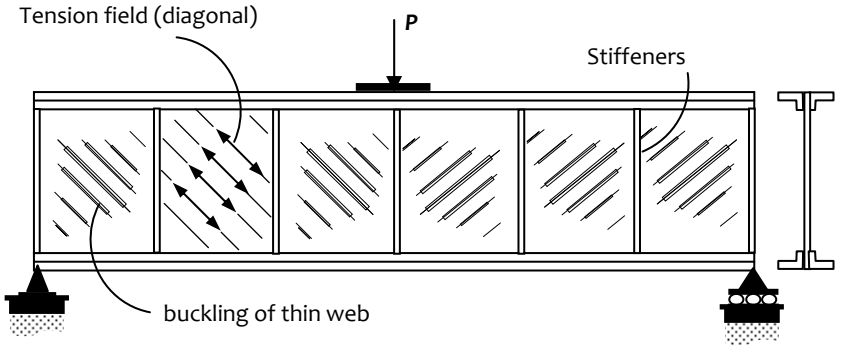

Figure 2.26: Tension field in thin-webbed metal girder under shear [Pillai and Menon, 2009]

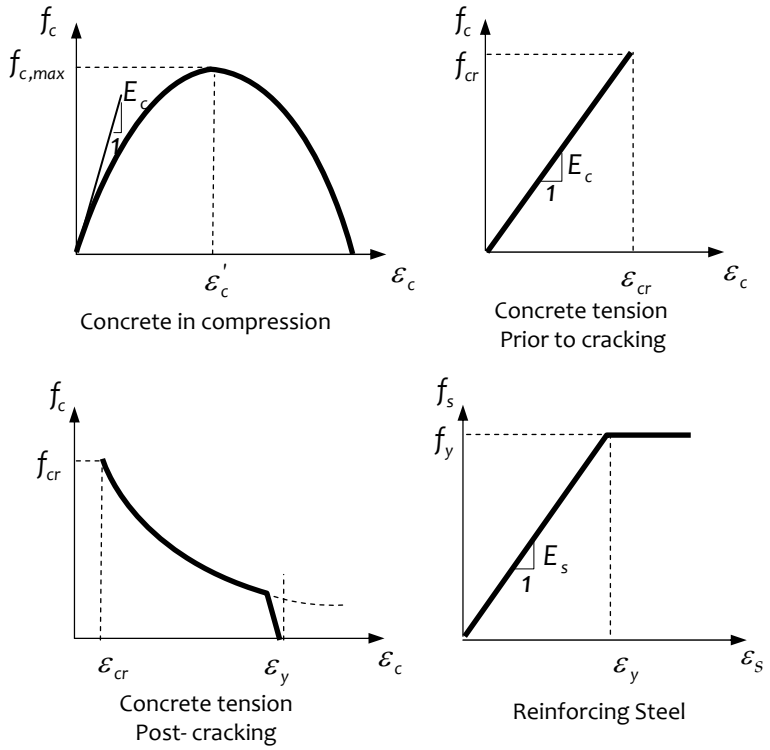

Figure 2.27: Constitutive relations for concrete and reinforcing steel [*reproduced from* Vecchio and Collins, 1988]

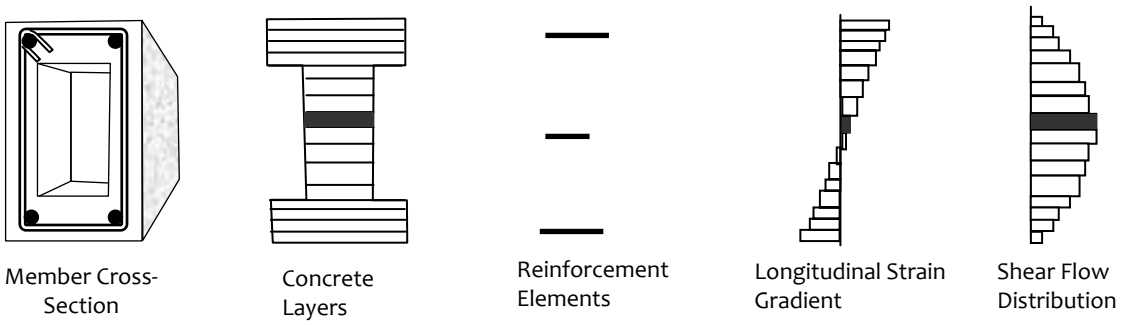

Figure 2.28: Beam section discretization*:* Estimates of longitudinal strain gradient and shear flow distribution across cross-section [*reproduced from* Vecchio and Collins, 1988]

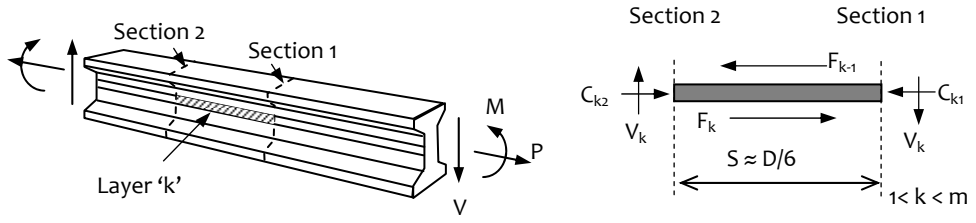

(a) **(b)**

Figure 2.29: Member discretization: (a) scheme, and (b) free body diagram for concrete layer *k* [*reproduced from* Vecchio and Collins, 1988]

Average strain used in calculations refers to strain measured over base lengths at least equal to the crack spacing; average stresses are calculated considering effects both at and between the cracks, and are distinct from the stresses calculated at cracks. Analytical procedure, which is summarized in Figure 2.30, requires longitudinal strain distribution and shear stress distribution across the section. For a given strain distribution, the bending moment, axial force and shear force capacities of the section were determined, and the *shear* stress-strain curve obtained. Though this model helped in predicting the capacity with good accuracy, and shear-flexure interaction was captured, it requires huge computational effort as both diagonal compression strain and strut angle need to be estimated iteratively for each layer, and shear strain profile obtained through equilibrium iteration of two adjacent sections. But, it provided a rational method for analysis and design of members with unusual complex geometry or loading [Vecchio and Collins, 1988].

To reduce the complexity involved in the calculations, approximate solution procedures were proposed based on constant shear flow or a parabolic shear strain [Collins *et al*, 1988]. Parabolic shear strain assumption overestimated the shear stresses in the compression region, giving un-conservative results, whereas constant shear flow assumption overestimated shear stresses in the tensile region, providing conservative predictions [Ceresa *et al*, 2007] .

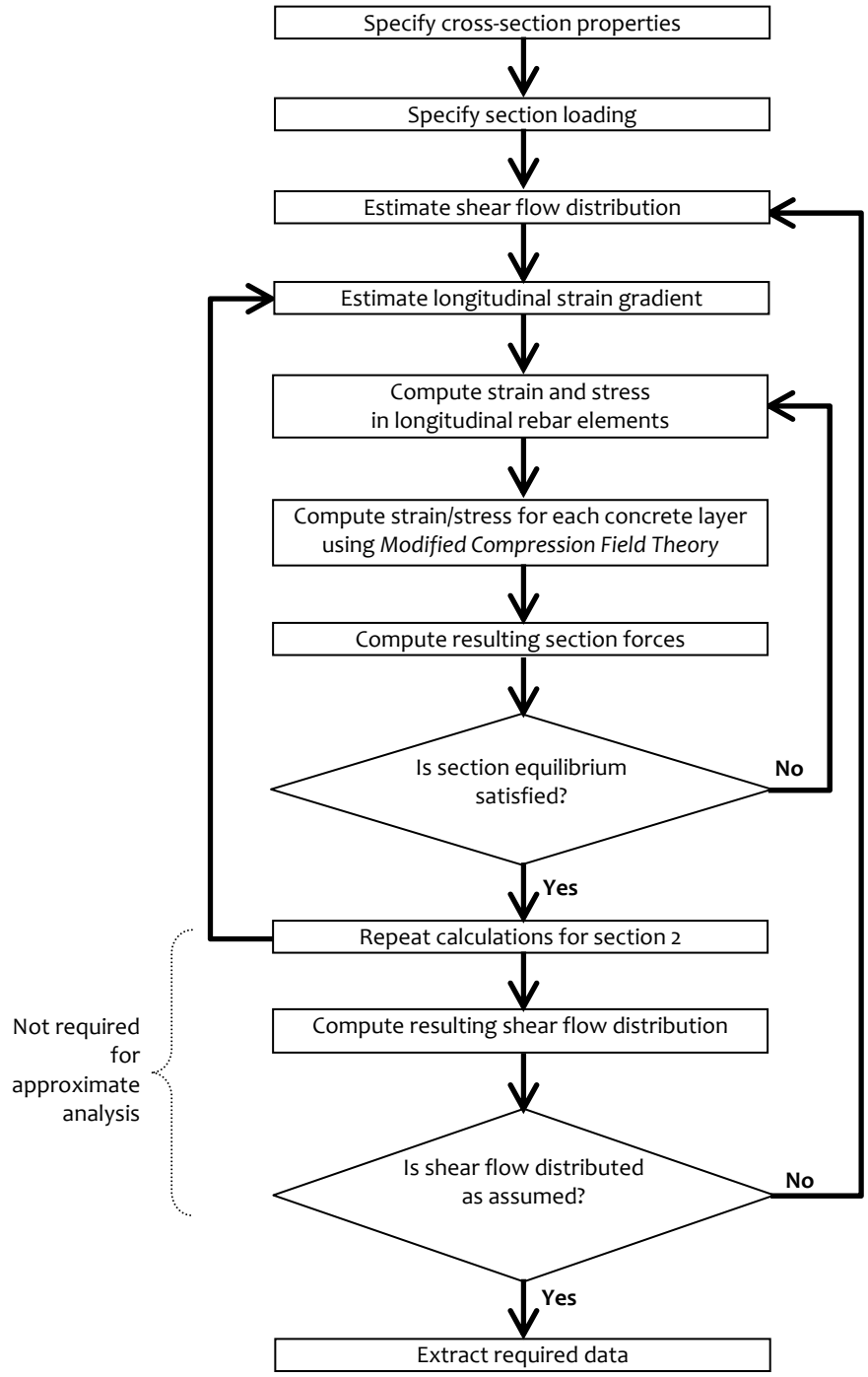

Figure 2.30: Solution procedure for beam analysis model [*reproduced from* Vecchio and Collins, 1988]

(c) Softened Truss Model

Alongside the development of *Modified Compression Field Theory*, another model was developed, known as *Rotating Angle Softened Truss Model* [Hsu, 1988; Belarbi and Hsu 1995], with two improvements over *Compression Field Theory*, namely: (i) tensile stress of concrete included, to predict deformations more accurately by defining a *softening coefficient* (a function of principal tensile strain), and (ii) average stress-strain

curve of reinforcement steel embedded in concrete was derived at the level of the crack for continuity, when used in *equilibrium* and *compatibility* equations. This was further improved to predict the concrete contribution by assuming cracks to be oriented at a fixed angle, rather than rotating angle [Pang and Hsu, 1995; Hsu and Zhang, 1996]. Later, the softening coefficient was redefined as a function of concrete compressive strength, and longitudinal to transverse steel ratios, in addition to the principal tensile strain of concrete. The solution procedure is similar to that using *Modified Compression Field Theory* (Figure 2.30).

Further, several numerical models were also proposed where *P-V-M* interaction is modelled using macro models [Mergos and Kappos, 2008, 2010 and 2012] and fibre beam-column elements [Petrangeli and Pinto, 1999; Marini and Spacone, 2006] with additional features to capture shear deformations. While some of these models used Timoshenko beam theory to formulate the shear resistance mechanism separately by considering equilibrium between concrete and transverse steel, and then superimposed the results with that from fibre beam element model for flexure, others used semi-empirical relations to consider the *P-V-M* interaction. For the purpose, nonlinear shear force-shear deformation relations are used to analyse RC members. In general, these models have proved to be efficient in the analysis of shear critical members.

2.3.3 Salient Observations

Extensive experimental and analytical studies were carried out, with the objective to identify the key parameters influencing the response of bridge piers and to arrive at suitable models to predict their behaviour. Experimental studies were useful particularly to identify the influence of various parameters on the behaviour of bridge piers. These studies investigated a number of aspects, including characteristics of constituent materials, the flexural strength, shear strength and ductility of bridge piers under simulated seismic loading with varying parameters. Among the many factors that influence the behaviour of bridge piers, important factors include *plan aspect ratio*, *amounts of transverse and longitudinal reinforcements* and their detailing, *material properties*, *axial load* on the pier, and *axial-shear-flexure (P-V-M) interaction* generated in the member during shaking. In addition, one key factor is *slenderness*; load transfer mechanism changes from *flexure-type* to *shear-type* with decrease in *span-to-depth ratio* (Figure 2.31) [Murty *et al*, 2012].

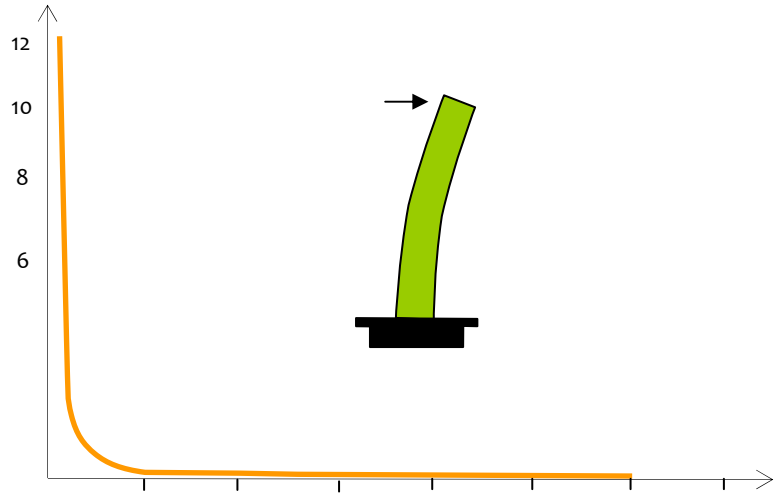

Figure 2.31: *Role of relative translational stiffness*: Influence of *L/D* ratio on ratio of flexural stiffness to shear stiffness of frame members [Murty *et al*, 2012]

In line with the experimental studies, analytical studies were conducted to simulate seismic behavior of RC members. Numerous theories and models were developed, mainly focusing on predicting the *lateral load capacity*. Most of these methods estimated the *flexural strength*, assuming *Bernoulli's Hypothesis*, and *shear strength* using the basic 45° *Truss Model*. The *estimated flexural strength* was reasonable, varying by not more than 10% of the experimental values, whereas the *estimated shear strength* overestimated the capacity by almost up to 200%. Consequently, new *refined* shear strength models were developed to improve estimates – these include *Variable Angle Truss Model*, additional concrete contribution term to the basic 45° *Truss Model*, *Equilibrium Plasticity Truss Model*, *Strut and Tie Model*, *Modified Compression Field Theory* and *Truss Arch Models*. Even though many of these models (*e.g.*, Strut and Tie Model, Modified Compression Field Theory, and Truss Arch Model) were able to forecast the behaviour with reasonable accuracy, the *P-V-M* interaction was not included. While *Strut and Tie Model* and *Modified Compression Field Theory* require huge computational effort, *Truss Arch Models* provide a totally novel approach, deviating from the traditional estimation methods. Also, basic assumption of linear strain variation adopted in many *Section Models*, like *Compression Field Theory* and other fiber models, limits their validity to forecast the behaviour of flexure dominated piers, and *Strut and Tie Model* approach is found useful mainly in forecasting the behaviour of disturbed regions of structural concrete. Strengths predicted using a *Section Model* and a *Strut and Tie Model* are

compared with experimentally determined shear strength [Collins and Mitchell, 1991; ACI 445R-99] (Figure 2.32). The main difficulty in developing general strength theory lies in non-homogenous nature of concrete, and the degree to which its behaviour at high stresses is influenced by cracking and other discontinuities.

2.4 SEISMIC DESIGN OF RC BRIDGE PIERS

Design specifications of national and international seismic codes are under constant revision by incorporating established outcomes of research and observations of practice. Countries that have made significant contributions in this area include European countries, Japan, New Zealand and USA. Seismic design requirements in Europe are approved by the *European Committee* for Standardisation, as a *European Pre-standard, Part 2* to *Eurocode 8 Earthquake Resistance Design of Bridges* [EC8-2, 2005]. In Japan, seismic design procedures are published by *Japan Road Association* as *Part V: Specifications for Highway Bridges: Seismic Design* (PWRI specifications) [Japan Road Association, 2002]. Specifications in New Zealand are issued by *Transit New Zealand* as *Bridge Manual: Earthquake Resistant Design: Section V* [NZS 3101, 2006]. USA has two national specifications for bridge design – the first is published by the *American Association of State Highway and Transportation Officials (AASHTO)* titled *Bridge Design Specifications* [AASHTO, 2007], and the second by the *Department of Transportation* of the

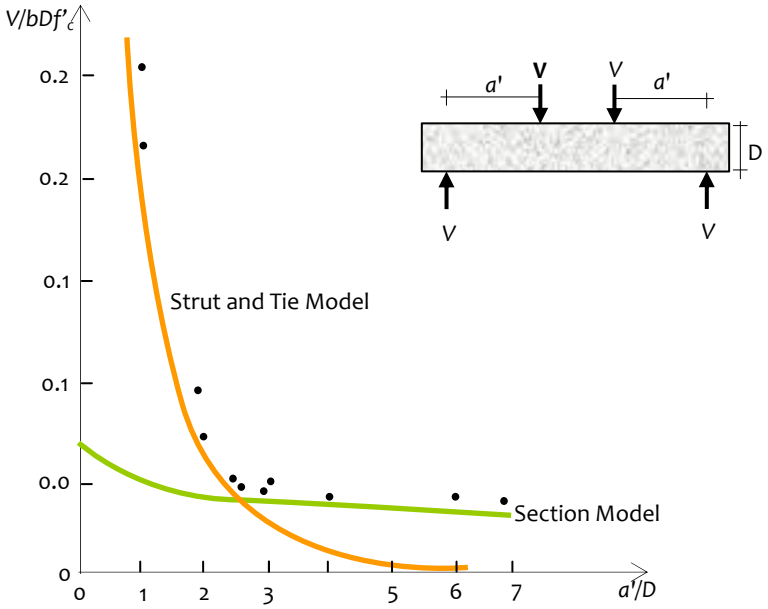

Figure 2.32: Applicability of fiber model, and strut and tie model for a series of beams tested with different *L/D* ratios [ACI 445R-99, 2000]

State of California titled *CALTRANS-Seismic Design Criteria* [CALTRANS, 2013]. Also, Indian code for highway bridges is issued by *Indian Roads Congress* as *IRC 112: Code of Practise for Concrete Road Bridges* [IRC 112, 2011]. Major developments done by these countries are explained in the subsections below.

2.4.1 Seismic Design Strategy

The seismic resistance of bridges is achieved normally by designing piers for both *strength* and *ductility*. It is not desirable to design a bridge pier to respond elastically to the lateral force demand induced by strong earthquakes. Hence, bridge piers are designed for a lower lateral force, allowing inelastic deformations, to dissipate seismic energy by forming of plastic hinges in piers. Seismic design of bridge piers consists of *strength design* and *capacity design*. *Strength design* provides adequate lateral strength to piers to limit ductility demands at critical sections to their ductility capacities, with appropriate safety factor. Force and deformation demands are obtained from factored loads. Elastic methods of analysis are used to determine distribution of forces and deformations throughout the pier. Flexural demand is calculated for the corresponding shear demand (Figure 2.33). The critical sections are designed for the shear H_d and moment M_d corresponding to the factored loads.

Capacity design controls the type of damage in structural elements, and sequence of damage between structural elements, ensuring adequate strength margin for non-ductile failure modes over designated ductile modes. Force demands are determined in

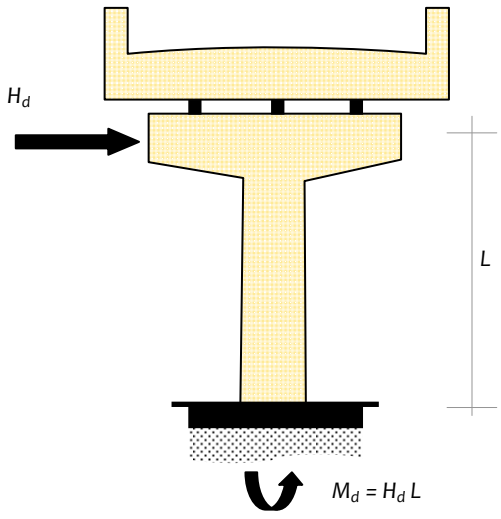

Figure 2.33: Illustrative example for strength design process

the inelastic range based on energy dissipation mechanism. In RC single column bridge piers, energy dissipation mechanism occurs through a single flexural plastic hinge in the pier. The maximum shear demand corresponds to overstrength flexural capacity of the section in the plastic hinge zone (Figure 2.34). Thus, the section is designed to have capacity greater than H_Ω. Hence, ductile inelastic flexural response is ensured.

Proper detailing of reinforcements is critical to ensure the required level of ductility in plastic hinges, thereby improving seismic resistance of bridge piers. The required ductile behavior of plastic hinge region can be ensured by providing necessary transverse reinforcement, for adequate confinement of concrete in them. Displacement ductility of piers is enhanced by increasing the amount of transverse reinforcement, which improves post-yield response.

2.4.2 Design Provisions

Design codes of different countries recommend different methods of analysis and design to meet the seismic demand through a desired structural behavior. Seismic design requirements from different design codes are discussed briefly in the following. In particular, specific requirements pertaining to flexure, shear, detailing and materials are presented.

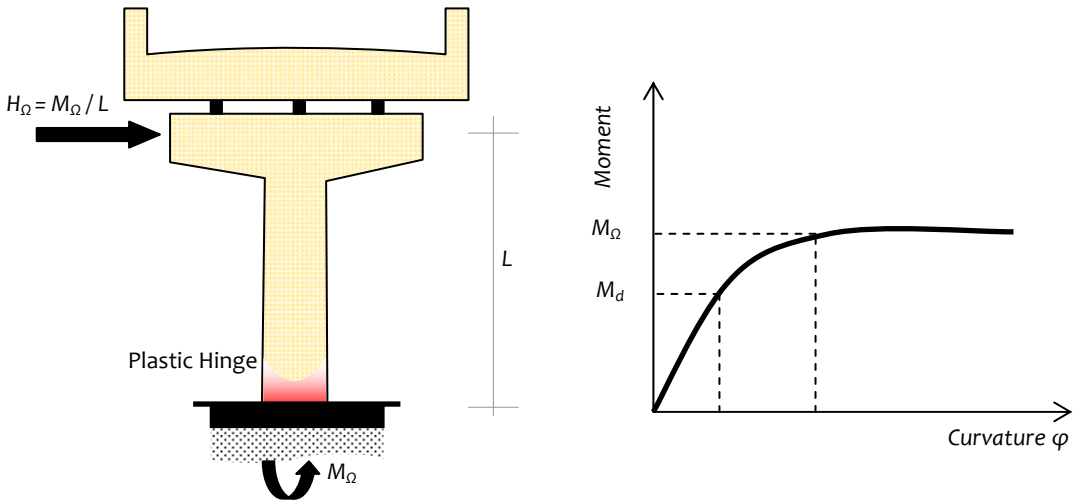

Figure 2.34: Plastic hinge condition assumed in capacity design process for estimating over strength-based design shear

2.4.2.1 Flexure

The bridge pier design in most international codes (including CALTRANS Seismic Design Criteria, NZS: 3101, Japan Road Association - Design Specifications for Highway Bridges, Euro Code 8-2 Earthquake Resistance Design of Bridges) follows the capacity design approach, while IRC 112-2011 specifications follows strength-based design. Generally, ultimate strength design is used for design of piers using material overstrength and capacity reduction factors to ensure flexural yielding before shear failure. Differences in these factors in various codes are mainly due to their attempt to balance economy and performance.

(a) CALTRANS – SDC analysis requirements

Flexural strength is ensured in design by this standard, by designing for the estimated plastic moment capacity of the pier at plastic hinge locations, based on expected material properties and not on nominal material strength. An idealised M-φ curve with an elastic perfectly plastic response, obtained by balancing the area under the curves, is used to estimate plastic moment capacity of the cross-section. The elastic portion of this idealised curve passes through the point of first yield of reinforcing bars. Code ensures at least a minimum flexural capacity against a lateral load of 10% of the tributary dead load applied at vertical mass centre of superstructure. The expected material properties are 1.3 times compressive strength of concrete and 1.1 times yield strength of reinforcing steel. Considering cost, no partial safety factor for materials is used to obtain design stress-strain curve of materials, and confinement effect is considered as per Mander's confinement model [CALTRANS, 2013].

(b) NZS 3101-2006 Concrete Structures Standard

Sufficient strength and adequate ductility of the structure are ensured at ultimate limit states through capacity-based design provisions given in this standard. It requires the use of capacity design approach for both *ductile structures* and *structures with limited ductility*, to restrict flexural yielding to selected regions, and to thereby protect the non-ductile regions. Minimum flexural strength requirement in regions of inelasticity is determined performing elastic analysis under specified loads, and sections are designed accordingly. Flexural capacity is obtained using a bilinear stress-strain curve for reinforcing steel and an equivalent stress block for concrete. Stress block corresponding to 80% and 130% of total axial load acting on the cross-section is considered; critical one

is used in design. Shear design at plastic hinge locations has to consider effects of formation of flexural hinges in members [NZS 3101, 2006].

(c) PWRI Design Specifications for Highway Bridges Part V

Two levels of seismic hazard are considered by this standard, namely (i) a highly probable seismic event, and (ii) a less probable, but strong, seismic event. Seismic design philosophy requires the structure to withstand the highly probable event with no damage, and to prevent fatal damage on structures of standard importance and to limit damage in bridges of high importance group under the less probable earthquake. Collapse is not allowed in any of the cases. Flexural capacity of the section, as per PWRI specifications, is estimated for the design seismic load. The cross-section is discretized into a number of fibres in the direction of lateral load, and the axial load, bending moment and curvature capacity are determined. Design bending strength is determined from the moment-curvature analysis considering the material properties specified by code, which can take a maximum value equal to design bending yield strength of the section [Japan Road Association, 2002].

(d) AASHTO Bridge Design Specifications 2007

Seismic design philosophy as per this standard requires: (i) no significant damage to structural components when subjected to small or moderate earthquake, and (ii) no collapse of the bridge or part of it under strong ground shaking during large earthquakes. The demand on each component of the bridge system is determined primarily by elastic analysis. Further, these are modified depending on the level of ductility desired, the redundancy, and its operational importance. Also, a load factor is applied and finally the demand ensured to be less than the capacity estimated. To ascertain that the structure has adequate ductility and yields in flexure, limits are provided for longitudinal reinforcement [AASHTO, 2007].

(e) Euro Code *8-2 Earthquake Resistance Design of Bridges*

Flexural resistance and ductile behaviour is ensured through capacity design by estimating flexural overstrength based shear demand; the flexural overstrength is obtained by multiplying design flexural strength of the section by an overstrength factor. Design flexural strength is based on the actual section geometry, including reinforcement, and material properties with partial safety factor of 1.5 for concrete and 1.15 for reinforcing steel. The value of over-strength factor reflects the probable deviation of material strength and strain hardening. Also, flexural resistance outside

plastic regions is checked and limited to a value lesser than the bending moment capacity of the section inside plastic hinge region [CEN, 2005].

(f) IRC Specifications for Concrete Road Bridges (IRC: 112-2011)

IRC 112 -2011 provides Force-based design criteria for RC bridges based on limit state method. Linear elastic analysis is recommended for normal bridges and nonlinear inelastic analysis for critical bridges. Elastic methods are recommended by the code to determine distribution of forces and deformations in the bridge. Also, plastic methods of analysis, as per specialised literature, are recommended by the code, provided, it can be shown that adequate ductility exists at plastic hinge locations. Capacity design method is not stated in the code, but length of plastic hinges and minimum spacing of transverse reinforcement in connection with buckling of longitudinal reinforcement, are mentioned separately [IRC 112, 2011].

2.4.2.2 *Shear*

The shear strength of RC members under inelastic loading is influenced by a number of parameters including *aspect ratio*, *level of axial load*, *transverse steel ratio* and *longitudinal steel ratio*. These parameters are considered in many of the specifications explicitly and implicitly in few.

(a) CALTRANS – SDC Analysis Requirements

The seismic shear demand is calculated based on the shear associated with the overstrength moment as per CALTRANS specifications. The shear capacity of the pier is calculated based on the nominal material strengths as:

$$\begin{aligned} &\phi V_n \geq V_0 \\ &V_n = V_c + V_s \end{aligned} \tag{2.10}$$

where V_c is concrete shear capacity designed for ductility considering effects of flexure and axial load, and V_s the shear reinforcement capacity. Shear contribution of steel is estimated using 45° *Truss Model* and that of concrete towards shear capacity (in MPa) given by:

$$V_c = \begin{cases} (Factor\,1)(Factor\,2)\sqrt{f_c'} & \text{inside the plastic hinge zone} \\ 0.25(Factor\,2)\sqrt{f_c'} & \text{outside the plastic hinge zone} \end{cases} \tag{2.11}$$

where

$$0.025 \leq Factor\,1 = \left(\frac{\rho_s f_{yt}}{0.15}\right) + 3.67 - \mu_d \leq 3 \text{, and} \tag{2.12}$$

$$Factor\ 2 = 1 + \left(\frac{P}{13.8 A_g} \right) < 1.5 . \tag{2.13}$$

In the above, $f_c^{'}$ is compressive strength of unconfined concrete, f_{yt} the nominal yield stress of transverse reinforcement, ρ_s the ratio of the spiral or hoop reinforcement to the core volume confined by the spiral or hoop reinforcement, A_g the gross cross-section area, μ_d the displacement ductility factor, and P the axial force in the column (Figure 2.35) [CALTRANS, 2013].

(b) NZS 3101-2006 Concrete Structures Standard

Acceptable values of member strengths to be provided in order to meet capacity design principles are given by the standard. The calculations of nominal strength in flexure include effects of confinement. The nominal shear strength is based on capacity design concept, and shear capacity check is given by:

$$\phi V^* < V_c + V_s , \tag{2.14}$$

where V^* is the design shear force obtained using capacity design approach considering the overstrength flexural actions at the plastic hinge regions with strength reduction factor taken as unity. Shear contribution from steel, V_s is estimated using 45˚ truss model and the shear resistance of concrete is obtained as:

$$V_c = v_c b d , \tag{2.15}$$

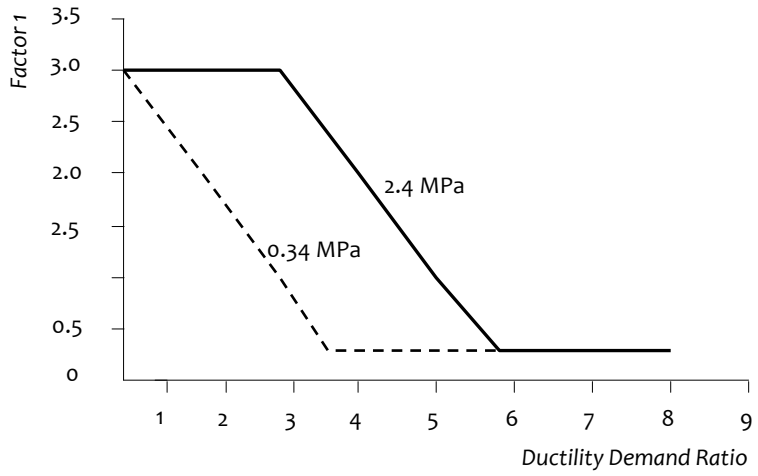

Figure 2.35: Effect of ductility on estimating shear strength

where v_c is the nominal shear stress resisted by concrete, and d is the distance from the extreme compression fiber to the centroid of the longitudinal reinforcement. In the potential hinge region, for axial load ratio $\left(3P/A_g f_c'\right) < 1$,

$$v_c = \begin{cases} 0 & \text{if } \dfrac{3P}{A_g f_c'} \le 1 \\ 4\left(0.07 + 10\rho_w\right)\sqrt{f_c'}\sqrt{\dfrac{3P}{A_g f_c'} - 1} & \text{if } \dfrac{3P}{A_g f_c'} > 1 \end{cases} \text{, in MPa} \tag{2.16}$$

Outside the potential hinge region, if axial load is present,

$$v_c = 4\left(0.07 + 10\rho_w\right)\sqrt{f_c'}\left[1 + \frac{3P}{A_g f_c'}\right] \text{, in MPa} \tag{2.17}$$

with limits of $0.08\sqrt{f_c'} < v_c < 0.2\sqrt{f_c'}$, where ρ_w is equal to the effective area of flexural reinforcement (the area of longitudinal reinforcement in the section lying between extreme tension reinforcement and a line located at a distance of one third of distance between extreme compression fiber and the extreme tension reinforcement measured from this reinforcement (Figure 2.36)), A_g the gross concrete area, f_c' the compressive strength of unconfined concrete and P the axial load [NZS 3101, 2006].

(c) PWRI Design Specifications for Highway Bridges Part V

Capacity design is followed by analyzing the deformation performance of RC bridge piers, considering all possible plastic hinges. Shear strength of concrete is evaluated including *scale effect*, and influence of cyclic loading is considered. The nominal shear capacity for the section is given as sum of concrete shear capacity V_c as

$$V_c = c_c c_e c_{pt} \tau_c b d \text{,} \tag{2.18}$$

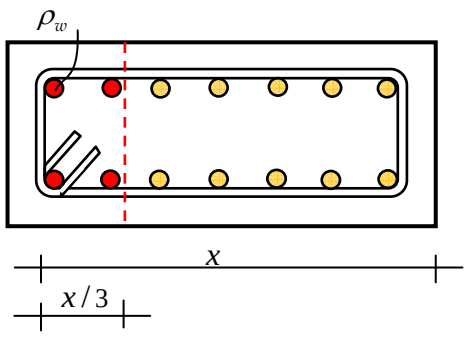

Figure 2.36: Area of longitudinal reinforcement effective in contributing towards shear [NZS 3101, 2006]

where c_c, c_e and c_{pt} are modification factors, τ_c the average shear capacity of concrete (which is a function of the grade of concrete). c_c accounts for reversed cyclic load effect, c_e for size effect, and c_{pt} for increase in shear capacity of concrete with increase in longitudinal steel (Figure 2.37), and V_s is estimated using 45° truss model.

Also, an allowable ductility factor is recommended by the code corresponding to the cyclic characteristics of seismic motion given by

$$\mu_a = 1 + \frac{(\delta_u - \delta_y)}{\alpha' \delta_y}, \tag{2.19}$$

where μ_a is the allowable ductility factor of RC bridge pier, δ_u the ultimate displacement, δ_y the yield displacement of RC bridge pier, and α' the safety coefficient [Japan Road Association, 2002].

(d) AASHTO Bridge Design Specifications

Design procedure for shear is derived from the *Modified Compression Field Theory*. The expressions for shear strength are modified for RC members to account for combined actions of axial load, bending moment, shear force and prestressing. The nominal shear capacity is taken as the sum of components of concrete, shear reinforcement, and prestressing, as:

$$V_n = V_c + V_s + V_p \tag{2.20}$$

The concrete contribution is controlled by the value of coefficient β as given by:

$$V_c = 0.0316\beta\sqrt{f_c'}\, b_v d_v \text{ . in kips} \tag{2.21}$$

A variable angle truss model is used to calculate the contribution of shear reinforcement. The angle of the field of diagonal compression θ is used to calculate number of stirrups.

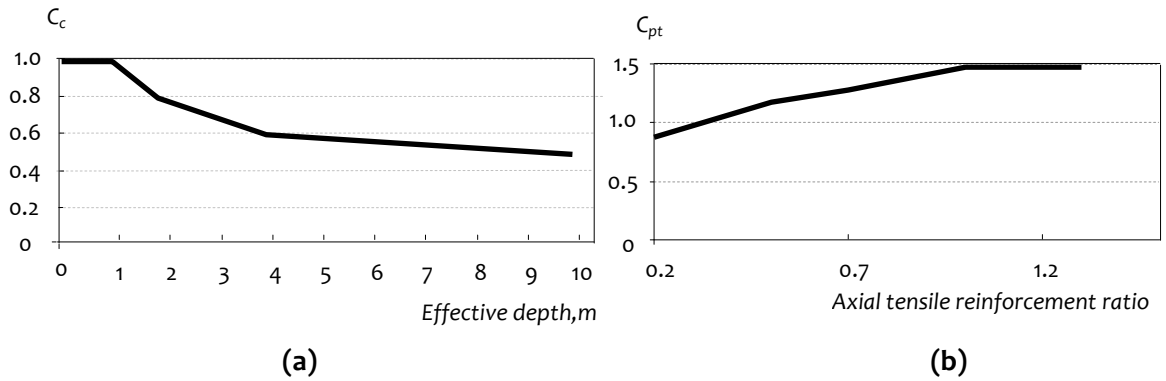

(a) **(b)**

Figure 2.37: Effect on contribution to shear strength: (a) reverse cyclic load, and (b) longitudinal reinforcement ratio [Japan Road Association, 2002]

$$V_s = \frac{A_h f_y d_v \cot\theta}{s_v}, \tag{2.22}$$

where $d_v = Max[0.9d; 0.72h]$. Values β and θ are given in terms of longitudinal strain ε_x and shear design stress ratio τ/f_c', where $\tau = V_u/(b_v d_v)$, in which b_v and d_v are width of web including adjustments for presence of ducts and effective shear depth respectively. d is the depth from compression face to centroid of tension reinforcement, h the overall depth of member, V_u the factored shear force at the section, and f_y the yield strength of reinforcing bars [AASHTO, 2007].

(e) Euro Code 8-2 *Earthquake Resistance Design of Bridges*

Design value of shear strength for member with shear reinforcement, as per this standard, is estimated based on the variable angle truss model by limiting the value of strut angle between 22˚ and 45˚ outside plastic hinge zone. Inside plastic hinge zone, strut angle is assumed to be 45˚. For members with shear reinforcement provided in the direction perpendicular to the longitudinal axis of the member outside the plastic hinge zone, shear resistance V_{Rd} is given as the smaller value of:

$$V_{Rd,s} = \frac{1}{\gamma_{Bd}}\left(\frac{A_v}{S_v} Z f_{yt} \cot\theta\right) \tag{2.23}$$

and

$$V_{Rd,\max} = \frac{1}{\gamma_{Bd}}\left(\frac{\alpha_{cw} b_w Z v_1 f_{cd}}{(\cot\theta + \tan\theta)}\right), \tag{2.24}$$

where,

$$\alpha_{cw} = \begin{cases} \dfrac{1+\sigma_{cp}}{f_{cd}} & 0 < \sigma_{cp} \le 0.25 f_{cd} \\ 1.25 & 0.25 f_{cd} < \sigma_{cp} \le 0.5 f_{cd} \\ 2.5\left(1 - \dfrac{\sigma_{cp}}{f_{cd}}\right) & 0.5 f_{cd} < \sigma_{cp} < 1.0 f_{cd} \end{cases} \tag{2.25}$$

For members with minimum or no shear reinforcement, concrete contribution to shear resistance given by

$$V_c = \frac{1}{\gamma_{Bd}}\left(C_{Rd,c} k (100\rho_l f_{ck})^{1/3} + K_1 \sigma_{cp}\right) b_w d \text{, in MPa} \tag{2.26}$$

where

$$k = \left(1 + \sqrt{\frac{200}{d}}\right) \leq 2, \text{ and} \tag{2.27}$$

$$\sigma_{cp} = \frac{P}{A_g} \leq 0.2 f_{cd}. \tag{2.28}$$

Here, A_v is the cross sectional area of shear reinforcement, S_v the spacing of stirrups, f_{yt} the yield strength of shear reinforcement, Z the inner lever arm approximate value normally considered as $0.9d$, where d is the effective depth of the section, f_{cd} design compressive stress in concrete, v_1 a strength reduction factor for concrete cracked in shear, a_{cw} a coefficient taking account of the state of the stress in the compression chord and σ_{cp} the mean compressive stress in concrete due to design axial force P over the gross cross sectional area A_g. $C_{Rd,c}$ and K_1 are constants depending on factors like concrete compressive strength and effective depth of section and γ_{Bd} is an additional factor of safety against brittle failure [CEN, 2005].

(f) IRC Specifications for Concrete Road Bridges (IRC: 112-2011)

IRC 112 -2011 provides concrete contribution to shear resistance given by

$$V_c = \left(0.12k(100\rho_l f_{ck})^{1/3} + 0.15\sigma_{cp}\right) b_w d, \text{ in MPa} \tag{2.29}$$

where

$$k = \left(1 + \sqrt{\frac{200}{d}}\right) \leq 2, \text{ and} \tag{2.30}$$

$$\sigma_{cp} = \frac{P}{A_g} \leq 0.2 f_{cd}. \tag{2.31}$$

Here, d is effective depth of cross-section and P/A_g axial stress. For members with shear reinforcement, variable angle truss model approach is adopted, considering shear resistance offered by stirrups alone. Eq.(2.29) is applicable for sections without shear reinforcement. The limiting values of truss angle θ recommended by the code lies between 22° and 45°. Shear resistance of concrete is assumed to be contributed by longitudinal steel in tension ρ_l [IRC 112, 2011].

2.4.2.3 Detailing

CALTRANS detailing criteria specify the amount of transverse reinforcement to be provided *inside* and *outside* the plastic hinge region, for adequate confinement and prevention of buckling of longitudinal reinforcement. The plastic hinge length is defined

as the larger of: (a) 1.5 times the cross-sectional dimension in the direction of bending, (b) the region of column where the moment exceeds 75% of maximum plastic moment and (c) 0.25 times length of the column from the point of maximum moment to the point of contraflexure. The maximum spacing of transverse reinforcement is restricted to the minimum of: (a) $1/5^{th}$ of the least dimension of the least cross-section dimension of piers, (b) 6 times the nominal diameter of longitudinal reinforcement, and (c) 203 mm, whichever is minimum. Maximum longitudinal reinforcement is limited to 4% of gross cross-sectional area, and minimum to 1% for columns and 0.25% for wall piers. Maximum diameter of longitudinal reinforcement is limited based on flexural bond consideration, given by:

$$d_l = 2.1\sqrt{f_c^{'}}\,\frac{L_b}{f_{yl}}, \tag{2.32}$$

where L_b=*L-0. 5D*. L_b is the length of column between the point of maximum moment and point of contra-flexure, and *D* the total depth of the section.

AASHTO Specifications limits maximum area of longitudinal reinforcement to 8% of the total cross-sectional area to ensure adequate ductility. Minimum area is limited to

$$\frac{(A_l)_{min} f_{yl}}{A_g f_c^{'}} \geq 0.135 \tag{2.33}$$

where f_{yl} is the yield strength of longitudinal bars. For bridges in higher seismic zones, to enhance the ductility, maximum and minimum areas are limited to 6% and 1% of the gross cross-sectional areas, respectively. Maximum spacing of transverse reinforcement is: *(a)* least cross-sectional dimension of the member, or *(b)* 300 mm, whichever is lesser to enhance confinement and prevent buckling of longitudinal reinforcement. Maximum spacing between longitudinal bars and lateral ties provided across the section, is not to exceed 150 mm. Transverse reinforcement has to be arranged in such a way that every corner and alternate longitudinal bar has lateral support provided by the corner of a tie bent at an angle of not more than 135˚.

PWRI Specifications present detailing requirements or transverse reinforcement inside plastic hinge zone in terms of spacing and bar diameter. A minimum diameter of 13 mm and maximum centre-to-centre spacing of 150 mm are recommended inside the plastic hinge zone. The maximum transverse reinforcement ratio allowed is 1.8%. The upper limit is imposed to limit the excessive enhancement of core confinement, which

may lead to reduction in plastic hinge length, thereby fracturing the longitudinal reinforcement.

Maximum area of longitudinal steel recommended by New Zealand Standards is 8%, similar to that specified by AASHTO. Minimum area is restricted to 0.8% of the gross sectional area. Special consideration is given for reinforcement provided in the plastic hinge to ensure ductile failure, by limiting the longitudinal reinforcement area to $18A_g/f_{yl}$. The smallest diameter of longitudinal bars provided has to be at least 2/3rd of the largest bar provided in a row. The maximum centre-to-centre spacing of cross-linked longitudinal bars across the cross-section has to be lesser of: (a) 1/4th the lateral dimension of cross-section in the direction of spacing, and (b) 200 mm. Maximum spacing of transverse reinforcement is limited to: (a) 1/3rd the least lateral dimension of the cross-section and, (b) 10 times diameter of the longitudinal bars tied by the stirrups. Again, in the plastic hinge zone, the spacing is reduced to: (a) 1/4th the least lateral dimension of the cross-section and, and (b) 6 times diameter of longitudinal bars tied by the stirrups. Minimum amount of transverse reinforcement required outside the plastic hinge zone is 70% of that inside the zone. For rectangular hoops and ties, minimum diameter of bars has to be: (a) 5 mm, if longitudinal bars are less than 20 mm in diameter, (b) 10 mm, if longitudinal bars are less than 20-32 mm in diameter, and (c) 12 mm, if longitudinal bars are 32 mm or more in diameter.

Euro Code 8-2 recommends confining reinforcement quantity for circular and rectangular sections by defining the mechanical reinforcement ratio

$$\omega_{wd} = \rho_T f_{yt} \ / f_{cd} \tag{2.34}$$

where, f_{yt} the yield strength of shear reinforcement, ρ_T the transverse reinforcement ratio and f_{cd} design compressive stress in concrete. Expressions are provided for minimum amount of confining reinforcement, to ensure minimum ductility and to prevent buckling of longitudinal bars. In addition, to avoid buckling of longitudinal reinforcement limits for spacing of transverse reinforcement is specified in the code not exceeding 200mm. Also, cross ties are required to be provided with 135˚ hook at one end and 90˚ hook at the other end. In case of spirals or hoops inside potential plastic hinge regions, mechanical couplers are preferred by the code. Further, splicing and lapping of longitudinal bars are not allowed inside plastic hinge region.

IRC 112-2011 recommends longitudinal bar diameter to be not less than 12mm and spacing between the bars to not exceed 200mm. Minimum area of longitudinal reinforcement is restricted to 0.2% of the gross sectional area or 10% of the ratio of design axial compression force to the design yield strength of longitudinal reinforcement, which ever is greater. Maximum area of longitudinal reinforcement is limited to 4% of gross sectional area. The diameter of transverse reinforcing bars shall not be less than 8mm or 1/4th the maximum diameter of longitudinal bar, which ever is greater. The spacing of transverse reinforcing bar shall not exceed the lesser of (i) 12 times the minimum diameter of longitudinal bars, (ii) least dimension of the column and (iii) 200mm. Use of mechanical devices is recommended by the code to ensure proper splicing. In potential plastic hinge regions, minimum transverse reinforcement is to be provided by defining mechanical reinforcement ratio same as that defined by Euro Code 8-2. Also, spacing of transverse reinforcement is limited to 1/3rd the diameter of the concrete core or 200 mm which ever is less. To avoid buckling of longitudinal bars, cross ties are recommended within a spacing not exceeding five times the diameter of smallest longitudinal bars. Also, cross ties are required to be provided with 135˚ hook at one end and 90˚ hook at the other end. Splicing and lapping of longitudinal bars are not allowed inside plastic hinge region.

2.4.2.4 Materials

Seismic design philosophy specified by codes, in general, requires ductile design of bridge piers. Primarily, this is based on the material properties within the column cross-section, including stress-strain behaviour of steel and concrete. Properties of concrete rely mainly on amount of transverse reinforcement providing confinement to the core region, which ensures ductile response of the pier. Various codes specify different amounts of reinforcement to be provided based on either: *(i) volumetric ratio* of transverse ties to concrete, or by *(ii) area ratio* of the stirrups within a given length along the member height.

CALTRANS design criteria and Euro Code 8-2 provide the transverse reinforcement ratio required depending on whether it is inside the plastic hinge zone or not. *Mander's Model* for stress-strain curve of confined concrete is recommended by both codes for ensuring adequate confinement. In addition to the expressions provided for shear capacity for both outside and inside plastic hinge region, the code imposes that

single members must have at least a minimum ductility capacity. Further, the section must be designed to meet a global displacement ductility demand of not less than 4, for single column bents.

New Zealand design code approach is similar to that adopted by CALTRANS criteria. The code expression includes certain limits imposed: (a) ratio of gross cross-sectional area to core area A_g/A_c, shall not be greater than 1, (b) yield strength of transverse reinforcement is not more than 800 MPa, and (c) $\left(A_{st}/A_g\right)\left(f_y/0.85f_c'\right) \le 4$. The ratio of transverse reinforcement is given by,

$$\rho_s = \begin{cases} \dfrac{(1-\rho_t m)}{2.4}\left(\dfrac{A_g}{A_c}\right)\left(\dfrac{f_c'}{f_{yt}}\right)\left(\dfrac{P}{\phi f_c' A_g}\right) - 0.0084 & \text{Inside the plastic hinge zone} \\ \dfrac{(1.3-\rho_t m)}{2.4}\left(\dfrac{A_g}{A_c}\right)\left(\dfrac{f_c'}{f_{yt}}\right)\left(\dfrac{P}{\phi f_c' A_g}\right) - 0.0084 & \text{Outside the plastic hinge zone} \end{cases} \quad (2.35)$$

where $\rho_t = \left(A_{st}/A_g\right)$ is ratio of flexural reinforcement, which is considered as the ratio of the area of longitudinal reinforcement in the section lying between extreme tension reinforcement and a line located at a distance of 1/3rd the distance between extreme compression fiber and the extreme tension reinforcement measured from this reinforcement to the gross cross-section area (Figure 2.36). m is lower characteristic yield strength of longitudinal steel, f_{yt} is lower characteristic yield strength of transverse steel, P is axial compressive load of column, and ϕ is the strength reduction factor (= 0.85 for columns not protected by capacity design).

AASHTO provides *volumetric ratio* of transverse reinforcement, in which effect of column size or strength is not accounted for. Minimum values of reinforcement ratio are provided based on the *Seismic Design Category*. For Seismic Design Category B, specified in the code, $\rho_s \ge 0.003$ and for Categories C and D, $\rho_s \ge 0.005$. Considering the rapid shear strength degradation in regions of high inelasticity, code specifies different reinforcement ratios for regions inside and outside the plastic hinge zone, as

$$\rho_s \ge \begin{cases} 0.12\dfrac{f_c'}{f_y} & \text{inside plastic hinge region} \\ 0.45\left(\dfrac{A_g}{A_c} - 1\right)\dfrac{f_c'}{f_y} & \text{outside plastic hinge region} \end{cases}, \quad (2.36)$$

where ρ_s is volumetric ratio of transverse reinforcement, f_{yh} the specified yield strength of transverse steel, f'_c the specified compressive strength of concrete, A_g the gross area of

cross-section, and A_c the core area of cross-section. Grades of reinforcing steel specified by the code are required to have yield strength in the range 414 - 538 MPa to ensure spread of plasticity.

As per PWRI specifications, transverse reinforcement to be provided to ensure adequate reinforcement, is given in terms of volumetric ratio of lateral restraining reinforcement, as

$$\rho_s = \frac{4A_h}{s_v d} \leq 0.018 \tag{2.37}$$

where A_h is the sectional area of lateral restraining reinforcement, s_v the spacing between lateral reinforcement, and d the largest value of length of core concrete divided and restrained by hoop ties and intermediate ties.

For providing adequate confinement at plastic hinge locations, IRC 112-2011 specifies transverse reinforcement in rectangular sections in terms of *volumetric ratio* given by:

$$\rho = \frac{A_{sw}}{s_v b} \tag{2.38}$$

where A_{sw} is the area of the stirrups and ties in one direction of confinement, s_v the spacing of hoops in the longitudinal direction, and b the dimension of the concrete core measured perpendicular to the direction of confinement under consideration.

2.4.3 Salient Observations

Most of the current design codes (NZS 3101, CALTRANS, PWRI and Euro Code) still adopt the 45° *Truss Model* with an additional concrete term to estimate the shear capacity, within plastic hinge region. While the NZS Code accounts for effect of aggregate size, axial load, and longitudinal reinforcement ratio in tension, the PWRI Specifications consider effect of repeated cyclic loads, longitudinal reinforcement ratio and effective depth for estimating the concrete contribution term. On the other hand, CALTRANS Specifications consider effect of flexural displacement ductility, confinement of concrete and axial load in estimating the concrete contribution term. IRC 112 considers the *Variable Angle Truss Model* to determine the shear capacity. The key influencing parameter *P-V-M* interaction is recognized in shear design by AASHTO code (using *simplified* Modified Compression Theory), and to a certain extent by CALTRANS (by considering effect of flexural displacement ductility). Table 2.1 provides a summary of the design provisions for bridge piers given in different codes. IRC

follows *strength design approach* for the design of bridge components with no clear focus on overstrength factors; this results in design of bridge components for the demands as per design loads (which are well below that of the overstrength plastic hinge based lateral shear force), which may cause brittle failure of bridges during earthquakes. Detailing of transverse reinforcement *inside* and *outside* plastic hinge zones provided in IRC is at par with those given in other codes for seismic regions, even though no clear guidance is provided on capacity design based shear design of piers. The PWRI specifications considers size effect, reversed cyclic load effect and displacement ductility in the shear strength calculation. Also, it provides an allowable limit for ductility; CALTRANS specifies the maximum limit for ductility as 4. IRC does not provide any specific limit for ductility. CALTRANS, PWRI, Euro Code, and New Zealand codes recognize the reduction of shear capacity due to the interaction of shear, axial and flexural actions particularly in regions of inelasticity, and have incorporated the same using certain empirical relations.

Table 2.1: Comparison of design provisions for bridge piers in different codes

Design Issue	***Design Code***			
	CALTRANS	***AASHTO***	***PWRI***	***EC 8-2; IRC***
Design	Capacity design approach			
Over strength Factors	1.2	1.3	Considered	Considered
Shear strength calculation	Inside plastic hinge $V_c = 0.25\lambda\gamma\sqrt{f_c'}$ Outside plastic hinge $V_c = 0.25\gamma\sqrt{f_c'}$	$V_c = 0.0316\beta\sqrt{f_c'}b_v d_v$ $V_s = \frac{A_h f_y d_v \cot\theta}{s_v}$	$V_c = C_e C_c C_{pt} bd$ $V_s = \frac{A_h f_y d}{s_v}$	Minimum of $V_{Rd,\max} = \frac{1}{\gamma_{Bd}}\left(\frac{\alpha_{cw} b_w Z v_1 f_{cd}}{(\cot\theta + \tan\theta)}\right)$ $V_{Rd,s} = \frac{1}{\gamma_{Bd}}\left(\frac{A_v}{S_v} Z f_{yt} \cot\theta\right)$
Size effect	Not Considered	Not Considered	Considered	Not Considered
Reversed cyclic load	Not Considered	Not Considered	Considered	Not Considered
Transverse renforcement inside plastic hinge zone for rectangular pier	$\rho_s = \frac{4A_b}{b_c d_c s_v}$	$A_h \geq 0.12 f_c / f_y$	$\rho_s = \frac{4A_h}{sd} \leq 0.018$	$\rho_s = \frac{A_{sw}}{s_v b}$
Note: $0.025 \leq \lambda = \left(\frac{\rho_s f_{yt}}{0.15}\right) + 3.67 - \mu_d \leq 3$ and $\gamma = 1 + \left(\frac{P}{13.8 A_g}\right) < 1.5$				

2.5 GAP AREAS

Single column RC bridges are prevalent around the world. Many of those collapsed during earthquakes due to insufficiency of bridge pier capacity to resist combined stresses induced during these earthquakes. Also, in general, single column piers behave like cantilever columns. Understanding of the behaviour of piers is challenging, because these piers are subjected to high *normal* and *shear stresses* during strong earthquake shaking. Often lateral load capacity is estimated, but failure modes and location of failure are overlooked; absence of a simple but comprehensive method (which captures the axial-shear-flexure interaction based load resisting mechanism of the piers) is cited as the reason for this. It is recorded that code designed RC bridge piers have failed mainly owing to inadequacy in *shear strength*, *flexural strength* or *ductility*. Considering these inadequacies, three typical and prominent modes of failure of RC piers are *flexure failure*, *combined flexure-shear failure*, and *shear failure* (Figure 2.38).

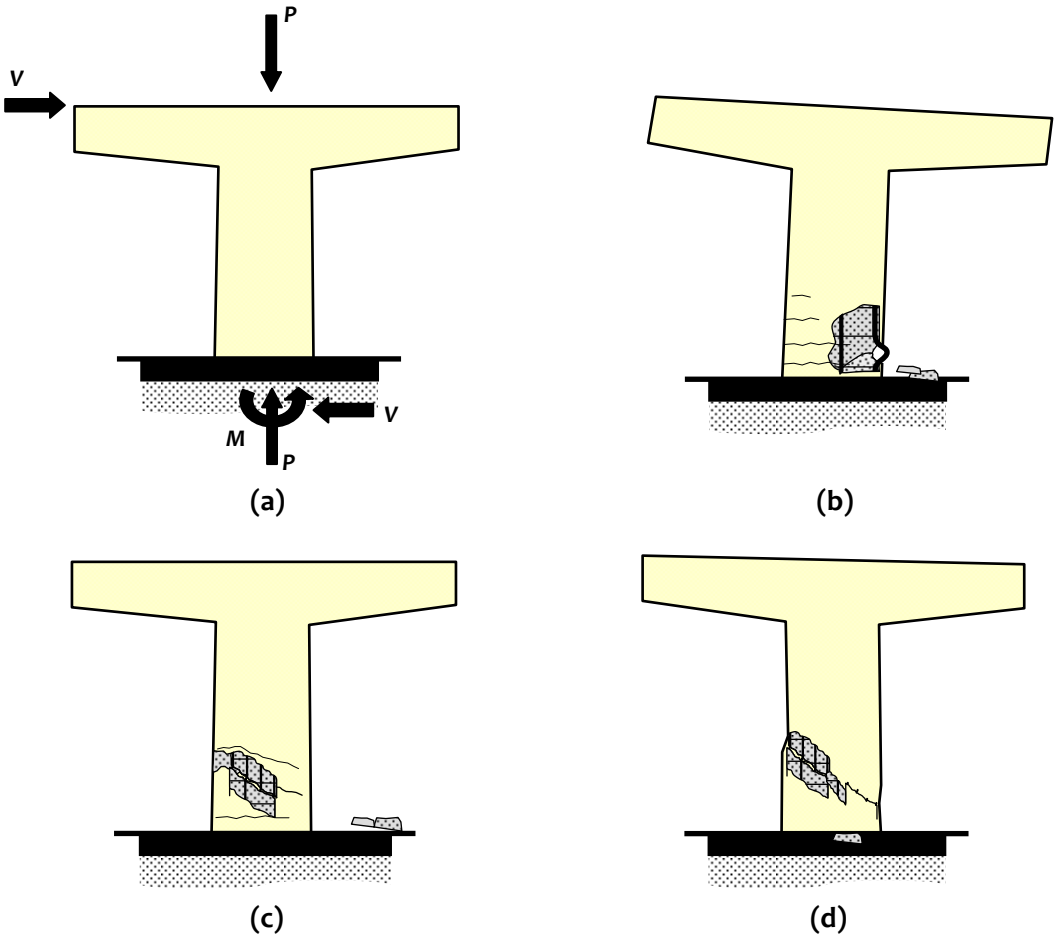

Figure 2.38: Predominant failure modes in RC bridge piers: (a) pier subjected to equivalent seismic loading, (b) flexure failure, (c) combined flexure-shear failure, and (d) shear failure

Flexure failure usually occurs in *slender piers*, where bending moment demand exceeds flexural capacity of a cross-section (Figure 2.39). *Flexure failure*, within plastic hinge regions, is characterized by spalling of cover concrete, yielding of longitudinal steel, initiation of cracking of core concrete at extreme outer layer in tension, and progression of the crack towards the inner layers of steel, with increased deformation demands [Zhu *et al*, 2007]. In extreme cases, buckling of longitudinal reinforcement in compression or crushing of core concrete in compression also occur. In laterally loaded slender cantilever piers, plastic hinging occurs at the bottom of the pier and is the principal source of energy dissipation [Paulay and Priestley, 1992]. Ensuring adequate amount and proper arrangement of reinforcement help achieve ductile mode of failure (Figures 2.40 and 2.41).

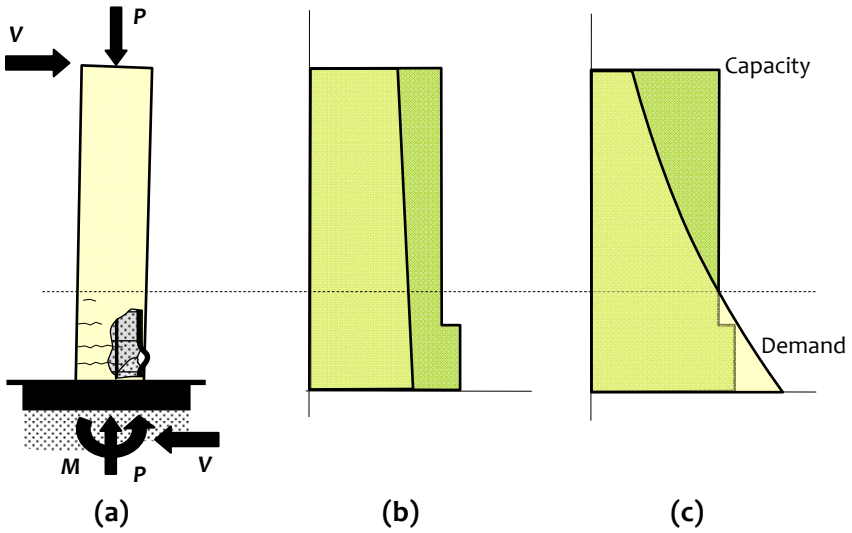

Figure 2.39: Flexure failure of bridge piers: (a) pier subjected to equivalent seismic loading, (b) shear force diagram, and (c) bending moment diagram

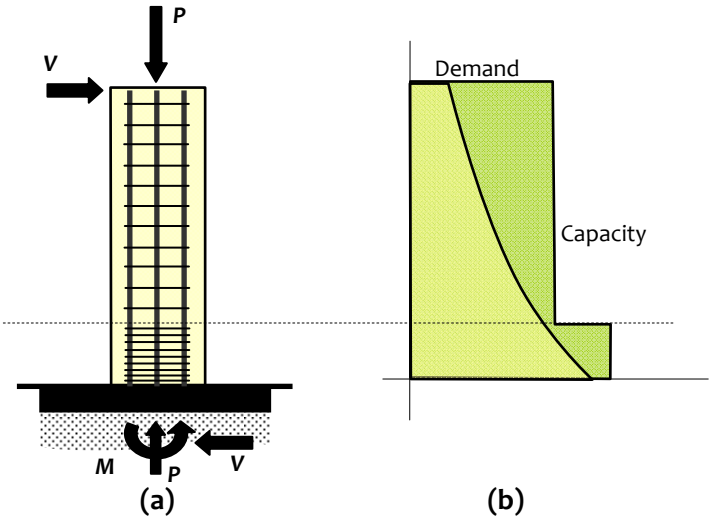

Figure 2.40: Influence of transverse reinforcement on flexural strength: (a) arrangement of reinforcement, and (b) enhancement in flexural strength capacity

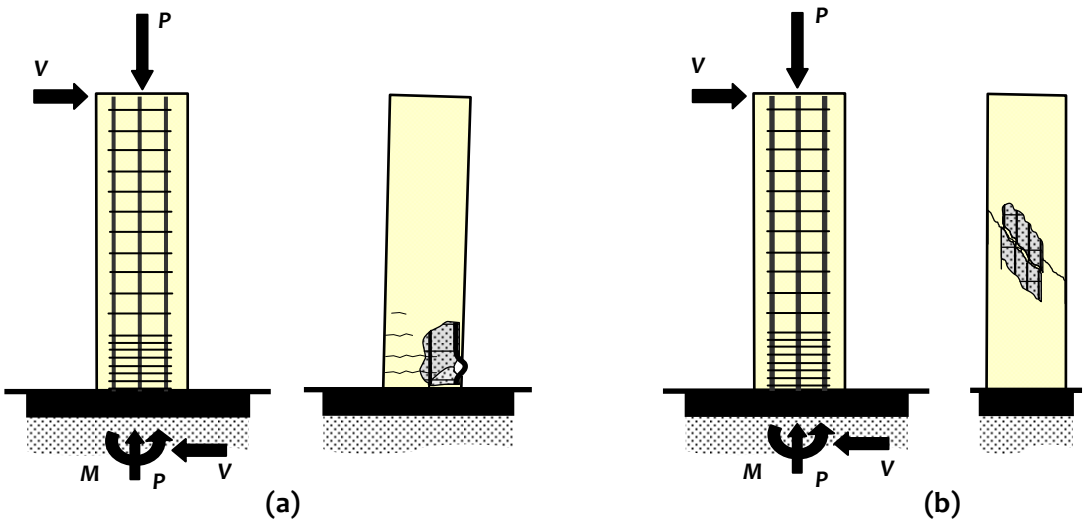

Figure 2.41: Influence of longitudinal reinforcement on flexural strength: (a) lightly reinforced, and (b) heavily reinforced piers

Bridge piers that are susceptible to the *combined flexure-shear failure* are *short columns* with a shear-to-span ratio 1.5-2.5; their ultimate performance is dominated by shear capacity [Sun *et al*, 2008]. Crack initiates as a flexural crack, but progresses in to becoming a diagonal shear crack. Flexural cracking is accompanied by yielding of longitudinal reinforcement leading to shear cracking of concrete. This is followed by concrete cover spalling, spiral reinforcement yielding, reinforcement exposing, longitudinal reinforcement buckling, and finally crushing of core concrete (Figure 2.42) [Zhu *et al*, 2007; Si *et al*, 2014]. At large displacements, shear cracks grow faster than flexural cracks, causing rapid reduction in shear strength resulting in premature brittle failure [Sun *et al*, 2008].

Shear Failure, brittle mode of failure is characterised by diagonal cracks in concrete, followed by rupture or opening up of transverse steel reinforcement and then by buckling of longitudinal steel reinforcement [Zhu, 2007]. This type of failure usually occurs in squat piers under high shear demand (Figure 2.43).

Location of failure in prismatic piers with varying reinforcement amount along the height shifts from the base of the pier, if not detailed properly. Usually, the amount of transverse reinforcement recommended by various design codes, outside the plastic hinge zone is almost 50% of that provided in the plastic hinge region. This reduction along with reduction in longitudinal reinforcement may meet the demand at that section, but may lead to undesirable brittle mode of failure, if not designed properly.

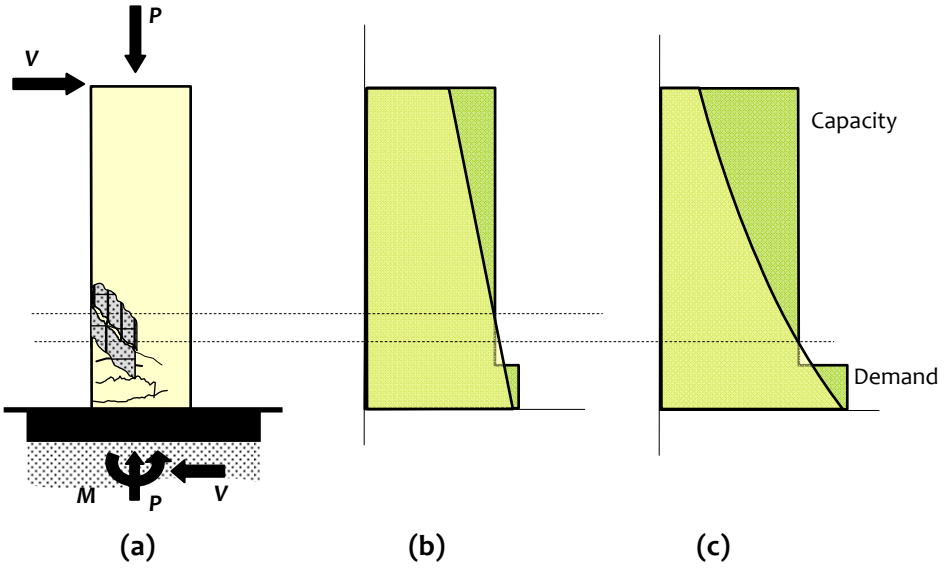

Figure 2.42: Combined flexure–shear failure of bridge piers: (a) pier subjected to equivalent seismic loading, (b) shear force diagram, and (c) bending moment diagram

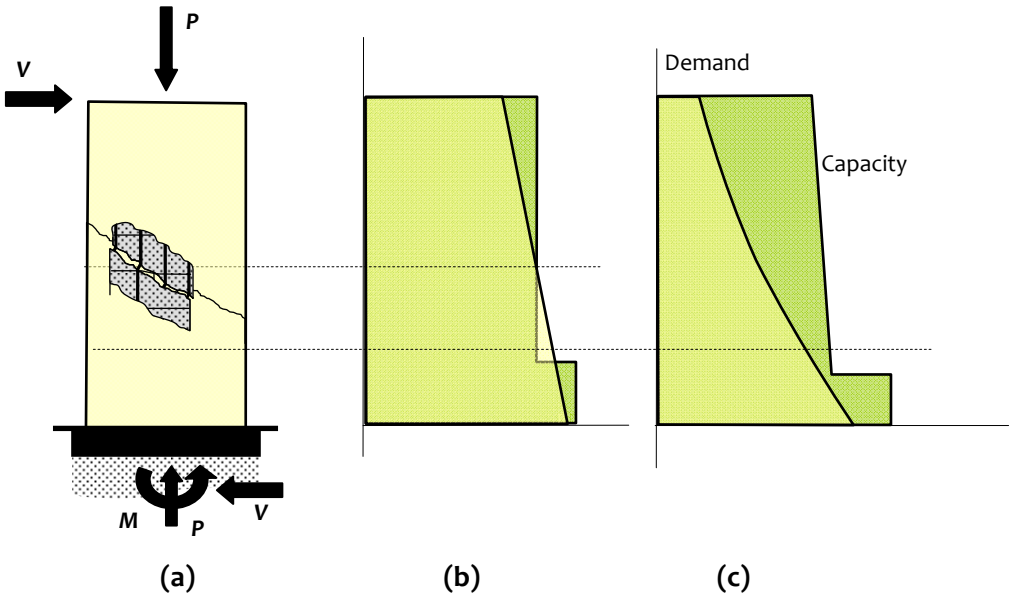

Figure 2.43: Shear failure in bridge piers: (a) pier subjected to equivalent seismic loading, (b) shear force diagram, and (c) bending moment diagram

When piers are flared, there is a gradual change in cross-section from a relatively narrow one to a wide one. Owing to this change, response of flared piers is quite involved under seismic action, because the flared part has larger flexural capacity. This causes failure location to shift away from the base. For a pier tapering upwards (Figure 2.44), flexural capacity increases towards the top, while demand increases towards base of the column. Two damage patterns are observed generally in these types of piers -

brittle failure at the bottom of the flare, and *flexural failure* near the base of the pier. When piers are flared towards bottom, (Figure 2.45) they have the advantage of increase in cross-sectional capacity in line with the demand. Here, the capacity is least near the top of flare, which is susceptible to failure.

Assessment of capacity of these piers necessitates an analytical tool that can mimic their response including the effects of deterioration of shear strength with increase in moment demand. Some analytical models are available to forecast the

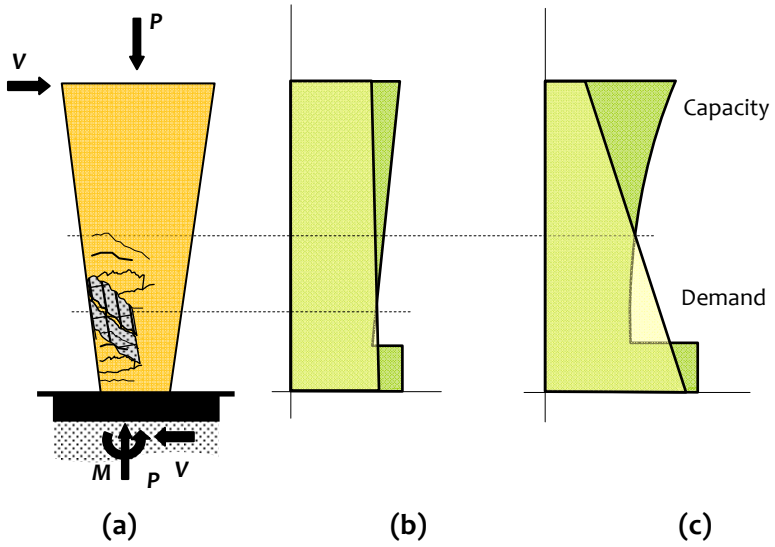

Figure 2.44: Location of failure of tapered bridge piers: (a) pier flared up, (b) shear force diagram, and (c) bending moment diagram

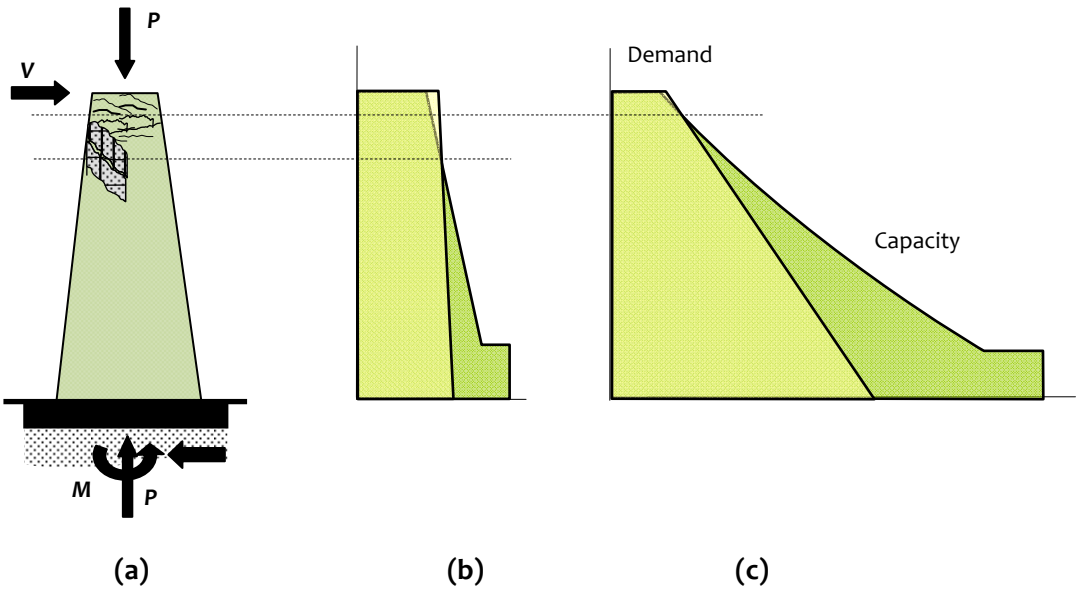

Figure 2.45: Location of failure of tapered bridge piers: (a) pier flared down, (b) shear force diagram, and (c) bending moment diagram

behavior of RC member (*e.g.*, *Strut and Tie Model*, *Modified Compression Field Theory etc.*), but they include complex analytical procedures that require *iterative* approach to arrive at end result; also, most of these methods are applicable for a limited range of slenderness (Figure 2.32). A consistent unified simple method is still lacking, which could predict the *failure load*, *failure mode* and *failure location* in single column RC bridge piers, to help practicing design engineers with assessment and seismic retrofit decision making of existing bridges.

2.5.1 Scope of Present Study

The present study focuses on the behavior of single column rectangular RC bridge piers subjected to combined earthquake and gravity loads. The following issues are addressed in the study:

(1) A consistent unified analytical method to predict initiation of damage in single column RC bridge piers of any slenderness with reliable accuracy, to arrive at a safe and conservative design;
(2) An adequate simplified method to assess the strength of piers, their failure type and location, when acted upon by combined stresses;
(3) The method should help explain step-wise progression of failure and contribution of main constituent materials towards shear resisting mechanism;
(4) Effects of key parameters in shifting the mode of failure from ductile to brittle, in piers, when pier geometry, reinforcement ratios, and axial load ratios vary.

The work is limited to study of behaviour of single column cantilever RC members with rectangular cross-section. Additional effects due to lateral deformation predominant in slender members, aggregate interlock, strain-rate and reversed-cyclic loading, and deficiencies in anchorage of reinforcement bars and bond strength are not considered.

3
RC Section Behaviour

3.0 INTRODUCTION

RC cross-sections are subjected to *combined axial, shear and bending action effects* during earthquakes. Neglecting the interaction of these combined effects overestimates the *lateral shear strength* of a RC pier, because shear strength reduces with increase in bending moment demand. In this chapter, an analytical method is proposed, to estimate *lateral shear strength* of a solid rectangular RC cross-section subjected to combined axial force, shear force and bending moment, and express the same as a function of geometric and mechanical properties of cross-section and its constituent materials.

3.1 BASIC CONSIDERATIONS

The mechanics of resistance of RC sections, under combined axial force, shear force and bending moment is established using *equilibrium* of forces and *compatibility* of strains within the cross-section, considering uniaxial *constitutive* relations of material. The *axial force – bending moment* envelope of the RC cross-section proposed in this chapter is in accordance with conventional method of strength estimation. The cross-section is discretized into a number of thin *fibres*, with width of each fibre being parallel to the axis of bending. Then, *shear force capacity* of *each fibre* of concrete is estimated, based on respective normal stresses acting on them, using the *normal stress – shear stress failure criterion*. *Confinement of concrete* and *strain-hardening of longitudinal reinforcement steel* are considered. For a specific *normal strain* distribution across the section, *normal stress* in concrete in each fibre is estimated using *average normal strain* in the fibre and the corresponding *uniaxial normal stress-strain relation* of concrete (Figure 3.1). Longitudinal reinforcing bars are represented by equivalent fibres at the centroid of each bar. *Normal stress* in longitudinal steel is computed using the *normal strain* at the equivalent fibre and the corresponding *uniaxial normal stress-strain relation* of reinforcing steel.

3.1.1 Basic Assumptions

The following assumptions are made in the proposed method:

(1) Plane sections normal to the longitudinal axis of the member remain plane even after deformation;
(2) Strength of concrete in tension is ignored for estimation of flexural strength;
(3) Concrete and reinforcing bars are perfectly bonded; and
(4) Normal stress-strain relations of concrete and steel are known, and can be expressed as general functions $\sigma_c=f(\varepsilon_c)$ and $\sigma_s=f(\varepsilon_s)$, respectively, where ε_c and ε_s are normal strains in concrete and steel, respectively.

3.1.2 Compatibility Conditions

Compatibility of strains in concrete and steel fibres is considered at all levels of load, thus neglecting bond slip and bond failure. Further, linear distribution of normal strain is assumed across the cross-section under flexural action (Figure 3.1). Thus, using strain compatibility conditions, the normal strain in each concrete and steel fibre (either in tension or compression) is given by,

$$\left.\begin{aligned} \varepsilon_{c,i} &= \varepsilon_o + y_i \Delta\varepsilon \\ \varepsilon_{sc,i} &= \varepsilon_o + y_i \Delta\varepsilon \\ \varepsilon_{st,i} &= \varepsilon_o + y_i \Delta\varepsilon \end{aligned}\right\}, \tag{3.1}$$

where

$$\varepsilon_o = \left(\frac{\varepsilon_{top} + \varepsilon_{bot}}{2} \right), \text{ and} \tag{3.2}$$

$$\Delta\varepsilon = \left(\frac{\varepsilon_{top} - \varepsilon_{bot}}{N} \right), \tag{3.3}$$

in which $\varepsilon_{c,i}$ is the average compressive strain in i^{th} fibre of concrete, $\varepsilon_{st,i}$ the average normal strain in i^{th} fibre of longitudinal steel in tension, $\varepsilon_{sc,i}$ the average normal strain in i^{th} fibre of longitudinal steel in compression, ε_o the average normal strain in the middle fibre, ε_{top} the average strain in the top concrete fibre, ε_{bot} the average strain in the bottom concrete fibre, N the total number of fibres, and y_i the distance to the centroid of the fibre i from the geometric centroidal axis of the cross-section.

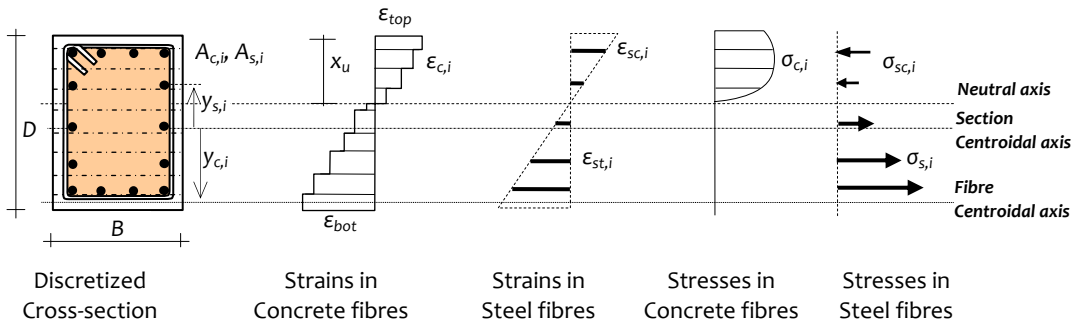

Figure 3.1: Discretization of cross-section and approximated normal strain and stress in fibres

3.1.3 Constitutive Relations

The stress-strain relations of constituent materials of the RC section significantly influence the axial, bending and shear strength of the RC member. The material constitutive law models depict the load-deformation relations of each fibre. Concrete and reinforcing steel constitute the materials of the RC cross-section. The *stress-strain relations* of *core* and *cover concretes* differ depending on the extent of confinement provided to the core concrete by transverse reinforcement; separate stress-strain relations are employed for *confined* and *unconfined concretes*. Similarly, stress-strain curve adopted for reinforcing steel has a *linear elastic portion*, and a *strain-hardening portion* that significantly affects the *moment-curvature estimate*. Hence, the constitutive relations reproduces the important nonlinear strength characteristics of both steel and concrete, and are described in the following subsections.

3.1.3.1 Steel

Stress-strain curve of reinforcing steel mentioned in IS:456-2000 is employed. It is modified by incorporating effect of *strain hardening*, to reasonably estimate normal stress with increase in normal strain. The stress-strain curve is smooth, with 15% strain hardening (Figure 3.2) (although about 25% strain hardening is reported for high strength deformed bars used for seismic applications [Paulay and Priestley, 1992]). Strain hardening is assumed to start soon after yielding, up to a maximum elongation of 20%, without any pure *elastic-plastic portion* [Park and Paulay, 1975].

3.1.3.2 Concrete

The monotonic stress-strain relations of *core* and *cover concretes* employed in this analytical method are as per the commonly used confinement model [Mander *et al*, 1988]. Figure 3.2 depicts envelopes of *confined* and *unconfined concretes* for the given material strengths and section geometry of RC member. Strain corresponding to 20%

drop in peak strength is considered as the ultimate strain in the study. Also, *normal stress - shear* stress interactions of concrete are considered separately for both core and cover concretes (Figure 3.2) as per a failure criterion developed for uniaxial shear and compression in 2D space [Bresler and Pister, 1958], and is given by:

$$\tau_{ci} = 0.1 f_c \sqrt{0.62 + 7.86\left(\frac{f_{ci}}{f_c}\right) - 8.46\left(\frac{f_{ci}}{f_c}\right)^2} \tag{3.4}$$

where τ_{ci} is the average shear stress, f_{ci} the average normal stress of i^{th} layer of concrete, and f_c the compressive strength of concrete.

3.2 *P-M* INTERACTION DIAGRAM

Axial-flexure (*P-M*) interaction curves used in design are traditionally developed using *Force-Based Method*. Design handbooks (*e.g.*, SP16-1978) provide design *P-M* curves for RC sections that are used commonly in design practice, thereby avoiding the computation of such curves by designers. This work uses *Strain-Based Method* to develop *P-M Curves* for use in nonlinear analysis, and proposes a strain-based, non-iterative, simplified procedure to obtain *Design P-M Curves* as per Indian design code for use in design (Annex A).

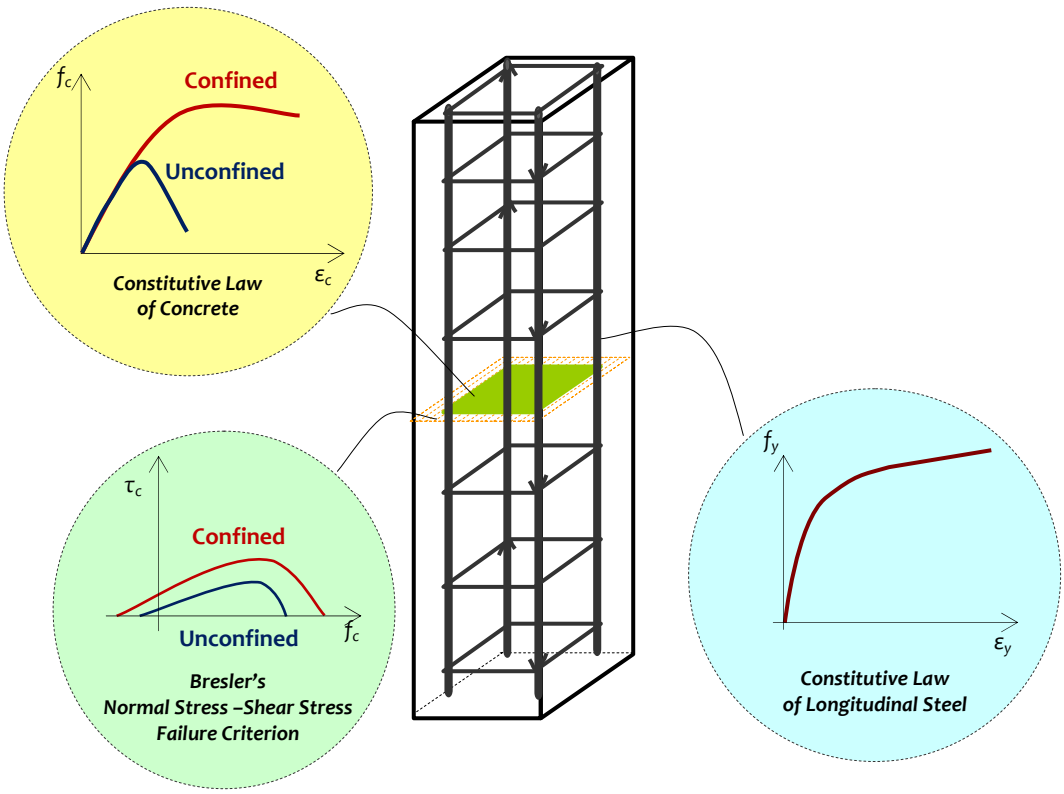

Figure 3.2: Schematic showing constitutive relationships considered in the analytical method

For developing *P-M Curves* (and thereby moment M – curvature φ curves at various axial load P levels), first the axial-flexure relation is determined of a section at a given axial load, by the *Strain-Based Method*, by increasing in increments the normal compressive strain in extreme compression concrete fibre. For each distribution of normal strain across the cross-section, the *normal strains* are computed in all concrete and steel fibres (using *compatibility conditions*) and *normal stresses* using the corresponding *normal stress - normal strain* constitutive relations. The axial force equilibrium is satisfied, as given by Eq.(3.5). Then, the bending moment capacity is computed (at the given axial load) using Eq.(3.6) for a given *normal strain distribution* representing a unique curvature.

$$\sum_{i=1}^{N_{cf}}(\sigma_{ci}A_{ci}) + \sum_{i=1}^{N_{sf}}(\sigma_{si}A_{si}) - P_{ext} = 0\,; \tag{3.5}$$

$$M = \sum_{i=1}^{N_{cf}}(\sigma_{ci}A_{ci}y_{ci}) + \sum_{i=1}^{N_{sf}}(\sigma_{si}A_{si}y_{si})\,; \tag{3.6}$$

where A_{ci} is the area of i^{th} layer of concrete, A_{si} the area of i^{th} layer of longitudinal steel, y_{ci} and y_{si} the distances to the centroids of the concrete and steel fibres i from the geometric centroidal axis of the cross-section, and N_{cf} and N_{sf} are total number of concrete and steel fibres, respectively.

P-M and *M-φ* curves of RC members of rectangular cross-section are generated numerically by a computer program. *M-φ* curves are determined of a given RC section at various levels of axial load, as discussed above. *M-φ* curves and *P-M* curve of a typical rectangular cross-section (of concrete of grade M30 and reinforcing steel of Fe415) are shown in Figures 3.3 and 3.4, respectively. With increase in compressive axial load, flexural rigidity increases, but the curvature corresponding to ultimate moment capacity reduces. The sharp reduction in moment capacity, as seen in Figure 3.3, occurs due to spalling of a portion of cover concrete (where the strain exceeds the unconfined concrete strain capacity), usually at higher axial load levels. Also, presence of axial loads significantly reduces curvature ductility of sections; at axial loads above the axial load P_b at balanced failure, curvature ductility is negligibly small even in an highly under-reinforced section. In general, curvature ductility of a section can be enhanced to a certain limit by providing confining transverse reinforcements with 135˚ hooks.

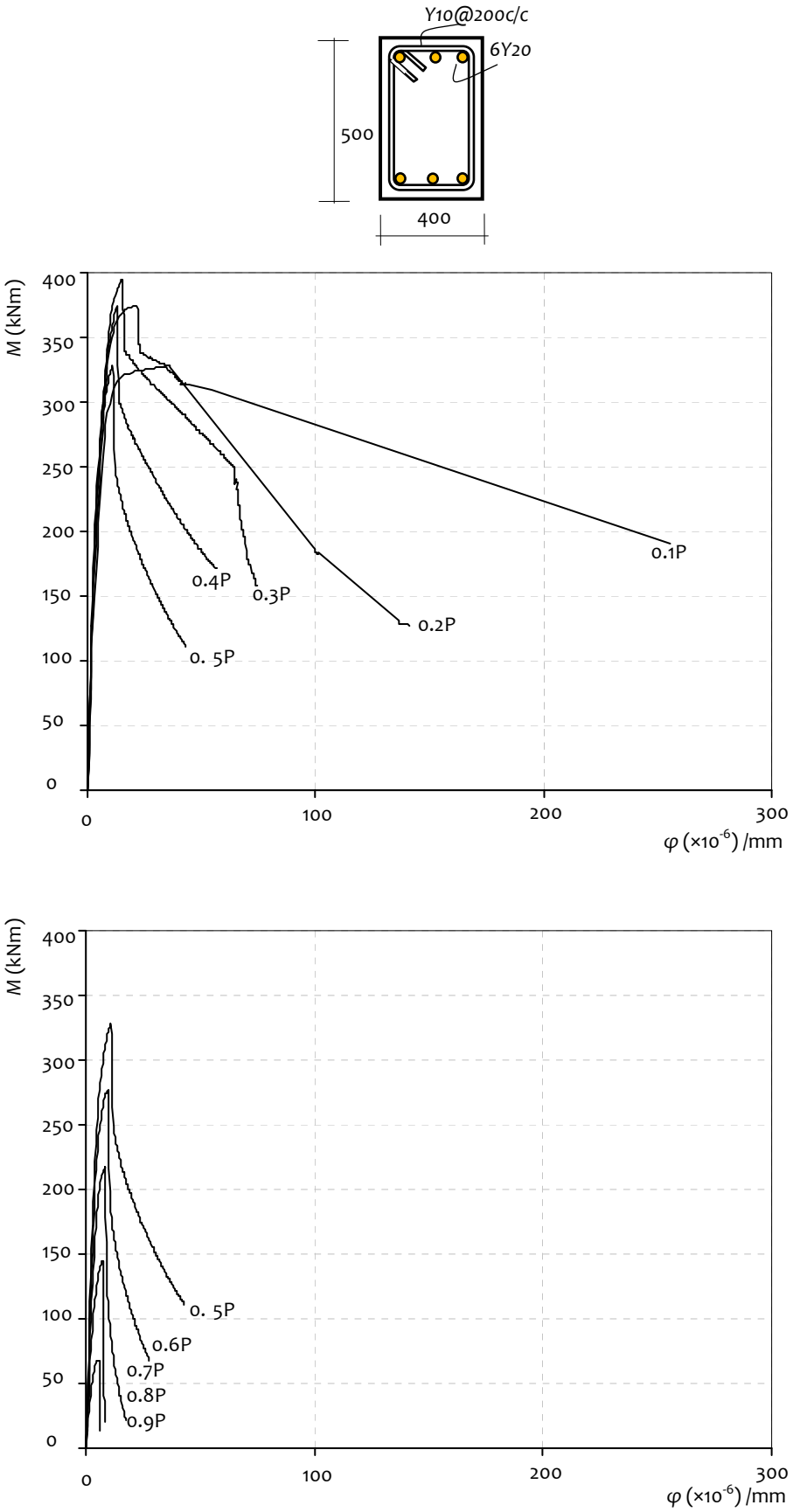

Figure 3.3: *M-φ* curves developed using proposed method at various axial loads

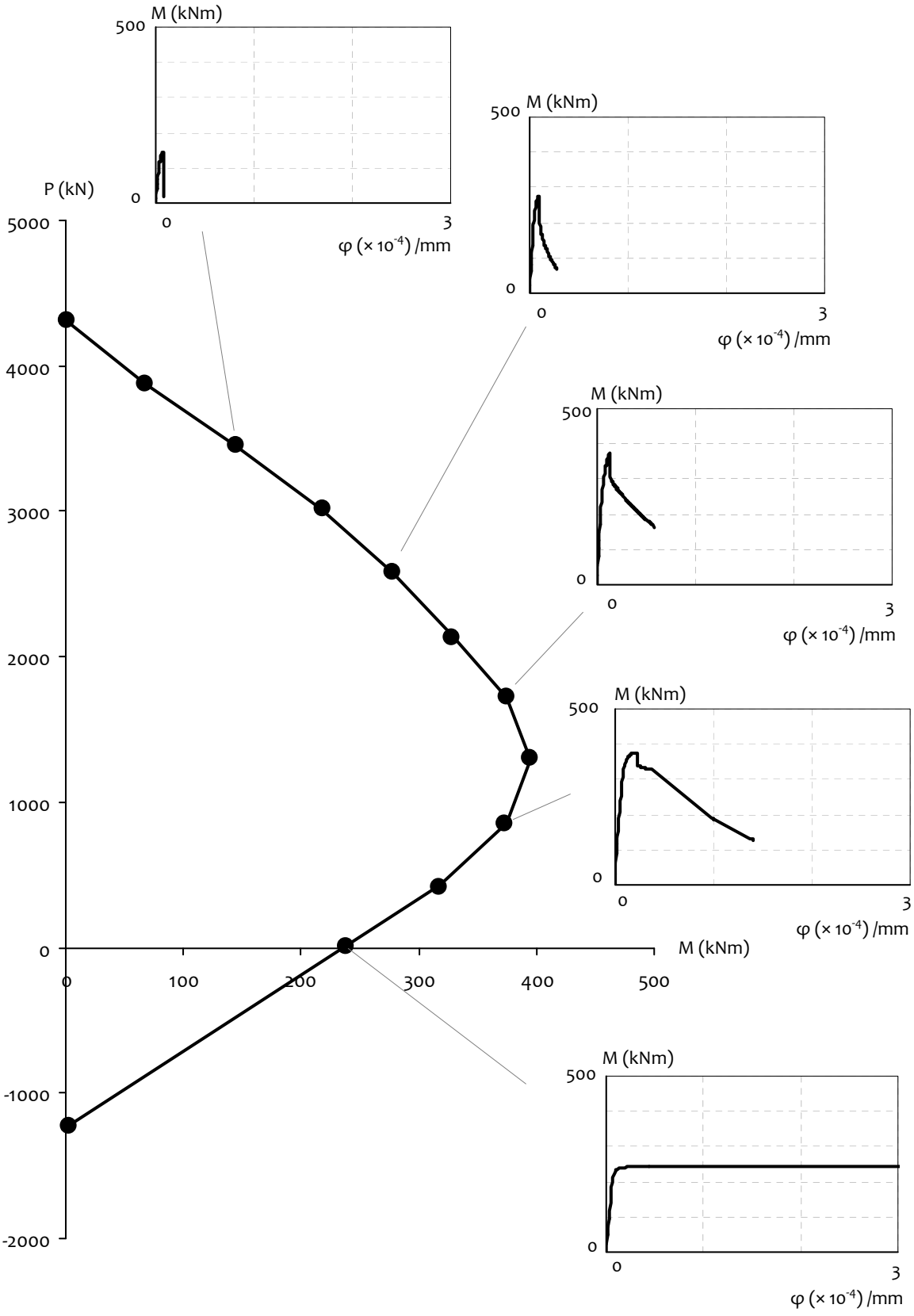

Figure 3.4: *P-M* interaction envelope: *M-φ* curves developed using proposed method at various axial loads

Results obtained using the proposed method are compared with *analytical* and *experimental M-φ* curves published in literature. Behaviour of both *short* and *slender* RC members are compared with different cross-sections and axial load levels. Column cross-section details are shown in Figures 3.5 and 3.6, along with results. Ultimate strength estimated using the proposed method is slightly on the higher side when compared to the published results of an analytical study (Figure 3.5), owing to different *concrete confinement models* used. The results of proposed method are compared with those from experimental studies conducted on RC cantilever column members subjected to constant axial load and cyclic lateral loads (Figure 3.6). The material laws incorporated in the proposed method do not account for effects of repeated loading on strengths and deformations. Two typical cases with shear span-to-depth ratios 2 and 5 are considered (with concrete cylinder strengths 34.5 MPa and 28 MPa, and yield strength of longitudinal reinforcing steel 375 MPa and 360 MPa respectively); a reasonable match is obtained of ultimate strength and ductility capacity in spite of neglecting the effect of repeated loading.

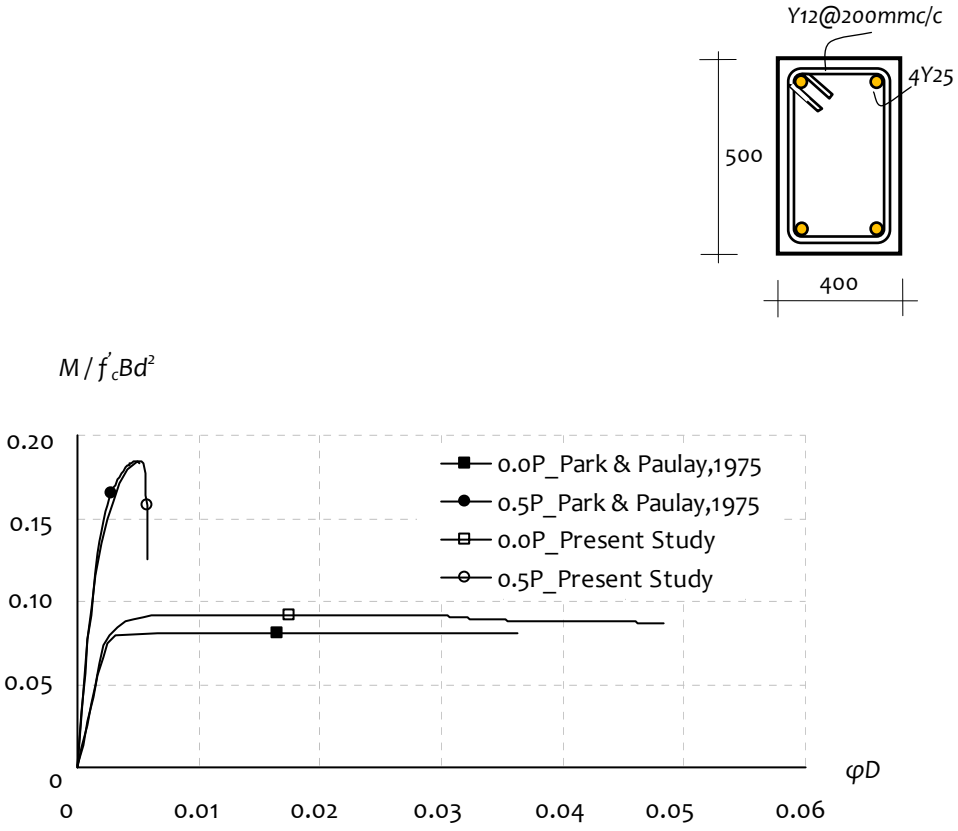

Figure 3.5: Comparison of *M-φ* curves developed using proposed method with those obtained from analytical method [Park and Paulay, 1975]

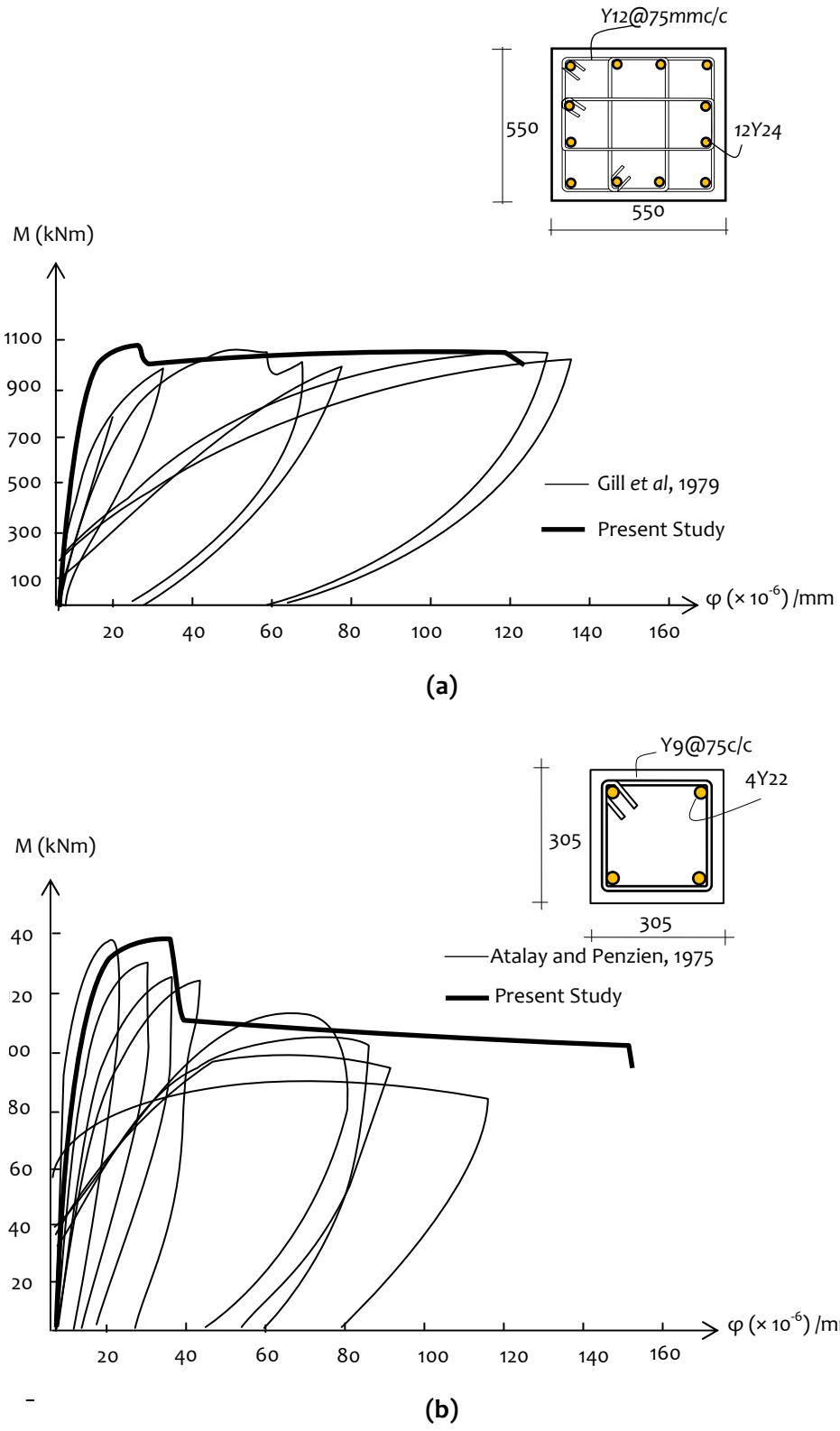

Figure 3.6: Comparison of *M-φ* curves developed using proposed method with those obtained from experimental results of specimens with (a) *a'/d* = 2 [Gill *et al*, 1979], and (b) *a'/d* = 5 [Atalay and Penzien, 1975]

3.3 PROPOSED METHOD OF ESTIMATING $P–V_c–M$ INTERACTION

The *P-M* interaction curve obtained by applying traditional section analysis satisfying the compatibility and equilibrium conditions (explained in the previous section), is coupled with *normal stress - shear stress* interaction. The shear force – bending moment interaction curves are estimated at the section level for each concrete fibre corresponding to the normal stress obtained from section analysis, using *normal-shear stress relation* proposed by *Bresler's Failure Criteria* [Bresler and Pister, 1958].

3.3.1 Axial – Shear ($P–V_c$) Interaction at Zero Bending Moment

To generate the P-V_c interaction curve, at zero bending moment, the procedure described below is followed. The *uniform* normal strain profile is estimated, corresponding to the maximum *pure* axial load compression capacity P_u of the section. Then, the coordinate 1 of the P-V_c curve (schematic shown in Figure 3.7) is established by summing up the shear forces of all fibres using Eq.(3.7); the shear stresses in each fibre being estimated corresponding to the normal stress using Eq.(3.4).

$$V_c = \sum_{i=1}^{N_{cf}} (\tau_{ci} A_{ci}), \tag{3.7}$$

where A_{ci} is area of i^{th} layer of concrete, τ_{ci} average shear stress of i^{th} layer of concrete, and N_{cf} the number of concrete fibres in the cross-section. At this stage, bending moment capacity of the section M_u =0, as it is estimated about the geometric centroidal axis of the section using Eq.(3.6). Now, the axial load level is reduced in steps (points 2, 3, etc., in

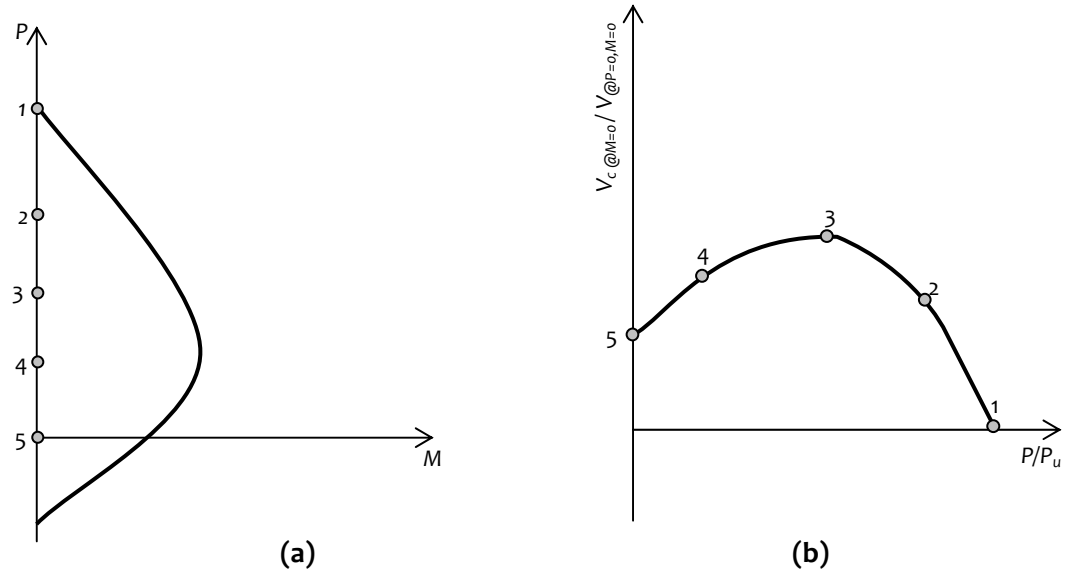

Figure 3.7: Schematic showing interaction envelopes for (a) axial–flexure interaction, and (b) axial–shear interaction corresponding to various axial load levels for reinforced concrete cross-section subjected to zero moment condition

Figure 3.7), and the stress profile corresponding to the uniform strain profile for the reduced axial load level pP_u is established and corresponding shear strength $V_{c\ @\ pPu}$ (concrete shear capacity V_c , at various level of axial load pP_u) evaluated. Shear strength of the section is *zero*, when the section is subjected to its maximum axial load capacity P_u, depicted by Point 1 in the Figure 3.7. Similarly, Point 5 represents the condition of *zero axial load* and *zero bending moment*.

3.3.2 Shear – Moment (V_c – M) Interaction at Axial Load Level

To generate the V_c - M interaction curve, at any given level of axial load, the procedure described below is followed. The uniform strain profile is first estimated corresponding to the given axial load level, pP_u. The coordinate 1 represented by $V_{c@P=pPu,M=0}$ (concrete shear capacity V_c at zero bending moment for various level of axial load pP_u) of the V_c-M curve (schematic shown in Figure 3.8) is established by summing up the shear forces in all layers using Eq.(3.7), which is estimated from the corresponding normal stress developed in each fibre using Eq.(3.4). Then, axial strain is increased in small steps of the topmost compression fibre, and the strain gradient is iterated until the resultant axial force is equal to the resultant applied load. Once the strain profile is determined, the stresses in the fibres are updated and the P and V_c generated are estimated using the equilibrium equations, Eqs.(3.5) and (3.7), respectively, thereby locating the next coordinate, coordinate 2 of V_c-M curve. The next increment to the strain profile is applied, and normal stresses in the fibres are updated, and the new stress profile is estimated to obtain the next point on the V_c-M curve.

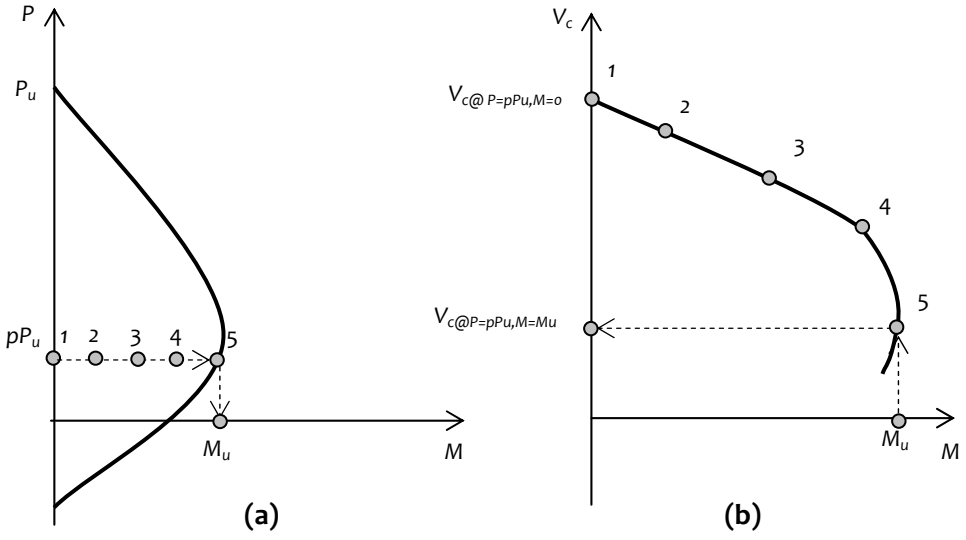

Figure 3.8: Schematic showing interaction envelopes for (a) axial–flexure interaction, and (b) shear–flexure interaction corresponding to pP_u for reinforced concrete cross-section subjected to combined stresses

Using the proposed method, V_c-M interaction envelope is developed for a prismatic rectangular RC section at different axial load levels; this envelope presents the effects of *axial force* and *bending moment* on *shear force capacity* of the cross-section considering contribution of concrete alone. Typical V_c-M curves are shown in Figure 3.10 of a square RC section; grade of concrete considered is M30 and both transverse and longitudinal reinforcement steels are Fe415.

Typical normalised interaction curves, namely *shear force capacity – axial load capacity*, and *shear force capacity – bending moment capacity*, of a square section obtained by the proposed method, are shown in Figures 3.9 and 3.10, respectively. The key observations made are:

(a) for any given level of axial load ratio p, shear strength V_c (at M=0) increases with increase in compressive axial load P up to about $0.5\ P_u$, and decreases sharply with further increase in axial load ratio; variation is shown in Figure 3.9 of normalized shear strength of concrete V_c (at $M=0$) with respect to the shear strength $V_{P=0,M=0}$ (at $P=0$ and $M=0$), as a function of axial load ratio p (= P/P_u).

(b) for any given level of axial load ratio p, shear strength V_c contributed by concrete decreases with increase in bending moment M demand of the section (Figure 3.10); the reduction is fast as the section approaches its *bending moment capacity*. This observation reinforces the concept that shear capacity is significantly reduced of RC sections due to flexural demand, as in potential plastic hinge regions, and thus, seismic design of such regions require consideration of P-V_c-M interaction.

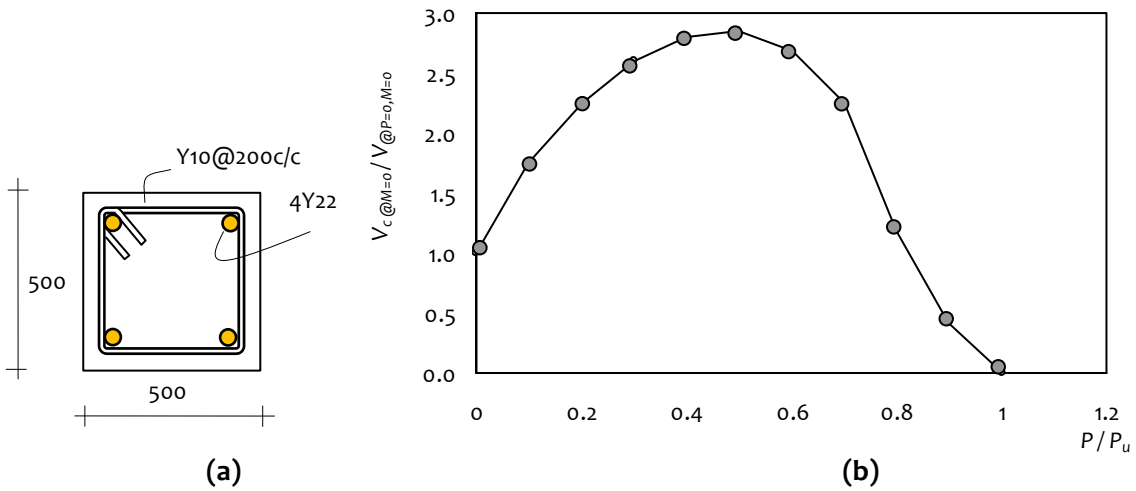

Figure 3.9: Shear capacity of concrete in a typical rectangular RC section: (a) cross section details, and (b) normalised shear force capacity of concrete at zero bending moment at various levels of axial load.

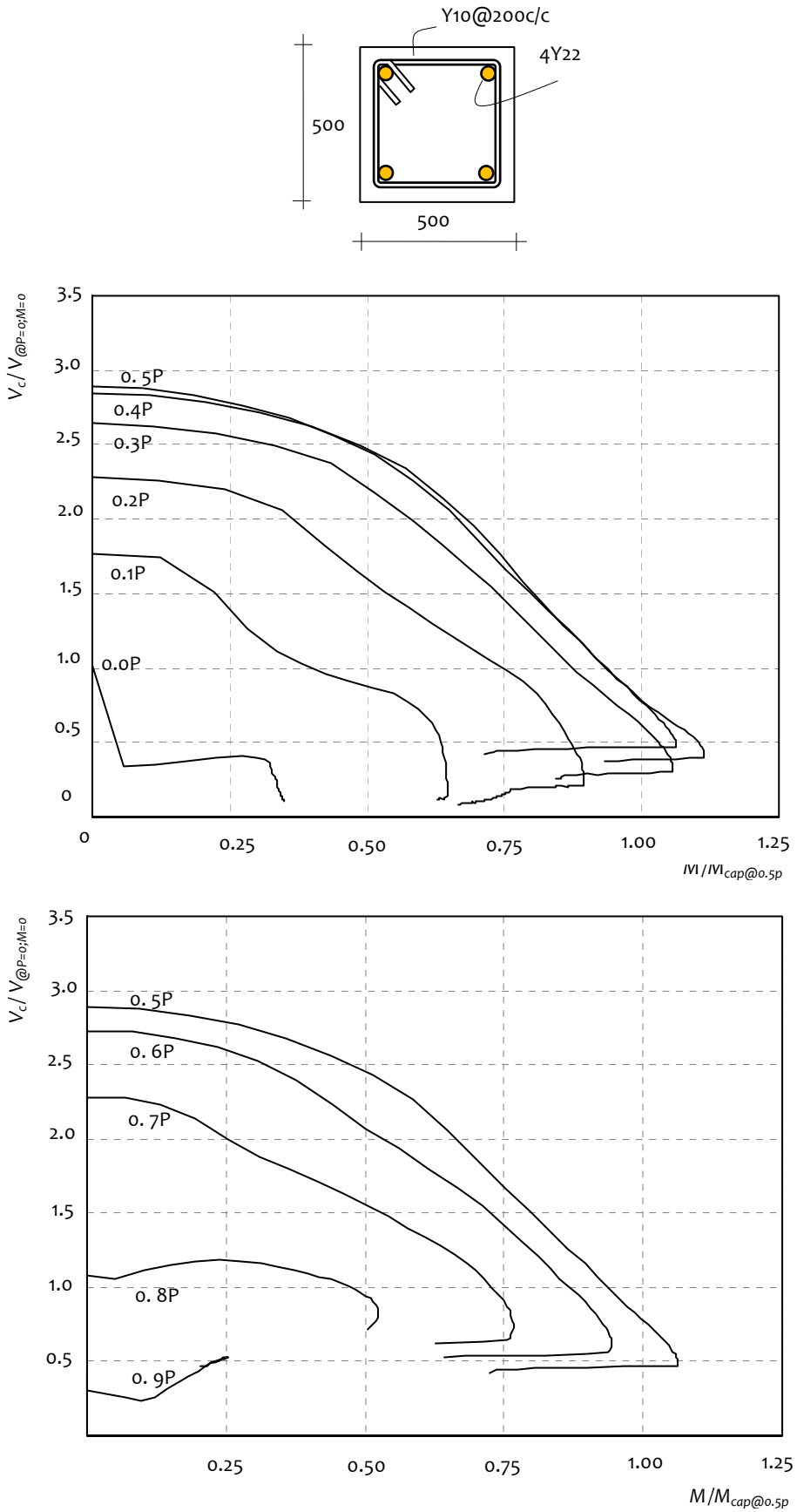

Figure 3.10: Shear strength of concrete for a typical rectangular RC section at different levels of axial load: Normalised V_c-M interaction curves

Further, increase in grade of concrete results in increase in shear force capacity of a RC section, although enhancement in moment capacity of the RC section with increase in compressive strength of concrete is not significant (Figure 3.11). This is because, moment capacity of an under-reinforced RC section is not significantly affected by compressive strength of concrete. On the other hand, the enhancement of shear strength is due to the increase in *shear stress* capacity of concrete with increase in compressive normal stress, as governed by Eq.(3.4), depicted in Figure 3.12. A detailed study is performed of shear capacity of *RC members* considering effect of five influencing parameters (namely member slenderness ratio, cross-sectional plan aspect ratio, transverse reinforcement ratio, longitudinal reinforcement ratio, and axial load ratio,); these results are presented in Chapter 4.

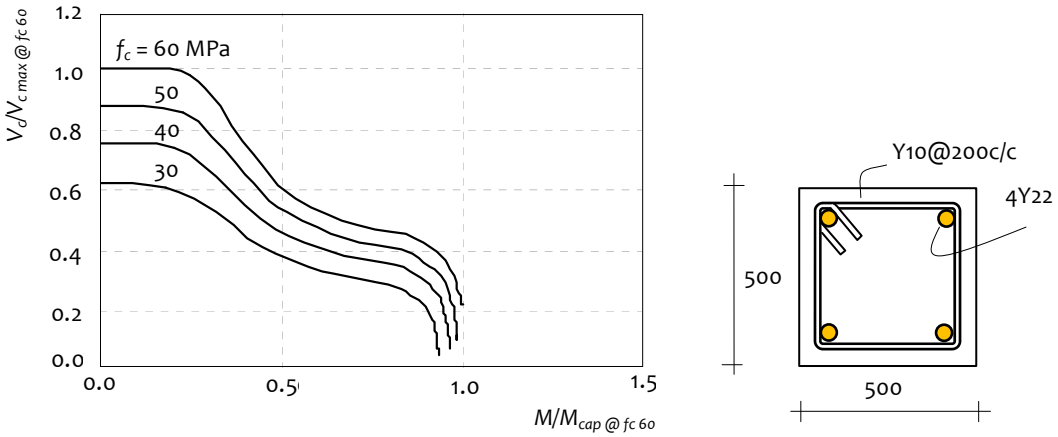

Figure 3.11 Effect of compressive strength of concrete on shear and flexural strengths of a RC section

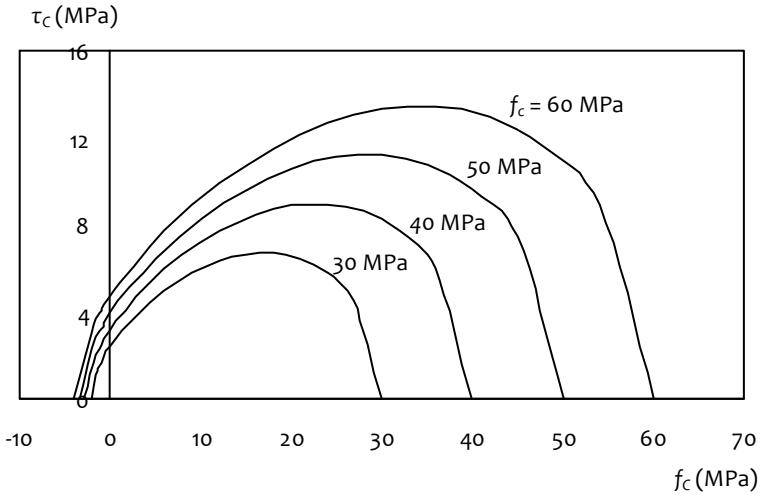

Figure 3.12: Shear stress – normal stress interaction curves of various grades of concrete

3.4 SUMMARY

A simplified *mechanics-driven method* is presented for estimating *P-V_c-M* interaction curves of rectangular RC cross-sections. Influences are included of *bending moment and axial load* on *shear force capacity* of rectangular RC sections, to account for combined effects of lateral and gravity loads, through a *shear stress capacity – axial stress capacity expression* and conventional sectional analysis. Also, a simple hand calculation based method is presented to obtain the design *P-M* curve, and numerical examples are shown in Appendix A to understand better the nuances in the method. The results from the analytical methods are compared with numerical and experimental results available in literature.

Blank page

4
RC Member Behaviour

4.0 INTRODUCTION

The three critical aspects required for understanding safety of a RC pier under the combined effects of *gravity loads* and *earthquake shaking* are: (i) *lateral shear force capacity*, (ii) *type* of failure, and (iii) *location* of failure. This chapter proposes a simple method to ascertain these three. The said method adopts a *simple mechanistic approach* to estimate lower bound *lateral shear force capacity* of a RC member. The *bending moment capacity* of the RC cross-section is estimated by traditional *moment-curvature analysis* using classical fibre discretization. In the proposed method, *shear force capacity* of each concrete fibre is estimated, using the *normal stresses* imposed on the fibre (caused by axial load and bending moment acting on the section); for this, *normal stress – shear stress failure criterion* is used as explained in Chapter 3. Contributions transverse and longitudinal reinforcing steels are considered, in addition to that by concrete, for estimating the behaviour of *RC members* of solid rectangular cross-sections.

4.1 MECHANISM OF RESISTANCE

Under earthquake ground shaking, shear force V is co-induced in RC piers with axial load P and bending moment M. Ignoring interaction between V and P & M leads to underestimation of deformation and overestimation of energy dissipation capacity of member, because premature shear failure is suppressed [Lee and Elnashai, 2001]. Design provisions of current Indian code, and many international codes, require that P-M interaction be considered separately in design of RC members, from V. Also, experimental data from *shear-sensitive* RC members suggest that the *type* of failure in such members is governed mainly by the *amount & spacing* of reinforcements, and *level* of axial load [Ranzo and Petrangeli, 1998]. Rational method to estimate shear force capacity of RC piers should include combined P-V-M effect induced during strong earthquake shaking.

4.1.1 Proposed Method for Estimating Overstrength Shear Force Capacity

P and M capacities of RC sections are determined using strength estimation approach explained in Chapter 3. In addition, the shear force capacity V of RC members is determined in *two stages*; in the first stage, contribution V_c of concrete is determined using *Section Strength Approach* (presented in Chapter 3), and in the second, contributions V_{st} and V_{sl} of transverse and longitudinal reinforcement, respectively, are determined using *Member Strength Approach* (which considers *direct tensile action* of transverse reinforcement and *dowel action* of longitudinal reinforcement), presented in the following. The *mechanism of resistance* of RC members (under combined action of P, V and M) is an outcome of the said process that uses:

(a) Equilibrium of forces,
(b) Compatibility of strains within the cross-section, and
(c) Uniaxial material constitutive relations.

Shear force demand is examined in light of the *P-V-M strength envelope* of the RC member to determine: (i) *mode of failure*, (ii) *location of failure*, and (iii) *load at failure*.

Contributions to shear force capacity V of RC members are determined by:

(a) Contribution V_c of concrete is estimated using Eq.(3.7), in which shear stress at a given section is calculated as summation of shear force capacities in fibres corresponding to normal stresses acting on them;
(b) Contribution V_{st} of transverse reinforcement (stirrups) intercepting shear cracks is estimated considering direct tensile action induced in them (which is governed by the angle of crack passing through the RC member); and
(c) Contribution V_{sl} of longitudinal reinforcement is estimated considering dowel action; this is activated only after the entire concrete section is cracked and the crack passes through the entire member cross-section.

Simple expressions are derived for computing crack angle and shear strength contributions of transverse and longitudinal reinforcements, respectively.

4.1.1.1 Contribution of Concrete

The shear force capacity contribution V_c of concrete (Figure 4.1) is estimated using Eq.(3.7) as the summation of shear forces capacity remaining in each concrete fibre (using shear stress τ_{ci} in fibre i at a given cross section corresponding to its normal stress f_{ci} imposed due to axial force and bending moment, using the *normal stress – shear stress*

strength envelope relation given by Eq.(3.4)). Thus, the shear force capacity at a section is a function of the level of axial force and bending moment at the section. For single cantilever piers, variation of axial force at different sections along the length of the member is considered to be negligibly small; only variation of bending moment is considered along the length of the member in estimating V_c at different sections.

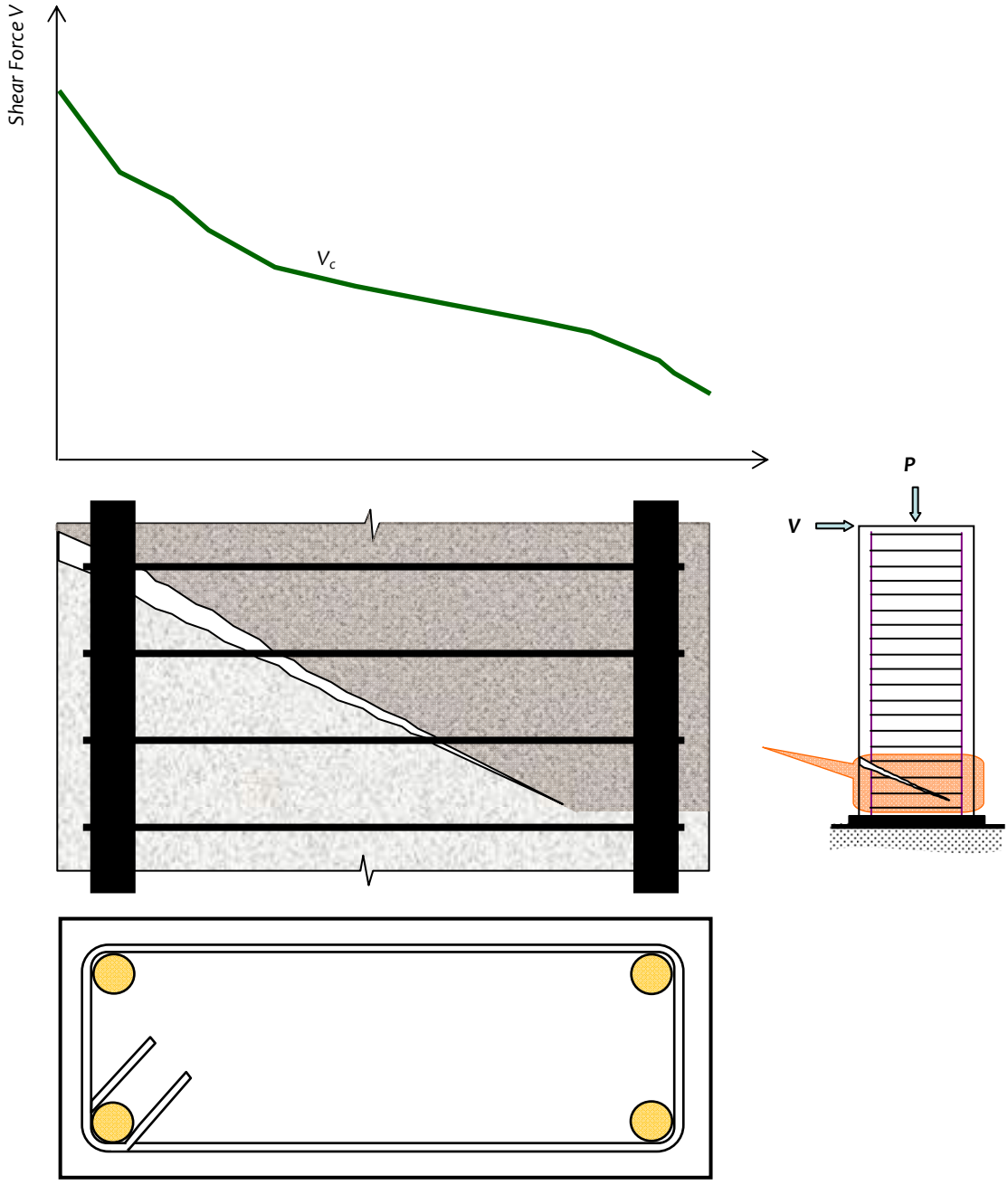

Figure 4.1: Uncracked portion of cross-section results in the contribution of concrete to shear strength

4.1.1.2 Contribution of Transverse Reinforcement

The crack angle α in a RC member is measured with respect to the normal to the longitudinal axis of the member. It takes values of 90˚, 45˚ and 0˚, respectively, when subjected to pure axial compressive force *P*, pure lateral shear force *V*, and pure bending moment *M*. In general, under the combined action of *P*, *V* and *M*, α can be estimated by:

$$\alpha = \frac{\pi}{4} + \frac{1}{2} tan^{-1}\left(\frac{P}{V}\right) - \frac{1}{2} tan^{-1}\left(\frac{M}{VD}\right). \tag{4.1a}$$

Using *V* (=*M*/*L*) in the Eq.(4.1a), α can be estimated by:

$$\alpha = \frac{\pi}{4} + \frac{1}{2} tan^{-1}\left(\frac{PL}{M}\right) - \frac{1}{2} tan^{-1}\left(\frac{L}{D}\right). \tag{4.1b}$$

When shear force *V* induced during *severe* earthquake shaking is large, α estimated using Eq.(4.1) is:

$$\alpha \begin{cases} \approx \frac{\pi}{4} & \text{for small } (L/D) \\ < \frac{\pi}{4} & \text{for large } (L/D) \end{cases}. \tag{4.2a}$$

Similarly, when shear force *V* induced during *minor* earthquake shaking is small, α estimated using Eq.(4.1) is given by:

$$\alpha \begin{cases} \approx \frac{\pi}{2} & \text{for small } (L/D) \\ \approx 0 & \text{for large } (L/D) \end{cases}. \tag{4.2b}$$

Thus, the range of possible crack angle α is 0˚< α <90˚. Depending on the crack angle α, the crack will be intercepted by a finite number of stirrups, which then contribute to shear force capacity of the RC member (Figure 4.2). The total shear strength contribution V_{st} of transverse reinforcement is given by:

$$V_{st} = \sum_{i=1}^{n} F_{yi} A_{sti}, \tag{4.3}$$

where F_{yi} is the yield strength of stirrup *i*, A_{sti} the total cross-sectional area of stirrup *i* intercepting the crack at a given section, and *n* the total number of stirrups intercepting the crack along the length of the RC member.

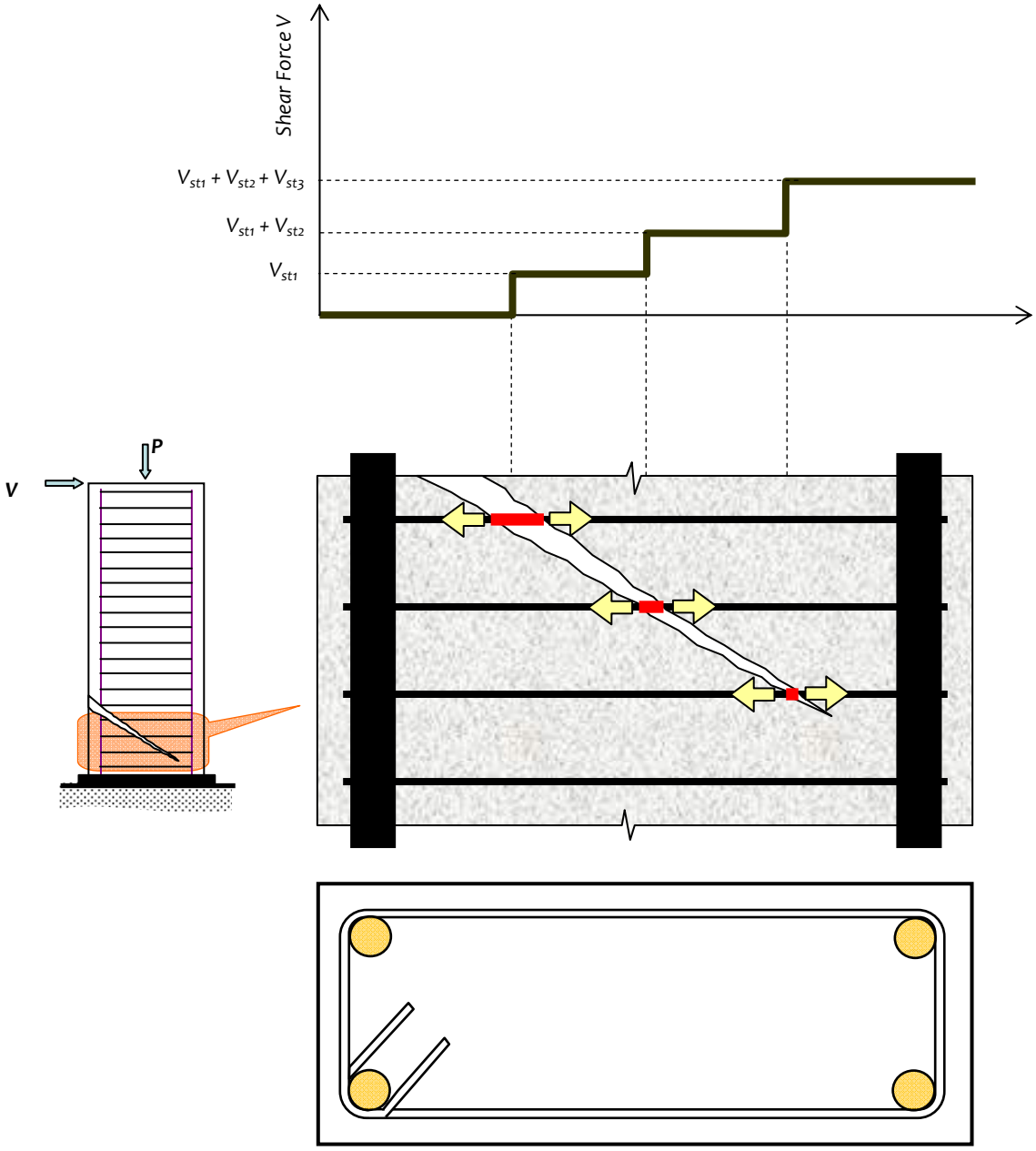

Figure 4.2: Shear crack crossing the transverse reinforcement results in the contribution of transverse reinforcement to shear strength

4.1.1.3 Contribution of Longitudinal Reinforcement

Assumptions are made in estimating contribution of longitudinal reinforcing bars through *dowel action* to shear resistance of RC members. When the crack is not through, longitudinal reinforcement offers some amount of shear resistance through dowel action; but this is relatively small [Hassan *et al*, 2008]. Similarly, effect of kinking of longitudinal bars is insignificant, because crack width of concrete remains small relative to the diameter of bar at the initiation of dowel action. With widening of cracks

or when the crack runs across the cross-section, the contribution of concrete to the shear resisting mechanism reduces and dowel action starts playing important role in shear resistance [He and Kwan, 2001; Tompos and Frosch, 2002; Park *et al*, 2012]. Thus, it is assumed that the predominant dowel action is due to unrestrained double curvature bending of the reinforcing bars between two adjacent stirrups with full rotational fixity (Figure 4.3). Thus, in the plastic hinge, plastic moment in the bar of radius r is given by:

$$M_p = \frac{4}{3} r^3 F_y , \tag{4.4}$$

The maximum displacement of the longitudinal bar between the two stirrups (where the longitudinal bar is assumed to be fixed) under double curvature bending can be estimated by:

$$\Delta_y = \frac{2}{9EI} L^2 r^3 F_y , \tag{4.5}$$

Thus, the shear resistance V_{sl} offered by dowel action of n_l longitudinal bars is given by:

$$V_{sl} = \frac{n_l d^3}{3 s_v} F_y , \tag{4.6}$$

where s_v is the spacing of stirrups, d the diameter of longitudinal bar, F_y the yield strength, E the modulus of elasticity, I the moment of inertia of cross-section of longitudinal bar, and n_l the total number of longitudinal bars. The total shear resistance V_{sl} offered by dowel action is considered to be mobilised only when the shear crack propagates across the entire cross-section (Figure 4.4).

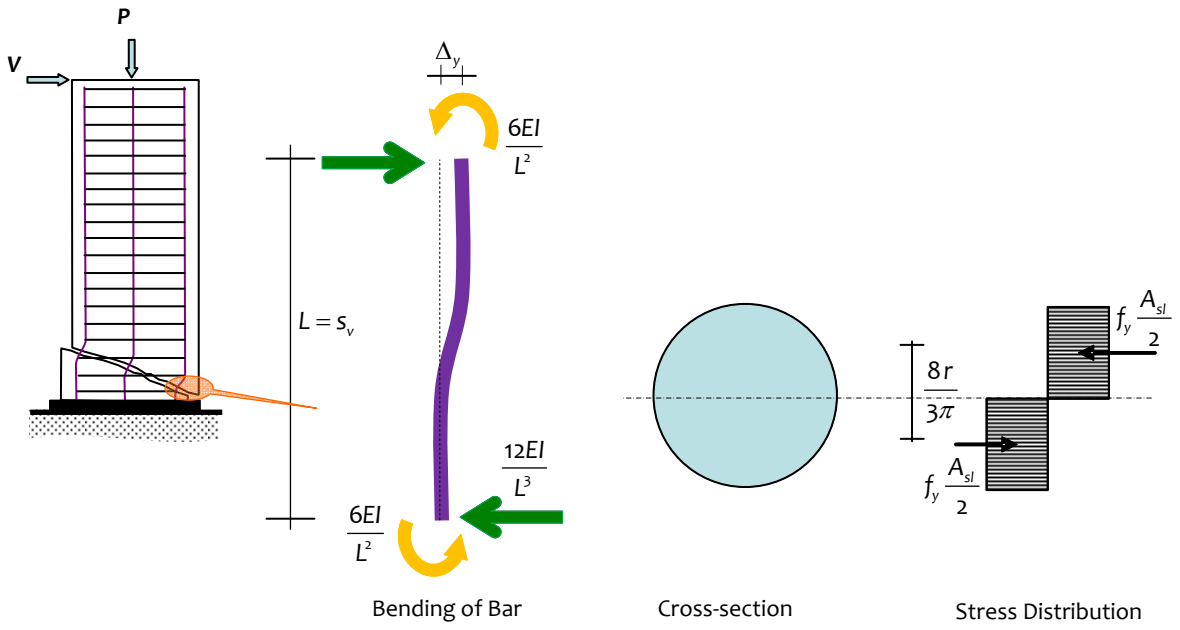

Figure 4.3: Schematic showing bending of longitudinal bar due to dowel action and the forces acting along the bar and across the section

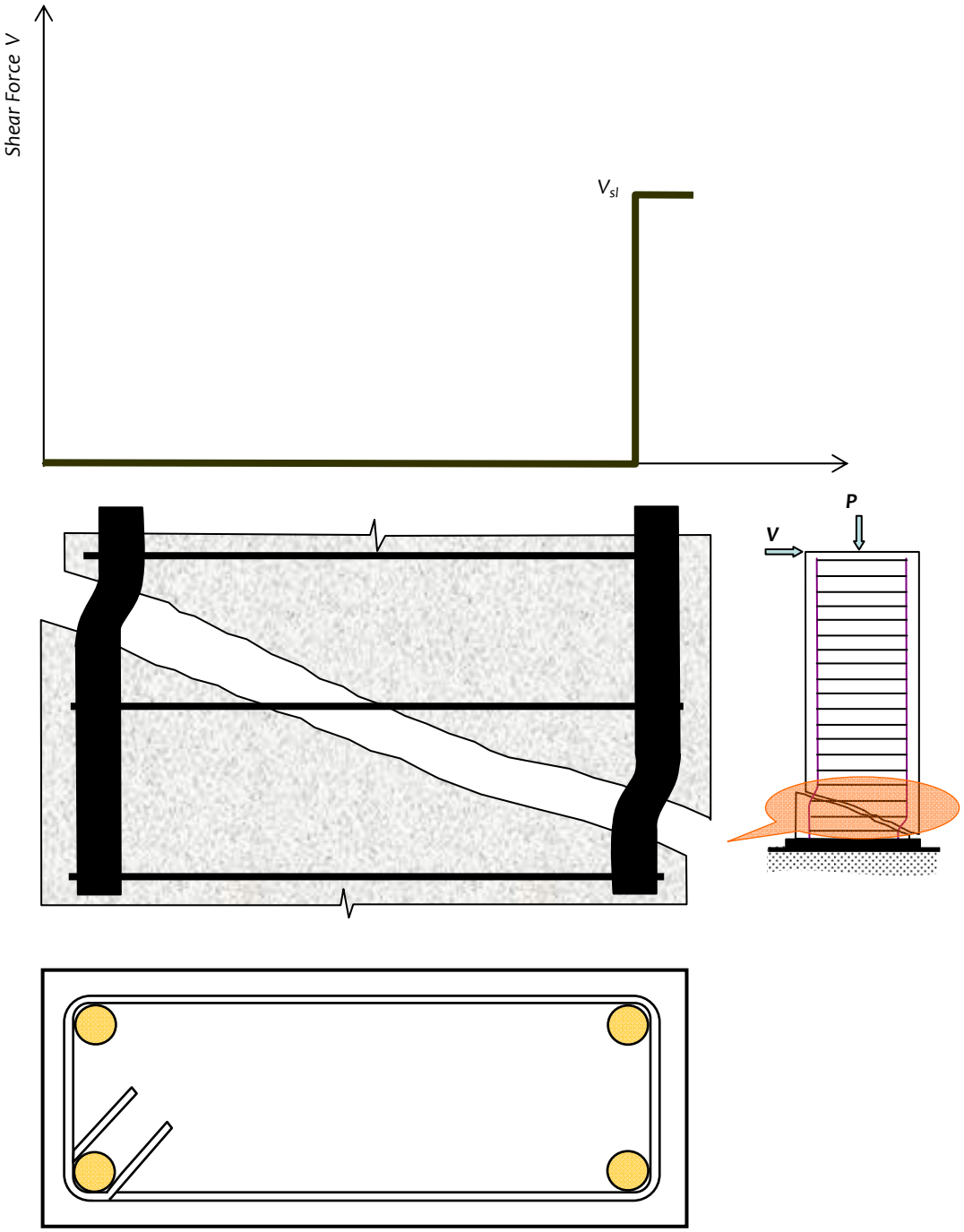

Figure 4.4: Shear crack crossing the longitudinal bars results in the contribution of longitudinal bar to shear strength

4.1.1.4 Lateral Shear Force Capacity of RC Members

Lateral shear force capacity of a RC member is estimated using V_c-M strength interaction envelop of the cross-section for a given axial load P, and contributions V_{st} and V_{sl} of transverse and longitudinal reinforcements. Schematically, Figure 4.5 shows how a prismatic cantilever RC member fails in *shear*, with uniform distribution of both transverse stirrups along the length of the member and longitudinal bars.

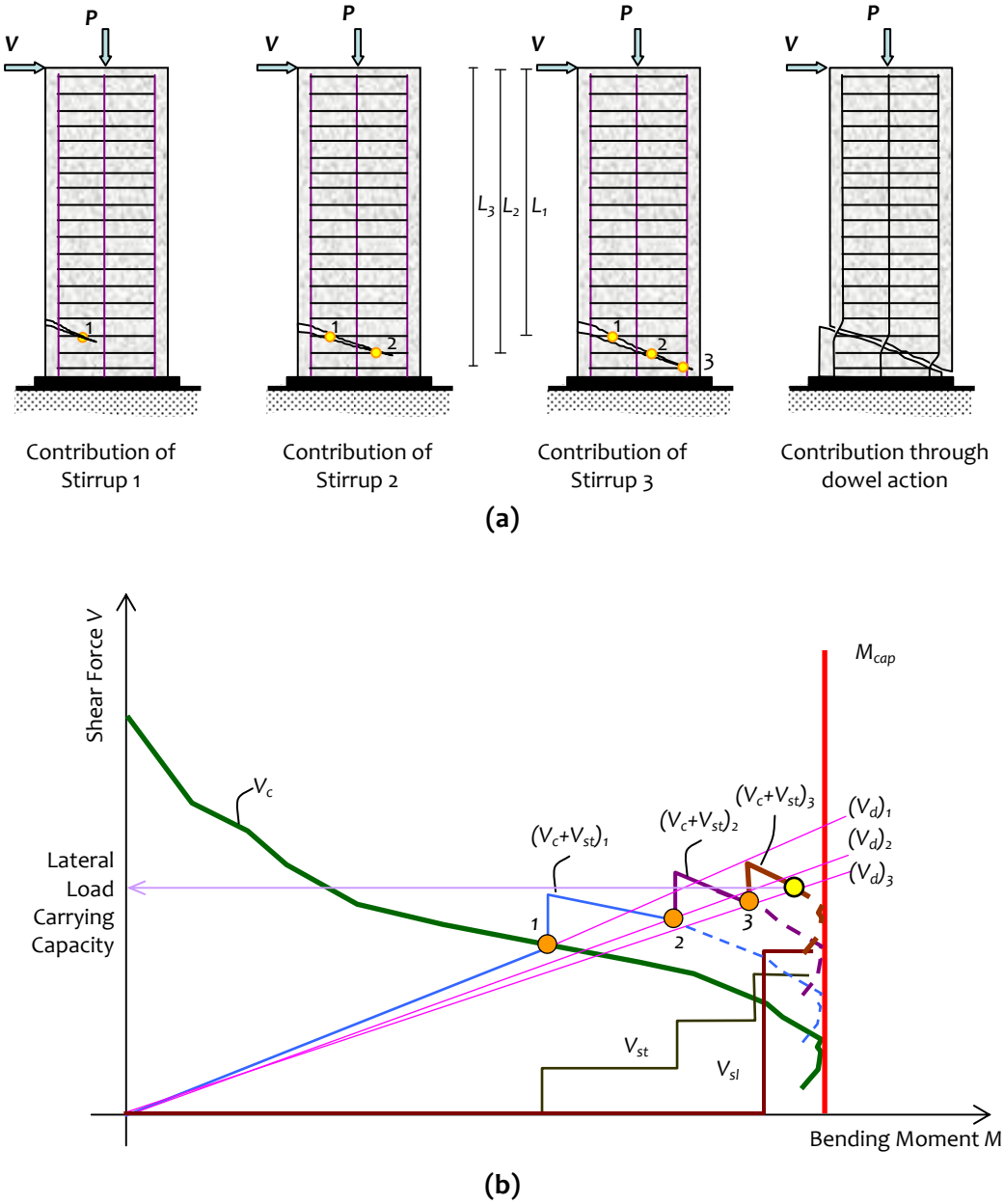

Figure 4.5: (a) Crack propagation across the member, and (b) shear resistance mechanism in a RC member, for a considered value of compressive axial load *P*

Salient features are discussed of the *V-M* interaction diagram (Figure 4.5b) and of the associated shear transfer mechanism in the member:

(a) Salient Features

The salient features of the member *V-M* interaction diagram (Figure 4.5b) are presented in Table 4.1.

Table 4.1: Descriptions of curves and lines on the *V-M* interaction diagram

Curve or Line	*Represents*
Curve V_c	Contributions of concrete (for given M and compressive P) to shear resistance of RC member
Line V_{st}	Contributions of stirrups through direct tensile action to shear resistance of RC member
Line V_{sl}	Contribution of longitudinal bars through dowel action to shear resistance of RC member
Line M_{cap}	Limit of flexural capacity of RC member at stirrups 1, 2 and 3; for a RC member with prismatic cross-section and uniform reinforcement, these three limits are the same
Lines $(V_d)_1$ $(V_d)_2$ $(V_d)_3$	Lateral shear force *demand* at stirrups 1, 2 and 3, respectively, corresponding to the bending moment at the stirrup levels
Curves $(V_c+V_{st})_1$ $(V_c+V_{st})_2$ $(V_c+V_{st})_3$	Contributions of concrete and stirrups to shear resistance of RC member

(b) Shear Resistance Mechanism

The shear resistance mechanism is discussed with reference to Figure 4.5b. The contribution of concrete to shear resistance reduces with increase in moment demand (*Curve* V_c). Initially, concrete alone contributes to shear resistance. As the imposed lateral deformation increases on the member, both shear force and bending moment increase linearly (demand *Line* $(V_d)_1$). When the demand line crosses the original concrete resistance *Curve* V_c (at point 1), the crack (defined by angle α in Eq.(4.1)) grows from the left side of the member until intercepted by stirrup 1 (at a distance L_1 from the loading point at top). Then, the stirrup also contributes to shear resistance (first jump in *Line* V_{st}). Thus, concrete and stirrup 1 (at level 1) together contribute to meet the demand (*Curve* $(V_c+V_{st})_1$). With further increase in lateral deformation, contribution V_c of concrete decreases with increase in bending moment (*Curve* $(V_c+V_{st})_1$) until the demand *Line* $(V_d)_2$ (at stirrup *2*) crosses the capacity *Curve* $(V_c+V_{st})_1$. At this stage, the shear crack grows further until intercepted by stirrup 2. Again, stirrup 2 (at a distance L_2) contributes to shear resistance (second jump in *Line* V_{st}). Thus, concrete and stirrups 1 & 2 together contribute to shear force capacity (*Curve* $(V_c+V_{st})_2$). This process continues as the crack propagates across the entire cross-section, and all n stirrups contribute step-by-step to shear force capacity. Once the crack passes through the entire section (point *3*), the contribution of concrete is exhausted, and *only then*, longitudinal reinforcement starts contributing to shear capacity through *dowel action* (demand *Line* (V_{sl})); this contributes to *residual* lateral shear force capacity of the member, along with stirrups (Figure 4.6).

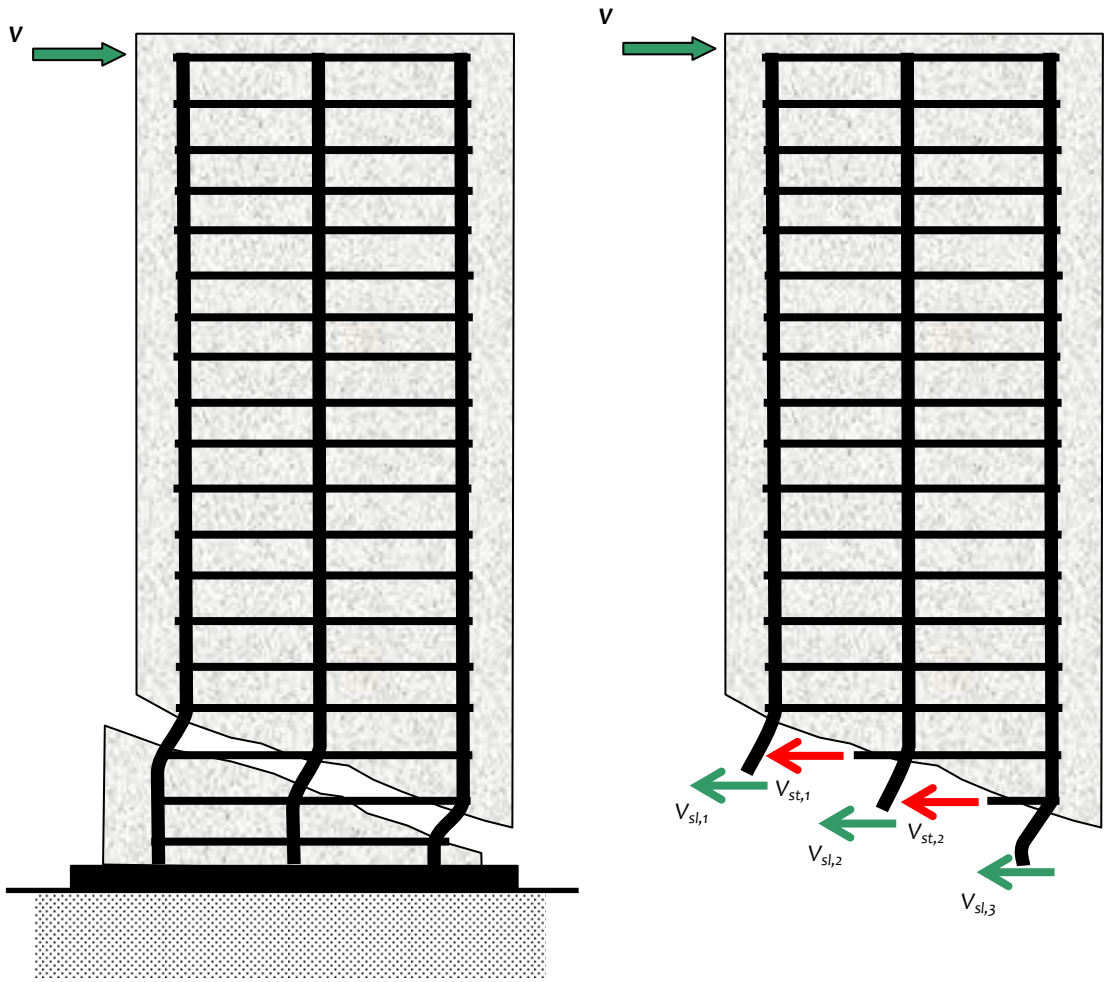

Figure 4.6: Residual shear resistance mechanism offered by longitudinal bars and transverse stirrups

(c) Mode of Failure

Failure mode of a RC member is determined using the shear force capacity curve ($(V_c+V_{st})_n$ with n=3 in Figure 4.5b), demand *Line* $(V_d)_n$ and moment capacity *Line* M_{cap}. The member will fail in *shear*, if the *demand Line* $(V_d)_n$ crosses the capacity *Curve* $(V_c+V_{st})_n$ at a lateral shear force smaller than that corresponding to intersection of demand *Line* $(V_d)_n$ and bending moment capacity *Line* M_{cap} (Figure 4.7a) The lateral shear force corresponding to intersection of $(V_d)_n$ and *Curve* $(V_c+V_{st})_n$ represents the shear force at *shear failure*. Further, the member will fail in *flexure*, if the demand *Line* $(V_d)_n$ crosses the moment capacity *Line* M_{cap} at a lateral shear force smaller than that corresponding to intersection of demand *Line* $(V_d)_n$ and capacity *Curve* (a) $(V_c+V_{st})_n$ (Figure 4.7b), or (b) V_c alone (Figure 4.7c). The shear force corresponding to intersection of $(V_d)_n$ and *Line* M_{cap} represents the shear force at *flexure* failure. And, the member will fail in *combined flexure-shear* mode, if the shear force corresponding to intersections of $(V_d)_n$ and M_{cap}, and that corresponding to intersection of $(V_d)_n$ and $(V_c+V_{st})_n$ are almost equal (Figure 4.7b).

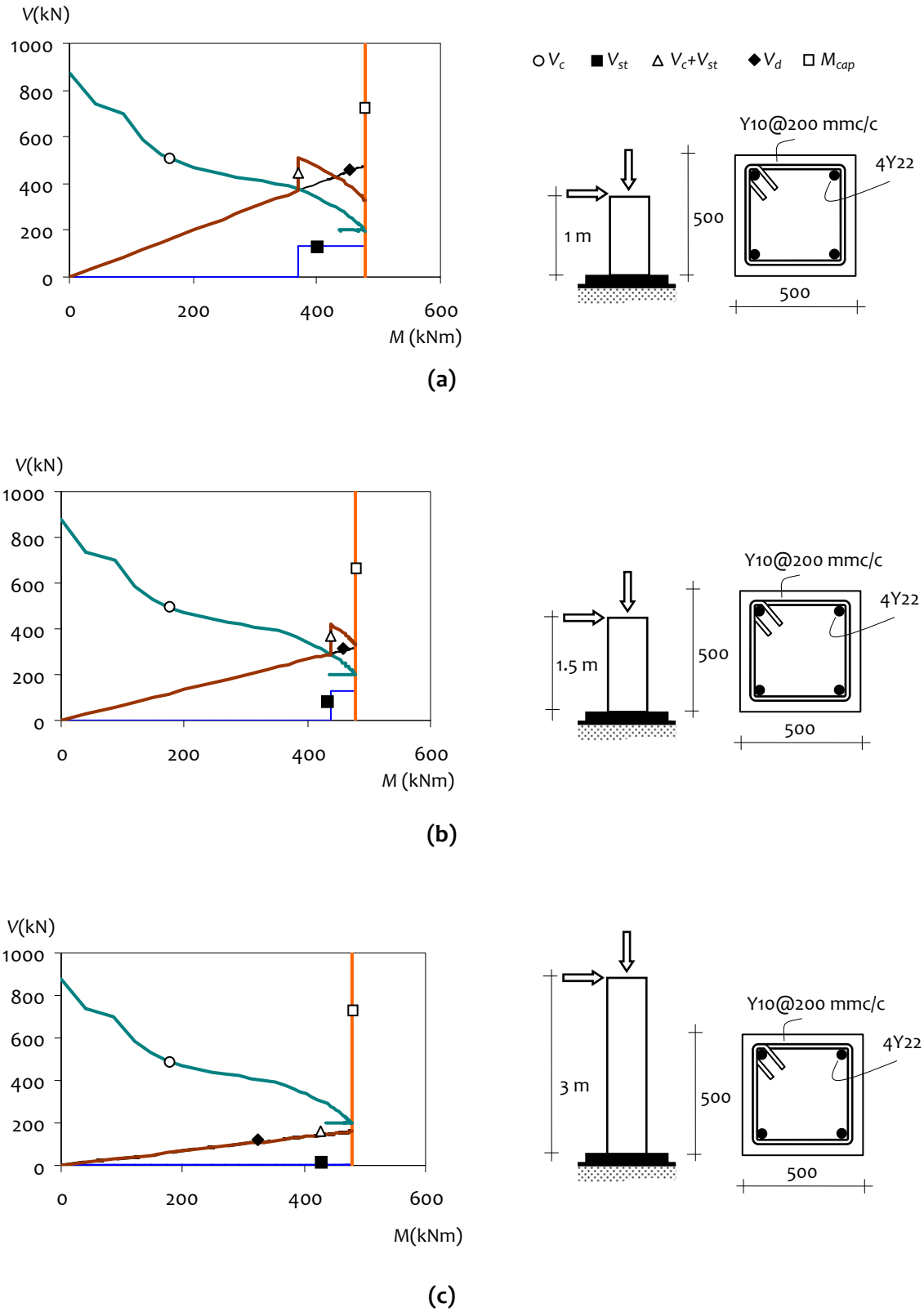

Figure: 4.7: Typical modes of failure based on demand-capacity interaction: (a) shear failure, (b) combined flexure–shear failure, and (c) flexure failure; M30 concrete and Fe415 reinforcing steel

4.1.2 Numerical Study

The accuracy of the proposed method is demonstrated by comparing *failure load* and *mode of failure* forecast using the proposed method with those observed in 107 RC specimens from *experimental* studies reported in literature [Wight and Sozen, 1973; Atalay and Penzien, 1975; Gill *et al*, 1979; Ang, 1981; Nagasaka, 1982; Umehara and Jirsa, 1982; Soesianawati *et al, 1986*; Zahn *et al, 1986*; Zhou *et al, 1985;* Saatcioglu and Ozcebe, 1989; Watson and Park, 1989; Tanaka and Park, 1990; Esaki, 1996; Taylor *et al*, 1997; Saatcioglu and Grira, 1999; Lynn, 1999; Mo and Wang, 2000; Ousalem *et al,* 2003; Yoshimura and Nakamura, 2003], and with four analytical models reported in literature [Priestley *et al*, 1994; Sezen, 2002; Pan and Li, 2012; Rossi, 2013]. Although other refined analytical models (*e.g.*, Mergos and Kappos, 2008) are available too, they are not considered in the present study as obtaining results from those models involve using specific finite element programs that are not readily available. The ranges of the main parameters of these 107 RC specimen are:

(a) Shear span-to-depth ratios : 1.0 – 6.6,
(b) Transverse reinforcement ratios : 0.0014 – 0.024,
(c) Longitudinal reinforcement ratios : 0.01 – 0.033,
(d) Axial load ratios, P/f_cA_g : 0.05 – 0.68,
(e) Concrete strengths : 20.2 – 49.3 MPa,
(f) Yield strengths of reinforcement : 255 – 580 MPa, and
(g) Type of loading : *Double curvature bending* (*DC*), *double ended* (*2C*), and *cantilever columns* (*C*); all subjected to reverse cyclic load effects.

The database is given in Table 4.2 comprising (1) *geometric* and *mechanical* properties of experimental specimens considered along with calculated and experimental test results (columns 2 to 14); and (2) observed mode of failure of the specimens and that forecast by the proposed method (columns 15 and 16).

The method proposed accurately forecasts the *mode of failure* as observed in the 105 experimental investigations reported in literature out of the 107 specimen. In general, the method proposed provides lower bound estimate of shear resistance at failure of RC members, particularly of those specimens whose behaviour is governed by *shear*, although it marginally overestimates failure load of specimens with *axial load*

Table 4.2: Details of experimental results and analytical solutions

S. No	Ref. No	Label	Loading Type	$B \times D$ mm x mm	f_c MPa	f_{yl} MPa	f_{yt} MPa	ρ_l %	ρ_t %	$\frac{M}{VD}$	Axial Load Ratio	V_{exp} kN	V_{prop} kN	Failure Mode		V_{theo}/V_{exp}				
														Exp.	Prop.	a	b	c	d	e
(1)	(2)	(3)	(4)	(5)	(6)	(7)	(8)	(9)	(10)	(11)	(12)	(13)	(14)	(15)	(16)	(17)	(18)	(19)	(20)	(21)
1	Ang, 1981	3	2C	400 x 400	23.6	427	320	1.51	1.76	4.39	0.27	192	180	F	F	0.86	0.86	0.86	0.97	0.94
2	Ang, 1981	4	2C	400 x 400	25.0	427	280	1.51	1.39	4.41	0.16	169	166	F	F	0.91	0.91	0.91	0.95	0.98
3	Sosian-awati *et al*, 1986	1	2C	400 x 400	46.5	446	364	1.51	0.78	4.43	0.16	200	186	F	F	0.88	0.88	0.88	0.88	0.93
4		2	2C	400 x 400	44.0	446	360	1.51	1.10	4.31	0.30	279	300	F	F	0.91	0.91	0.91	0.97	1.08
5		3	2C	400 x 400	44.0	446	364	1.51	0.73	4.28	0.28	277	249	F	F	0.93	0.93	0.93	0.97	0.90
6		4	2C	400 x 400	40.0	446	255	1.51	0.52	4.31	0.29	265	232	F	F	0.90	0.90	0.90	0.93	0.88
7	Zahn *et al*, 1986	7	2C	400 x 400	28.3	440	466	1.51	1.13	4.67	0.18	213	181	F	F	0.76	0.76	0.76	0.81	0.85
8		8	2C	400 x 400	40.1	440	466	1.51	1.44	5.15	0.33	269	242	F	F	0.78	0.78	0.78	0.88	0.90
9	Watson *et al*, 1989	5	2C	400 x 400	41.0	474	372	1.51	1.06	4.58	0.44	292	244	F	F	0.83	0.83	0.83	0.99	0.84
10	Tanaka and Park, 1990	1	2C	400 x 400	25.6	474	333	1.57	1.46	4.34	0.16	167	159	F	F	0.93	0.93	0.93	0.99	0.95
11		5	2C	550 x 550	32.0	511	325	1.25	1.42	3.32	0.09	386	367	F	F	0.89	0.89	0.89	0.91	0.95
12		7	2C	550 x 550	32.1	511	325	1.25	1.16	3.31	0.25	588	481	F	F	0.81	0.81	0.81	0.87	0.82
13	Atalay and Penzien, 1975	2S1	2C	305 x 305	30.7	367	363	1.63	0.48	6.07	0.09	61	56	F	F	0.84	0.84	0.84	0.84	0.92
14		3S1	2C	305 x 305	29.2	367	363	1.63	0.80	6.04	0.10	57	55	F	F	0.90	0.90	0.90	0.90	0.96
15		4S1	2C	306 x 305	27.6	429	363	1.63	0.48	5.96	0.18	49	60	F	F	1.16	1.16	1.16	1.16	1.22
16		5S1	2C	307 x 305	29.4	429	392	1.63	0.80	6.16	0.18	74	73	F	F	0.93	0.93	0.93	0.93	0.99
17		6S1	2C	308 x 305	31.8	429	392	1.63	0.48	6.25	0.17	75	75	F	F	0.91	0.91	0.91	0.92	1.00
18		9	2C	309 x 305	33.3	363	392	1.63	0.80	6.14	0.18	79	79	F	F	0.97	0.97	0.97	0.98	1.00
19		10	2C	310 x 305	32.4	363	392	1.63	0.48	6.35	0.27	78	79	F	F	0.95	0.95	0.95	0.96	1.01
20		12	2C	312 x 305	31.8	363	373	1.63	0.48	6.60	0.27	78	78	F	F	0.91	0.91	0.91	0.92	1.00
21	Gill *et al*, 1979	Gill1	2C	550 x 550	23.1	375	297	1.79	1.11	2.32	0.24	657	556	F	F	0.85	0.85	0.85	0.89	0.85
22		Gill2	2C	550 x 550	41.4	375	316	1.79	1.70	2.27	0.28	764	813	F	F	0.99	0.99	0.99	1.02	1.06

S. No	Ref. No	Label	Loading Type	$B \times D$ mm x mm	f_c MPa	f_{yl} MPa	f_{yt} MPa	ρ_l %	ρ_t %	$\frac{M}{VD}$	Axial Load Ratio	V_{exp} kN	V_{prop} kN	Failure Mode		V_{theo}/V_{exp}				
														Exp.	Prop.	a	b	c	d	e
(1)	(2)	(3)	(4)	(5)	(6)	(7)	(8)	(9)	(10)	(11)	(12)	(13)	(14)	(15)	(16)	(17)	(18)	(19)	(20)	(21)
23		Gill3	2C	550 x 550	21.4	375	297	1.79	1.18	2.31	0.44	642	557	F	F	0.90	0.90	0.90	0.99	0.87
24		Gill4	2C	550 x 550	23.5	375	294	1.79	2.06	2.36	0.68	697	541	F	F	0.81	0.81	0.81	1.02	0.78
25	Saatcioglu and Grira, 1999	BG1	C	350 x 350	34.0	456	570	1.95	1.16	5.41	0.38	169	144	F	F	0.87	0.87	0.87	0.95	0.85
26		BG2	C	350 x 350	34.0	456	570	1.95	1.16	5.32	0.35	164	131	F	F	0.90	0.90	0.90	1.02	0.80
27		BG3	C	350 x 350	34.0	456	570	1.95	0.76	5.21	0.16	148	131	F	F	0.88	0.88	0.88	0.92	0.89
28		BG4	C	350 x 350	34.0	456	570	2.93	0.77	5.60	0.36	171	163	F	F	0.94	0.94	0.94	1.09	0.95
29		BG5	C	350 x 350	34.0	456	570	2.93	1.54	5.55	0.33	173	168	F	F	0.94	0.94	0.94	1.11	0.97
30		BG6	C	350 x 350	34.0	478	570	2.29	1.48	5.53	0.38	188	159	F	F	0.90	0.90	0.90	0.98	0.85
31		BG7	C	350 x 350	34.0	456	580	2.93	0.76	5.52	0.35	178	165	F	F	0.93	0.93	0.93	1.08	0.93
32		BG8	C	350 x 350	34.0	456	580	2.93	0.76	5.19	0.18	180	162	F	F	0.93	0.93	0.93	0.98	0.90
33		BG9	C	350 x 350	34.0	428	580	3.28	0.77	5.58	0.36	185	162	F	F	0.89	0.89	0.89	1.04	0.88
34		BG10	C	350 x 350	34.0	428	570	3.28	1.57	5.55	0.34	177	162	F	F	0.93	0.93	0.93	1.10	0.92
35	Mo and Wang, 2000	C1-1	C	400 x400	24.9	497	460	2.13	0.95	3.66	0.08	250	239	F	F	0.85	0.85	0.85	0.90	0.96
36		C1-2	C	400 x400	26.7	497	460	2.13	0.95	3.71	0.11	243	198	F	F	0.86	0.86	0.86	0.92	0.81
37		C1-3	C	400 x400	26.1	497	460	2.13	0.02	4.10	0.15	243	208	F	F	0.79	0.79	0.79	0.84	0.86
38		C2-1	C	400 x400	25.3	497	460	2.13	0.01	4.10	0.08	241	240	F	F	0.87	0.87	0.87	0.92	1.00
39		C2-2	C	400 x400	27.1	497	460	2.13	0.01	4.10	0.11	250	200	F	F	0.88	0.88	0.88	0.93	0.80
40		C2-3	C	400 x400	26.8	497	460	2.13	0.01	4.10	0.15	271	209	F	F	0.79	0.79	0.79	0.83	0.77
41		C3-1	C	400 x400	26.4	497	460	2.13	0.01	4.10	0.07	228	240	F	F	0.93	0.93	0.93	0.97	1.05
42		C3-2	C	400 x400	27.5	497	460	2.13	0.01	4.10	0.11	248	200	F	F	0.89	0.89	0.89	0.94	0.81
43		C3-3	C	400 x400	26.9	497	460	2.13	0.01	4.10	0.15	286	209	F	F	0.81	0.81	0.81	0.86	0.73
44	Nagasaka, 1982	HPRC10-63	DC	200 x 200	21.6	371	344	1.27	1.22	1.55	0.13	87	90	F	F	0.97	0.97	0.97	0.91	1.03
45		HPRC19-32	DC	200 x 200	21.0	371	344	1.27	2.14	1.53	0.26	111	107	F	F	0.97	0.97	0.97	0.94	0.96
46	Tanaka and	85PDC-1	DC	300 x 250	24.8	374	352	1.35	0.54	3.11	0.09	85	74	F	F	0.79	0.79	0.79	0.77	0.87

S. No	Ref. No	Label	Loading Type	$B \times D$ mm x mm	f_c MPa	f_{yl} MPa	f_{yt} MPa	ρ_l %	ρ_t %	$\frac{M}{VD}$	Axial Load Ratio	V_{exp} kN	V_{prop} kN	Failure Mode		V_{theo}/V_{exp}				
														Exp.	Prop.	a	b	c	d	e
(1)	(2)	(3)	(4)	(5)	(6)	(7)	(8)	(9)	(10)	(11)	(12)	(13)	(14)	(15)	(16)	(17)	(18)	(19)	(20)	(21)
47	Park, 1990	85PDC-2	DC	300 x 250	27.9	374	506	1.35	0.54	3.15	0.09	75	74	F	F	0.89	0.89	0.89	0.88	0.99
48		85PDC-3	DC	300 x 250	27.9	374	506	1.35	0.54	3.15	0.09	75	74	F	F	0.89	0.89	0.89	0.88	0.99
49		85STC-1	DC	300 x 250	27.9	374	506	1.35	0.54	3.16	0.08	76	76	F	F	0.88	0.88	0.88	0.86	1.00
50		85STC-2	DC	300 x 250	27.9	374	506	1.35	0.54	3.10	0.08	80	76	F	F	0.85	0.85	0.85	0.83	0.95
51		85STC-3	DC	300 x 250	27.9	374	506	1.35	0.54	3.16	0.08	76	76	F	F	0.88	0.88	0.88	0.86	1.00
52	Esaki, 1996	H-2-1/5	DC	200 x 200	23.1	362	364	2.65	0.85	2.09	0.20	108	93	F	F	0.89	0.89	0.89	0.85	0.86
53		HT-2-1/5	DC	200 x 200	20.2	362	364	2.65	0.57	2.09	0.20	108	105	F	F	0.85	0.85	0.85	0.78	0.97
54		H-2-1/3	DC	200 x 200	23.1	362	364	2.65	1.06	2.11	0.33	121	115	F	F	0.83	0.83	0.83	0.85	0.95
55		HT-2-1/3	DC	200 x 200	20.2	362	364	2.65	0.71	2.13	0.33	118	99	F	F	0.79	0.79	0.79	0.79	0.84
56		H-1-1/8	DC	200 x 200	24.6	333	354	2.65	2.12	1.03	0.13	173	170	S	S	1.02	1.02	1.02	0.87	0.98
57		HT-1-1/8	DC	200 x 200	29.5	333	354	2.65	1.41	1.04	0.13	199	198	F	F	0.93	0.92	0.93	0.78	0.99
58		H-1-1/3	DC	200 x 200	22.9	333	354	2.65	2.12	1.05	0.33	187	195	S	F	1.03	1.03	1.03	0.88	1.04
59		HT-1-1/3	DC	200 x 200	22.5	333	354	2.65	1.41	1.05	0.33	184	189	F	F	1.04	1.04	1.04	0.84	1.03
60	Saatcioglu and Ozcebe, 1989	U3	C	350 x 350	34.8	430	470	3.21	0.89	3.04	0.10	267	284	F	F	1.05	1.05	1.05	1.05	1.06
61		U4	C	350 x 350	32.0	438	470	3.21	1.33	3.17	0.10	324	269	F	F	0.82	0.82	0.82	0.83	0.83
62		U6	C	350 x 350	37.3	437	425	3.21	1.26	3.16	0.10	341	316	F	F	0.81	0.81	0.81	0.81	0.93
63		U7	C	350 x 350	39.0	437	425	3.21	1.26	3.16	0.10	340	320	F	F	0.81	0.81	0.81	0.82	0.94
64	Ousalem *et al*, 2003	15	DC	300 x 300	26.1	447	398	2.36	1.11	1.68	0.23	328	309	F	F	0.88	0.88	0.88	0.85	0.94
65	Yoshimura and Nakamura, 2003	8	DC	300 x 300	30.7	402	392	1.05	0.18	2.20	0.20	174	154	F	S	0.91	0.91	0.85	0.84	0.89
66		6	DC	300 x 300	30.7	402	392	1.77	0.26	2.16	0.20	219	188	FS	FS	0.94	0.94	0.83	0.83	0.86
67		7	DC	300 x 300	30.7	402	392	1.77	0.18	2.18	0.20	213	173	FS	S	0.99	0.95	0.78	0.85	0.81
68	Umehara and Jirsa,	CUS	DC	230 x 410	34.9	441	414	3.01	0.32	1.13	0.14	324	268	S	S	1.33	0.88	1.09	1.12	0.83
69		2CUS	DC	230 x 410	42.0	441	414	3.01	0.32	1.14	0.27	412	423	S	S	1.39	0.86	1.09	1.03	1.03

S. No	Ref. No	Label	Loading Type	$B \times D$ mm x mm	f_c MPa	f_{yl} MPa	f_{yt} MPa	ρ_l %	ρ_t %	$\frac{M}{VD}$	Axial Load Ratio	V_{exp} kN	V_{prop} kN	Failure Mode		V_{theo}/V_{exp}				
														Exp.	Prop.	a	b	c	d	e
(1)	(2)	(3)	(4)	(5)	(6)	(7)	(8)	(9)	(10)	(11)	(12)	(13)	(14)	(15)	(16)	(17)	(18)	(19)	(20)	(21)
70	1982	CUW	DC	410 x 230	34.9	441	414	3.01	0.64	2.03	0.14	265	229	S	S	1.15	1.08	1.04	0.99	0.86
71	Wight and Sozen, 1973	25.033	2C	152 x 305	33.6	496	345	2.45	0.27	3.00	0.07	84	66	S	S	0.93	0.93	0.93	0.93	0.79
72		40.033	2C	152 x 305	33.6	496	345	2.45	0.27	3.02	0.11	89	88	S	S	0.92	0.92	0.92	0.91	0.99
73		40.033a	2C	152 x 305	34.7	496	345	2.45	0.27	3.04	0.11	95	91	S	S	0.93	0.93	0.93	0.92	0.96
74		40.048	2C	152 x 305	26.1	496	345	2.45	0.38	3.03	0.15	98	90	S	S	0.88	0.88	0.88	0.87	0.92
75		40.067	2C	152 x 305	33.4	496	345	2.45	0.53	3.17	0.11	89	96	S	S	0.94	0.94	0.94	0.94	1.08
76		40.092	2C	152 x 305	33.5	496	345	2.45	0.76	3.15	0.11	111	118	S	S	0.76	0.76	0.76	0.76	1.06
77		40.147	2C	152 x 305	33.5	496	345	2.45	1.21	3.14	0.11	109	94	--	FS	0.78	0.78	0.78	0.78	0.86
78	Lynn, 1999	3CLH18	DC	457 x 457	26.9	331	399	3.04	0.10	3.28	0.08	277	242	S	S	1.08	0.83	0.98	0.91	0.87
79		2CLH18	DC	457 x 457	33.1	331	399	1.94	0.10	3.35	0.07	241	216	S	S	0.91	0.91	0.91	0.83	0.90
80		3SLH18	DC	457 x 457	26.9	331	399	3.04	0.10	3.26	0.08	270	242	S	S	1.11	0.86	1.01	0.93	0.90
81		2SLH18	DC	457 x 457	33.1	331	399	1.94	0.10	3.30	0.07	229	204	S	S	0.97	0.97	0.97	0.88	0.89
82		2CMH18	DC	457 x 457	25.5	331	399	1.94	0.10	3.37	0.27	306	241	S	FS	0.91	0.91	0.91	0.87	0.79
83		3CMH18	DC	457 x 457	27.6	331	399	3.04	0.10	3.36	0.27	328	295	S	S	1.08	0.92	0.97	0.95	0.90
84		3CMD12	DC	457 x 457	27.6	331	399	3.04	0.25	3.37	0.22	355	312	S	S	0.99	0.99	0.99	0.97	0.88
85		CSMD12	DC	457 x 457	25.5	331	399	3.04	0.25	3.43	0.24	367	301	S	S	0.92	0.92	0.92	0.91	0.82
86	Sezen, 2002	SC-2.4-0.2	DC	350 x 350	22.6	409	393	2.05	0.21	2.58	0.20	219	200	S	S	1.03	0.95	0.95	0.90	0.91
87		SC-2.4-0.3	DC	350 x 350	49.3	409	393	3.21	0.21	2.80	0.30	357	382	S	S	1.14	0.94	0.98	1.06	1.07
88		SC-2.4-0.5	DC	350 x 350	24.2	409	393	2.05	0.21	2.88	0.50	238	207	S	FS	0.96	0.96	0.96	0.96	0.87
89		SC-1.7-0.05	DC	350 x 350	29.8	409	393	2.05	0.21	1.74	0.05	276	215	S	S	1.03	0.80	0.81	0.79	0.78
90		SC-1.7-0.2	DC	350 x 350	27.5	409	393	2.05	0.21	1.82	0.20	294	272	S	S	1.19	0.96	0.93	0.96	0.93
91		SC-1.7-0.35	DC	350 x 350	25.5	409	393	2.05	0.21	1.86	0.35	336	282	S	S	1.06	0.95	0.91	0.87	0.84
92		SC-1.7-0.5	DC	350 x 350	26.4	409	393	2.05	0.21	1.91	0.50	376	300	S	FS	0.96	0.96	0.93	0.79	0.80
93		RC-1.7-0.05	DC	250 x 490	32.5	409	393	2.05	0.21	1.79	0.05	283	229	S	S	1.01	0.90	0.88	0.88	0.81

S. No	Ref. No	Label	Loading Type	$B \times D$ mm x mm	f_c MPa	f_{yl} MPa	f_{yt} MPa	ρ_l %	ρ_t %	$\frac{M}{VD}$	Axial Load Ratio	V_{exp} kN	V_{prop} kN	Failure Mode		V_{theo}/V_{exp}				
														Exp.	Prop.	a	b	c	d	e
(1)	(2)	(3)	(4)	(5)	(6)	(7)	(8)	(9)	(10)	(11)	(12)	(13)	(14)	(15)	(16)	(17)	(18)	(19)	(20)	(21)
94		RC-1.7-0.2	DC	250 x 490	24.5	409	393	2.05	0.21	1.84	0.20	306	261	S	S	1.00	0.95	0.91	0.90	0.85
95		RC-1.7-0.35	DC	250 x 490	27.1	409	393	2.05	0.21	1.91	0.35	346	296	S	S	0.97	0.97	0.93	0.93	0.86
96		RC-1.7-0.5	DC	250 x 490	26.8	409	393	2.05	0.21	1.98	0.50	355	286	S	S	0.93	0.93	0.93	0.86	0.81
97	Ousalem *et al*, 2003	1	DC	300 x 300	27.7	447	398	1.77	0.55	1.03	0.22	341	316	S	S	1.16	0.85	0.96	0.88	0.93
98		11	DC	300 x 300	28.2	447	398	2.36	0.18	1.56	0.21	243	206	S	S	1.15	0.87	0.88	0.97	0.85
99		12	DC	300 x 300	28.2	447	398	2.36	0.18	1.57	0.21	250	206	S	S	1.11	0.84	0.85	0.94	0.82
100		13	DC	300 x 300	26.1	447	398	2.36	0.55	1.58	0.23	266	273	S	S	1.15	1.08	1.04	1.03	1.03
101		14	DC	300 x 300	26.1	447	398	2.36	0.55	1.60	0.23	296	273	S	S	1.02	0.96	0.93	0.92	0.92
102		16	DC	300 x 300	26.1	447	398	1.77	0.55	1.04	0.23	341	306	S	S	1.12	0.83	0.95	0.84	0.90
103	Yoshimura and Nakamura, 2003	1	DC	300 x 300	30.7	402	392	2.68	0.26	2.09	0.20	234	208	S	S	1.14	0.97	0.85	0.93	0.89
104		2	DC	300 x 300	30.7	402	392	2.68	0.18	2.06	0.20	230	190	S	S	1.10	0.92	0.79	0.92	0.83
105		3	DC	300 x 300	30.7	402	392	2.68	0.13	2.10	0.20	230	197	S	S	1.03	0.86	0.76	0.88	0.86
106		4	DC	300 x 300	30.7	402	392	2.68	0.26	2.13	0.30	261	234	S	S	1.03	0.96	0.82	0.92	0.90
107		5	DC	300 x 300	30.7	402	392	2.68	0.26	2.18	0.35	275	233	S	S	0.96	0.93	0.81	0.88	0.85

a	Priestley *et al*, 1994	F	Flexure
b	Sezen, 2002	S	Shear
c	Pan and Li, 2012	FS	Combined Flexure-Shear
d	Rossi, 2013		
e	Proposed Method		

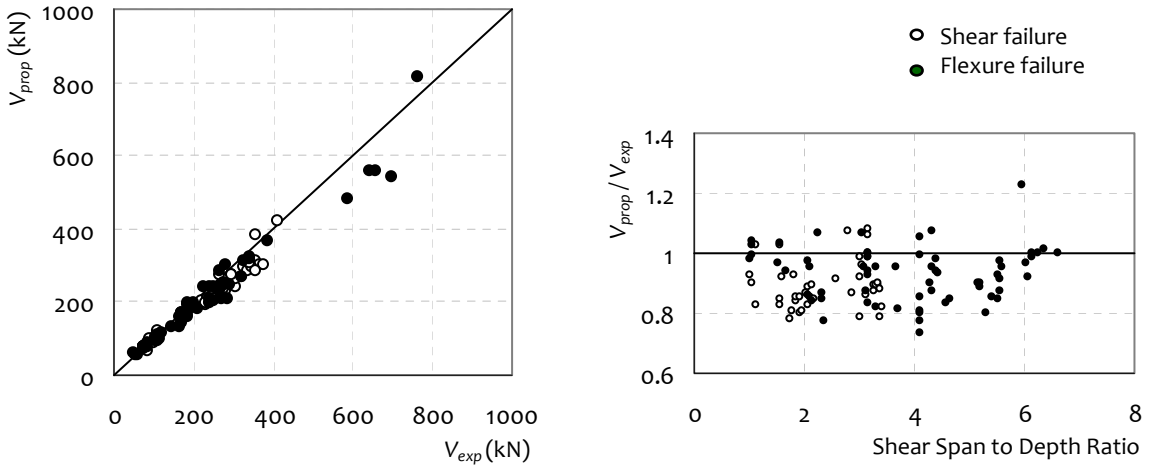

Figure 4.8: (a) Comparison of numerical estimates of lateral load (shear) capacity of 107 specimens to experimental values, and (b) ratio of proposed to experimental shear capacity across various shear span-to-depth ratio

ratio 0.5 or more. Absolute values are compared in Figure 4.8a of the shear resistance at failure using method proposed V_{prop} with experimental values V_{exp}, and ratio V_{prop}/V_{exp} is shown in Figure 4.8b as a function of shear span-to-depth *(L/D)* ratio. The numerical estimates of the failure load of the 107 specimens correlate well with the experimental values. Also, ratios are shown in Figure 4.9 of analytical estimates of shear force V_{theo} of the tested specimens using the method proposed and four commonly used analytical methods [Priestley *et al*, 1994; Sezen, 2002; Pan and Li, 2012; Rossi, 2013] to the experimental values V_{exp}. It depicts acceptability of the method proposed for both *shear-critical* and *flexure-critical* members with reasonable accuracy; the numerical values are listed in Table 4.2 (columns *17* through *21*) of ratio V_{theo}/V_{exp} of the 107 specimens. Statistical analysis is given in Table 4.3 of analytical estimates of failure load obtained using the method proposed and four other analytical methods – all specimens taken together, and *shear-critical* and *flexure-critical* specimens taken separately. The results indicate that the method proposed is as effective as any of the other methods, for *estimating failure load* and *identifying failure mode*; the advantage of the method proposed is the additional insight it provides into the shear resistance mechanism in RC members, as explained through Figure 4.5. Sample calculations using the proposed method for two specimens are presented in Annex B.

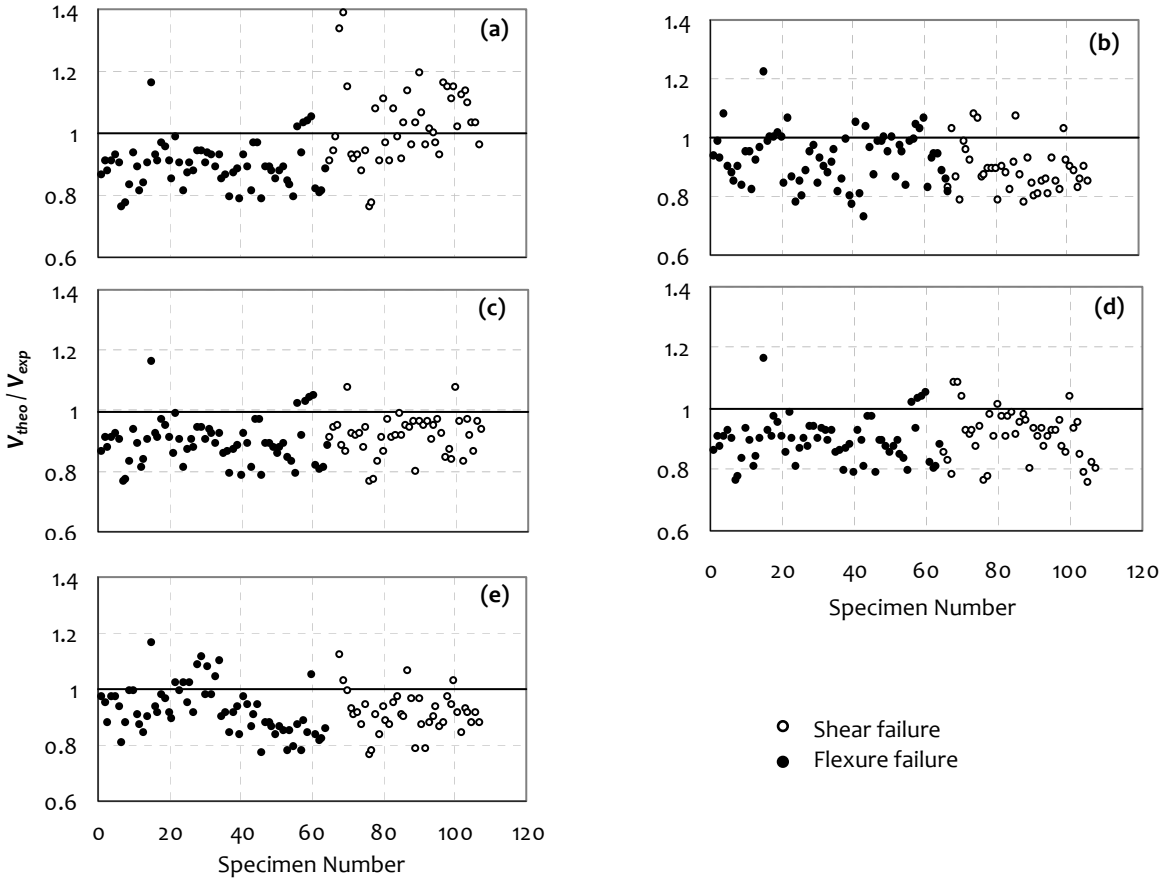

Figure 4.9: Comparison of ratio of theoretical to experimental shear capacity of 107 RC specimens: (a) Priestley *et al*, 1994, (b) Sezen, 2002, (c) Pan and Li, 2012, (d) Rossi, 2013, and (e) Proposed

Table 4.3: Statistical variation of theoretical results obtained from the proposed and other analytical methods

Parameter	V_{theo} / V_{exp}				
	Priestley *et al*, 1994	Sezen, 2002	Pan & Li, 2012	Rossi, 2013	Proposed
ALL SPECIMENS					
Mean	0.950	0.900	0.900	0.920	0.910
Standard Deviation	0.116	0.070	0.077	0.082	0.087
Coefficient of Variation	12.3	7.8	8.6	9.0	9.5
Maximum	1.390	1.160	1.160	1.160	1.220
Minimum	0.760	0.760	0.760	0.760	0.730
SHEAR FAILURE					
Mean	1.03	0.92	0.92	0.91	0.89
Standard Deviation	0.128	0.067	0.081	0.074	0.078
Coefficient of Variation	12.4	7.3	8.9	8.2	8.8
Maximum	1.39	1.08	1.09	1.12	1.08
Minimum	0.76	0.76	0.76	0.76	0.78
FLEXURE FAILURE					
Mean	0.90	0.90	0.89	0.92	0.93
Standard Deviation	0.073	0.072	0.073	0.087	0.089
Coefficient of Variation	8.1	8.0	8.2	9.4	9.6
Maximum	1.16	1.16	1.16	1.16	1.22
Minimum	0.76	0.76	0.76	0.77	0.73

Further, a study is carried out to investigate influence of distribution and properties of the constituent materials, on the behaviour of prismatic RC member with solid rectangular cross-sections. The main objective of this study is to understand responses of prismatic RC members with reinforcement varying along the span. A method is presented to identify *quantitatively* the possible *location of failure* for prismatic cantilever RC bridge piers with varying reinforcements along the span.

In practical design of RC bridge piers, the amounts of transverse and longitudinal reinforcements change gradually, with *more transverse reinforcement* ensuring enough strength and confinement in the *critical plastic hinge zone*, especially to meet the bending moment and associated shear force demands. Usually, the amount of transverse reinforcement recommended in various design codes, outside the plastic hinge zone is about 50% of that provided in the plastic hinge region. Also, longitudinal reinforcement is reduced corresponding to the flexural demand at the cross-section considered. This reduction in reinforcement may meet the flexural demand required at that section, but may lead to undesirable brittle shear mode of failure, if not designed properly. A typical case when this happens is considered to illustrate the behaviour of such prismatic piers.

To identify the probable *location* and *type of failure* in a prismatic RC member with solid rectangular cross-section, when subjected to earthquake shaking (Figure 4.10), the base of the RC member is considered to be rotationally fixed at the top of the foundation. Hence, the member is idealised as a *cantilever*; details of cross-section of the member considered are shown in Figure 4.10. Axial load P is taken as 10% of the axial load capacity, and the grades of steel and concrete are taken as Fe415 and 30 MPa, respectively; also, details are shown of *longitudinal* and *transverse* reinforcements provided along the height of the pier.

Shear-flexure interaction diagram is developed for the RC member at two cross-sections (Figure 4.11). Lateral shear force capacity is estimated of the RC member at each of these cross-sections, as the *smaller* of that corresponding to *shear* and *flexure* modes of failure. At a section, lateral load capacity in flexure-critical mode is computed as *flexural moment capacity* divided by distance of that section from the top of the cantilever. The results are summarised in Table 4.4, and are discussed in detail in the following.

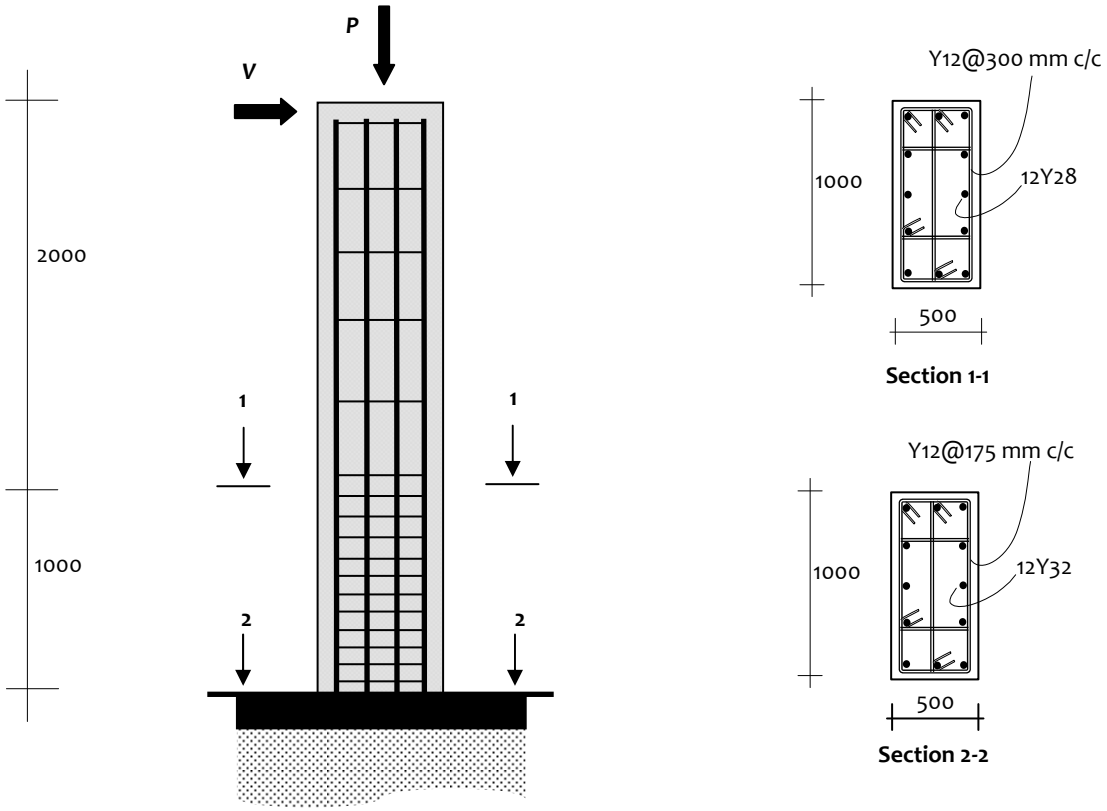

Figure: 4.10: Schematic showing elevation and cross-section details of prismatic study pier

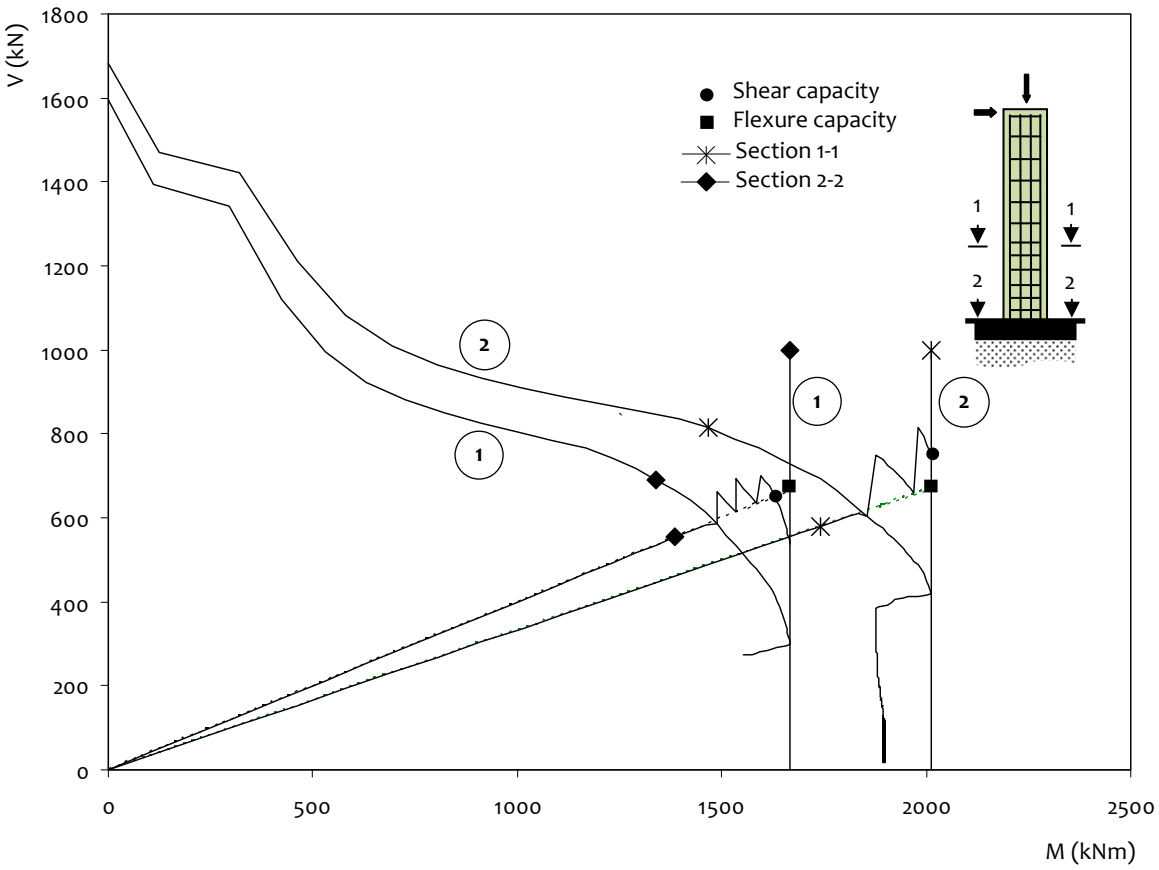

Figure 4.11: Shear-flexure interaction curves showing lateral load capacity and failure modes of prismatic RC member inside (1) and outside plastic hinge zones (2)

Table 4.4: Failure modes at different sections along height of prismatic piers and failure load and failure mode of member

At Section Level				At Member Level		
Section	*Lateral Shear Force (kN) corresponding to*		*Failure Mode*	*Failure Load (kN)*	*Failure Mode*	*Failure Location*
	Shear Failure	*Flexure Failure*				
1-1	652	1,656	Shear	652	Shear	1-1
2-2	756	671	Flexure			

The critical section of a prismatic cantilever pier is at its base, where bending moment is maximum. In this study, the pier is provided with sufficient *transverse* and *longitudinal* reinforcement to ensure that flexure failure occurs at the critical section. Because bending moment demand reduces gradually towards the top of the pier, designers wish to reduce the amount of reinforcement along the height. Section 1-1 (in Figure 4.11) shows the reinforcement details provided at a cross-section outside the plastic hinge zone; longitudinal steel meets requirements of flexural demand, and transverse steel is reduced to almost half of that provided inside the plastic hinge zone. Though it meets all detailing criteria, shear strength reduction is not accounted for at Section 1-1 corresponding to the moment demand, and hence, the member will fail in shear along Section 1-1, before the moment capacity is exhausted at the base. Figure 4.11 shows that Section 1-1 outside plastic hinge zone has a lateral shear force capacity of 652 kN, which is less than that at Section 2-2 of 671 kN (moment capacities at Sections 1-1 and 2-2 are 1656 kNm, 2013 kNm, respectively, leading to shear force capacities of 828 kN, and 671 kN, respectively). Thus, in this case, shear failure is likely to occur in pier outside plastic hinge zone. Undesirable brittle shear failure occurs, if amount of transverse reinforcement is reduced beyond plastic hinge zone without due consideration of shear strength, although shear force capacity at critical section is more than that at other sections.

4.1.3 Conclusions

The capacity is estimated of solid RC members with rectangular cross-section and prismatic span considering interaction of axial, shearing and bending stresses generated under earthquake shaking; a simple procedure is presented for estimating lower bound *failure load* and *mode of failure*. Shear force capacity of the member is estimated by summing up contributions of *concrete* (computed using a well established relation between normal and shear stresses), *transverse reinforcement* (depending on the crack angle estimated based on the applied stresses) and *longitudinal* reinforcement

(based on dowel action considered only after the contribution of concrete is exhausted). Therefore, the shear force capacity V of a RC member is contributed by: (a) Concrete V_c, and, (b) Transverse reinforcement (stirrups) V_{st} through direct tensile action and longitudinal reinforcement V_{sl} through dowel action. Together V_c, V_{st} and V_{sl} result in the lateral shear force capacity of a RC member.

Comparison of results obtained by the proposed method with those from experimental studies (available in literature) shows that the proposed method is reliable in capturing both *failure load* and *mode of failure*, of both *shear-critical* and *flexure-critical* RC members. Also, the *V-M* interaction diagram derived using the proposed method, provides insight into the mechanism of shear resistance of RC members subjected to combined action of axial force, shear force and bending moment. And also, the method proposed can help identify possible *location of failure* in RC members, in addition providing estimate of failure load and predict mode of failure.

4.2 CRITICAL PARAMETERS CONTROLLING MEMBER BEHAVIOUR

Lateral shear force capacity (*failure load*) and *mode of failure* in RC members depend on geometric properties of the member and mechanical properties of the constituent materials. In this section, effects are studied of the key parameters controlling *load at failure* and *mode of failure* (either in *flexure* or in *shear*) of RC bridge members with rectangular cross-section, under combined actions of gravity loads and earthquake shaking effects. These key parameters are identified based on the previous analytical and experimental studies (reported in literature) related to estimation of lateral shear force capacity and mode of failure.

4.2.1 Influence of Parameters

Earthquake damage of RC bridge piers critically depends on:

(i) Slenderness s, ratio of shear span (or length L of cantilever) to cross-sectional depth D of the pier, *i.e.*, $s = L/D$,

(ii) Geometry of cross-section along the height of the piers, including plan aspect ratio a, defined as ratio of depth D to width b, *i.e.*, $a = D/b$,

(iii) Design and detailing of transverse steel reinforcement, represented by *volumetric ratio* of transverse reinforcement ρ_T, expressed in percent,

(iv) Design and detailing of longitudinal steel reinforcement, represented by *area ratio* of longitudinal reinforcement ρ_L, expressed in percent, and

(v) Level of axial load, expressed as axial load ratio p of axial compressive load P to the ultimate compressive axial load capacity P_u, *i.e.*, $p = P/P_u$.

Parametric study is carried out considering possible combinations of these key influencing parameters on RC piers with rectangular cross-section, using analytical method discussed in Chapters *3* and in the earlier sections of this chapter. Although increase in compressive strength of concrete enhances shear strength and axial load capacity of RC sections, the effect on flexural strength is not significant and can be neglected. Flexural strength is governed by longitudinal reinforcement in RC members, particularly when reinforcement is distributed evenly throughout the cross-section leading to under-reinforced section design; usually this is the case with piers. Therefore, increasing concrete grade increases the lateral shear force capacity, and changes the mode of failure from *brittle shear failure* to *ductile flexure failure* [Sotoud and Aboutaha, 2014]. Also, to avoid brittle shear failure mode, grade of steel is recommended in literature to be kept in the range 400-500 MPa [Priestley and Benzoni, 1996; FIB, 2007]. Hence, in this study, influence of concrete compressive strength is *not* considered; a reasonably low grade of concrete, 30MPa, and grade of longitudinal and transverse reinforcements of Fe415 (*i.e.*, with yield strength of 415 MPa at 0.2% proof strain) are considered. Also, width b of the cross-sections is taken as 500 mm. Longitudinal bars are distributed uniformly along the four sides of the cross-sections with clear cover of 50 mm. Summary is listed in Table 4.5 of the range parameters considered for the study.

The influence of each key parameter considered is examined, with other parameters kept constant. A total of 5,040 combinations are considered to study mode of *initiation* of failure and lateral load capacity of prismatic RC members of rectangular cross-section. The mode of failure can be *flexure*, *combined flexure-shear* or *shear* failure, depending on slenderness ratio s, amount of transverse reinforcement ρ_T, amount of longitudinal reinforcement ρ_L, and level of axial load P. Maximum lateral shear force capacity of piers at failure H_{max}, is normalised with flexural overstrength based shear demand V_Ω $(= M_\Omega / L)$, where M_Ω is flexural overstrength capacity, and L the length of single column cantilever pier (Figure 4.12). Thus, $H_{max}/V_\Omega < 1$ indicates *shear failure*, while $H_{max}/V_\Omega = 1$ indicates flexure failure.

Table 4.5: Variables considered for parametric study

Parameter	Range	Increment
Shear Span-to-Depth Ratio	$1 \le s \le 6$	0.5
Plan Aspect Ratio	$1 \le a \le 6$	1.0
Transverse Reinforcement Ratio	$0.4\% \le \rho_T \le 1.6\%$	0.1%
Longitudinal Reinforcement Ratio	$1.0\% \le \rho_L \le 2.5\%$	0.5%
Axial Load Ratio	$0.1 \le p \le 0.5$	0.1

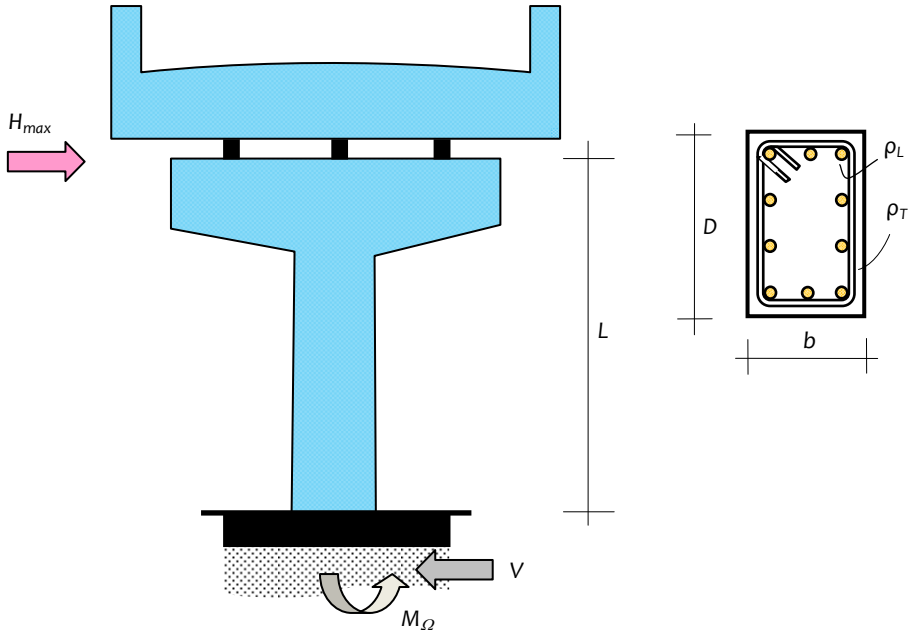

Figure 4.12: Geometry of prismatic single column RC bridge pier

4.2.1.1 Slenderness

Slenderness s (=L/D) is a critical factor governing lateral shear force capacity and mode of failure in RC bridge piers. With increase in slenderness, failure mode changes from *shear-controlled* to *flexure-controlled* (Figure 4.13). In the first case (Figure 4.13a), with ρ_T = 0.4%, ρ_L = 1.0%, p = 0.1 and plan aspect ratio a in the range *1- 6*, failure occurs in *flexure* at slenderness s of 2.5 or more. Here, plan aspect ratio does not seem to affect the *mode of failure*, but does affect the *lateral shear force capacity*. Next, with a = 1, ρ_L = 1.0% and p = 0.1, failure occurs in flexure at slenderness s of 2.5 or more, with transverse reinforcement ratio ρ_T in the range 0.4%- 1.4% (Figure 4.13b). Minimum transverse reinforcement of 0.4% is adequate to prevent shear failure in piers with even larger slenderness (of 2.5 or more), but flexure failure occurs with higher amount of transverse reinforcement in less slender piers.

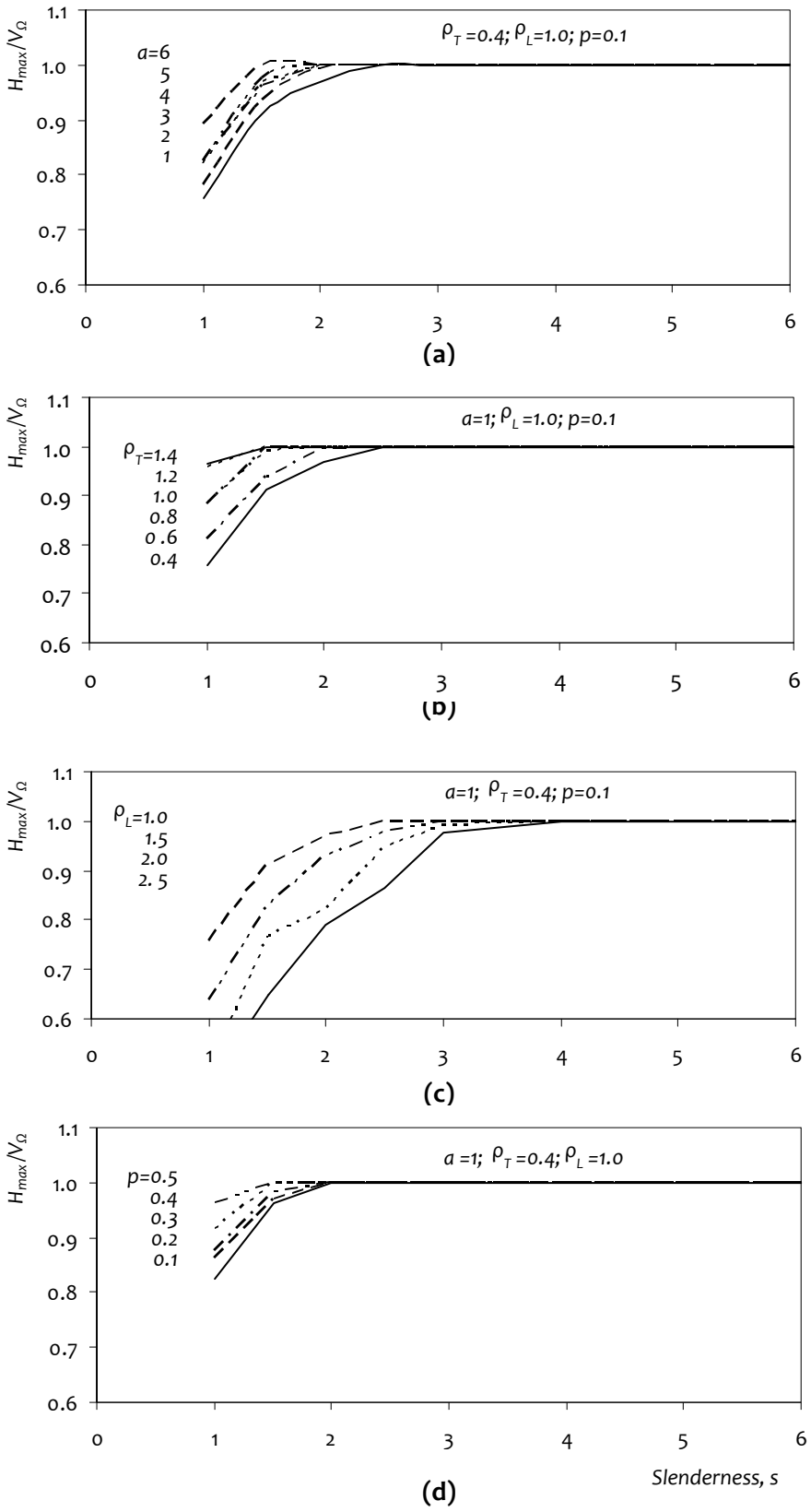

Figure 4.13: Effect of slenderness ratio *s* on response of piers for varying: (a) aspect ratio *a*, (b) percentage of transverse reinforcement ρ_T, (c) percentage of longitudinal reinforcement ρ_L, and (d) axial load ratio *p*

Similarly, with a = 1, ρ_T = 0.4% and p = 0.1, flexure failure occurs at slenderness s of 4.0 or more, with longitudinal reinforcement ratio ρ_L in the range 1.0%-2.5% (Figure 4.13c). With increase in longitudinal reinforcement ratio ρ_L, the flexural capacity increases; this increases likelihood of shear failure, except in piers with larger slenderness (of 4 or more). Finally, with a = 1, ρ_T = 0.4% and ρ_L = 1.0%, flexure failure occurs at slenderness s of 2.5 or more, with axial load ratio p in the range 0.1-0.5 (Figure 4.13d). Increase in axial load p ratio (up to about 0.5) increases shear capacity of member, but piers with larger slenderness (of 2.5 or more) do not rely on this enhancement of shear capacity to prevent shear failure. In summary, members fail in *shear*, when slenderness $s<2$, and in *flexure*, when $s>4$; the mode of failure depends on values of other three parameters when $2<s<4$.

4.2.1.2 Plan Aspect Ratio

Again, higher slenderness s causes *flexure mode of failure* (even with increase in plan aspect ratio a), with transverse reinforcement ratio, longitudinal reinforcement ratio and axial load ratio of ρ_T = 0.4%, ρ_L = 2.0% and p = 0.1 (Figure 4.14a). In particular, slenderness s of 4 (or more) causes *flexure failure* for typical ranges of the parameters, including plan aspect ratio a in the range of 1- 6. And, small transverse reinforcement ratio ρ_T causes *flexure failure* with increase in plan aspect ratio a, with slenderness, longitudinal reinforcement ratio and axial load ratio of s = 2, ρ_L = 2.5% and p = 0.1 (Figure 4.14b). Higher plan aspect ratio a (=D/b) requires larger D (for constant b), which, in turn, requires longer member length L to maintain constant slenderness s (=L/D). This increase in length L increases the moment demand on the member for a given lateral force, and thus, increases the possibility of *flexure failure*. This explains why transverse reinforcement requirement is lesser in members with large plan aspect ratio a (*e.g.*, walls) than those with small plan aspect ratio a (*e.g.*, beams or columns), but of the same slenderness s.

Similarly, lesser amount of longitudinal reinforcement ratio ρ_L is required to ensure flexural mode of failure with increase in plan aspect ratio a, with slenderness, transverse reinforcement ratio and axial load ratio of s = 2, ρ_T = 0.4% and p = 0.1 (Figure 4.14c). Here, increase in plan aspect ratio a, through increase in cross-sectional depth D (for constant width b), leads to a higher increase in *flexure capacity* compared to *shear*

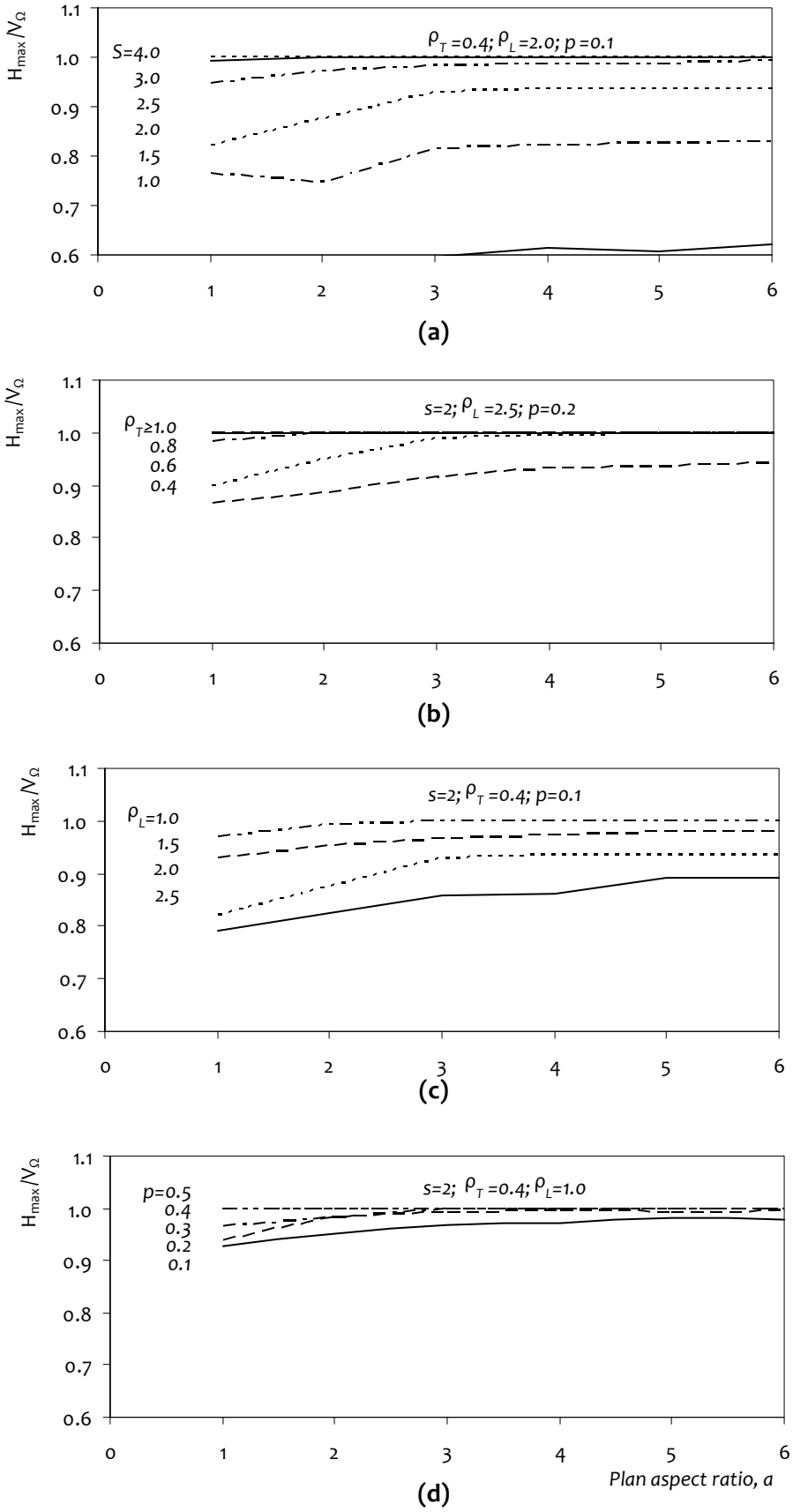

Figure 4.14: Effect of plan aspect ratio *a* on response of piers for varying: (a) slenderness *s*, (b) percentage of transverse reinforcement ρ_T, (c) percentage of longitudinal reinforcement ρ_L, and (d) axial load ratio *p*

capacity of the section, thereby increasing the likelihood of *shear failure*. Finally, as in the case of transverse reinforcement ratio, smaller amount of axial load ratio p is required to ensure *flexure mode of failure* with increase in plan aspect ratio a, with slenderness, transverse reinforcement ratio, and longitudinal reinforcement ratio of $s = 2$, $\rho_T = 0.4\%$ and $\rho_L = 1.0\%$ (Figure 4.14d).

In general, lateral shear force capacity of piers:

(a) Increases with increase in plan aspect ratio a (= D/b) for a given slenderness s (Figure 4.15), because larger cross-section depth D increases for the same width b; and

(b) Decreases with increase in slenderness s, for any given plan aspect ratio a, because moment demand increases with increase in slenderness, which in turn, reduces the shear capacity as discussed in Chapter 3.

4.2.1.3 Transverse Reinforcement Ratio

Increase in transverse reinforcement enhances confinement of concrete, which enhances *lateral shear force capacity* of the pier. But, amount of transverse reinforcement does not enhance significantly the failure load, except in very short piers (with $s<2$, Figure 4.16). In less slender members, moment demand is less, and shear failure can be prevented by providing larger transverse reinforcement (which increases lateral shear force capacity). In members with high slenderness, ratio of *moment demand* to *flexure capacity* is higher, and hence *flexure capacity* is exhausted much before *shear capacity* is, which leads to flexure failure.

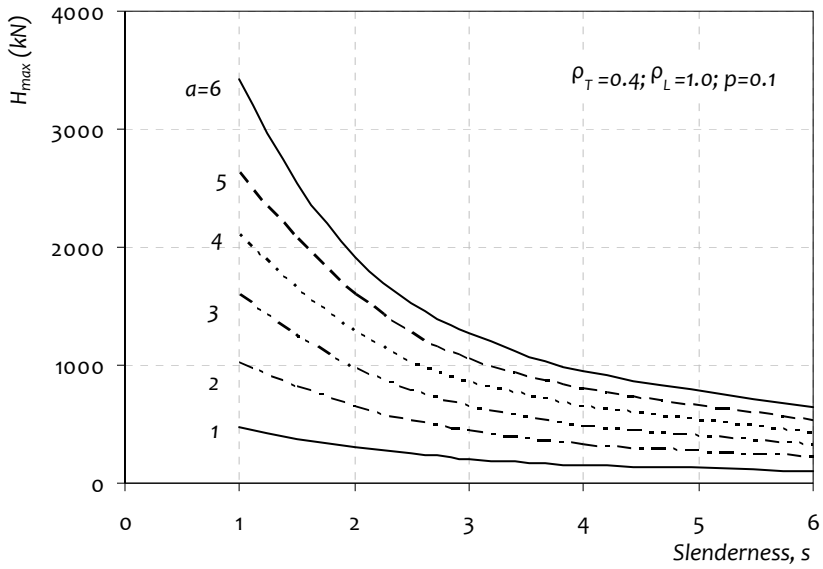

Figure 4.15: Effect of plan aspect ratio, a on lateral load capacity of piers for varying slenderness, s

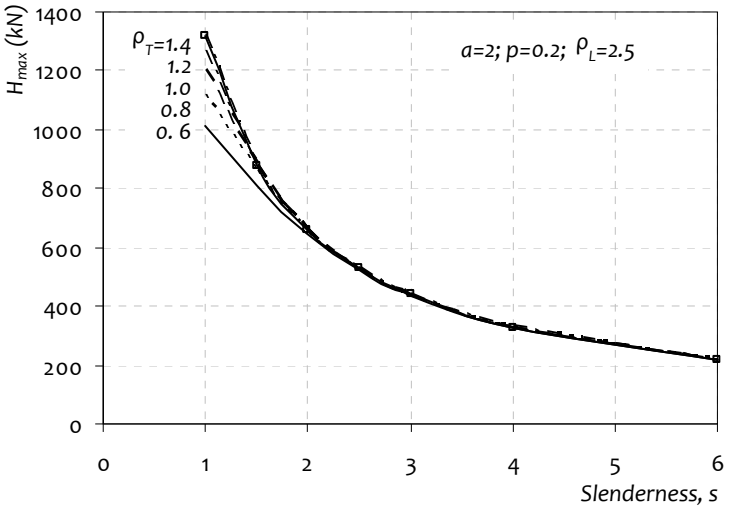

Figure 4.16: Effect of transverse reinforcement ratio, ρ_T on lateral load capacity of piers for varying slenderness, *s*

Further, in short members (*e.g.*, *s*=1, Figure 4.17a), moment demand is less; they are susceptible to *shear failure*. Increasing transverse reinforcement ratio *does not* help change the mode of failure, but helps increase its lateral shear force capacity; shear force capacity is enhanced, with plan aspect ratio, longitudinal reinforcement ratio and axial load ratio of $a=3$, ρ_L = 1.0% and p = 0.1 (Figure 4.17a). On the other hand, in less slender members ($1<s<2.5$), shear failure can be prevented by providing suitable amount of transverse reinforcement. Again, for a given slenderness ratio *s (L/D)*, increase in plan aspect ratio *a* (*D/b*) increases length of the member, which, in turn, increases flexural demand on the member, making it susceptible to flexure failure (with slenderness, longitudinal reinforcement ratio and axial load ratio of $s=2$, ρ_L = 1.0% and p = 0.1) (Figure 4.17b). Members with low aspect ratios have less flexural demand, and tend to fail in shear; in such cases, providing more transverse reinforcement will help alter mode of failure from *shear* to *flexure*.

Next, more transverse reinforcement ratio ρ_T is required to ensure flexure failure with increase in longitudinal reinforcement ratio ρ_L (with slenderness, plan aspect ratio and axial load ratio of s = 2, $a=3$ and p = 0.1) (Figure 4.17c). Increase in *longitudinal* reinforcement ratio increases *bending moment capacity*, and increase in *transverse* reinforcement ratio increases *shear force capacity*. Hence, desirable mode of flexure failure can be ensured with larger transverse reinforcement. Similarly, higher transverse reinforcement ratio ensures flexure failure in members subjected to low axial load level (with slenderness, plan aspect ratio, and longitudinal reinforcement ratio of s = 2, $a=3$ and ρ_L = 1.0%) (Figure 4.17d); increase in transverse reinforcement results in increased confinement, which, in turn, increases shear force capacity and prevents shear failure.

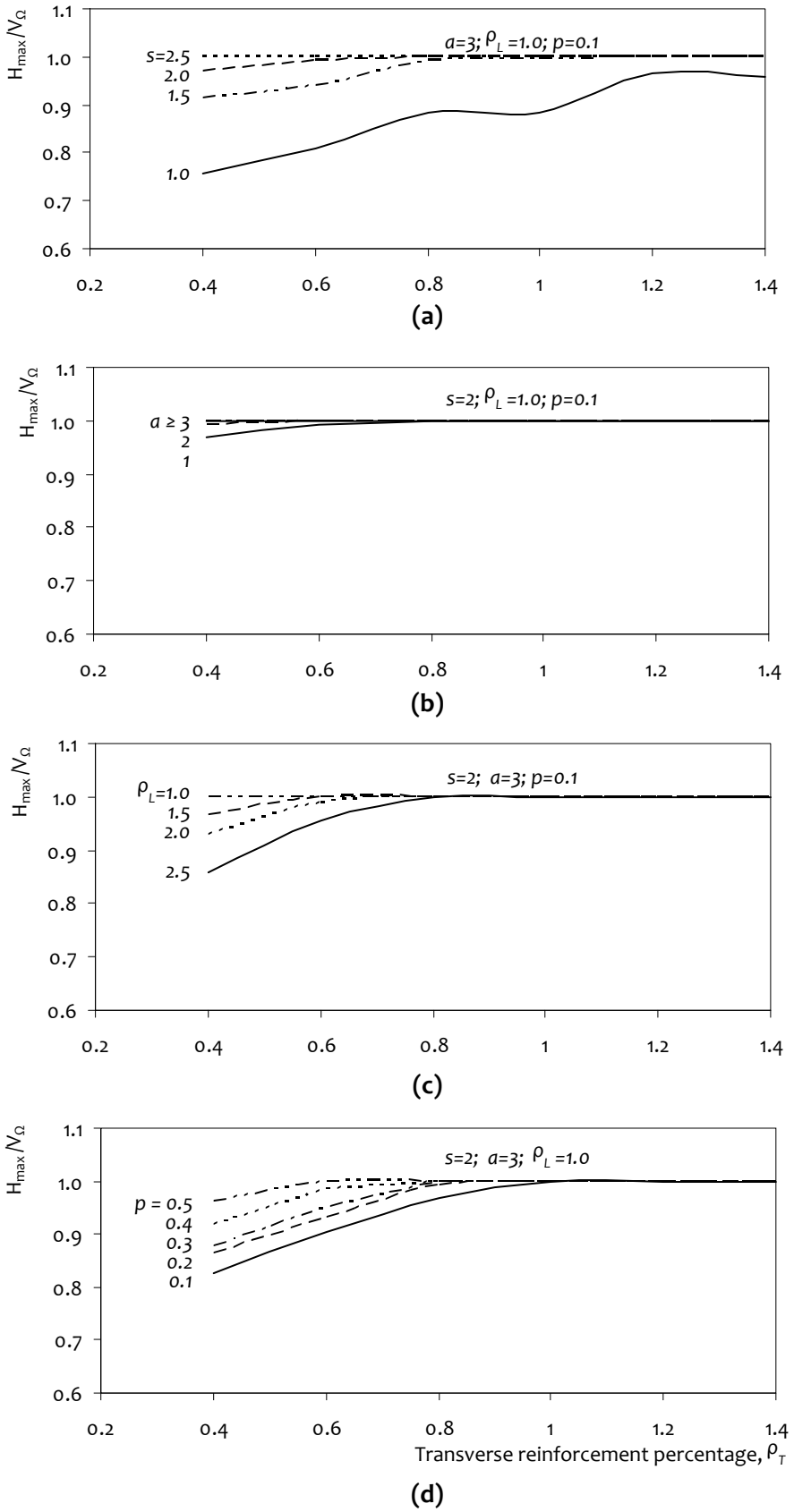

Figure 4.17: Minimum ρ_T required for preventing shear failure in piers for varying (a) slenderness *s*, (b) aspect ratio *a*, (c) percentage of longitudinal reinforcement ρ_L, and (d) axial load ratio *p*

4.2.1.4 Longitudinal Reinforcement Ratio

Increase in longitudinal reinforcement increases moment capacity and, increase in slenderness increases flexural demand. Hence, in less slender members (s<2.5) (with plan aspect ratio, transverse reinforcement ratio and axial load ratio of $a=3$, ρ_T = 0.4% and p = 0.1) (Figure 4.18a), moment demand is less; providing more longitudinal reinforcement does not help, because failure is controlled by shear force capacity (neglecting the nominal resistance that would be offered through dowel action). In slender members, providing more flexure reinforcement is useful in increasing their lateral shear force capacity, because slender members with s>4 are susceptible to *ductile failure* owing to increase in moment demand.

For plan aspect ratio of a = 3 (Figure 4.18b), mode of failure changes from *shear* to *flexure*, when longitudinal reinforcement is reduced (with slenderness, transverse reinforcement ratio and axial load ratio of $s=2$, ρ_T = 0.4% and p = 0.1) (Figure 4.18b), because flexural capacity is reduced with lesser longitudinal reinforcement. As aspect ratio is increased, the trend is the same, but there is likelihood of preventing brittle mode of failure, because length of member increases with increase in aspect ratio for a given slenderness ratio.

Next, transverse reinforcement required to prevent shear failure increases with increase in longitudinal reinforcement ratio (with slenderness, plan aspect ratio and axial load ratio of s = 2, a = 2 and p = 0.2) (Figure 4.18c), because increase in longitudinal reinforcement ratio increases *flexure capacity*, and increase in transverse reinforcement ratio increases *shear force capacity*. Similarly, *brittle mode* of failure is changed with increase in longitudinal reinforcement ratio to *ductile mode* at higher axial loads (with slenderness, plan aspect ratio and transverse reinforcement ratio of s = 2, a = 3 and ρ_T = 0.4%) (Figure 4.18d), because shear capacity is enhanced with increase in axial force, up to about fifty percent of the axial load capacity.

Thus, in general, increasing longitudinal reinforcement ratio in piers enhances flexural capacity. But, this does not help in less slender members, because failure in them is controlled by shear force capacity. As a member becomes more slender, failure is controlled by *flexure capacity* (Figure 4.19); bending moment capacity increases, but this enhancement is not significant, because increase in slenderness also leads to a higher flexural demand under the same lateral load.

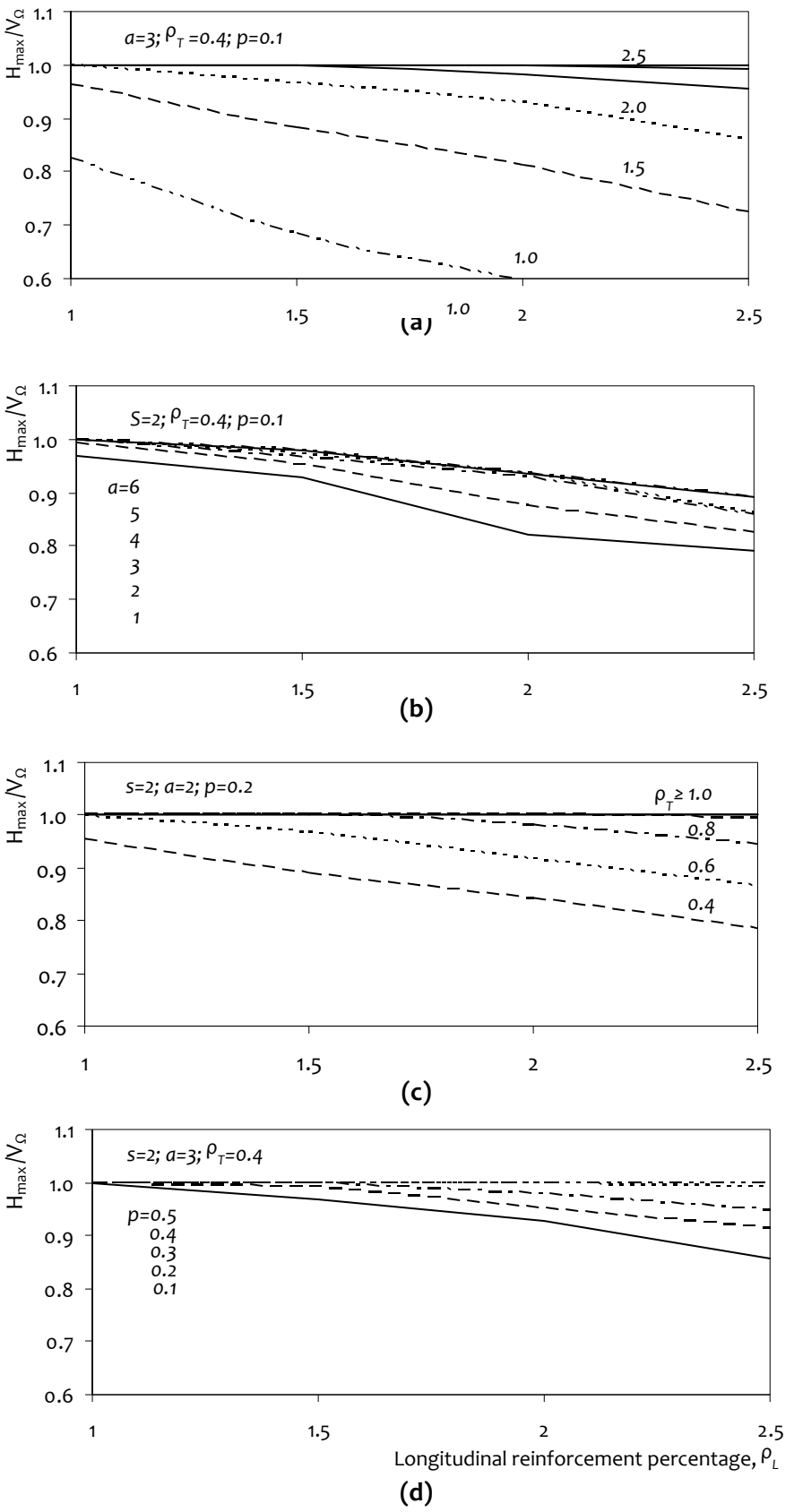

Figure 4.18: Effect of longitudinal reinforcement percentage ρ_L on response of piers for varying: (a) slenderness *s*, (b) aspect ratio *a*, (c) percentage of transverse reinforcement ρ_T, and (d) axial load ratio *p*

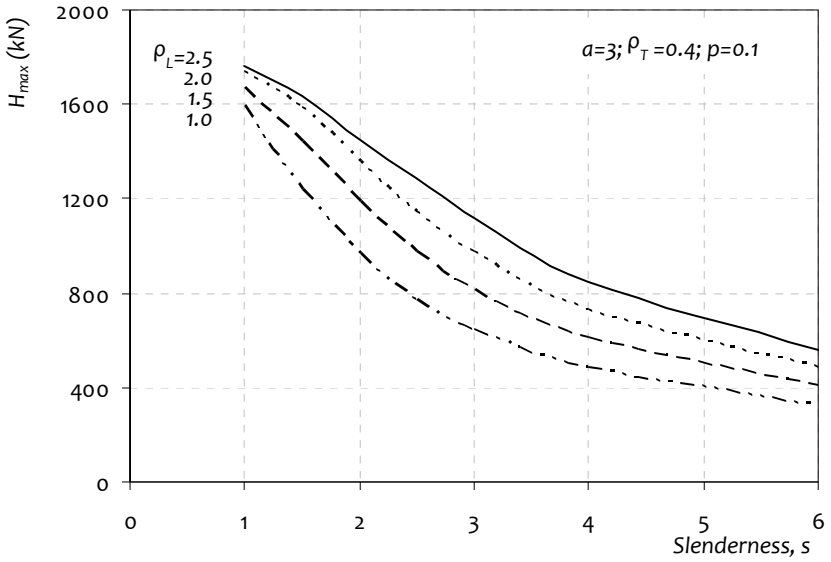

Figure 4.19: Effect of longitudinal reinforcement ratio ρ_L on lateral load carrying capacity of piers with different slenderness *s*

4.2.1.5 Axial Load Ratio

Again, in less slender members, higher axial load ratio is required to ensure flexure mode of failure (with plan aspect ratio, transverse reinforcement ratio and longitudinal reinforcement ratio of a = 3, ρ_T = 0.4% and ρ_L = 1.0%) (Figure 4.20a), because failure of less slender members is governed by their shear force capacity, and axial load helps in enhancing shear force capacity. Again, for given slenderness *s*, as plan aspect ratio a increases, the length of the member increases, which, in turn, increases flexural demand (with slenderness, transverse reinforcement ratio and longitudinal reinforcement ratio of s=2, ρ_T = 0.4% and ρ_L = 1.0%) (Figure 4.20b); this leads to failure in ductile mode even at low levels of axial load. Next, increase in both axial load ratio p and transverse reinforcement ratio ρ_T enhances shear force capacity, thereby preventing shear failure (with slenderness, plan aspect ratio and longitudinal reinforcement ratio of s = 2, a = 3 and ρ_L = 2.0%) (Figure 4.20c). Finally, as longitudinal steel is reduced, its flexural capacity reduces (with slenderness, plan aspect ratio and transverse reinforcement ratio of s = 2, a = 3 and ρ_T = 0.4%) (Figure 4.20d). Hence, it fails in flexure.

Ideally, RC piers are designed such that, *design axial load* is 10-20% of the *uniaxial axial force capacity*. Increase in axial load ratio helps in increasing shear force carrying capacity of less slender members, because increase in *axial load stress* enhances *shear stress capacity*. But, in slender members, no significant effect is observed, when axial load ratio is increased, because mode of failure is governed by slenderness (Figure 4.21).

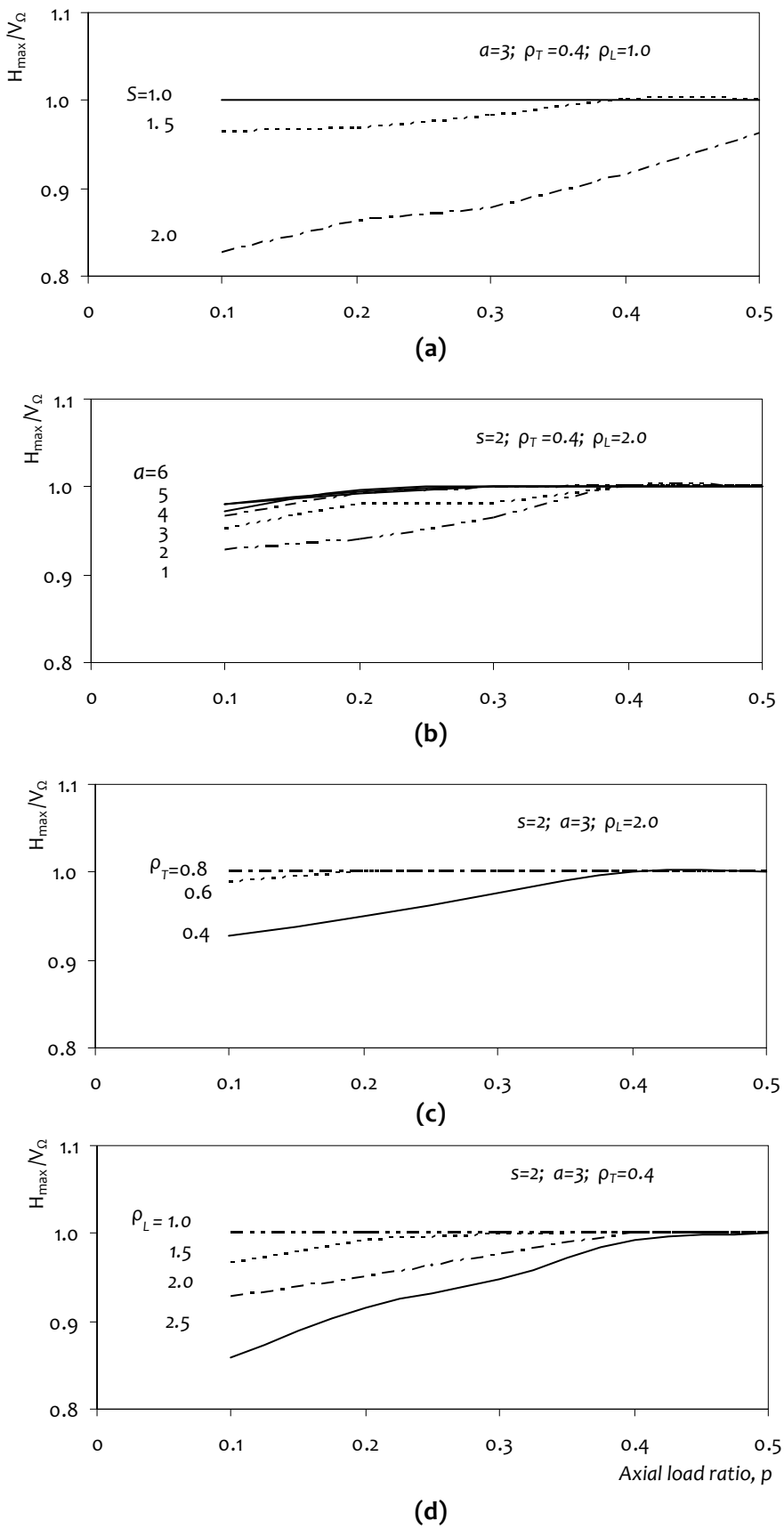

Figure 4.20: Effect of axial load ratio *p* on response of piers for varying (a) slenderness *s*, (b) aspect ratio *a*, (c) percentage of transverse reinforcement ρ_T, and (d) longitudinal reinforcement ratio ρ_L

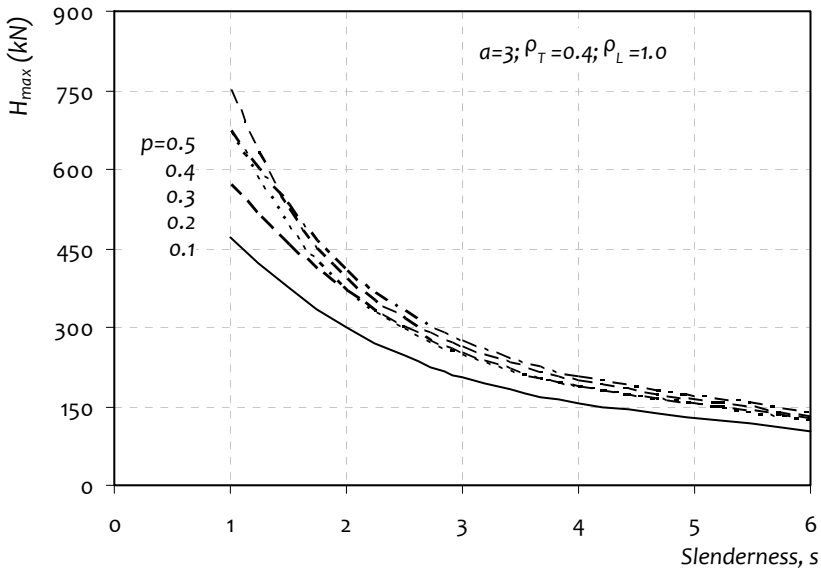

Figure 4.21: Effect of axial load ratio *p* on lateral load capacity of piers for varying slenderness *s*

4.2.1.6 Recommendations

The analytical study (using the proposed method for estimating lateral shear force capacity and *P-V-M* interaction) discussed in this chapter highlights *five main points* on the behaviour of prismatic rectangular RC piers, namely:

(1) Piers with s<4 exhibit shear behaviour predominantly;

(2) Piers with s<2 fail in shear, irrespective of a, ρ_T, ρ_L and p;

(3) Decreasing shear span-to-depth ratio increases shear force capacity of the pier, but leads to failure of pier in brittle shear mode;

(4) Spacing of transverse reinforcement, with constant ρ_T , does not seem to affect shear force capacity of the piers , but, has a major influence on their mode of failure; and

(5) Increasing longitudinal steel enhances flexural capacity of the section, but causes the pier to fail in brittle shear mode.

4.2.2 Conclusions

Effect is studied of different parameters governing the response of prismatic RC members with rectangular cross-sections. Critical parameters that influence mode of failure of RC members are slenderness s and transverse reinforcement ratio ρ_T. Spacing of transverse reinforcement does not have significant effect on lateral load carrying capacity, but prevents brittle shear failure with reduced spacing. On the other hand, increase in longitudinal reinforcement ratio enhances lateral shear force capacity, but causes shear failure. Lateral shear force capacity is found to reduce with increase in

slenderness, irrespective of plan aspect ratio. Further, increase in axial load ratio helps in increasing lateral shear force capacity, even of members with less slenderness. In summary, with a judicious choice of the key parameters, RC members can be made to fail in a ductile mode, for a required lateral shear force capacity.

4.3 BEHAVIOUR OF FLARED RC MEMBERS

Flared RC bridge piers are used widely for their aesthetic appeal; often, a gradual change is provided in cross-section from a relatively narrow one at the base to a wide one at the top. In most flared piers, positioning of longitudinal reinforcement follows the shape of the pier, whereas in some piers, the flared segments are treated as *architectural features* and minimally reinforced. Owing to change in size of cross-section along the height of the pier, design becomes involved of flared piers to resist earthquake effects; poor behaviour of flared piers was observed during past earthquakes due to enhanced flexure capacity in the flared part [Nada *et al*, 2003]. Such increased capacity shifts location of failure away from the base towards the bottom of the flare; even a slender pier that is flared behaves as if it was much shorter, leading to undesirable brittle shear failure mode [Saiidi *et al*, 2001].

The analytical study on prismatic rectangular RC piers presented in Section 4.3 highlights two main points, namely: (i) Piers with s<4 exhibit predominant *shear behaviour*, and (ii) Piers with s<2 fail in *shear*, irrespective of a, ρ_T, ρ_L and p. In flared piers, it is difficult to define s. Also, both *shear* and *flexure* capacities increase simultaneously at different sections in the direction of the flare. Damages to such piers in past earthquakes suggest that damage moves closer to the narrower cross-section (Figure 4.22). An investigation is made to ascertain probable *location* and *type* of failure in such flared piers under earthquake effects; flared piers are studied with square cross-section using the proposed method. Boundary condition at the base of such piers may be taken as hinged [Saiidi *et al*, 2001], and the pier can be idealised as a cantilever with downward flare (Figure 4.22b). Also, a pier with upward flare is considered in the study, for comparison. Details of cross-section of flared piers considered are as shown in Figures 4.23 and 4.24; axial load P considered is 10% of axial force capacity P_u of pier, and grades of steel and concrete are taken as Fe415 and 30 MPa, respectively. Alongside, a prismatic pier is considered with cross-section equal to the narrowest part of flared pier (Figure 4.25). Longitudinal reinforcement is provided along the shape in the flared region. Percentages of transverse and longitudinal steels are kept constant along the height.

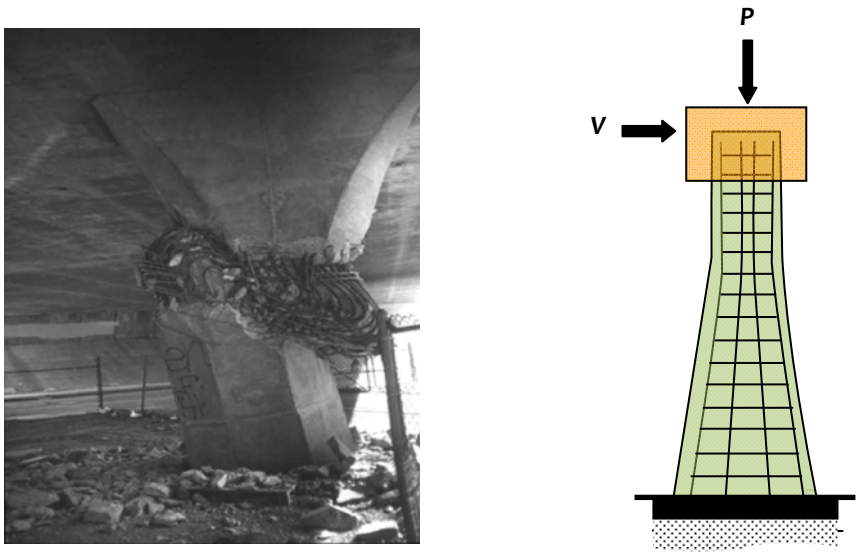

Figure 4.22: (a) Shear failure in flared piers of Mission-Gothic Bridge during 1994 Northridge earthquake [Mitchell *et al*, 1996], and (b) Idealized boundary conditions of flared piers

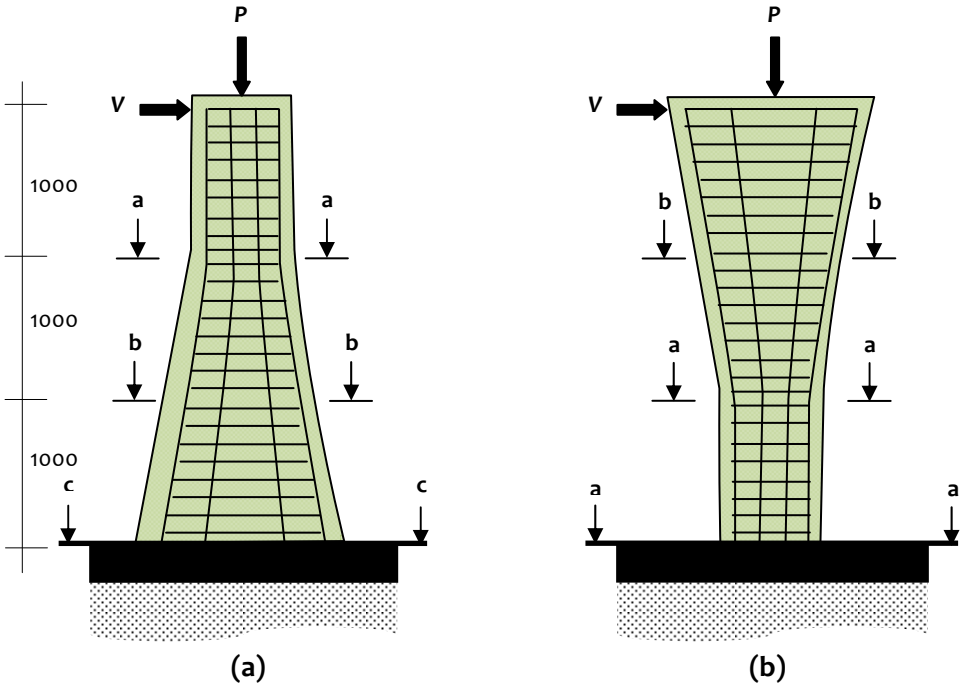

Figure 4.23: Geometry of flared RC piers considered: (a) flared down, and (b) flared up

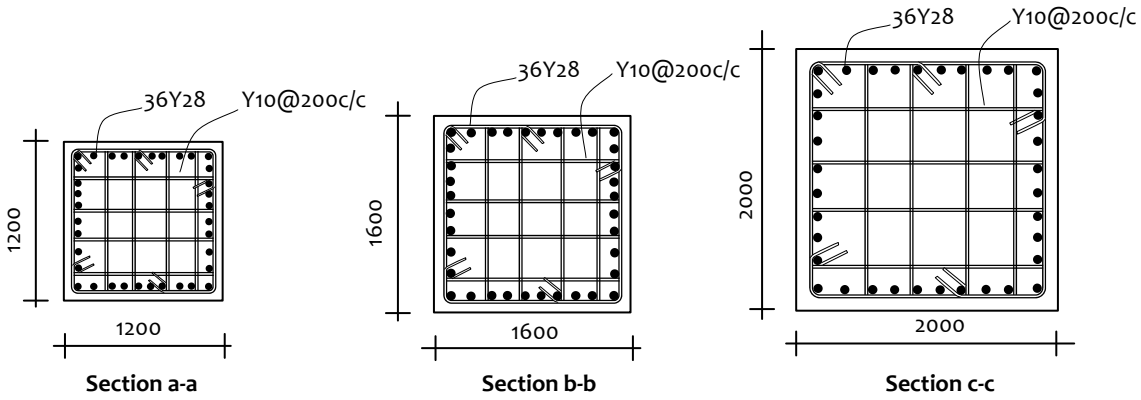

Figure 4.24: Cross-sectional details of flared and prismatic RC pier considered in the study

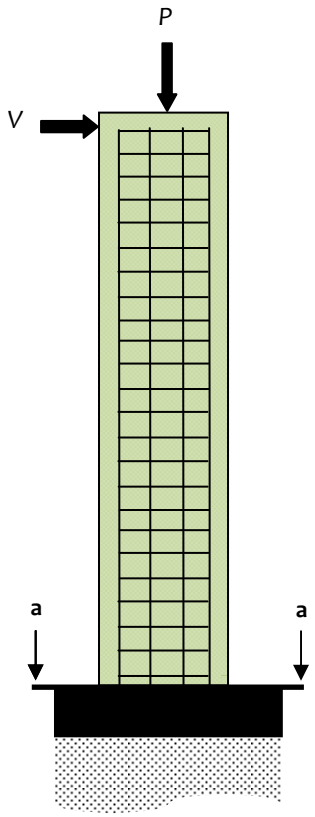

Figure 4.25: Geometry of prismatic RC pier considered in the study

V-M interaction diagrams are obtained at different cross-sections of the members to determine *location* and *mode* of failure in them (Figures 4.26, 4.27). Lateral shear force capacities are estimated at different cross-sections in both flared and prismatic piers. At a section, lateral shear force capacity is computed considering *flexure* failure, as flexural capacity divided by distance of that section from top of the pier. In *flared down* piers, the critical section is at Section 1-1 (Figure 4.26a; refer Section a-a in Figure 4.24 for cross-sectional details); the behaviour is governed by *shear* and the pier has a *shear force capacity* of 3,601 kN (moment capacities at Sections 1-1, 2-2 and 3-3 are 6,306 kNm, 10,606 kNm, and 16,368 kNm, respectively, leading to corresponding flexural overstrength based lateral shear force demand of 6,306 kN, 5,303 kN and 5,456 kN, respectively). Thus, shear failure is likely to occur in the flared down pier at the interface between flared and prismatic portions. On the other hand, in the case of *flared up* piers, the critical section is at Section 3-3 (Figure 4.26b; refer Section a-a of Figure 4.24 for cross-sectional details); the behaviour of the pier is governed by *flexure* and the pier has a *shear force capacity* of 2,102 kN (moment capacity at Section 3-3 is 6,306 kNm, leading to lateral shear force 2,102 kN governed by flexure capacity).

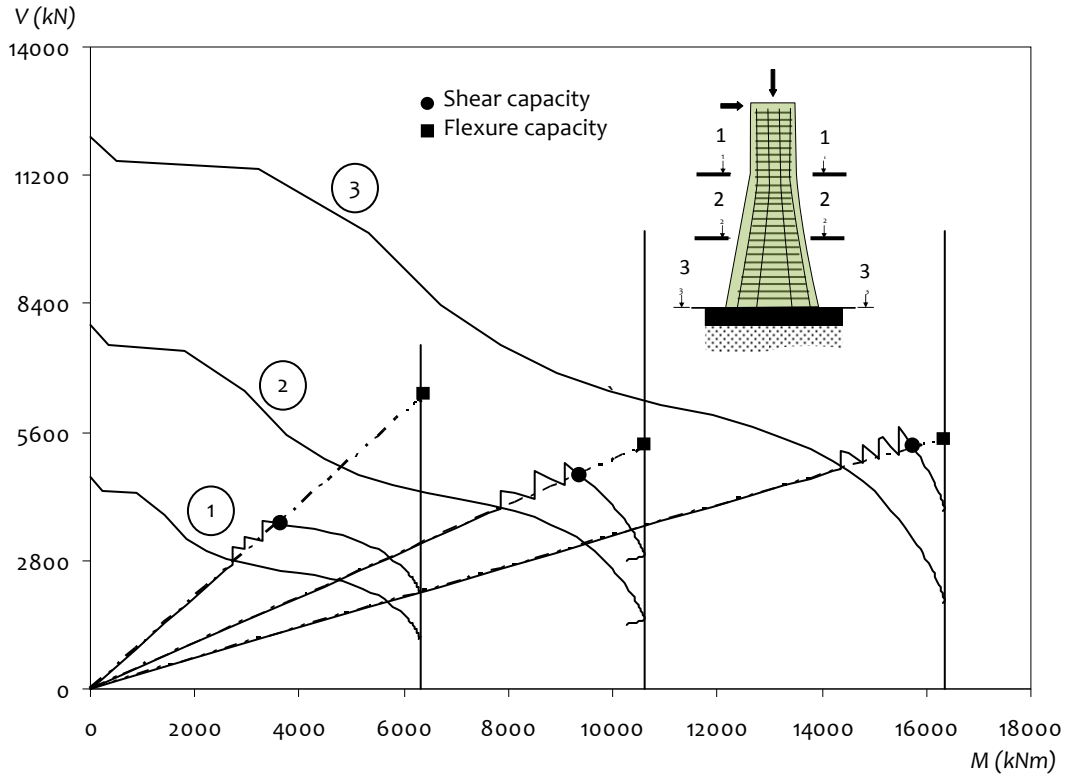

(a)

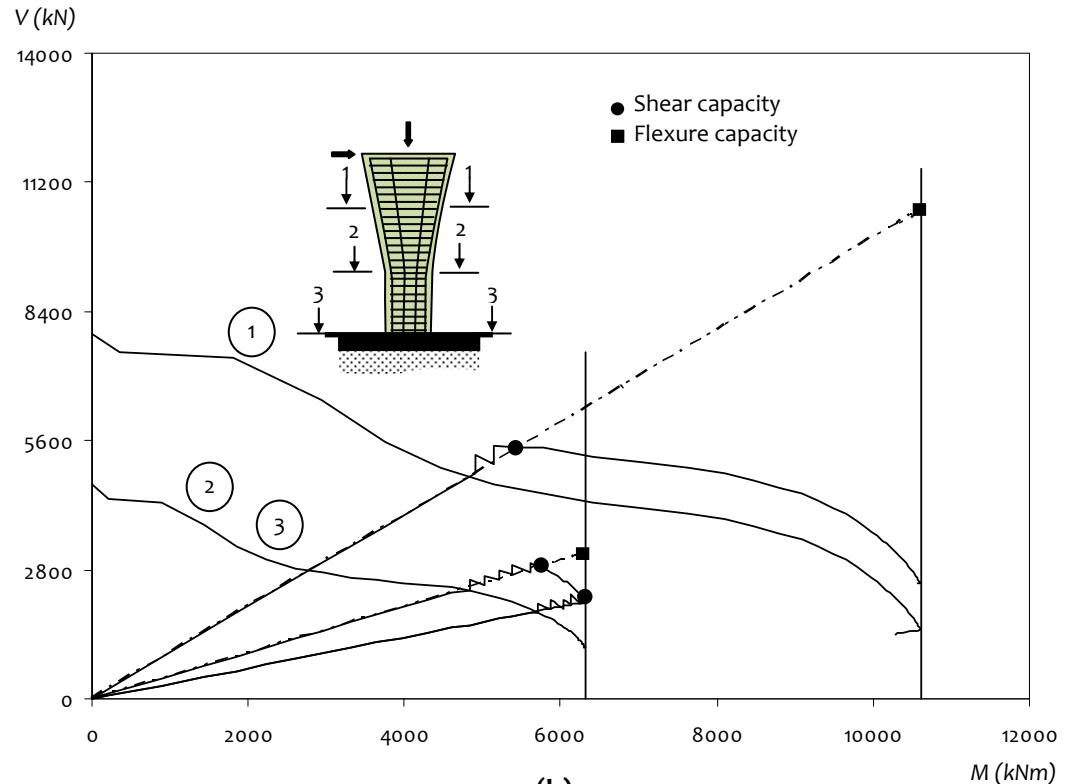

(b)

Figure 4.26: Shear–flexure interaction curves showing lateral load capacity and failure modes for piers (a) flared down, and (b) flared up at various cross-sections

As in the case of flared up, in a prismatic pier, the critical section is at Section 3-3 (Figure 4.27, refer Section a-a of Figure 4.24 for cross-sectional details), and governed by flexure and is 2,102 kN (moment capacity at Section 3-3 is 6,306 kNm, leading to lateral shear force capacity 2,102 kN governed by flexure capacity). This indicates that *flexure failure* is likely to occur in *prismatic* and *flared up* piers at locations of maximum bending moment only. But, *flaring* the piers can lead to undesirable brittle shear failure, although lateral shear force capacity of flared pier is more than that of the corresponding prismatic pier. Results are summarized in Table 4.6.

4.3.1 Conclusions

The analytical study to identify *location* and *mode* of failure of both *prismatic* and *flared* piers requires proper evaluation of shear force capacity as a function of moment demand. Detailing of reinforcement along the height for both *prismatic* and *non-prismatic* piers should account for effect of moment demand on shear force capacity of the section. Contribution is not considered to shear capacity of flared piers by longitudinal reinforcement, particularly when positioning of longitudinal reinforcement follows the shape of the pier; additional investigation is required to ascertain the same.

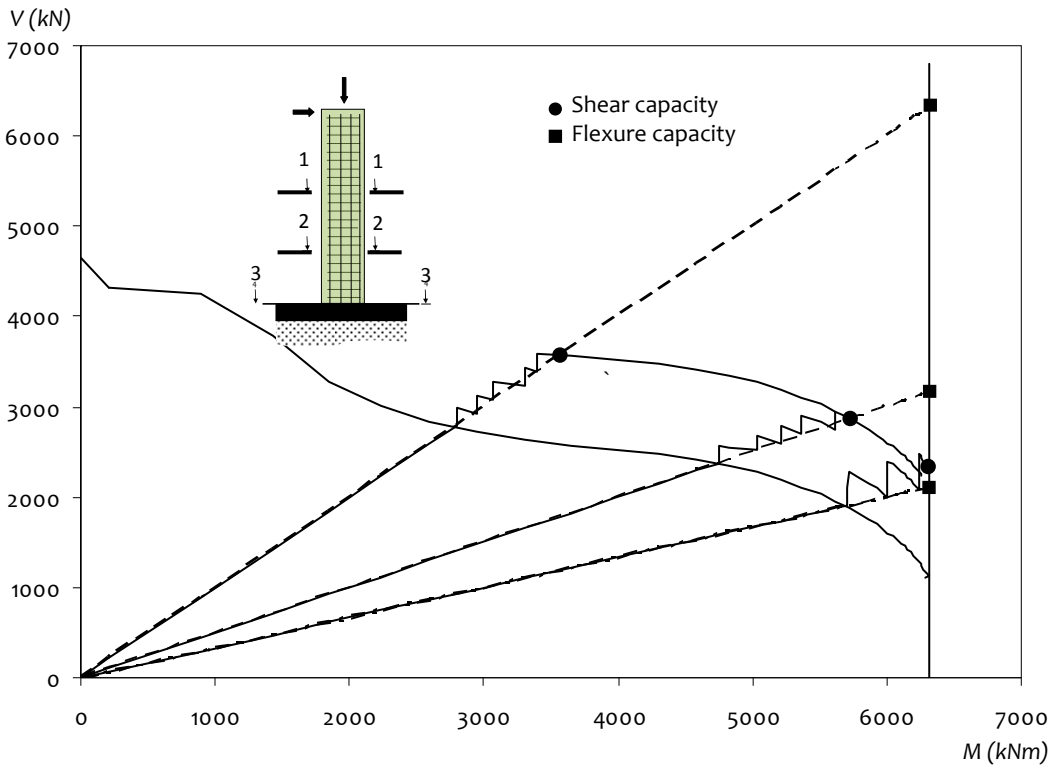

Figure 4.27: Shear-flexure interaction curves showing lateral load capacity and failure modes for prismatic member at various cross-sections

Table 4.6: Failure modes at different levels along height of flared and prismatic piers

At Section Level				At Member Level		
Section	*Lateral Shear Force (kN) corresponding to*		*Failure Mode*	*Failure Load (kN)*	*Failure Location*	*Failure Mode*
	Shear Failure	*Flexure Failure*				
Flared Down						
1-1	3,601	6,306	Shear	3,601	1-1	Shear
2-2	4,670	5,303	Shear			
3-3	5,250	5,456	Shear			
Flared Up						
1-1	5,465	10,606	Shear	2,102	3-3	Flexure
2-2	2,870	3,109	Shear			
3-3	2,127	2,102	Flexure			
Prismatic						
3-3	2,127	2,102	Flexure	2,101	3-3	Flexure

4.4 ANALYTICAL STEPS INVOLVED IN PROPOSED METHOD

Applying the proposed method, the *combined axial-flexure-shear behaviour* of a RC member can be evaluated without difficulty, to estimate *failure load, failure mode* and *failure location* with reasonable accuracy. The proposed analytical method simplifies modelling of RC members, by considering *P-M interaction* and *normal stress - shear stress interaction* based on classical fibre discretization approach as given in Section 3.1. Both cover and core concretes are considered separately; *normal stress – normal strain relation* for confined and unconfined is determined using *Mander's Model* [Mander *et al*, 1998], and *shear stress-shear strain relation* is estimated using *Bresler's Failure Envelope* [Bresler and Pister, 1958]. Then, *P-M interaction envelope* and *M-φ curves* for a given axial load are determined using compatibility conditions given by Eq.(3.1) and equilibrium equations given by Eqs.(3.5) and (3.6). The *P-M interaction envelope* and *σ–τ interaction envelope* are coupled to get *P-V-M* interaction at a section, as explained in Section 3.3. The lateral shear force capacity of a RC member is derived based on the shear resistance mechanism of member presented in detail in Section 4.1, which considers the contributions from concrete, transverse and longitudinal reinforcements. *V-M strength envelope* for a given level of axial load thus generated for a given RC member using the proposed method provides a simple approach to capture the *failure load, failure mode* and *failure location*.

Also, limits are identified (Table 4.7) of amount of transverse reinforcement, depending on slenderness, for use in preliminary understanding of expected mode of

Table 4.7: Limits of transverse reinforcement with varying slenderness ratio and the resulting mode of failure

Slenderness	**Transverse Reinforcement Ratio (%)**			
s	*0.4-0.6*	*0.6-0.8*	*0.8-1.0*	*>1.0*
< 2	Shear	Shear	Shear	Shear
2-3	Shear	Shear	Shear	Flexure
3-4	Shear	Flexure	Flexure	Flexure
> 4	Flexure	Flexure	Flexure	Flexure
Note:: Limits applicable over a range of axial load ratio of 0.1-0.5, longitudinal reinforcement ratio of 1.0%-2.5%, and plan aspect ratio of 1-6				

failure of existing RC prismatic piers, based on parametric study presented Section 4.2. Thus, these limits, together with the proposed method, may help in quick assessment of expected seismic behaviour of existing single column RC bridge piers of rectangular cross-section.

4.5 KEY CONCLUSIONS

An analytical method is proposed to determine mode of failure, location of failure and lateral load at failure, of rectangular RC bridge piers; the same is validated with experimental data published in literature. A parametric study performed with this method identified influence of various parameters on response of bridge piers. Key factors influencing behaviour of RC members are identified as *slenderness* and *transverse reinforcement ratio*; the minimum transverse reinforcement ratio is quantified as a function of varying slenderness for practical range of axial load ratio, plan aspect ratio and longitudinal reinforcement ratio, which will ensure member to fail in flexure mode.

Blank page

5
Summary and Conclusions

5.0 GENERAL

Determining possible behaviour of single RC piers a priori during design process is critical to assure that the overall earthquake response of RC bridges is acceptable. Similarly, predicting possible behaviour of existing stock of RC bridge piers is important in undertaking retrofit strategies. Precluding brittle shear failure of RC piers is essential, especially under increased axial and flexural demands imposed during *strong* earthquake shaking. Towards these goals, estimation is necessary of *shear force capacity* of RC members under combined *Axial Force P – Shear Force V – Bending Moment M*. The present study presents a simple analytical method, which estimates effectively the *failure load*, *failure mode* and *failure location* of RC members, thereby providing better understanding of shear resistance mechanism in RC members.

5.1 SUMMARY

The summary is presented in this section of key activities undertaken as part of the present study.

5.1.1 Section Behaviour

Shear resistance mechanism is postulated of solid RC pier of rectangular cross-sections, which accounts for the interaction of axial, shear and flexural stresses. For assessing the efficacy of this mechanism to capture earthquake behaviour of RC piers:

1. An analytical method is proposed to forecast the inelastic behaviour of solid *RC* piers with rectangular cross-sections under combined action of axial force *P*, shear force *V* and bending moment *M*;
2. Shear strength of concrete is estimated using *normal stress* σ – *shear stress* τ relation and the *three-parameter* Bresler-Pister failure criterion; and

3. Shear–flexure (V_c-M) strength envelope is generated of a RC section, considering *equilibrium equations, compatibility conditions* and *constitutive relations*, for an imposed axial load P.

5.1.2 Member Behaviour

The lateral shear force capacity of a RC member is determined and the key parameters are identified, which influence its behaviour. For establishing this:

1. A simple analytical method is proposed for estimating *shear force capacity* of *RC members* considering contributions of concrete V_c and steel reinforcement bars (V_{st} and V_{sl}));
2. An expression is presented, which estimates the crack angle in RC members under combined actions of axial force P, shear force V and bending moment M, even though the crack angle is assumed to remain constant throughout the path of propagation of the crack;
3. Shear force capacity contributions of steel reinforcement are estimated from:
   (a) Transverse reinforcement V_{st} based on *number of stirrups that intercept the crack*, and on the expression proposed for the *crack angle*; and
   (b) Longitudinal reinforcement V_{sl} based on *dowel action of longitudinal reinforcement bars*, assuming that they are clamped at stirrup levels; and
4. Shear–moment (V-M) *capacity envelope* is derived analytically for solid RC members with rectangular cross-section; this *envelope* is superposed with the *demand diagram* to determine *failure load, failure mode* and *failure location*;
6. The influences are evaluated of prominent structural parameters (namely *axial load ratio*, *plan aspect ratio*, *slenderness*, and *longitudinal & transverse reinforcement ratios*) on response of *prismatic* and *non-prismatic* solid RC members of rectangular cross-section using the proposed analytical method. In particular, influences are studied (through a parametric study) of the above parameters on the shifting of the mode of failure from *brittle shear* failure to *ductile flexure* failure. From this, the key parameters are identified; and
7. Minimum transverse reinforcement to be provided in RC piers is proposed for inclusion as requirements for seismic design of solid RC bridge piers with rectangular cross-section, of different slenderness.

5.2 CONCLUSIONS

The *key* conclusions drawn from the present study are:

1. The analytical method proposed:
   (a) Is effective in estimating *failure load*, identifying *failure mode* and identifying *failure location* in solid RC members with rectangular cross-section; the accuracy of results is comparable to that obtained using *more complex* existing methods;
   (b) Provides simple explanation of *shear resistance mechanism* in RC members subjected to combined action of axial force, shear force and bending moment; and
   (c) Is applicable to solid RC piers of slenderness 1 and more;
2. RC members with slenderness *less than* 2.0 are likely to fail in *shear*, irrespective of *transverse reinforcement ratio*, *longitudinal reinforcement ratio*, *plan aspect ratio* and *axial load ratio*;
3. Shear force capacity reduces with increase in flexural demand, and this should be considered for affecting change in *detailing of reinforcements* along height of both *prismatic* and *non-prismatic* RC members; and
4. The minimum transverse reinforcement required in earthquake-resistant design increases with *decrease* in slenderness of solid RC bridge piers with rectangular cross-section.

5.3 LIMITATIONS OF PRESENT STUDY AND SCOPE FOR FUTURE WORK

The present study is *limited* to understanding behaviour of solid cantilever RC piers with rectangular cross-sections; effects of aggregate interlock, size, and strain rate are not considered. Also, deficiencies are neglected in lap length, anchorage of reinforcement bars and bond strength. Further, the effect is neglected of additional bending moment arising from large lateral deformations in slender RC piers with high axial load. Furthermore, the present study does not estimate lateral *deformation*; only estimate of *shear force capacity* is. In addition, the method of estimation of lateral shear force capacity presented in the study is for *monotonic loading*; effect is not accounted of cyclic loading on shear resistance mechanism.

The comparison of these analytical estimates with the experimental values from tests (reported in literature) based *cyclic loading*, suggests the need for examining effects of cyclic loading on shear resistance mechanism, and incorporating the same in the

analytical method. Thus, based on results of present study and on the unaddressed issues, the scope for possible future work in this area could be:

1. Investigate *P-V-M* strength interaction of *other RC cross-sectional shapes* (like solid circular, and hollow circular & rectangular cross-sections);
2. Investigate *deformability* and *ductility* capacities of RC piers considering *P-V-M* interaction, especially those with high slenderness; and
3. Investigate *shear force* and *lateral deformation capacities* of RC members under *bi-directional lateral loading*, *i.e.,* investigate *P-V-*M_1*-*M_2 interaction.
4. Investigate shear resistance mechanism (failure load, failure mode and failure locations) of non-prismatic solid RC members by undertaking experimental studies on flared piers.
5. Investigate shear resistance mechanism (failure load, failure mode and failure locations) and lateral deformation capacity of *hollow* RC members.

References

[1] AASHTO, (2007), *LRFD Bridge Design Specifications*, 4th Edition, American Association of State Highway and Transportation Officials, Washington, DC., USA

[2] ACI 318-77, (1977), *Building Code Requirements for Reinforced Concrete*, American Concrete Institute, Farmington Hills, USA

[3] ACI 318-83, (1983), *Building Code Requirements for Reinforced Concrete*, American Concrete Institute, Farmington Hills, USA

[4] ACI-ASCE 445/ACI *445R*-99, (2000), *Recent Advances to Shear Design of Structural Concrete*, American Concrete Institute, Farmington Hills, USA

[5] Ang,B.G., (1981), "Ductility of reinforced concrete bridge piers under seismic loading," Report No.81-3, Department of Civil Engineering, *University of Canterbury*, Christchurch, New Zealand

[6] Ang,B.G., Priestley,M.J.N., and Paulay,T., (1989), "Seismic shear strength of circular reinforced concrete columns," *ACI Structural Journal*, Vol.86, No.1, pp 45-59

[7] Atalay,M.B., and Penzien,J., (1975), "The seismic behavior of critical regions of reinforced concrete components as influenced by moment, shear and axial force," Report No.EERC 75-19, *University of California, Berkeley*, USA

[8] Belarbi,A., and Hsu,T.T.C., (1995), "Constitutive laws of softened concrete in biaxial tension-compression," *ACI Structural Journal*, Vol. 92, No.5, pp 562-573

[9] Birgisson,S.R., (2011), "Shear Resistance of Reinforced Concrete Beams without Stirrups," Doctor of Philosophy Thesis, *Reykjavik University, Iceland*

[10] Boys,A.G., (2009), "Assessment of the Seismic Performance of Inadequately Detailed Reinforced Concrete Columns," Master of Engineering Thesis, *University of Canterbury*, New Zealand

[11] Bresler,B., and Pister,K.S., (1958), "Strength of concrete under combined stresses," *ACI Structural Journal*, Vol. 55, No.9, pp 321-345

[12] Burgueno,R., Liu,X., and Hines,E.M., (2014), "Web crushing capacity of high-strength concrete structural walls: Experimental study," *ACI Structural Journal*, Vol. 111, No. 2, pp 235-246

[13] CALTRANS 2006, (2006), *Visual Catalog of Reinforced Concrete Bridge Damage, Structure: Maintenance and Investigations*, CALTRANS, Sacramento, USA

[14] CALTRANS SDC, (2013), *Caltrans Seismic Design Criteria*, Version 1.7, California Department of Transportation, Sacramento, California, USA

[15] Carlo,P., Gustavo,A., Fabio,T., and Artur,P., (2007), "Simplified models/procedures for estimation of secant-to-yielding stiffness, equivalent damping, ultimate deformations and shear capacity of bridge piers on the basis of numerical analysis," LESSLOSS Project/Sub-Project 8: Deliverable 69 – Displacement-Based Design Methodologies, *JRC Scientific and Technical Reports, Italy*, ISSN 1018-5593

[16] CEB-FIP, (2000), "Ductility of reinforced concrete structures," *Bulletin d'Information*, Report No. 242, Thomas Telford Ltd., Lausanne, Switzerland, pp 332

[17] CEN, (2005), *Eurocode 8-Design Design of Structures for Earthquake Resistance-Part 2: Bridges*, EN 1998-2, Brussels, Belgium

[18] Ceresa,P., Petrini,L., and Pinho,R., (2007), "Flexure-shear fibre beam-column elements for modelling frame structures under seismic loading-state of the art," *Journal of Earthquake Engineering*, Taylor & Francis, Vol. 11, Supplement No. 1, pp 46-88

[19] Chan,W.W.L., (1955), "The ultimate strength and deformation of plastic hinges in reinforced concrete frameworks," *Magazine of Concrete Research*, ICE publishing, London, Vol.7, No.21, pp 121-132

[20] Chen,W.F., (2007), *Plasticity in Reinforced Concrete*, J. Ross Publishing, New York, USA, ISBN: 978-1-932159-74-5

[21] Cladera,A., Marí,A., Bairán,J., Oller,E., and Ribas,C., (2015), "Predicting the shear-flexural strength of slender reinforced concrete T and I shaped beams,", *Engineering Structures*, Elsevier, Vol.101, pp 386-398

[22] Collins,M.P., and Mitchell,D., (1991), *Prestressed Concrete Structures*, Prentice Hall, Englewood Cliffs, New Jersey, USA, ISBN: 978-0-136916-35-2

[23] Collins,M.P., Mitchell,D., Adebar,P., and Vecchio,F.J., (1996), "A general shear design method," *ACI Structural Journal*, Vol.93, No.1, pp 36-45

[24] Davey, B.E., (1974), "Reinforced Concrete Bridge Piers under Seismic Loading," Master of Engineering Thesis, *University of Canterbury*, New Zealand

[25] Esaki,F., (1996), "Reinforcing effect of steel plate hoops on ductility of R/C square column," Proceedings of the *11th World Conference on Earthquake Engineering*, Paper No.199, Acapulco, Mexico

[26] FIB, (2007), "Seismic bridge design and retrofit: structural solutions; State-of-art Report," *FIB Bulletin 39,* The International Federation for Structural Concrete (Fib), Lausanne, Switzerland

[27] Geraldine,S.C., and Stone,W.C., (1990), "Behavior of 1/6-Scale Model Bridge Columns Subjected to Inelastic Cyclic Loading," *ACI Structural Journal*, Vol.87, No.6, pp 630-638

[28] Gill,W.D., Park,R., and Priestley,M.J.N., (1979), "Ductility of rectangular reinforced concrete columns with axial load," Report 79-1, Department of Civil Engineering, *University of Canterbury*, Christchurch, New Zealand

[29] Goswami,R., (2002), "Investigation of Seismic Shear Design Provisions of IRC Code for RC Bridge Piers Using Displacement-Based Pushover Analysis," Master of Technology Thesis, Department of Civil Engineering, *Indian Institute of Technology Kanpur*, India

[30] Goswami,R., and Murty,C.V.R., (2005), "Seismic vulnerability of RC bridge piers designed as per current IRC codes including Interim IRC: 6-2002 provisions," *The Indian Roads Congress Journal*, Vol.66, No.2, pp 379-426

[31] Hassan,A.A.A., Hossain,K.M.A., and Lachemi,M., (2008), "Behavior of full-scale self-consolidating concrete beams in shear," *Cement and Concrete Composites*, Elsevier, Vol.30, No.7, pp 588-596

[32] He,X.G., and Kwan,A.K.H., (2001), "Modeling dowel action of reinforcement bars for finite element analysis of concrete structures", *Computer and Structures*, Vol. 79, No.6, pp 595-604

[33] Higai,T., Rizkalla,S.H., Saadat,F., and Ben Omran,H., (1985), "Response of RC bridge piers to large deflection reversals," Technical Report, Department of Civil Engineering, *University of Manibota, Winnipeg*, Manibota, Canada, pp 35

[34] Hoshikuma,J., Kawashima,K., Nagaya,K., and Taylor,A.W., (1997), "Stress-strain model for confined reinforced concrete in bridge piers," *Journal of Structural Engineering, ASCE*, Vol.123, No.5, pp 624-633

[35] Hoshikuma,J., Unjoh,S., and Nagaya,K., (2001), "Size effect on ductile behaviour of reinforced concrete columns under cyclic loading," Proceedings of the *17th US – Japan Bridge Engineering Workshop*, Tsukuba, Japan, pp 421-434

[36] Hoshikuma,J., Unjoh,S., and Nagaya,K., (2002), "Flexural ductility of full-scale bridge columns subjected to cyclic loading," *First FIB Congress*, Osaka, Japan

[37] Hsu,T.T.C., (1988), "Softened truss model theory for shear and torsion," *ACI Structural Journal*, Vol.85, No.6, pp 624–635

[38] Hsu,T.T.C., and Zhang,L.X., (1996), "Tension stiffening in reinforced concrete membrane elements," *ACI Structural Journal*, Vol.93, No.1, pp 108-115

[39] Hsu,Y.T., and Fu,C.C., (2004), "Seismic effect on highway bridges in Chi-Chi earthquake," *Journal of Performance of Constructed Facilities, ASCE*, Vol.18, pp 47-53

[40] IRC 11: 2011, (2011), *Code of Practise for Concrete Road Bridges*, Indian Road Congress, New Delhi, India

[41] IS 456: 2000, (2000), *Indian Standard Code of Practise for Plain and Reinforced Concrete*, Bureau of Indian Standards, New Delhi, India

[42] Japan Road Association 2002, (2002), *Specifications for Highway Bridges, Part V, Seismic Design*, PWRI, Tokyo, Maruzen

[43] James,F.D., (2001), *Nonlinear Analysis of Thin Walled Structures: Statics, Dynamics and Stability*, Springer, ISBN 0-387-95216-0

[44] Kawashima,K., Sasaki,T., Matsumoto,T., Watanabe,G., Nagata,S., Ukon,H., and Kajiwara,K., (2007), "Failure mechanism of column components and systems of bridges," *Proceedings of 2007 Structures Congress*, Structural Engineering Research Frontiers, California, USA, pp 1-16

[45] Kent,D.C., and Park,R., (1971), "Flexural member with confined concrete," *Journal of Structural Engineering, ASCE*, Vol.97, No.7, pp 1969-1990

[46] Kim,T.H., Kim,B.S., Chung,Y.S., and Shin,H.M., (2006), "Seismic performance assessment of reinforced concrete bridge piers with lap splices," *Engineering Structures*, Elsevier, Vol.28, No.6, pp 935-945

[47] Konstantinidis,D., Kappos,A.J., and Izzuddin,B.A., (2004), "Analytical model for unconfined and confined high strength concrete under cyclic loading," *Proceedings of 13th World Conference on Earthquake Engineering*, Vancouver, B.C., Canada, Paper No.2064, pp 1-13

[48] Konstantinidis,D., Kappos,A.J., and Izzuddin,B.A., (2007), "Analytical stress-strain model high strength concrete members under cyclic loading," *Journal of Structural Engineering*, ASCE, Vol.133, No.4, pp 484-494

[49] Kupfer,H., (1964), "Extension to the truss analogy of Morph using the principle of minimum potential energy," *CEB Bulletin d'Information,* Paris, France, No.40, pp 44-57

[50] Lampert,P., and Thurlimann,B., (1971), "Ultimate strength and design of reinforced concrete beams in torsion and bending," Publication No. IABSE 31-I, *IABSE, Zurich*, pp 107-131

[51] Lee,D.H., and Elnashai,A.S. (2001), "Seismic analysis of RC bridge columns with flexure-shear interaction," *Journal of Structural Engineering, ASCE*, Vol.127, No.5, pp 546-553

[52] Lehman,D.E., and Moehle,J.P., (2000), "Seismic performance of well confined concrete bridge columns," PEER Report No. 1998/01, *University of California, Berkeley,* USA

[53] Leondardt,F., (1965), "Reducing the shear reinforcement in reinforced concrete beams and slabs," *Magazine of Concrete Research*, Thomas Telford Ltd., Vol.17, No.53, pp 187–198

[54] Lynn,A., (1999), "Seismic Evaluation of Existing Reinforced Concrete Building Columns," Doctor of Philosophy Thesis, *University of California, Berkeley*, USA

[55] Machida,A., and Abdelkereem,K.H., (2000), "Effect of shear reinforcement on failure mode of RC bridge piers subjected to strong earthquake motions," *Proceedings of the 12th World Conference on Earthquake Engineering*, Auckland, New Zealand, Paper No.1011

[56] Mander,J.B., Priestly,M.J.N., and Park,R., (1988), "Theoretical stress-strain model for confined concrete," *Journal of Structural Engineering, ASCE,* Vol.114, No.8, pp 1804-1826

[57] Mari,A., Bairan,J., Cladera,C., Oller,E., and Ribas,C., (2014), "Shear-flexural strength mechanical model for the design and assessment of reinforced concrete beams," *Journal of Structure and Infrastucture Engineering: Maintenance, Life-Cycle Design and Performance*, Taylor & Francis, Vol.8, No.4, pp 337-353

[58] Martinez-Rueda, J.E., (1997), "Energy dissipation devices for seismic upgrading of RC structures," Doctor of Philosophy Thesis, *Imperial College*, University of London, London

[59] Marini,A., and Spacone,E., (2006), "Analysis of reinforced concrete elements including shear effects," *ACI Structural Journal*, Vol.103, No.5, pp 645–655

[60] Mergos,P.E., and Kappos,A.J., (2008), "A distributed shear and flexural flexibility model with shear–flexure interaction for R/C members subjected to seismic loading," *Earthquake Engineering & Structural Dynamics*, John Wiley & Sons Ltd, Vol. 37, pp 1349–1370

[61] Mergos,P.E., and Kappos,A.J., (2010) "Seismic damage analysis including inelastic shear–flexure interaction," *Bulletin of Earthquake Engineering*, Vol. 8, pp 27–46

[62] Mergos,P.E., and Kappos,A.J., (2012), "A gradual spread inelasticity model for R/C beam-columns, accounting for flexure, shear and anchorage slip," *Engineering Structures*, Elsevier, Vol.44, pp 94–106

[63] Mitchell,D., Bruneau,M., Willilams,M., Anderson,D., Saatcioglu,M., and Sexsmith,R., (1995), "Performance of bridges in the 1994 Northridge Earthquake," *Canadian Journal of Civil Engineering*, NRC Research Press, Vol.22, No.2, pp 415-427

[64] Mo,Y.L., and Wang,S.J., (2000), "Seismic behavior of RC columns with various tie configurations," *Journal of Structural Engineering, ASCE*, Vol.126, No.10, pp 1122–1130

[65] Moretti,M.L., and Tassios,T.P., (2006), "Behaviour and ductility of reinforced concrete short columns using global truss model," *ACI Structural Journal*, Vol.103, No.3, pp 319–327

[66] Munro,I.R.M., (1976), "Seismic Behaviour of Reinforced Concrete Bridge Piers," Master of Engineering Thesis, *University of Canterbury*, New Zealand

[67] Murty,C.V.R., Goswami,R., Vijaynarayanan,A.R., and Vipul,V.M., (2012), *Some Concepts in Earthquake Behaviour of Buildings*, Gujarat State Disaster Management Authority, Gandhinagar, India

[68] Muttoni,A., and Ruiz,M.F., (2008), "Shear strength of members without transverse reinforcement as function of critical shear crack width," *ACI Structural Journal*, Vol.105, No.2, pp 163-172

[69] Nada,H., Sanders,D.H., and Saiidi,M.S., (2003), "Seismic performance of RC bridge frames with architectural flared columns," Report No.CCEER 03-01, *University of Nevada, Reno*, USA

[70] Nagasaka,T., (1982), "Effectiveness of steel fiber as web reinforcement in reinforced concrete column," *Trans Japan Concrete Institute*, Vol.4, pp 493–500

[71] Ngo,D., and Scordelis,A.C., (1967), "Finite Element Analysis of Reinforced Concrete Beams," *ACI Journal Proceedings*, Vol.64, No.3, pp 152-163

[72] NZS 3101:2006, (2006), *Concrete Structures Standard, Part 1: The Design of Concrete Structures Standards*, Standards New Zealand, Wellington, New Zealand

[73] Ousalem,H., Kabeyasawa,T., and Tasai,A., (2004), "Evaluation of ultimate deformation capacity at axial load collapse of reinforced concrete columns," *Proceedings of 13th World Conference on Earthquake Engineering*, Vancouver, BC, Canada, Paper No. 370

[74] Ousalem,H., Kabeyasawa,T., Tasai,A., and Iwamoto,J., (2003), "Effect of hysteretic reversals on lateral and axial capacities of reinforced concrete columns," *Proceedings of the Annual Conference of Japan Concrete Institute*, Kyoto, Japan, Vol.25, No.2, pp 367–372

[75] Pan,Z., and Li,B., (2012), "Truss–Arch model for shear strength of shear-critical reinforced concrete columns," *Journal of Structural Engineering, ASCE*, Vol.139, No.4, pp 548–560

[76] Pang,X.B., and Hsu,T.T.C., (1995), "Behaviour of reinforced concrete membrane elements in shear," *ACI Structural Journal*, Vol.92, No.6, pp 665-679

[77] Park,H., and Eom,T., (2007), "Truss model for nonlinear analysis of RC members subject to cycling loading," *Journal of Structural Engineering, ASCE*, Vol.133, pp 1351–1363

[78] Park,H.G., Choi,K.K., and Wight,J.K., (2006), "Strain-based shear strength model for slender beams without web reinforcement," *ACI Structural Journal*, Vol.103, No.6, pp 783-793

[79] Park,H.G., Yu,E.J., and Choi,K.K., (2012), "Shear-strength degradation model for RC columns subjected to cyclic loading," *Engineering Structures*, Elsevier, Vol.34, pp 187–197

[80] Park,R., and Paulay,T., (1975), *Reinforced Concrete Structures*, John Wiley & Sons, UK

[81] Paulay,T., and Priestley,M.J.N., (1992), *Seismic Design of Reinforced Concrete and Masonry Buildings*, John Wiley and Sons, New York, ISBN: 978-0-471-54915-4

[82] Penelis,G.G., and Kappos,A.J., (1997), *Earthquake Resistant Concrete Structures*, E&FN Spon, Chapman & Hall, London, ISBN: 0-419-18720-0

[83] Penzien,J., Seible,F., Bolt,B.A., Idriss,I.M., Nicoletti,J.P., Preece,F.R., and Roberts,J.E., (2003), "The race to seismic safety (Protecting California's transportation system)," *Caltrans Seismic Advisory Board*, California, USA

[84] Petrangeli,M., Pinto,P.E., and Ciampi,V., (1999), "Fiber Element for Cyclic Bending and Shear of R/C Structures, Part I: Theory," *Journal of Engineering Mechanics*, ASCE, Vol. 125, No. 9, pp 994-1001

[85] Pillai,S.U., and Menon,D., (2009), *Reinforced Concrete Design*, 3rd Edition, Tata McGraw-Hill Publishing Company Limited, New-Delhi, India, ISBN-13: 978-0-070-14110-0

[86] Priestley,M.J.N., and Benzoni,G., (1996), "Seismic performance of circular columns with low longitudinal reinforcement ratios," *ACI Structural Journal*, Vol.93, No.4, pp 474-485

[87] Priestley,M.J.N., and Park,R., (1987), "Strength and ductility of concrete bridge columns under seismic loading," *ACI Structural Journal*, Vol.84, No.1, pp 61-76

[88] Priestley,M.J.N, Seible,F., and Calvi,G.M., (1996), *Seismic Design and Retrofit of Bridges*, John Wiley and Sons, New York, ISBN-13: 978-0471579984

[89] Priestley,M.J.N., Verma,R., and Xiao,Y., (1994), "Seismic shear strength of reinforced concrete columns," *Journal of Structural Engineering, ASCE*, Vol.120, No.8, pp 2310–2329

[90] Ramirez,J.A., and Breen,J.E., (1991), "Evaluation of a modified truss-model approach for beams in shear," *ACI Structural Journal*, Vol.88, No.5, pp 562–571

[91] Ranzo,G., and Petrangeli,M., (1998), "A fibre finite beam element with section shear modelling for seismic analysis of RC structures," *Journal of Earthquake Engineering*, Taylor & Francis, Vol.2, No.3, pp 443–473

[92] Razvi,S.R., and Saatcioglu,M., (1994), "Strength and deformability of confined high-strength concrete columns," *ACI Structural Journal*, Vol.91, No.6, pp 678-687

[93] Recupero,A., D'Aveni,A., and Ghersi,A., (2003), "N-M-V Interaction Domains for Box I-shaped Reinforced Concrete Members," *ACI Structural Journal*, Vol.100, No. 1, pp 113-119

[94] Rodrigues,H., Arede,A., Varum,H., and Costa,A.G., (2013), "Experimental evaluation of rectangular reinforced concrete column behaviour under biaxial cyclic loading," *Earthquake Engineering Structural Dynamics*, John Wiley & Sons Ltd, Vol.42, No.2, pp 239–259

[95] Rossi,P.P., (2013), "Evaluation of the ultimate strength of R.C. rectangular columns subjected to axial force, bending moment and shear force," *Engineering Structures*, Elsevier, Vol.57, pp 339-355

[96] Roy,H.E.H., and Sozen, .A., (1964), "Ductility of concrete," *Proceedings of the International Symposium on Flexural Mechanics of Reinforced Concrete*, Miami, pp 213-224

[97] Saadeghvaziri,M.A., and Foutch,D,A., (1988), "Inelastic response of RC bridges under horizontal and vertical earthquake motions," Structural Research Series No.540, Civil Engineering Studies, *University of Illinois, Urbana–Champaign*, Illinois, USA

[98] Saatcioglu,M., and Grira,M., (1999), "Confinement of reinforced concrete columns with welded reinforcement grids," *ACI Structural Journal*, Vol.96, No.1, pp 29–39

[99] Saatcioglu,M., and Ozcebe,G., (1989), "Response of reinforced concrete columns to simulated seismic loading," *ACI Structural Journal*, Vol.86, No.1, pp 3–12

[100] Saatcioglu,M., and Razvi,S.R., (1992), "Strength and ductility of confined concrete," *Journal of Structural Engineering, ASCE*, Vol.118, No.6, pp 1590-1607

[101] Saiidi,M.S., Wehbe,N.I., Sanders,D.H., and Caywood,C.J., (2001), "Shear Retrofit of Flared RC Bridge Columns Subjected to Earthquakes," *Journal of Bridge Engineering, ASCE* , Vol.6, No.3, pp 189-197

[102] Sakai,K., and Sheikh,S.A., (1989), "What do we know about confinement in reinforced columns?," *ACI Structural Journal*, Vol.86, No.2, pp 192–207

[103] Schlaich,J., Schafer,K., and Jennewein,M., (1987), "Toward a Consistent Design of Structural Concrete," *Journal of the Precast/Prestressed Concrete Institute*, Vol.32, No.3, pp 75-149

[104] Scott,B.D., Park,R., and Priestley,M.J.N., (1982), "Stress-strain behaviour of concrete confined by overlapping hoops at low and high strain rates," *ACI Structural Journal*, Vol.79, No.1, pp 13-27

[105] Sezen,H., (2002), "Seismic Behavior and Modeling of Reinforced Concrete Building Columns," Doctor of Philosophy Thesis, *University of California, Berkeley*, USA

[106] Sheikh,S.A., and Uzumeri,S.M., (1982), "Analytical model for concrete confinement in tied columns," *Journal of Structural Engineering, ASCE*, Vol.108, No.12, pp 2703-2722

[107] Si,B.J., Sun,Z.G., Ai,Q.H., Wang,D.S., and Wang, Q.X., (2014), "Experiments and simulation of flexural-shear dominated RC bridge piers under reversed cyclic loading," *Proceedings of the 14th World Conference on Earthquake Engineering*, Beijing, China

[108] Soesianawati,M.T., Park,R., and Priestley,M.J.N., (1986), "Limited ductility design of reinforced concrete columns," Report 86-10, Department of Civil Engineering, *University of Canterbury*, Christchurch, New Zealand

[109] Sotoud,S., and Aboutaha,R.S., (2014), "Performance of RC bridge columns subjected to lateral loading," *Proceedings of the Istanbul Bridge Conference*, Istanbul, Turkey

[110] SP 16: 1980, (1980), *Design Aids for Reinforced Concrete Structures*, Bureau of Indian Standards, New Delhi

[111] Stone,W.C., and Geraldine,S.C., (1989), "Inelastic behavior of full-scale bridge columns subjected to cyclic loading," NIST Building Science Series 166, *National Institute of Standards and Technology*, US Department of Commerce, Washington, USA

[112] Sun,Z.G., Si,B.J., Wang,D.S., and Guo,X., (2008), "Experimental research and finite element analysis of bridge piers failed in flexure-shear modes," *Earthquake Engineering and Engineering Vibration*, Springer, Vol.7, No.4, pp 403–414

[113] Tanaka,H., and Park,R., (1990), "Effect of lateral confining reinforcement on the ductile behavior of reinforced concrete columns," Report 90-2, Department of Civil Engineering, *University of Canterbury*, New Zealand

[114] Tarakji,G., (1992),''Lessons not learned from 1989 Loma Prieta earthquake," *Journal of Professional Issues in Engineering Education and Practice, ASCE*, Vol.118, No.2, Paper No. 1302

[115] Taylor,A.W., Kuo,C., Wellenius,K., and Chung,D., (1997), "A summary of cyclic lateral load tests on rectangular reinforced concrete columns," *National Institute of Standards and Technology*, US Department of Commerce, Washington, Report NISTIR 5984

[116] Tegos,I.A., and Penelis,G.G., (1988), "Seismic resistance of short columns and coupling beams reinforced with inclined bars," *ACI Structural Journal*, Vol.85, No.1, pp 82–88

[117] Tim,B., (2014), Seismic Performance of Reinforced Concrete Bridge Columns Constructed with Grade 80 Reinforcement, Master of Science Thesis, *Oregon State University*, USA

[118] Tompos,E.J., and Frosch,R.J., (2002), "Influence of beam size, longitudinal reinforcement, and stirrup effectiveness on concrete shear strength," *ACI Structural Journal*, Vol.99, No.5, pp 559–67

[119] Tureyen,A.K., and Frosch,R.J., (2003), "Concrete shear strength: Another perspective," *ACI Structural Journal*, Vol.100, No.5, pp 609-615

[120] Umehara,H., and Jirsa,J.O., (1982), "Shear strength and deterioration of short reinforced concrete columns under cyclic deformations," PMFSEL Report No. 82-3, Department of Civil Engineering, *University of Texas, Austin*, Texas, USA

[121] Vecchio,F.J., and Collins,M.P., (1986), "The modified compression field theory for reinforced concrete elements subjected to shear," *ACI Structural Journal*, Vol. 83, No.2, pp 219–231

[122] Vecchio,F.J., and Collins,M.P., (1988), "Predicting the response of reinforced concrete beams subjected to shear using the modified compression field theory," *ACI Structural Journal*, Vol.85, No.3, pp 258–268

[123] Watson,S., and Park,R., (1989), "Design of reinforced concrete frames of limited ductility," Report 89-4, Department of Civil Engineering, *University of Canterbury*, Christchurch, New Zealand

[124] Wight,J.K., and Sozen,M.A., (1973), "Shear strength decay in reinforced concrete columns subjected to large deflection reversals," Structural research series no. 403, Civil Engineering Studies, *University of Illinois, Urbana–Champaign*, Illinois, USA

[125] Wong,Y.L., Paulay,T., and Priestley,M.J.N., (1993), "Response of circular reinforced concrete columns to multidirectional seismic attack," *ACI Structural Journal,* Vol.90, No.2, pp 180–191

[126] Xie,Y.P., Li,Z.B., Song,J., and Du,X.L., (2011), "Shear size effect analysis of reinforced concrete column based on Truss-Arch Model," *Applied Mechanics and Materials*, Trans Tech Publications Ltd., Vols. 90-93, pp 3145-3150

[127] Yap,S.L., (2012), "Strut and tie modelling of reinforced concrete short span beams," *Proceedings of the 1st Civil and Environmental Engineering Student Conference*, London, UK

[128] Yeh,Y.K., Mo,Y.L., and Yang,C.Y., (2002), "Seismic performance of rectangular hollow bridge columns," *Journal of Structural Engineering, ASCE*, Vol.128, No.1, pp 60-68

[129] Yoshimura,M., and Nakamura,T., (2003), "Axial collapse of reinforced concrete short columns," *Proceedings of the 4th US–Japan Workshop on Performance Based Earthquake Engineering Methodology for Reinforced Concrete Building Structures*, Toba, Japan, pp 187–198

[130] Zahn,F.A., Park,R., and Priestley,M.J.N., (1986), "Design of reinforced bridge columns for strength and ductility," Report 86-7, Department of Civil Engineering, *University of Canterbury*, Christchurch, New Zealand

[131] Zhou,X., Satoh,T., Jiang,W., Ono,A., and Shimizu,Y., (1985), "Behavior of reinforced concrete short column under high axial load," *Trans Japan Concrete Institute*, Vol.9, pp 541–548

[132] Zhu,L., Elwood,K.J., and Haukaas,T., (2007), "Classification and seismic safety evaluation of existing reinforced concrete columns," *Journal of Structural Engineering, ASCE*, Vol.133, No.9, pp 1316-1330

Annex A
Design *P-M* Interaction

A.1 METHODOLOGY

A simple mechanics driven, hand calculation based method is proposed for use in design practice to develop *P-M* interaction curves for RC sections. Such a simplified approach overcomes the large computational effort required for generating *Design P-M Curves*. This method follows IS 456 [IS 456, 2000] of employing the limiting strains of constituent materials, *i.e.*, concrete and reinforcing steel, to determine the *design strength* of RC sections subjected to combined *axial load P* and *uniaxial bending moment M*. Hence, the following considerations are made in computing *design strength* of RC sections in line with IS 456:

(i) Plane sections normal to the axis of the member remain plain after bending, indicating the normal strain distribution to be linear across the cross-section;

(ii) Design stress-strain curves of concrete and reinforcing steel are as shown in Figure A.1;

(iii) Tensile strength of concrete is ignored;

(iv) Limiting strain in concrete in compression is 0.0035; and

(v) Limiting strain in reinforcing steel, both in compression and in tension, is $0.002+(f_y/1.15E_s)$.

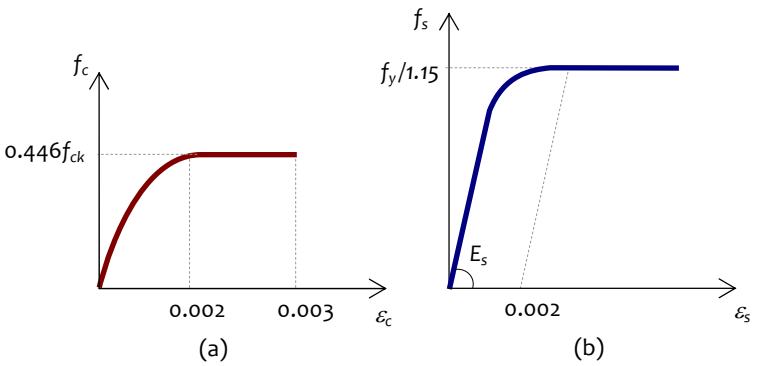

Figure A.1: Design stress-strain curves (a) concrete and (b) steel [IS 456, 2000]

Thus:

(a) In RC sections, whose strength is governed primarily by concrete in compression (commonly called *over-reinforced sections*), the limit state is reached when the strain in the *highly compressed edge* reaches a limiting strain of 0.0035;

(b) In RC sections, whose strength is governed simultaneously by both concrete in compression and reinforcing steel in tension (commonly called *balanced sections*), the limit state is reached when simultaneously, the strain in the *highly compressed edge* reaches a *limiting strain of* 0.0035 and the strain in the *outermost tensile reinforcing steel* reaches a *limiting strain of* $0.002+(f_y/1.15E_s)$, and

(c) In RC sections, whose strength is governed primarily by reinforcing steel in tension (commonly called *under-reinforced sections*), the limit state is reached when the strain in the outermost tensile reinforcing steel reaches limiting strain of $0.002+(f_y/1.15E_s)$.

While most of the considerations are same as given in IS 456, the limiting strain of concrete under uniform compression is taken as 0.0035, in contrast to 0.002 specified in IS 456. Under *strain-controlled loading* (as is the case of *earthquake shaking*), strain in concrete can attain a value of 0.0035 under uniform compression without significantly altering the strength capacity of the section. Thus, the first two limiting strains of concrete and reinforcing steel are used to facilitate a *consistent* computational approach for arriving at the *Design P-M Interaction Curve* of RC sections.

Design P-M Interaction Curve of RC sections can be constructed with a series of straight lines joining the *eight* salient points characterised by their *unique* normal strain distribution diagrams, as shown in Figure A.2. These eight salient points are:

(1) *Point A* represents the condition of *uniform axial compression* – the entire cross-section is at the *limiting compressive strain* of 0.0035; the stress in both top and bottom reinforcing steels are that corresponding to a strain of 0.0035;

(2) *Point B* represents the condition when the *strain in the least compressed (bottom) edge is* 0.002, and *that in the highly compressed (top) edge* 0.0035 – stresses in top and bottom reinforcing steels are different, although stress in concrete is constant (at $0.446f_{ck}$) over the entire cross-section;

(3) *Point C* represents the condition of *onset of cracking of concrete* – the strain in the bottom edge of concrete is *zero* and that in the topmost compressed edge of concrete 0.0035. Beyond this state, a portion of concrete is subjected to tensile strain, and

therefore, cracking starts; the full *nonlinear* design stress block of concrete in compression is mobilised over the entire depth of the cross-section.

(4) *Point D* represents the condition where *strain in the outermost layer of reinforcing steel (near the bottom edge) is zero*, and *that in the highly compressed (top) edge of concrete* 0.0035 – neutral axis depth is equal to the effective depth of the cross-section.

(5) *Point E* represents the condition of *balanced failure* – the highly compressed (top) edge of concrete in compression and the outermost layer of reinforcing steel in tension are at their corresponding limiting strain values, namely 0.0035 and $0.002+(f_y/1.15E_s)$ respectively; neutral axis depth is computed directly from the strain distribution diagram.

(6) *Point* F represents the condition where *strain in the outermost layer of reinforcing steel in tension is* $0.002+(f_y/1.15E_s)$, and that *in the innermost layer of steel (near the compressed concrete edge) is zero*.

(7) *Point G* represents the condition where *strain in the outermost reinforcing steel layer is* $0.002+(f_y/1.15E_s)$, and that *in the topmost edge of concrete is zero*.

(8) *Point H* representing the condition of *pure axial tension* – the entire cross-section is at a tensile strain of $0.002+(f_y/1.15E_s)$.

For each of these points, simple step-wise calculation is enough to estimate the axial load P and bending moment M values using the said strain distribution; it does not require any iterative procedure. This provides a simple hand calculation based method to develop the *Design P-M Interaction Curves* of rectangular RC sections.

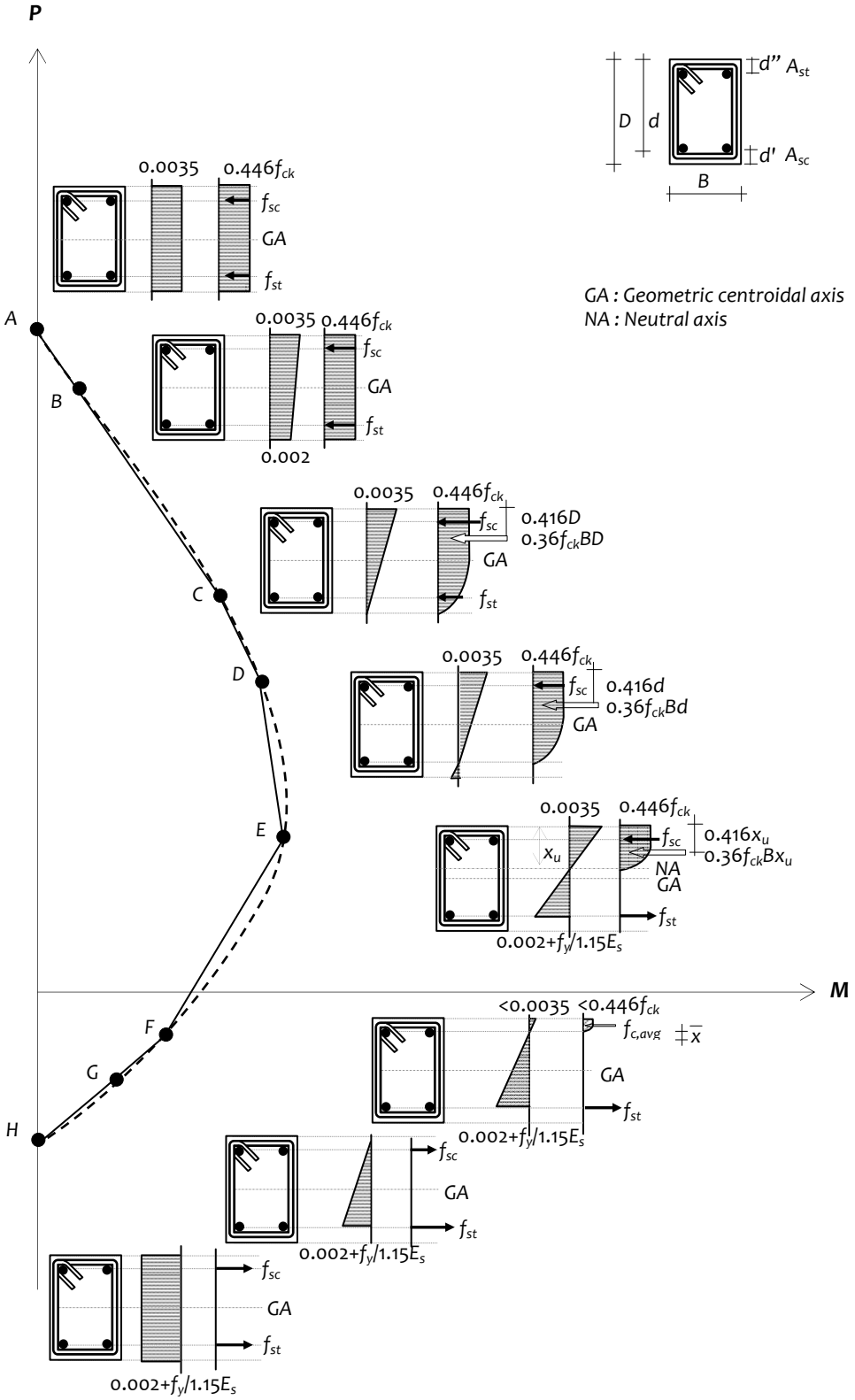

Figure A.2: Normal strain and stress distributions in a RC section corresponding to the eight salient points on its design *P-M* interaction diagram

A.2 EXPRESSIONS OF DESIGN *P* AND *M* AT SALIENT POINTS

Expressions for estimating *P* and *M* corresponding to the said eight salient points on the design *P-M* interaction curve are:

Point A

$$\begin{aligned} P_A &= 0.45 f_{ck} BD + (f_{sc} - 0.45 f_{ck}) A_{sc} + (f_{st} - 0.45 f_{ck}) A_{st} \\ M_A &= 0 \end{aligned} \tag{A.1}$$

Point B

$$\begin{aligned} P_B &= 0.45 f_{ck} BD + (f_{sc} - 0.45 f_{ck}) A_{sc} + (f_{st} - 0.45 f_{ck}) A_{st} \\ M_B &= (f_{sc} - 0.45 f_{ck}) A_{sc} \left[\frac{D}{2} - d'' \right] - (f_{st} - 0.45 f_{ck}) A_{st} \left[\frac{D}{2} - d' \right] \end{aligned} \tag{A.2}$$

Point C

$$\begin{aligned} P_C &= 0.36 f_{ck} BD + (f_{sc} - f_{csc}) A_{sc} + (f_{st} - f_{cst}) A_{st} \\ M_C &= 0.36 f_{ck} BD \left[\frac{D}{2} - 0.416 D \right] + (f_{sc} - f_{csc}) A_{sc} \left[\frac{D}{2} - d'' \right] - (f_{st} - f_{cst}) A_{st} \left[\frac{D}{2} - d' \right] \end{aligned} \tag{A.3}$$

Point D

$$\begin{aligned} P_D &= 0.36 f_{ck} B(D - d') + (f_{sc} - f_{csc}) A_{sc} \\ M_D &= 0.36 f_{ck} B(D - d') \left[\frac{D}{2} - 0.416(D - d') \right] + (f_{sc} - f_{csc}) A_{sc} \left[\frac{D}{2} - d'' \right] \end{aligned} \tag{A.4}$$

Point E

$$\begin{aligned} P_E &= 0.36 f_{ck} B x_u + (f_{sc} - f_{csc}) A_{sc} - f_{st} A_{st} \\ M_E &= 0.36 f_{ck} B x_u \left[\frac{D}{2} - 0.416 x_u \right] + (f_{sc} - f_{csc}) A_{sc} \left[\frac{D}{2} - d'' \right] + f_{st} A_{st} \left[\frac{D}{2} - d' \right] \end{aligned} \tag{A.5}$$

Point F

$$\begin{aligned} P_F &= f_{c,avg} B d'' - f_{st} A_{st} \\ M_F &= f_{c,avg} B d'' \left[\frac{D}{2} - (d'' - \bar{x}) \right] + f_{st} A_{st} \left[\frac{D}{2} - d' \right] \end{aligned} \tag{A.6}$$

Point G

$$\begin{aligned} P_G &= -f_{sc} A_{sc} - f_{st} A_{st} \\ M_G &= -f_{sc} A_{sc} \left[\frac{D}{2} - d'' \right] + f_{st} A_{st} \left[\frac{D}{2} - d' \right] \end{aligned} \tag{A.7}$$

Point H

$$\begin{aligned} P_H &= -f_{sc} A_{sc} - f_{st} A_{st} \\ M_H &= 0 \end{aligned} \tag{A.8}$$

In the above expressions, compressive loads are considered positive, and tensile loads negative. Further, the above expressions are for solid RC members with rectangular cross-sections and uniform distribution of reinforcing steel on *two faces*.

In RC sections with uniform distribution of reinforcing steel on *four faces*, strain and stress distributions at the eight salient points remain identical as in the case of RC sections with uniform distribution of reinforcing steel on two faces presented earlier. Typical strain and stress distributions on a rectangular RC section for a general case are shown in Figure A.3. Strain and stress in the intermediate layers of steel reinforcing bars are considered in addition to those in the innermost and outermost layers, for estimating design *P* and *M* capacities of the section. Expressions for design *P* and *M* for the typical state shown in *Figure 3* are:

$$\begin{aligned} P &= f_{c,avg} B x_u + \sum_{i=1}^{n} f_{sc,i} A_{sc,i} - \sum_{i=1}^{n} f_{st,i} A_{st,i} \\ M &= f_{c,avg} B x_u \left[\frac{D}{2} - \left(d_i'' - \bar{x} \right) \right] + \sum_{i=1}^{n} f_{sc,i} A_{sc,i} \left[\frac{D}{2} - d_i'' \right] + \sum_{i=1}^{n} f_{st,i} A_{st,i} \left[\frac{D}{2} - d_i' \right] \end{aligned} \quad \text{(A.9)}$$

Average compressive stress $f_{c,avg}$ in concrete, compressive stress f_{csc} in concrete at the level of innermost reinforcing steel in compression, and distance $\bar{x}$ of resultant compressive force in concrete from the neutral axis, are:

$$f_{c,avg} = \begin{cases} 0.45 f_{ck} \left[\left(\dfrac{\varepsilon_c}{0.002} \right) - \dfrac{1}{3} \left(\dfrac{\varepsilon_c}{0.002} \right)^2 \right] & 0 \le \varepsilon_c \le 0.002 \\ 0.45 f_{ck} \left[1 - \dfrac{1}{3} \left(\dfrac{0.002}{\varepsilon_c} \right) \right] & 0.002 \le \varepsilon_c \le 0.0035 \end{cases} \quad \text{(A.10)}$$

$$f_{csc} = \begin{cases} 0.45 f_{ck} \left[2 \left(\dfrac{\varepsilon_c}{0.002} \right) - \left(\dfrac{\varepsilon_c}{0.002} \right)^2 \right] & 0 \le \varepsilon_c \le 0.002 \\ 0.45 f_{ck} & 0.002 \le \varepsilon_c \le 0.0035 \end{cases} \quad \text{(A.11)}$$

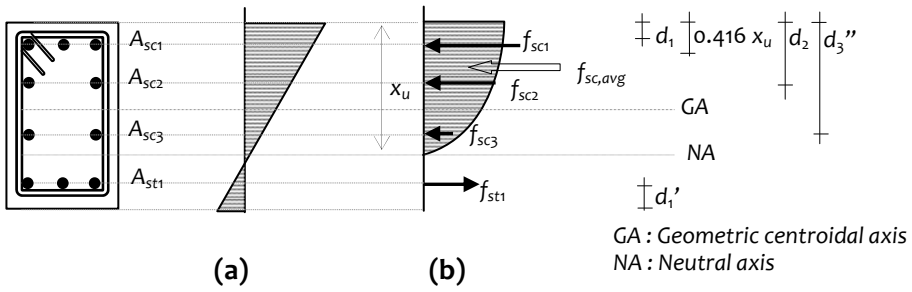

Figure A.3: General case of a rectangular RC section with uniform distribution of reinforcing steel on all four faces: (a) strain distribution, and (b) stress distribution

$$\bar{x} = \begin{cases} \dfrac{\left[\dfrac{2}{3} - \dfrac{1}{4}\left(\dfrac{\varepsilon_c}{0.002}\right)\right]}{\left[1 - \dfrac{1}{3}\left(\dfrac{\varepsilon_c}{0.002}\right)\right]} x_u & 0 \le \varepsilon_c \le 0.002 \\ \dfrac{\left[\dfrac{1}{2} - \dfrac{1}{12}\left(\dfrac{0.002}{\varepsilon_c}\right)^2\right]}{\left[1 - \dfrac{1}{3}\left(\dfrac{0.002}{\varepsilon_c}\right)\right]} x_u & 0.002 \le \varepsilon_c \le 0.0035 \end{cases} \qquad \text{(A.12)}$$

In Eqs.(A.1) to (A.12) that follow, f_{ck} is the characteristic cube strength of concrete, f_{sc} the stress in reinforcing steel in compression; f_{csc} the stress in concrete at the level of reinforcing steel in compression; f_{st} the stress in reinforcing steel in tension; A_{st} the area of reinforcing steel in tension; A_{sc} the area of reinforcing steel in compression; d' the distance of the centre of reinforcing steel in tension from the least compressed or tensile edge; d'' distance of the centre of reinforcing steel in compression from the highly compressed; B, D and d the width, overall depth and effective depth of the rectangular RC section; and P and M are the design axial load and moment.

Design P-M Curves obtained by the proposed method are compared with those obtained using SP 16 [SP 16, 1980] (Figure A.4*)* for two rectangular RC sections – the first section has reinforcing steel bars uniformly distributed on two faces, and second, on all four faces. The maximum difference of design values obtained by the proposed method from that obtained using SP 16 (in the range CD and DE) is less than 9%; this is attributed to the proposal of multi-linear curve in place of the otherwise nonlinear curve.

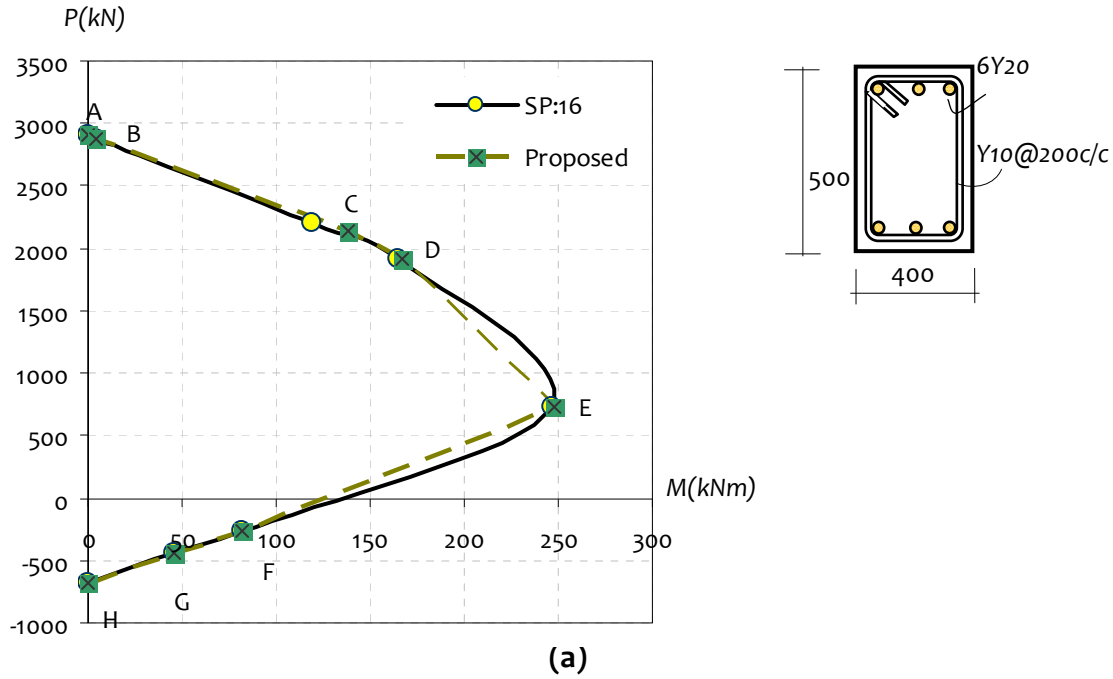

(a)

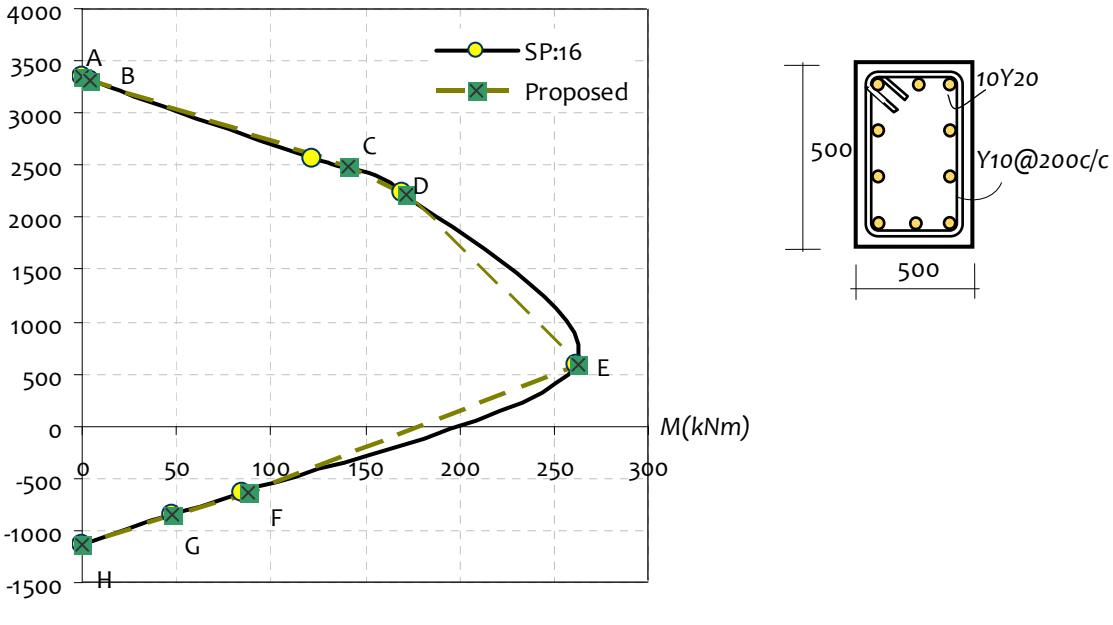

(b)

Figure A.4: Design *P-M* interaction curves as per SP 16 and proposed method of example rectangular RC sections with uniform distribution of reinforcing steel on: (a) two faces, and (b) four faces

Annex B
Sample Calculations

B.1 METHODOLOGY

Sample calculations, using the method proposed in Chapters 3 and 4, for estimation of shear strength of columns with rectangular cross-section subjected to combined axial force, shear force and bending moments are presented in the following. Although the main computations are carried out using a computer program developed for the purpose, only key results and salient calculations are presented here for two members, one that (i) fails in flexure, and another that (ii) fails in shear.

B.2 FLEXURE FAILURE

A typical case in which the specimen fails in flexure is considered (1st specimen in Table 4.2; Specimen 3 from Ang *et al*, 1981). The specimen has a square cross-section with reinforcement details as shown in Figure B.1, and height of 1.6m. First, the moment – curvature (M-φ) and the shear-flexure (V_c-M) interaction diagrams are obtained. Then, the bending moment capacity M_{cap} = 286kNm is determined from the M-φ diagram for the specimen (Figure B.2 (a)) and the shear resistance mechanism of the member is ascertained as discussed in Section 4.1.1.4 (Figure B.2 (b)).

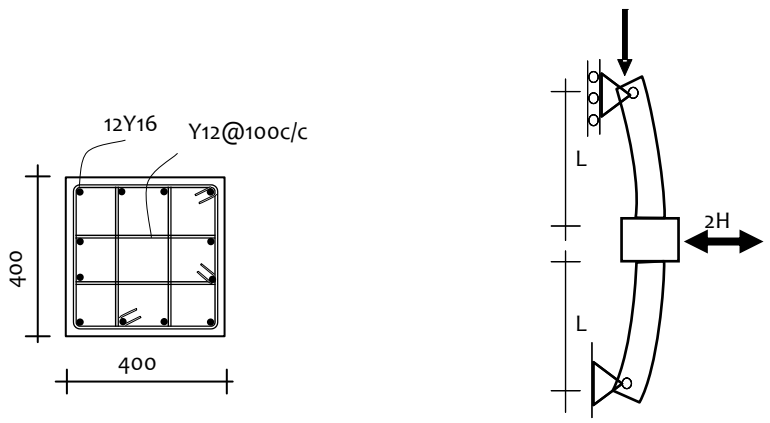

Figure B.1: (a) Cross-section details of column, (b) schematic of loading pattern of double ended specimen (2C) considered in the referred study [*reproduced from* Ang *et al*, 1981]

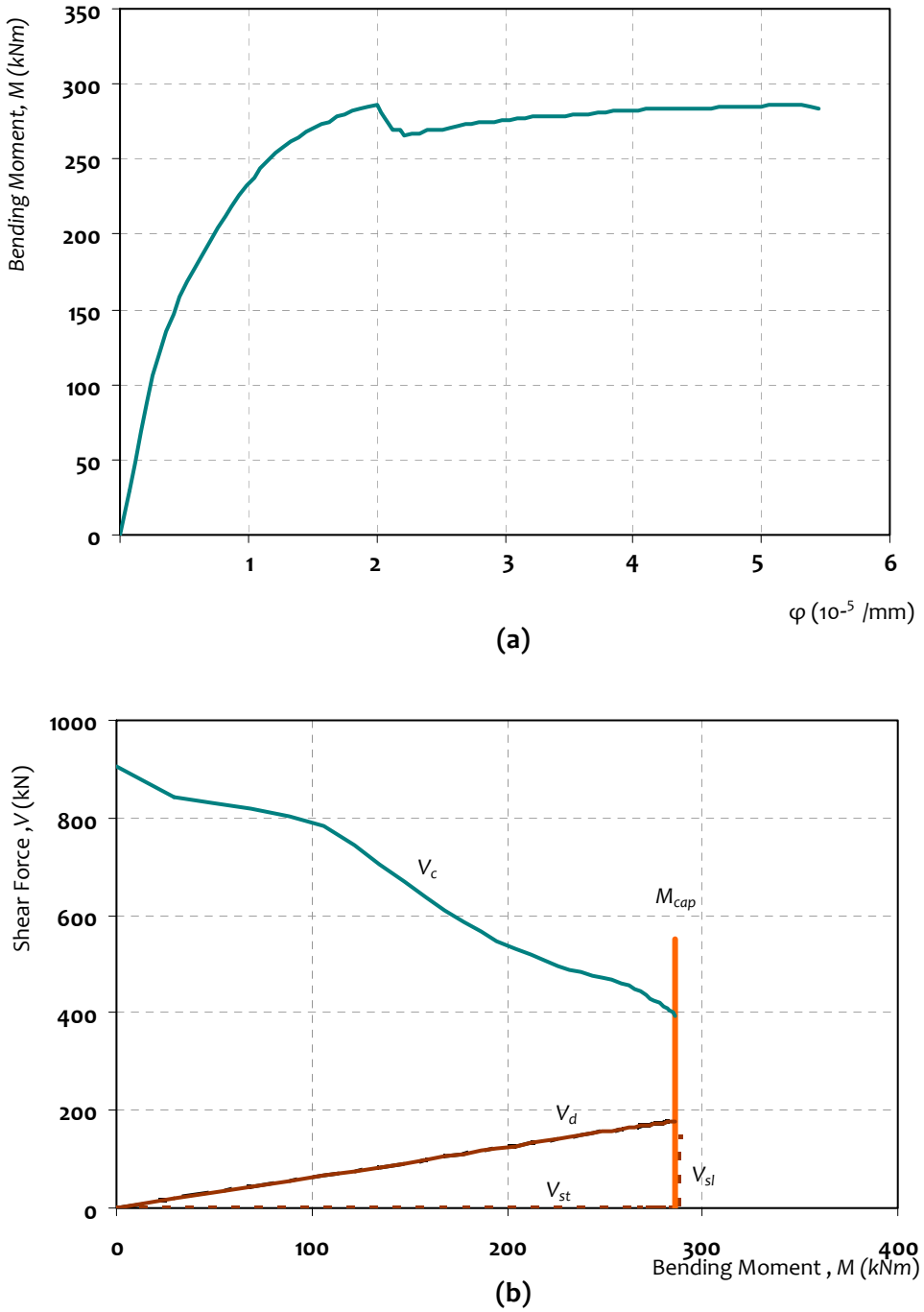

Figure B.2: (a) *M-φ* curves developed of the section, and (b) shear resistance mechanism in the member failing in flexure as per proposed method

In this case, the demand *Line* V_d crosses the moment capacity *Line* M_{cap} at a lateral shear force of 179kN; demand *Line* V_d does not intersect the V_c-M envelope indicating that the member would fail in flexure. Thus, the shear force of 179kN, corresponding to intersection of V_d and *Line* M_{cap} represents the shear capacity at *flexure* failure. It is to be

noted that although the estimate of crack angle of 48° suggests three stirrups to be intercepted by the crack, the concrete contribution alone is able to resist the shear demand. Thus, shear cracks are not developed and hence none of the stirrups contribute towards shear resistance. Consequently, the contribution of longitudinal reinforcement of 70kN through dowel action is not required to be mobilised at the initiation of flexure failure. The pertinent calculations are shown below.

Effective cover c_e	= 34.5 mm
Effective depth d	= 365.5 mm
Grade of unconfined concrete f_{ck}	= 29.5 MPa
Limiting strain in unconfined concrete	= 0.002
Ultimate strain in unconfined concrete	= 0.004
Yield strength of longitudinal steel	= 427 MPa
Yield strength of transverse steel	= 320 MPa
Axial compressive load applied P	=1435 kN
Net axial capacity of column cross-section P_u	= 5242 kN
Factor of axial load $p = \frac{1435}{5242}$	= 0.273
Crack angle $\alpha = \left(\frac{\pi}{4} + 0.5 \times tan^{-1}\left(\frac{1435 \times 1.6}{286}\right) - 0.5 \times tan^{-1}\left(\frac{1.6}{0.4}\right)\right) \times \frac{180}{\pi}$	= 48º
Spacing of transverse reinforcement s_v	= 100 mm
Number of stirrups intercepted by crack = $int(d \tan\alpha / s_v)$	= 3
Shear resistance from stirrups $V_{st} = 320 \times 4 \times \frac{\pi}{4} \times 12^2$	= 145 kN
Shear resistance from longitudinal steel $V_{sl} = \frac{12 \times 16^3 \times 427}{3 \times 100 \times 1000}$	= 70 kN

Shear strength for the specimen as reported from the experimental study is 192kN. Thus, it is observed that the strength of 179kN obtained using the proposed method is lower by about 6%. The numerical values corresponding to Figure B.2 (b) are presented in Table B.1, as obtained from the computer program developed.

Table B.1: Analysis results for specimen failing in f*lexure*

M	V_d	V_c	V_{st}	V_c+V_{st}	*Failure Load*
kNm	kN	kN	kN	kN	kN
0	0	904	0	904	-
29	18	841	0	841	-
49	31	832	0	832	-
69	43	819	0	819	-
88	55	803	0	803	-
106	66	782	0	782	-
122	76	745	0	745	-
135	84	703	0	703	-
147	92	668	0	668	-
158	99	637	0	637	-
168	105	611	0	611	-
178	111	588	0	588	-
187	117	567	0	567	-
195	122	549	0	549	-
204	128	533	0	533	-
212	133	518	0	518	-
219	137	507	0	507	-
226	141	497	0	497	-
232	145	489	0	489	-
238	149	484	0	484	-
244	153	477	0	477	-
249	156	472	0	472	-
254	159	467	0	467	-
258	161	460	0	460	-
262	164	455	0	455	-
265	166	448	0	448	-
268	168	443	0	443	-
271	169	436	0	436	-
273	171	431	0	431	-
275	172	425	0	425	-
278	174	420	0	420	-
280	175	415	0	415	-
282	176	409	0	409	-
283	177	404	0	404	-
285	178	400	0	400	-
286	**179**	395	0	395	**179**

B.3 SHEAR FAILURE

A typical case in which the specimen fails in shear is considered (68th specimen in Table 4.2; Specimen CUS from Umehara and Jirsa, 1982). The specimen has a square cross-section with reinforcement details as shown in Figure B.3, and height of 457mm. First, the moment – curvature (M-φ) and the shear-flexure (V_c-M) interaction diagrams are obtained. Then, the bending moment capacity M_{cap} = 133kNm is determined from the M-φ diagram for the specimen (Figure B.4 (a)) and the shear resistance mechanism of the member is ascertained as discussed in Section 4.1.1.4 (Figure B.4 (b)).

In this case, the demand *Line* V_d first intercepts the V_c curve at lateral force of 227kN, before meeting the moment capacity *Line* M_{cap}. This indicates propagation of a shear crack which is going to be intercepted by stirrups. The estimate of crack angle of 52° suggests six stirrups to be intercepted by the crack. The revised capacity line (V_c+V_{st}) is continued until the demand line V_d is again intercepted by the capacity line (V_c+V_{st}). This occurs at a shear force 290kN which is less than 292kN required to initiate flexure failure. This indicates a possible shear failure of the specimen. Also, the contribution of longitudinal reinforcement of 158kN through dowel action is not enough to prevent the shear failure; that would act as the residual strength of the specimen. The pertinent calculations are shown below.

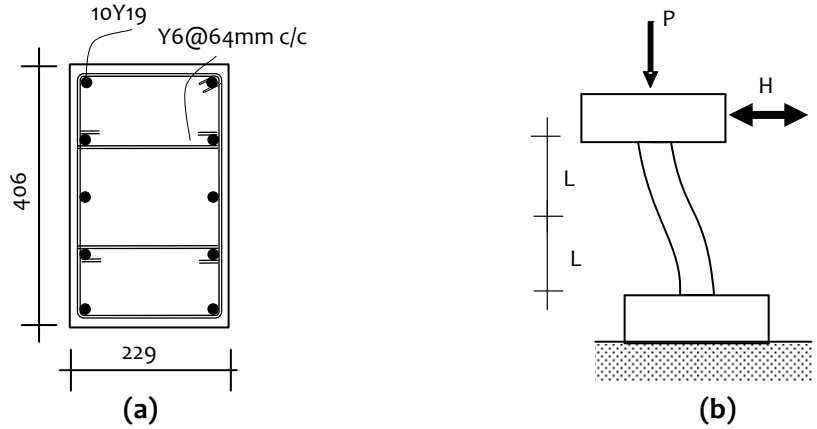

Figure B.3: (a) Cross-section details of column, (b) schematic of loading pattern of double cantilever specimen (DC) considered in the study [*reproduced from* Umehara and Jirsa, 1982]

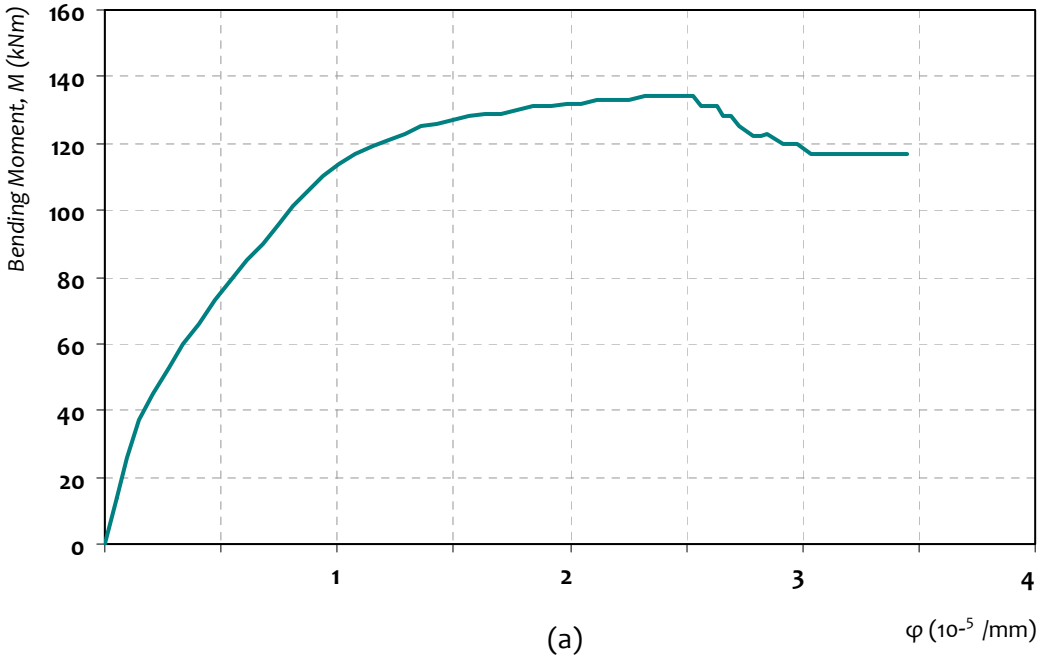

(a)

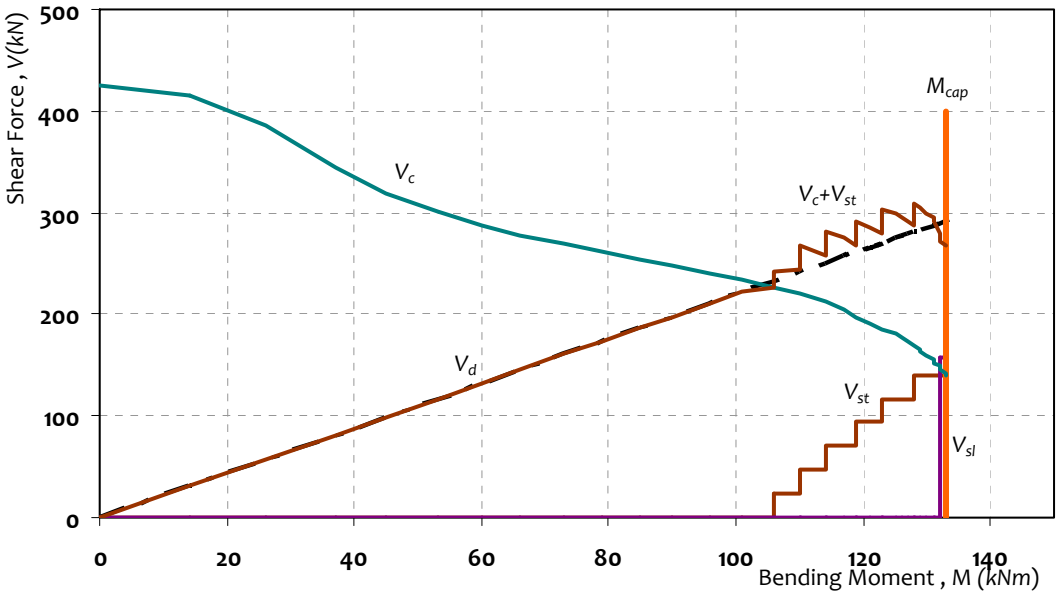

(b)

Figure B.4: (a) *M-φ* curves developed for the member, and (b) shear resistance mechanism in the member failing in shear using proposed method

Effective cover c_e	= 50.0 mm
Effective depth d	= 360.0 mm
Grade of unconfined concrete f_{ck}	= 42.0 MPa
Limiting strain in unconfined concrete	= 0.002

Ultimate strain in unconfined concrete = 0.004

Yield strength of longitudinal steel = 441 MPa

Yield strength of transverse steel = 414 MPa

Axial compressive load applied P = 534 kN

Net axial capacity of column cross-section P_u = 3904 kN

Factor of axial load $p = \frac{534}{3904}$ = 0.137

Crack angle $\alpha = \left(\frac{\pi}{4} + 0.5 \times tan^{-1}\left(\frac{534 \times 0.457}{133} \right) - 0.5 \times tan^{-1}\left(\frac{0.457}{0.41} \right) \right) \times \frac{180}{\pi}$ = 52°

Spacing of transverse reinforcement s_v = 64 mm

Number of stirrups intercepted by crack = $int(d \tan\alpha / s_v)$ = 6

Shear resistance from stirrups $V_{st} = 414 \times 2 \times \frac{\pi}{4} \times 6^2$ = 23.4 kN

Shear resistance from longitudinal steel $V_{sl} = \frac{10 \times 19^3 \times 441}{3 \times 64 \times 1000}$ = 158 kN

Shear strength for the specimen as reported from the experimental study is 324kN. Thus, it is observed that the strength of 290kN obtained using the proposed method is lower by about 9%. The numerical values corresponding to Figure B.4(b) are presented in Table B.2, as obtained from the computer program developed.

Table B.2: Analysis results for specimen failing in shear

M	V_d	V_c	V_{st}	V_c+V_{st}	*Failure Load*
kNm	kN	kN	kN	kN	kN
0	0	425	0	425	-
14	31	416	0	416	-
26	57	386	0	386	-
37	81	345	0	345	-
45	99	319	0	319	-
53	116	302	0	302	-
60	132	288	0	288	-
66	145	278	0	278	-
73	160	269	0	269	-
79	174	261	0	261	-
85	187	254	0	254	-
90	198	248	0	248	-
96	211	241	0	241	-
101	222	234	0	234	-
106	233	227	0	227	-
106	233	227	23	250	-
110	242	220	23	243	-
110	242	220	47	267	-
114	251	212	47	259	-
114	251	212	70	282	-
117	257	205	70	275	-
119	262	197	70	267	-
119	262	197	94	291	-
121	266	191	94	285	-
123	270	186	94	280	-
123	270	186	117	303	-
125	275	182	117	299	-
126	277	178	117	295	-
127	279	174	117	291	-
128	281	170	117	287	-
128	281	170	140	310	-
129	284	166	140	306	-
130	286	159	140	299	-
131	288	152	140	**292**	-
132	**290**	139	140	279	**290**
133	292	128	140	268	-

Aysha Zeneeb Majeed
Department of Civil Engineering
Indian Institute of Technology Madras

August 2016